UNIVERSIDAD COMPLUTENSE DE MADRID

FACULTAD DE CIENCIAS GEOLÓGICAS

TESIS DOCTORAL

Magmatic processes and lithosphere dynamics: insights into crustal evolution

Procesos magmáticos y dinámica litosférica: ahondando en la evolución cortical

MEMORIA PARA OPTAR AL GRADO DE DOCTOR

PRESENTADA POR

Daniel Gómez Frutos

Directores

Antonio Castro
Javier Fernández Suárez

Madrid

UNIVERSIDAD COMPLUTENSE DE MADRID
FACULTAD DE CIENCIAS GEOLÓGICAS

TESIS DOCTORAL

MAGMATIC PROCESSES AND LITHOSPHERE DYNAMICS: INSIGHTS INTO CRUSTAL EVOLUTION

PROCESOS MAGMÁTICOS Y DINÁMICA LITOSFÉRICA: AHONDANDO EN LA EVOLUCIÓN CORTICAL

MEMORIA PARA OPTAR AL GRADO DE DOCTOR

PRESENTADA POR

Daniel Gómez Frutos

DIRECTORES

Antonio Castro, Javier Fernández Suárez

Universidad Complutense de Madrid

Facultad de Ciencias Geológicas

PROCESOS MAGMÁTICOS Y DINÁMICA LITOSFÉRICA: AHONDANDO EN LA EVOLUCIÓN CORTICAL

MAGMATIC PROCESSES AND LITHOSPHERE DYNAMICS: INSIGHTS INTO CRUSTAL EVOLUTION

Daniel Gómez Frutos

Directores: Antonio Castro, Javier Fernández Suárez

Doctorado en Geología e Ingeniería Geológica

AGRADECIMIENTOS

Una tesis doctoral supone una amalgama de experiencias diferentes, marcadas en todo caso por el paso de numerosas personas. Hoy tengo la fortuna de deber gratitud a la mayoría de ellas, y nombrar a todas las que han contribuido a haber llegado hasta aquí resultaría imposible. No obstante, sí puedo destacar a los que más han influenciado el devenir de mi etapa predoctoral.

En primera instancia, agradecer a mi entorno más cercano, familia y amigos, de los que he recibido apoyo incondicional desde que comencé esta etapa, y que siempre han sido los primeros en celebrar mis éxitos.

Por supuesto reconocer y agradecer el apoyo mostrado por mis directores, Antonio Castro y Javier Fernández Suárez. Sin su guía esta tesis doctoral no habría tenido lugar.

Agradezco también a mis colaboradores en estos últimos años, en especial a Gabriel Gutiérrez Alonso y Jesús de la Rosa, cuya ayuda me ha servido para aprender y pulir mis conocimientos, métodos e ideas.

Deseo agradecer la amabilidad recibida por parte de mis colegas del ETH Zurich, muy en especial de Taras Gerya y Attila Balázs, que hicieron de mi estancia en el ETH Zurich no solo un aprendizaje de valor pedagógico incalculable, sino en su totalidad una experiencia inolvidable.

Y por último, muestro mi gratitud a todas las personas no nombradas aquí, pero que sí se mostraron afables conmigo en los últimos años.

Esta tesis doctoral fue posible gracias al apoyo de los proyectos de la Agencia Estatal de Investigación PGC2018-096534-B-I00 (Proyecto IBERCRUST) y PID2021-126347NB-I00/AEI/10.13039/501100011033/FEDER,UE (Proyecto IBERCRUST II).

Index

Resumen

El origen y la evolución de la corteza continental continúa siendo uno de los enigmas más significativos y fundamentales en las Ciencias de la Tierra. A lo largo de la historia del planeta, la corteza continental ha sufrido innumerables eventos responsables de su creación, destrucción y modificación. Dichos procesos son la causa de que el registro rocoso represente una amalgama de la continua evolución de la corteza continental, ocultando las evidencias claras sobre su origen y los mecanismos responsables de su creación. En este sentido, el crecimiento cortical puede describirse como un proceso ígneo que involucra la segregación de material ígneo desde el manto y su subsiguiente incorporación y preservación a largo plazo en la corteza continental. Por consiguiente, el estudio de la petrogénesis del magmatismo más voluminoso del mundo representado por las dos suites constituyentes del magmatismo tipo I, a saber los magmas post-colisionales y cordilleranos, resulta de máxima prioridad a la hora de determinar el origen y evolución de la corteza continental. En esta disertación doctoral se aborda el problema de la evolución de la corteza continental usando una perspectiva ígnea. Para dicha tarea, una profunda comprensión del origen del magmatismo tipo I, actualmente sujeto a importantes controversias que siguen sin resolver, supone un requisito crucial. A través de diversas metodologías que incluyen relaciones de campo, geoquímica, petrología experimental y modelización numérica, se ofrece un análisis integral y conciliador sobre las fuentes magmáticas de los magmas tipo I. La interpretación clásica sobre el magmatismo post-colisional lo interpreta como de origen cortical. Por contrario, las evidencias geoquímicas y experimentales obtenidas sugieren que los magmas post-colisionales, representados principalmente por la suite silícea, la suite sanukitoide y los enclaves microgranulares máficos, tienen su fuente en un manto modificado. Las diferencias composicionales se pueden atribuir a la diferenciación magmática, que provoca una signatura geoquímica específica en última instancia definida por una línea de descenso de líquidos y en la que los magmas sanukitoides representan el magma parental de los granitos. La evidencia numérica apoya un origen en el manto litosférico comprendido en rangos de temperatura y contenidos en agua razonables. Complementariamente, los magmas cordilleranos se originan a partir de un precursor intermedio que puede encontrarse como glóbulos máficos en zonas de interacción de

magmas, donde la congelación súbita previene la fraccionación y preserva la composición parental intermedia que coincide con los modelos experimentales. Las implicaciones de estas evidencias petrológicas y geodinámicas son usadas para abordar el problema de la evolución cortical como resultado de procesos magmáticos y dinámica litosférica, estableciendo el rol pasivo de los continentes en la evolución a largo plazo de la corteza continental.

Abstract

The origin and evolution continental crust remains one of the most significant and fundamental issues in Earth Sciences. Throughout the history of the planet, the continental crust has undergone innumerable events that are responsible for its creation, destruction and modification. Such processes have resulted in the rock record representing an amalgamation of the ongoing evolution of the continental crust, hindering clear evidence on its origin and the mechanisms responsible for its creation. In this regard, crustal growth can be conceptualised as an igneous process involving the segregation of igneous material from the mantle and its subsequent incorporation and long-term preservation into the continental crust. Consequently, constraining the petrogenesis involving the most voluminous magmatism as represented by the two constituent suites of I-type magmatism, namely post-collisional and cordilleran magmas, is of paramount importance in constraining the origin and evolution of the continental crust. In this doctoral dissertation the problem of the evolution of the continental crust is addressed using a magmatic perspective. A crucial pre-requisite for this task is a deep understanding on the mechanisms surrounding the origin of I-type magmatism, currently subjected to important controversies that remain unsolved. Through a variety of different research methods that include field relations, geochemistry, experimental petrology and numerical modelling, an integrated and conciliatory analysis of the ongoing problem of I-type magmatic sources is offered. Classic interpretation of post-collisional magmatism considers it to be crustal in origin. Contrary to this, the herein provided geochemical and experimental evidence suggest that post-collisional magmas, mostly represented by the silicic suite, the sanukitoid suite and the mafic microgranular enclaves, are sourced in a modified mantle. Compositional differences can be attributed to magmatic differentiation, which shapes a specific geochemical signature that is ultimately fixed by a liquid line of descent, with sanukitoid rocks representing the parental composition to the granitic magmas. Numerical evidence supports a lithospheric mantle origin within reasonable temperature ranges and water contents. Complementarily, cordilleran magmas originate from an intermediate precursor that can be found as mafic globules in magma mingling zones, where quenching phenomena preclude fractionation and preserve pristine intermediate compositions that match

those predicted by the experimental models. The implications of such petrological and geodynamical constrains are used to address crustal evolution as a result of magmatic processes and lithosphere dynamics, subsequently establishing the passive role of the continents in the long-term development of the continental crust.

1. Introduction

The lithosphere, an essential component of the Earth's intricate structure, plays a vital role in shaping the geology of the planet, its climate, and ultimately life. It comprises the uppermost part of the mantle, and the solid, rocky material that conforms the crust. It is an ever-changing part of the Earth, driving global phenomena like plate tectonics and orogenic processes. Within the lithosphere, the crust, both continental and oceanic, constitutes the outermost layer. This dynamic region houses diverse geological features, from towering mountain ranges to the depth of ocean basins. Its behaviour and interaction with the underlying mantle are integral factors in the comprehension of the Earth's geological history and its ongoing evolution, potentially related to modern day challenges.

Among the constituent parts of the lithosphere, the crust is the support for life on Earth as we know it. Particularly, the continental crust is of special interest, given that is presumably responsible for modifying the composition of the mantle during its differentiation (Taylor and McLennan, 1995; Windley, 2010). It contains the highest complexity in terms of petrological and geodynamical processes, actively affecting the surrounding subsystems as a result of plate tectonics (Condie, 2013a). Thus, it is safe to assume that the continental crust has played a major role in the evolution of planet Earth, with the inquiries regarding its origin arguably representing one of the biggest unresolved mysteries in Earth Sciences.

Tackling the challenges concerning the origin and evolution of the continental crust proves to be a difficult crusade. A multitude of interrelated factors are responsible for this difficulty, each with its independent study methodology, often involving completely different disciplines. Among them, the most immediate are the geological complexity, with the continents representing an amalgamation of rocks with varying compositions, ages and origins, and formed by equally diverse mechanisms; the limited geological record, with processes like metamorphism partially erasing many of the original features of the rocks, or others like subduction destroying them; the obscure mechanisms of crustal recycling and their effect in crustal growth over time; and ultimately the scientific complexity that implies the study of such a multifarious system, requiring the expertise

in many different fields of geology, including petrology, geochemistry, geodynamics or tectonics. It is not far-fetched to affirm that any attempt to reconcile such variety of observations, methods and techniques starts with a basic understanding of the nature of the continental crust.

The initial classification of the Earth into its three major structural components, namely the crust, mantle and core, was established in 1909 by Andrija Mohorovičić on significant discontinuities in both compressional (P) and shear wave velocities (S). Following works allowed for higher resolution in determining the structure of the continental crust, mostly after complementing geophysical observations with the petrological information provided by xenoliths carried in extrusive magmatism. This allowed for the subsequent division of the continental crust into two geophysical and geochemically distinct layers, an upper section with granodioritic composition and a lower section with basaltic composition (Rudnick and Fountain, 1995). Further advances in geophysical and geochemical techniques resulted in the steady improvement of the characterisation of these layers (e.g. Heier, 1973; Holland and Lambert, 1972; Smithson, 1978). Currently, the consensus separates an upper crust, containing high concentrations of alkalis, calcium, and silicon, as well as the majority of incompatible elements present in the geosphere, producing a global composition similar to that of a granodiorite (Rudnick and Gao, 2003). On the other hand, the lower crust is mostly mafic and is depleted in incompatible elements, displaying a global/average composition that resembles a diorite (Heier, 1973; Rudnick and Fountain, 1995; Rudnick and Gao, 2003).

The efforts to characterise the nature of the crust allowed for the determination of a bulk composition for the continental crust. The continental crust is andesitic on average (Rudnick and Gao, 2003), representing a composition that is not in equilibrium with the underlying peridotitic mantle (Hacker et al., 2011; Rudnick and Gao, 2003). This observation is central to the ongoing debate on the origins of the continental crust, and several attempts to reconcile the evidence have been made in the past decades. More specifically, a plethora of processes may account for this compositional discrepancy, such as differentiation from the mantle, differentiation from a crustal magmas or magma mixing, all of which will be discussed thoroughly in the following sections of this thesis.

Of special relevance to this subject is the emergence of experimental petrology, which has greatly contributed to solve this challenge. Although an arguably longstanding methodology (Boyd and England, 1960; Eugster, 1971), it has fulfilled the desire of petrologists and geochemists by enabling the simulation of the Earth's interior in a laboratory setting. Petrological experiments provide a controlled environment to study the properties and behaviour of rocks and minerals. More specifically, they helped characterising the behaviour of rocks under heating and cooling, providing significant thermodynamic constrains to the field of petrology. Concepts like magmatic differentiation, crystallization or the existence and influence of liquid lines of descent, all of which are currently university-level geological education, owe their understanding to experimental petrology. This allowed for further determining the evolutionary trajectories of crustal rocks under known conditions, bringing important insights into virtually every geological discussion. Up to this day, they continue to serve as an invaluable source of information that help constrain existing geological problems.

The development of petrology and experimental petrology and the attempts to constrain crustal evolution brought into the discussion the role of intensive parameters such as temperature, either as scalar for petrological experiments and thermobarometric calculations or in the form of heat flux for thermomechanical calculations; pressure, resulting from stresses linked to geodynamic process or from sheer lithostatic load; and age/time.

Temperature is a critical parameter that strongly controls the rheological behaviour of the lithosphere and the occurrence of igneous process like melting and crystallization. The Earth's thermal regime was established early in its history, and since its inception, a gradual decrease in the global temperature has been occurring, causing the planet to transition from magma oceans to its current relatively solid yet mobile state (Ballmer et al., 2017; Nakajima and Stevenson, 2015; Tonks and Melosh, 1993). In contrast with the rapid cooling showcased by other planets in the Solar system, the causes of Earth's steady yet relatively slow cooling are twofold. Firstly, the low thermal diffusivity of the crust makes it an effective thermal isolator for the underlying mantle, with the lower continental crust exhibiting exceptionally good insulating properties (Whittington et al., 2009). Secondly, heat production in the Earth's interior has continued ever since its

origin, primarily due to the persistent presence of multiple heat sources maintaining its warmth. These heat sources comprise radiogenic heating, caused by the radiogenic decay of radioactive elements; and shear heating, resulting by the dissipation of mechanical energy due to geodynamic processes. Two additional processes that have a comparatively lesser impact can influence heat generation and dissipation, namely adiabatic heating or cooling, linked to the changes in pressure causing compression or decompression; and latent heating or cooling, resulting from energy released or absorbed in thermodynamic reactions during melting or crystallization of magmas, respectively (Gerya, 2019).

The thermal complexity of the planet has led to a dynamic and thermally evolving planet, wherein the transfer of thermal energy is quantified through the heat flux. Heat flux values are characterised by their non-uniformity, and only mantle upwelling zones exhibit the highest measured values. Alternatively, active margins show midterm values, while tectonically inactive settings like continental plateaus reach the lowest heat flux values. Although these observations represent a complex dynamic of everchanging thermal regimes, as well as heat flux measurements are related to surface and shall not be indicative of deep temperatures due to a number of processes (e.g. local heat due to volcanism, shallow water convection, local erosion or sediment blanketing), one fundamental feature remains unaltered: temperatures steadily increase with depth and can be described as a gradient.

Heat flux and gradient measurements are exclusively related to surface-level values. Models extrapolating these values to deeper sections led to unrealistically high crustal and mantle temperatures, directly conflicting with petrological and geophysical evidence predicting the lack of large-scale melting under these conditions. These observations justify the assumption that the gradient decreases with temperature, which is supported by the observation that the upper crust concentrates the largest amounts of radioactive elements, and it is only logical that radioactive heating decreases with depth. This discussion culminated with the definition of the steady-state geotherm (Turcotte and Schubert, 2002, and references therein). Further work correlated the predictions from continental geotherms with heat flow and heat production (Artemieva and Mooney, 2001; Chapman, 1986; Hasterok and Chapman, 2011), the range of seismic velocities in

the continental lithosphere (Goes and van der Lee, 2002; Priestley and McKenzie, 2006; Röhm et al., 2000; Shapiro and Ritzwoller, 2004) and xenolith thermobarometry (O'Reilly and Griffin, 2006; Rudnick et al., 1998).

The interconnectivity of all the aforementioned factors allowed for tighter constrains on the temperature ranges within the lithosphere and the continental crust. Most existing evidence points to average Moho temperatures of 600 ^{o}C in an average 40 km thick continental crust (Goes et al., 2020; Rudnick et al., 1998). Higher temperatures have been registered in active tectonic settings during subduction, occasionally reaching temperatures of 800-900 ^{o}C (Schutt et al., 2018), or during post-orogenic extension, reaching temperatures up to 700-800 ^{o}C (Gaudemer et al., 1988; Huet et al., 2011). Melt inclusions in granulite xenoliths from the lower crust exceptionally record ultra-high temperatures above 900 ^{o}C (Clark et al., 2011; Laurent et al., 2023). Complementarily, the steady-state geotherm predicts temperatures up to 1200-1300 ^{o}C in the underlying lithospheric mantle, occasionally reaching >1300 ^{o}C during mantle upwelling in post-orogenic extension. These considerations provide a solid framework for temperature values in experimental and numerical work.

While comparatively less influential than the temperature in rock and magma generation, pressure is an important variable conditioning most lithospheric processes. Pressure is dictated by the lithostatic gradient, defined as a function of the product of depth, gravity and the average density of the overlying rock from the measurement point. For the continental lithosphere, the upper crust, constituted mainly by felsic rocks rich in lighter elements (such as alkalis, calcium and silicon), has an average value of 2700 km/m^3; the lower crust, with predominantly mafic composition and richer in heavier elements (such as iron, magnesium and titanium), has average values from 2800 km/m^3, up to 3000 km/m^3 increasing with the predominance of the most mafic compositions (Ranalli, 1995); and lastly, a MORB-like lithospheric mantle composed mainly by dry peridotite has an average density of 3300 km/m^3 (Ranalli, 1995). On the other hand, crustal thickness is a variable that depends on the occurrence and on-going stage of orogenic processes. Thus, measurements of the surface waves from seismic tomography show a considerably large variation interval. A crustal thickness of 30 to 35 km is registered in inactive continental settings like the African, South American or Australian

cratons, while values up to 45 to 50 km can be found in orogens with active magmatism like the Andes, Sierra Nevada or Tibet (e.g. Meier et al., 2007; Soller et al., 1982). Exceptionally high values above 50 km are found in the Tibet due to the ongoing continental collision between India and the Eurasian plate (e.g. Rao et al., 2015; Tewari et al., 1997).

Using these density and crustal thickness values allows for calculation of the pressure regime in the Moho discontinuity and in the lithospheric mantle. Pressure values at the Moho may vary from 1.0 GPa in the thinner and more felsic crust, to 1.3 GPa in the thicker and more mafic continents. The mantle lithosphere yields higher values, ranging from 1.5 to 2.5 GPa depending on depth and crustal thickness. Note that these variations of ±0.2 GPa are acceptable uncertainty intervals for most techniques, mainly due to phase equilibria mostly depending on temperature and having wider pressure stability fields (Philpotts and Ague, 2009).

The efforts aimed at understanding the effect of intensive parameters in the evolution of the continental crust have provided a solid construct for their use in experimentation. Nevertheless, the wide range of rock ages within the lithosphere and present-day geodynamics brings the spotlight into an important bias that must be addressed prior to any in-depth discussion of the subject. That is, research within geology is limited by the availability of the rock record and the current state of the planet, likely causing biases in the observations (Fig. 1). While experimental petrology provides direct and timeless evidence of the thermodynamic laws involved in igneous processes that is equally valid from the Archean until now, the context for this petrological information (i.e. evolution of the Earth's temperature and dynamics) remains obscure.

In this regard, a relatively recent technique has allowed the Earth Sciences community to propel forward the reconstruction of the geodynamic history of the planet. Numerical modelling emerged as a complementary method to study the thermal and kinematic evolution of the mantle (Torrance and Turcotte, 1971) or active margins, either during subduction (Matsumoto and Tomoda, 1983; Minear and Toksöz, 1970) or the subsequent collision (Bird, 1978; Daignieres et al., 1978). While initially hampered by computational limitations, coupled development of computer engineering and

numerical methods eventually allowed geodynamical numerical modelling to evolve into its current state as a fully-fledged discipline.

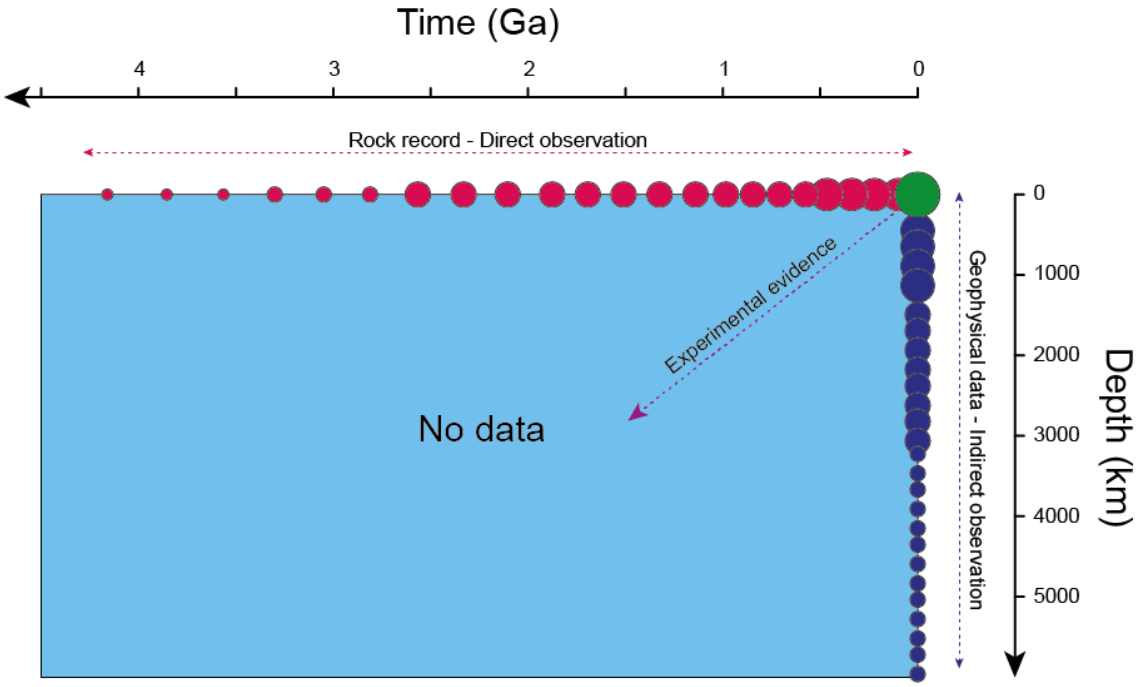

Figure 1. Time–depth diagram showing the availability of data from the Earth's interior. Although the rock record is the manifestation of processes operating in the Earth's interior, pervasive modification of the rocks over the geological time limits the information they provide. Experimental methods are the only reliable source of information, either petrological or numerical. Modified from Gerya, 2014.

The development of new thermomechanical codes helped to compensate the missing pieces of the rock record and inability to study the past configuration of the deep Earth. Studying the time dependency of geodynamical processes became an achievable goal, and so several phenomena affecting the lithosphere received a new approach for their characterisation, such as delamination (Bird, 1979; Göğüş and Pysklywec, 2008; Li et al., 2016; Ueda et al., 2012), Rayleigh-Taylor instabilities removal (e.g. Gorczyk et al., 2012; Plag and Jüttner, 1995), or subduction (Gerya, 2022 for review). Most importantly, although models may lose reliability with extended simulation times due to the yet irreproducible complexity of nature, they constitute a consistent source of information on the evolution of temperature, pressure, and, ultimately, the lithosphere and the crust over time.

In this context, the discussion around the evolution of the continental crust has proved to be a challenge for the geological community. Its history can be strictly correlated to the evolution of supercontinents, with the classical interpretation being that crustal growth correlates to periods of enhanced production of magma (Condie, 1998; Taylor and McLennan, 1995; Wang et al., 2009). However, the advancement of geophysics and numerical methods allowed for the identification and characterisation of mechanisms responsible for recycling crust into the mantle. The correlation of crustal growth estimation maxima through zircon crystals with the assembly of supercontinents shifted the focus towards the preservation of continents, pointing to it as the most crucial factor influencing how crustal growth is measured (Hawkesworth et al., 2009; Kemp et al., 2006).

In this unresolved puzzle of interconnected and often conflicting evidence, an important consideration is that any process regarding crustal growth must satisfy three preliminary conditions: (1) the segregation and differentiation of igneous material form the mantle, (2) the incorporation of such material into the pre-existing continental crust, and (3) its long-term preservation in the form of large igneous bodies (Condie et al., 2011; Couzinié et al., 2016; Hawkesworth et al., 2009). In essence, crustal evolution can be entirely conceived as an igneous process. Furthermore, these very igneous mechanisms are also the ultimate drivers behind the bulk composition of the continental crust. As a result, igneous rocks inherently emerge as the most effective tracers for understanding crustal evolution.

In this context, I-type magmatism constitutes the most voluminous type of magmatism on Earth. The two nominal subtypes within I-type magmas, the Andean-type and the Caledonian-type magmas, take their names after their two most notable representants, namely the Andes cordillera in South America and the Caledonian orogen in the British Isles. I-type magmas appear associated with most collisional orogens across the world as a response to lithospheric-scale events that trigger extensive magmatism (Fig. 1.2). Archean cratons are also relevant in the I-type discussion, with pericratonic magmatism sharing a number of features with post-Archean I-type magmas (Fowler and Rollinson, 2012).

The mechanisms surrounding the origin of these magmas have long been a matter of controversy, spawning a wide range of hypotheses, some of them contradictory. The only thing that remains unchanged from their original definition is their link to specific stages of the orogenic process. This causes their alternative, arguably more popular names to exist. Andean-type magmatism, also known as arc magmatism, occurs during subduction in an active margin, resulting in either a continental arc if the subduction is between an oceanic and a continental plate, or an oceanic arc if the subduction is between two oceanic plates. On the other hand, Caledonian-type magmatism, also known as post-collisional magmatism, takes place during the post-collisional stage of an orogenic process, after ocean closure and continent collision.

Due to its relevance in addressing crustal evolution and in petrology itself, I-type magmatism has been studied by almost all available methods in Earth sciences, including petrological, geophysical and numerical methods. Although resulting from different stages of the subduction process, the two magmatism types are believed to result from different sources and geodynamic mechanisms. This apparent independence causes their particular range of controversy to be relatively self-contained and, a priori, deserving of a separate discussion.

In this doctoral project the problem of the evolution of the continental crust was addressed using a magmatic perspective. A crucial pre-requisite for this task is a deep understanding on the mechanisms and constraints surrounding the origin of I-type magmatism, currently subjected to important controversies that remain unsolved. Through a variety of different research methods, including field relations, geochemistry, experimental petrology and numerical modelling, an integrated and conciliatory analyses of the ongoing problem of crustal evolution is offered.

This doctoral dissertation sets its first milestone in addressing the comparatively more unknown Caledonian-type magmatism, with a sequential and organized characterisation of all its constituent features using petrological experiments and geochemical analyses. The mantle origin of Caledonian-type magmas is subsequently established, challenging the majority of previous crustal growth models. In parallel, field relations and geochemical analyses are used to identify the missing natural example that matches the experimental models on the intermediate parental to Andean-type magmas. After the

thorough characterisation of I-type magmas and bringing new important cues to their petrogenesis, numerical models are used to constrain the dynamics, the temperature and pressure conditions and the potential volatile contents involved in the mantle source for I-type magmatism. A final set of petrological experiments uses all collected evidence to constrain the controls on each type of magmatism. The role of crustal recycling in crustal evolution is then appropriately discussed, concluding in the passive role of the crust and major involvement of the lithosphere. The major conclusion of this dissertation points to the lithosphere, and more specifically to crust-lithospheric mantle interactions, as the main factor driving crustal growth through voluminous I-type magmatism.

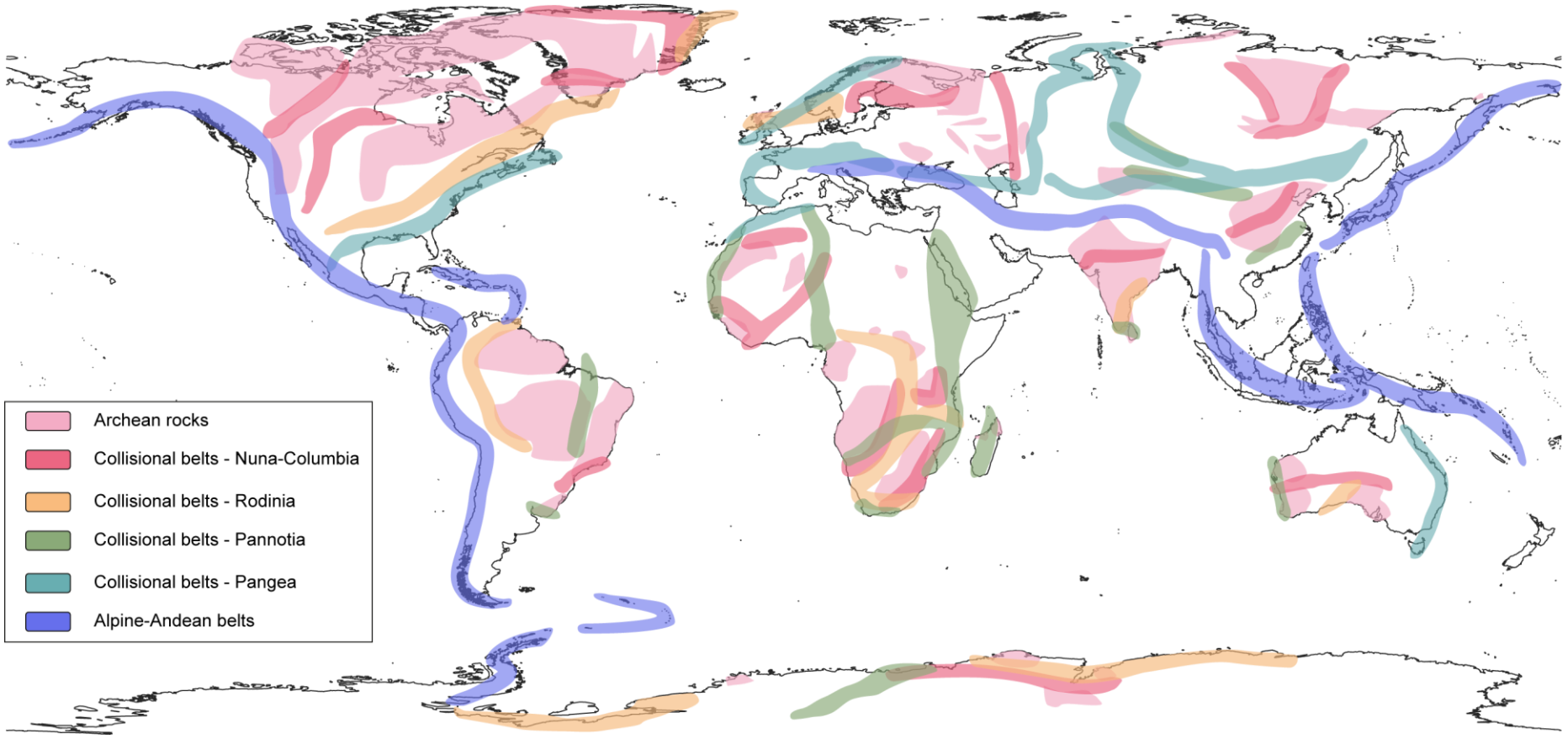

Figure 1.2. Collisional belt world map. I-type magmatism occurs associated to the domain of a collisional belt. Archean cratonic shields are also included, commonly bearing pericratonic magmatism. References used for the elaboration of this map are the following: Condie, 2013; Kirscher et al., 2021; Kusky and Polat, 1999; Li et al., 2017; Spencer et al., 2015; Stampfli et al., 2013; Wang et al., 2017; Wareham et al., 1998; Zhao et al., 2011.

2. State of the art – existing challenges

2.1 Crustal growth and evolution

The evolution of the continental crust can be described by igneous processes, causing the incorporation of igneous material from the mantle into the crust and subsequent growth; and by geodynamic processes, resulting in the recycling of crustal material back to the mantle and subsequent destruction. The balance between these two competing processes ultimately determines the evolution of the continental crust over the geologic history.

A vast number of models have attempted to constrain the evolution of the continental crust, balancing growth and destruction processes. Among them, important discrepancies may be found, with some suggesting that a large portion of the continental crust formed during the Archean, and a slower rate of growth or decrease in the continental net volume through time; others estimating rapid growth at the onset of plate tectonics (circa 3.0 Ga) and steady crustal growth over the Proterozoic; and finally, some pointing to episodic growth since the onset plate tectonics (Fig. 2, and references therein). These differences are due to the use of a wide range of techniques and methods to estimate crustal evolution, proving the conciliation of such varied sources of information a difficult task.

Mass balance calculations indicate that more than 80% of the continental crust was created in destructive plate margins (Rudnick, 1995). This observation means that I-type magmatism can be considered the main driver behind the creation of new continental crust. Consequently, granitic rocks have been widely studied for their role into this discussion, mainly through the use of zircon chronology and geochemistry.

Zircons constitute the only record available for the ancient (Hadean) Earth, with the development of micro-analytical, integrated U-Pb and Hf isotope techniques allowing for new observations. In this regard, Hf isotopes have been the most successful at discerning crustal and mantle sources, allowing for the elaboration of zircon datasets with model ages for separation of the igneous protolith from the mantle (Griffin et al., 2000; Kemp et al., 2006; Payne et al., 2016). Further work on zircon grains also allowed for broader

connections to large scale lithospheric processes. There is a direct correlation between peaks in crustal growth and supercontinent formation (Condie, 1998; Condie and Aster, 2010), in which supercontinent assembly represents optimal time periods for the long-term preservation of igneous material newly incorporated to the continental crust (Condie et al., 2011; Hawkesworth et al., 2009).

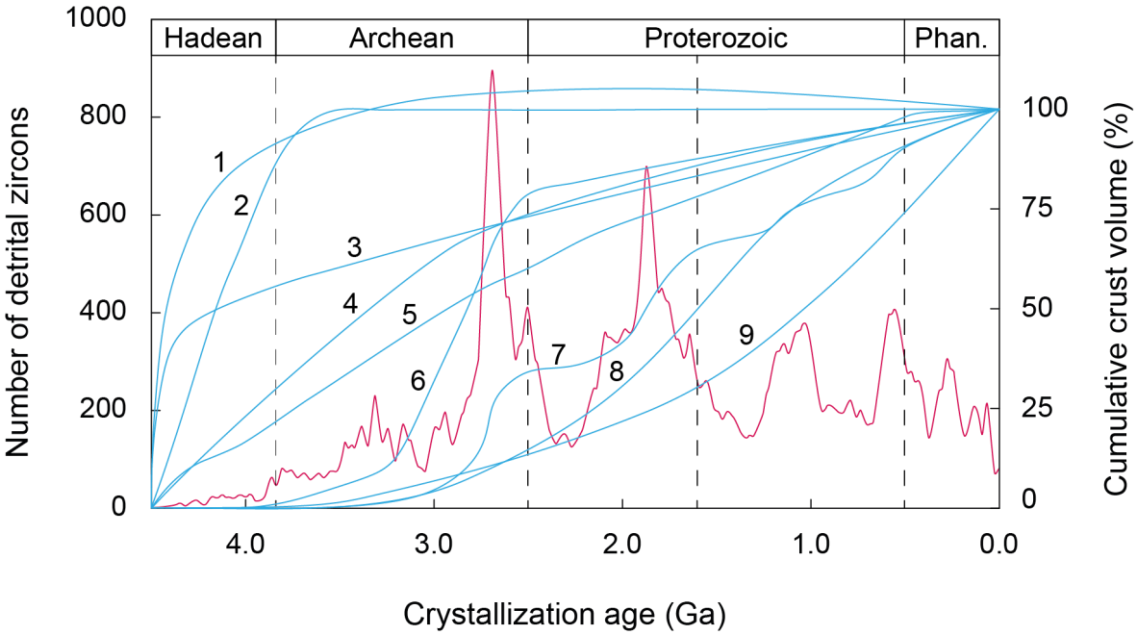

Figure 2.1. Diagram showing the evolution of the net crust volume over time. Number of detrital zircons are plotted for reference (Condie, 2014). Numbers inside the diagram refer to blue lines, representing crustal evolution models from different authors: 1.Fyfe, 1978; 2. Armstrong, 1981; 3. Reymer and Schubert, 1984; 4. Dhuime et al., 2012; 5. Belousova et al., 2010; 6. Taylor and McLennan, 1985; 7. Condie and Aster, 2010; 8. Allègre et al., 1983; 9. Hurley and Rand, 1969.

However, information on the igneous source given by the zircon record is limited, considering that Lu-Hf systematics suffer from similar problems to the Sm-Nd system (Arndt and Goldstein, 1987). That is, the isotopic configuration of rocks is affected by every magma entrainment in the system, including those from different sources, hence the isotopes representing a hybrid age (Belousova et al., 2010; Payne et al., 2016; Roberts and Spencer, 2015). These works rely on the number of sampled detrital zircons, uncertainly assuming their weathered igneous source and producing fictitious density

maxima (Arndt, 2013; Hawkesworth et al., 2019; Voice et al., 2011). Furthermore, discrepancies between calculated model ages and crystallization ages in arc rocks strongly suggest that the incorporation of preexisting crustal material into the mantle source of new continental crust has been a long-standing feature (Dhuime et al., 2011). Thus, crustal growth estimations through the use of isotopes in zircon are not straightforward.

The destruction of the continental crust is the other side of the coin when addressing crustal evolution. A number of processes contribute to the destruction of continental crust, most of which are related to subduction. Among them, delamination is the most significant in terms of volume, and its qualitative influence in lithosphere destruction has already been discussed (Kay and Kay, 1993). Furthermore, the dismantling of orogens and continental arcs undergoing erosion represent major sinks for crustal material (Clift and Vannucchi, 2004). Numerical modelling on collisional orogens predict that significant volumes of subducted continental crust, either in the form of sediments or large continental blocks, are recycled into the mantle (Faccenda et al., 2009). This recycling takes places either in the form of relaminated material, delamination (e.g. Ueda et al., 2012) or slab break-off (e.g. Duretz et al., 2011; van Hunen and Allen, 2011). Recycling of continental crust during collision proves an interesting observation when compared with crustal growth models: for being recycling and erosion an important crust destruction mechanism during collision, crustal growth models should predict net volume loss during the collisional stage of supercontinent assembly. Contrary to this, crustal growth models predict stable continental growth (Fig. 2.1), implying that the elimination of mass from the continents must be compensated by the addition of new mass from the mantle.

Following the aforementioned limitations of zircon studies at estimating crustal growth, an alternative must be used to overcome these challenges. Thorough characterisation of the mechanisms behind crustal growth and destruction is key for understanding crustal evolution. Considering I-type magmas as the main drivers behind crustal growth, a re-evaluation of the origin of their two nominal classes, namely Caledonian-type and Andean-type, is an immediate prerequisite to address the crustal evolution discussion. Petrological and numerical evidence highlighted the relevance of mantle-crust

interaction throughout continent formation events, a contradictory observation when considering the classic interpretations on the origin of I-type magmas.

2.2 The post-collisional magmatism

Caledonian-type magmas, or post-collisional magmas, comprise large silicic igneous bodies emplaced substantially later than the aftermath of the orogenic edifice building and its subsequent collapse. This type of magmatism was initially described in the Caledonian orogen in Scotland, where a vast number of granitic intrusions served as a testing ground for the many theories of granite petrogenesis (Hamilton et al., 1980; Read, 1961). In the Scottish Highlands, the contrasting nature between the older and less voluminous S-type magmatism, indicative of enhanced anatexis, and the newer granitic intrusions, exhibiting a broader compositional range spanning from gabbro-diorite-granodiorite-granite, drew significant attention to this type of magmatism. Their most notable features were their apparent similarities with arc magmatism, including the calc-alkaline affinity, the presumed involvement of the continental crust, and their occurrence during a subduction process. However, the exact role of subduction in post-collisional magma generation and the interaction between mantle-derived magmas and the compositional effect of traversing the crust during ascent was quickly put into question (Harmon et al., 1984; Plant, 1983). Although sharing some clear characteristics with arc magmatism, the particularities of the newer granites from Scotland and the intrigues surrounding their relationship with the subduction process (Stephens and Halliday, 1984) caused them to be considered a new I-type association in future works (Pitcher, 1987). Further works on the British Highlands stressed the relevance of mantle-derived magmas in the genesis of the recently established Caledonian-type magmas (Fowler, 1988), pointing to a multicomponent source region and bringing important cues to the crustal evolution discussion (Fowler, 1992; Fowler and Henney, 1996; Tarney and Jones, 1994).

Since the early works in the Caledonian orogen, Caldonian-type magmatism has been identified in recent decades in a multitude of places around the world, notably in all the most studied Phanerozoic collisional orogens. Extensive petrological work on post-collisional magmatism has been carried in the European Variscan belt, either in Iberia

(e.g. Fernández-Suárez et al., 2000; Orejana et al., 2009), the French Massif Central (Couzinié et al., 2016; Moyen et al., 2017) and Bohemian Massif (Janoušek et al., 2000; Laurent et al., 2014; Słaby and Martin, 2008); in the European Alpine orogen (Frisch et al., 2000), in the Central Asian Orogenic Belt (Chung et al., 2005); in the Zagros orogen and its surroundings (Aghazadeh et al., 2011; Castro et al., 2013a; Moghadam et al., 2023; Pang et al., 2013); in the Grenville orogen (Goswami and Bhattacharyya, 2014); in the Anatolian province (Gencalioglu Kuscu and Geneli, 2010); or in the different Pan-African orogen terrains (de Lima et al., 2021; Ferré et al., 1998), among others.

Further constrains to post-collisional magmatism were given by numerical works on continental collision, effectively identifying the most influential parameters affecting the collision style and its consequences (e.g. Burg and Gerya, 2005; Faccenda et al., 2008; Pfiffner et al., 2000; Pysklywec, 2001). Existing models predict the critical influence of convergence rate leading to different collision styles, with asymmetrical collision developing extensional regimes and mantle upwelling (Faccenda et al., 2008; Ghazian and Buiter, 2013) that are optimal for magmatism. The thermal age of the oceanic crust has a direct effect on the thermal structure of the orogen, with younger and hotter oceans driving increased orogenic temperatures and enhancing melting processes (Dymkova et al., 2016). The amount of subducted continental crust depends on the rheological coupling of the lithosphere, with the most coupled rheologies leading to lower crust sinking into the asthenosphere (Faccenda et al., 2009).

The combined efforts within the fields of petrology and numerical modelling allowed for a general vision on the nature of post-collisional magmas. Post-collisional magmas occur as large silicic magmatism in a relatively narrow timespan after continental collision, and mostly comprise two distinctive suites: (1) the silicic suite, composed of voluminous felsic intrusions mostly represented by granodiorites, that are metaluminous (ASI<1) to slightly peraluminous (ASI≥1.0) [ASI (Alumina Saturation Index) = molar $Al_2O_3/Na_2O+K_2O+(CaO-3.3\times P_2O_5)$]; and (2) the mafic-intermediate suite, embodied by smaller intrusions of metaluminous high-K calc-alkaline geochemistry that ranges from mafic to intermediate. The overall geochemistry resembles that of Andean-type magmatism by sharing roughly similar major oxides concentrations (SiO_2, 63–70 wt.%; FeO^T, 2–5 wt.%; MgO, 1–3 wt.%; CaO, 3–5 wt.%; Na_2O, 2–4 wt.%; and K_2O, 2–4 wt.%;

Castro, 2020, see section 2.3 for Andean-type magmas), with the main difference being that Caledonian-type magmas usually display enriched geochemistry, particularly in K_2O, large ion litophile elements (LILE) and light rare earth elements (LREE). Caledonian-type magmas show enriched isotopic signatures, with features that resemble a crustal source with a significant contribution from a juvenile source. Moreover, post-collisional magmas occur as a consequence of the complex dynamics involved during continental collision, commonly resulting in extensional forces in the upper plate driven by mantle upwelling (see references above) and/or slab break-off (Hildebrand and Bowring, 1999; Whalen and Hildebrand, 2019), and altered thermal regimes that may cause the production of melt from a variety of different potential sources (e.g. Dymkova et al., 2016).

Along with this extensive work, a prevalent perspective on the origin of post-collisional magmas cemented within the Earth Sciences community. A dichotomous interpretation on the petrogenesis of post-collisional magmatism was based in the distinction of the mantle-sourced mafic-intermediate suite, and the crustal-sourced silicic suite caused by decompression during post-collisional extension and heat transfer by the mafic magmas into the lower crust (Bonin, 2004; Couzinié et al., 2016; Moyen et al., 2017; Murphy, 2020). According to this petrogenetic model, the silicic suite results from lower crust melting after decompression during post-collisional extension and heat transfer by the underplated mafic magmas (Annen et al., 2006; Liégeois et al., 1998, 1996; Ma et al., 1998; Pitcher, 1987). However, a number of problems arise when considering these existing hypotheses:

1) The lower crust is mafic on average (Rudnick and Fountain, 1995). A hypothetical basalt precursor in the lower crust for the batholiths entails the need for the elimination of an ultramafic residue from the lower crust in order to produce the observed bulk composition. This ultramafic residue is unaccounted for and lacks natural evidence.
2) The lower crust is essentially depleted. Simple melting of the lower crust cannot reproduce the enriched signature of post-collisional batholiths. An additional element in the process needs to be involved.
3) Given the refractory nature of the lower crust, it showcases unrealistically high solidus temperatures (>850–1000 ^{o}C) that are incapable of producing significant

amounts of liquids. Only scarce, arguably marginal petrogenetic evidence support ultra-high temperatures in the lower crust (Clark et al., 2011; Laurent et al., 2023); and numerical models on collisional orogens predict thermal perturbations at the Moho that barely exceed >700 ^{o}C (see references above).

4) Mafic magma underplating is an inefficient process at heating the lower crust even when periodic influx is invoked (Bonin, 2004), requiring large volumes of mafic magma to intrude in sills (Annen et al., 2006). Such sill swarms have not been observed in any exposed lower crust section around the world.
5) Water is commonly argued to lower solidus temperatures (Aranovich et al., 2014; Castro, 2020; Collins et al., 2021, 2020, 2016; Weinberg and Hasalová, 2015), but even with the most conservative estimations of 4 wt.% H_2O dissolved in the parental magma (Plank et al., 2013) the water content in a residual granitic liquid that represents a 0.2 melt fraction will have ~20 wt.% H_2O. This water amount in residual liquid is unrealistic and is supported neither by the observed igneous textures in the rocks nor by the scarcity of pegmatitic dykes or amphibole-rich cumulates in the plutons. Not only that, but also post-collisional silicic magmas rarely present LOI values above ~1 wt.%.
6) Fully recycled lower crust inherently implies a fully recycled isotopic signature. Nevertheless, post-collisional magmatism is characterised by recycled isotopic signatures yet with an important juvenile component that cannot be accounted for by crustal melting.
7) Modelling collision results in a wide range of potential magmatic sources, among which the mantle is almost always involved. Nonetheless, the upper plate lower crust remains relatively cold during the process, and rarely becomes a magmatic source.
8) The alternative presented by numerical models are not satisfactory either, given that vast windows of molten asthenosphere are not supported by the existence of surface flood basalts or picrites, and the duration of magmatism does not match the comparatively narrower time span of post-collisional magmatism.
9) Variability of isotopic values does not correlate to any changes in the geochemical trends of the magmas, implying that crustal assimilation was limited and that the isotopic variability was configured in the source.

Addressing these challenges has proven to be a difficult task. In the grand scheme of this riddle, available techniques have been unsuccessful at solving the limitations of the classical model. Prior to any attempt at solving this problem, further contextualization must be made regarding the three ubiquitous and constituent features of post-collisional magmas. These are the silicic suite, comprising the large silicic bodies that represent the largest volumetric fraction of the batholiths, to which this section was dedicated; the mafic-intermediate suite, representing relatively smaller intrusions of dioritic to quartz-dioritic nature; and the mafic microgranular enclaves, appearing as hand-size to sometimes meter-sized globules surrounded by the granites.

2.2.1 The mafic-intermediate/sanukitoid suite

Mafic-intermediate suite is a general term to refer mafic to intermediate intrusions that occur associated with the larger felsic intrusions. Although volumetrically much smaller than the granites in mid to upper crustal sections, tilted sections of arc continental crust reveal that mafic rocks become dominant with increasing depth (Garrido et al., 2006; Martin et al., 2009; Otamendi et al., 2009). It should also be noted that magmas of the same composition have received a whole range of different names, such as vaugnerites (e.g. Bea et al., 2021; Galán et al., 1997; von Raumer et al., 2014), durbachites (e.g. Parat et al., 2010; von Raumer et al., 2014), appinites (e.g. Castro et al., 2003; Molina et al., 2012; Murphy, 2013) or sanukitoids (e.g. Fowler and Rollinson, 2012). The latest term, sanukitoid, is of special relevance, given their relatively recent inclusion in the post-collisional magmatism discussion. That is, rocks known by the name “sanukitoid” are the best characterised among all the previous nomenclatures, and although currently used as a synonym to refer to the mafic-intermediate suite of post-collisional batholiths they were once linked to an Archean series. Thus, exploring the geochemical features and origin of sanukitoid rocks is particularly relevant in the post-collisional magmatism discussion.

Sanukitoid intrusions were first described in the Roaring River Complex, Superior Province (Shirey and Hanson, 1984), as a particular type of Archean intrusions linked to Tonalite-Trondhjemite-Granodiorite (TTG) magmatism. These intrusions closely resembled the high magnesium andesites of the Steouchi Volcanic Belt, known as

"sanukites" (Tatsumi and Ishizaka, 1982). Sanukitoid rocks were eventually recognized as an important component in most Archean terrains (Martin et al., 2009, 2005). The Archean link of sanukitoid magmatism was progressively put to the test, with further works stressing the similarities between Archean sanukitoids and Phanerozoic, post-collisional mafic-intermediate magmas (Castro et al., 2013a; Fowler and Rollinson, 2012; López-Moro and López-Plaza, 2004; Moyen et al., 2017).

Since then, the term sanukitoid has been accepted as equivalent to post-collisional mafic-intermediate magma, and has been successfully identified in virtually every collisional belt and Archean craton around the world. This includes the Superior Province in Canada (Shirey and Hanson, 1984; Stern and Hanson, 1991; Stevenson et al., 1999; Sutcliffe et al., 1990); the Pilbara and Yilgarn cratons in Australia (Smithies and Champion, 2000); the Zimbabwe craton in South Africa (Kampunzu et al., 2003); the Dharwar and Budelkhand cratons in India (Jayananda et al., 2018; Singh et al., 2019); the North China craton (Jiang et al., 2016; Yu et al., 2021); the Río María Suite in Brazil (de Oliveira et al., 2010, 2009; dos Santos and Oliveira, 2016); the Karelia and Kola provinces in the Baltic Shield (Halla, 2005; Heilimo et al., 2010; Käpyaho et al., 2006; Kudryashov et al., 2013; Lobach-Zhuchenko et al., 2005); the Sarmatian craton in the Baltic Shield (Terentiev and Santosh, 2018); the Svecofennian Orogen in the Baltic Shield (Andersson et al., 2006; Eklund et al., 1998); the Wester Junggar in Northern Tibet (Duan et al., 2019; Yin et al., 2015); the British Caledonian Province (Fowler et al., 2008; Fowler and Henney, 1996; Fowler and Rollinson, 2012); the Iberian Massif (Castro et al., 2003; López-Moro and López-Plaza, 2004; Molina et al., 2012), the French Massif Central (Couzinié et al., 2016; Moyen et al., 2017) and the Bohemian Massif in Europe (Bowes and Košler, 1993; Holub, 1997; Janoušek et al., 2000); the Dabie and Sulu orogens (e.g. Tang et al., 2009; Wang et al., 2005; Xu et al., 2012; Zhang et al., 2012); the Setouchi Volcanic Belt (Kawabata and Shuto, 2005; Tatsumi and Ishizaka, 1982); the Alborz magmatic belt (Castro et al., 2013a; Nabatian et al., 2016); and the Tibetan Plateau (e.g. Guo et al., 2013, 2006; Huang et al., 2015; Liu et al., 2015). The almost ubiquitous association between sanukitoid and silicic post-collisional magmatism points to the critical role of sanukitoids in post-collisional magma generation.

Sanukitoid rocks (i.e. mafic-intermediate post-collisional magmas) are characterised by a clear mantle signature with an enrichment in compatible elements, such as Mg, Cr, Ni and #Mg; combined with large ion litophile elements (LILE), particularly Ba, Sr (as in the high Ba–Sr granites in the Caledonian Province – Fowler and Rollinson, 2012), K, and light rare earth elements (Heilimo et al., 2013, 2010; Lobach-Zhuchenko et al., 2008; Stern et al., 1989). They plot in the alkaline field of the TAS (total alkalis versus silica) diagram (Miyashiro, 1974) and in the shoshonitic and high-K domains of the K_2O-silica classification diagram (Peccerillo and Taylor, 1976). While initially restricted to an exclusively mafic to intermediate series with a strict definition of SiO_2=55–60 wt.%, MgO>6 wt.%, Mg#>60, Sr>600–1800 ppm, Ba>600–1800 ppm, Cr>100 ppm and Ni>100 ppm (Stern et al., 1989), sanukitoid magmas are currently considered to represent a broader series that comprise diorites, tonalites, granodiorites, monzonites, and even gabbros that are magnesian, mostly metaluminous and water-bearing (Halla, 2005; Heilimo et al., 2010; Lobach-Zhuchenko et al., 2005).

Regarding the origin of sanukitoid magmas, there is a wide agreement that they are mantle sourced (see references above). However, given their enriched nature and intermediate composition, a purely peridotitic source is unable to reproduce their composition. For this reason, a metasomatized mantle is most commonly invoked as the source for sanukitoid magmatism. Given the need for an external component to enrich the continental lithospheric mantle, mantle metasomatism is attributed to the recycling of continental crust into the mantle via subduction (Heilimo et al., 2013).

As for the nature of such metasomatized mantle, no consensus has been reached yet. A majorly peridotitic source yields unrealistic degrees of melting without the presence of additional phases such as amphibole or phlogopite (Bailey, 1982). In this regard, experimental studies provided important constrains on the stability of amphibole and phlogopite in upper mantle conditions and their relationship with ultrapotassic magmas (Conceição and Green, 2004), and constrained pressures between ~1 GPa and 0.3 GPa to be the most influential in phase equilibria (de Oliveira et al., 2010). Moreover, further petrological studies on mantle xenoliths from kimberlite pipes support the presence of phlogopite in the upper mantle (Giuliani et al., 2016; Kargin et al., 2019). Contrary to this, high-Mg signatures were successfully reproduced via experiments using a

harzburgitic source (Wood and Turner, 2009), proving conflicting evidence with the mantle metasomatism evidence.

Within the context of of post-collisional magmatism, sanukitoid rocks have received special attention in recent years. This interest stems from the observation that they carry the geochemical budget absent in the lower crust, otherwise necessary to reproduce the enriched signature of the granite batholiths. Additionally, their water-bearing nature renders them ideal candidates to lower the solidus of the lower crust (Castro, 2020; Collins et al., 2020; Smithies et al., 2021). Hence, although their relationship with granitic magmas remains unclear, sanukitoid magmas can contribute in the petrogenesis of Caledonian-type magmas in four potential and complementary ways: (1) they are parental to the granites by differentiation; (2) they supply water for water-fluxed melting of the lower crust; (3) they constitute the mafic endmembers in a magma/hybridization process; (4) they advect heat from the lithospheric mantle to the lower crust to produce extensive melting (Castro, 2020).

Whatever the case, the recurring presence of sanukitoid rocks in collisional orogens represents a critical cue that the lithospheric mantle plays an important role in post-collisional magma generation. Existing work on the sanukitoid series has apparently identified all its major geochemical features, but are yet to provide a satisfactory explanation on their geochemical trends, the effect of intensive parameters on phase equilibria, the exact nature of the source of this magmatism and, ultimately, its relationship with the Caledonian-type granites.

2.2.2 The mafic microgranular enclaves

Mafic microgranular enclaves are a ubiquitous feature of both I-type and S-type magmas, consisting of fine-grained, usually dark globules surrounded by the host felsic rocks. These features make them distinct from other types of enclaves (xenoliths) commonly included in igneous rocks, such as migmatite resisters or metamorphic rocks. Microgranular enclaves were first described in association with different types of volcanic rocks, in which they were considered magmatic enclaves that held intimate relationship with the genesis of intermediate lavas (Lacroix, 1893), soon to be identified in granitic rocks from the Pyrenees as well (Lacroix, 1898). No further advances were

made on the topic until several decades later, when a monography on granites and enclaves reviewed the role of mafic enclaves in the post-collisional magmatism from the French Massif Central (Didier, 1973, 1964). Subsequent works successfully identified microgranular enclaves in S-type granitoids, as well as in both Andean-type and Caledonian-type batholiths, highlighting them as one of the main features of I-type magmatism (e.g. Barbarin, 1991; Barbarin and Didier, 1992; Vernon, 1984).

Since then, extensive effort has been expended into thoroughly characterising microgranular enclaves and their petrogenetical meaning (Bacon, 1986; Barbarin, 2005; Barbarin and Didier, 1992; Cantagrel et al., 1984; Coombs et al., 2003; Didier, 1973; Paterson et al., 2004; Vernon, 1984; Wiebe, 2016; Yongfeng, 1994; Zhang et al., 2015). Microgranular enclaves occur in different forms, usually shaped as globular bodies, but also occasionally angular, suggesting the involvement of brittle mechanics in their genesis (Rodríguez and Castro, 2019). They range in size from a few centimetres to several meters, and appear either relatively isolated and scattered throughout the host granite (Paterson et al., 2016); or clustered in confined concentrations or swarms in restricted areas, separated by minimal host material in which they may reach above 60% in volume (Barbarin, 2005; Paterson et al., 2016; Wiebe and Adams, 1997). Similarly, enclave swarms can present different morphologies, spanning from small lenses to tabular bodies or dykes (Tobisch et al., 1997), determined by the variability in the viscous behaviour and velocity of the host magma during ascent (Rodríguez and Castro, 2019).

Microgranular enclaves are usually more melanocratic than the surrounding granite (*s.l.*), owing to their comparatively more basic nature, usually dioritic to tonalitic. There is wide agreement that they represent the mantle component during magma generation (see references above), yet with a significant crustal contribution as suggested by isotopic evidence (Clemens et al., 2017). Their dark appearance has caused them to be commonly referred to as mafic microgranular enclaves, although their composition is not homogeneous, and ranges from the less abundant mafic terms to the more common intermediate enclaves. This compositional variability is consequently displayed in the mineral assemblage in post-collisional settings, with the most mafic enclaves containing larger amounts of biotite and amphibole, and increasing contents of quartz and plagioclase with increasing silica (Rodríguez and Castro, 2019). Similar to sanukitoid post-

collisional rocks, amphibole is often present as polycrystalline mafic aggregates in microgranular enclaves, interpreted to result from pyroxene-melt re-equilibration either through grain-boundary diffusion or direct contact (Castro and Stephens, 1992).

Moreover, the compositional range causes an equally variable compositional contrast with their host rocks, from instances with no contrast, in which case they are identified as autoliths (Rodríguez and Castro, 2019, and references therein), to varying degrees of mineralogical and geochemical contrast. Interestingly enough, this compositional contrast does not translate into chemical interactions between enclaves and host rocks, given the limited evidence from reaction rims in the enclaves (e.g. Castro and Stephens, 1992; Clemens et al., 2017, and references therein).

Many models have been proposed to explain the origin of microgranular enclaves. Among the initial works, the most relevant ones either consider the enclaves a result from restite unmixing and accounting for the variability within series of granitic rocks (Chappell, 1996; Chappell and Wyborn, 2012; Chen et al., 1989; White et al., 1999; White and Chappell, 1977); considering them the result of disrupted dykes during the ascent of new pulses of magma (Didier, 1991); the consideration that they are the result of basalt injection into the crust and magma mixing (Didier and Lameyre, 1969; Huppert and Sparks, 1988; Wiebe, 1991); and considering them autoliths from a closed differentiation system (Dodge and Kistler, 1990; Fershtater and Borodina, 1977; Pabst, 1928). Following works on the topic allowed for some consensus to be reached, considering that the enclaves are igneous in origin (see Clemens et al., 2017, for review). Pervasive quenching textures in microgranular enclaves favour this consideration, likely resulting from rapid cooling in ascent conduits during the first magma pulses in which the continental crust is hot (Donaire et al., 2005). Latest works on this topic favour the autolith model, considering the enclaves to represent chilled margins from the ascent conduits dragged by posterior high-energy pulses (e.g. Rodríguez and Castro, 2019; Xu et al., 2020).

Whereas the discussion on the origin of mafic microgranular enclaves has provided plausible descriptions of their formation mechanisms, it has yet to give a satisfactory explanation for their relationship with their host rocks. The consistent appearance of mafic microgranular enclaves in contrasting magmatic settings (I-type and S-type

magmas, both batholiths and volcanism) suggest that they are likely to result from an intrinsic process during magma generation. Moreover, given that enclaves of autolithic nature represent quenched pulses of parental magma, they can constitute valuable tracers of the petrogenetic process of post-collisional magmas.

2.3 The cordilleran magmatism

Cordilleran magmas, also known as Andinotype, Andean-type or arc magmas, represent a calc-alkaline, silicic type of magmatism that occurs linked to the oceanic stage of a subduction process. The 1960s and 1970s were pivotal for the development of the paradigm of plate tectonics, providing a sound framework to study and explain arc magmatism. Researches quickly focused on magmas linked to subduction zones, and began to contextualize conceptual petrological work on their respective tectonic setting (Allen and Boettcher, 1978; Cawthorn and O'Hara, 1976). In the following decades, much effort was dedicated to describe the origin of subduction magmas from the Pacific ring of fire (e.g. Hervé et al., 1988; Tatsumi and Ishizaka, 1981). Soon enough destructive plate margins were considered a severely influential factor in crustal evolution, representing the most significant cause of crustal and lithosphere destruction. Contrary to this, Andean-type magmas were considered the most important mechanism contributing to crustal growth.

The prevalence of destructive margins along the Pacific in recent geologic times has enhanced cordilleran magma production, which, as of yet, has not encountered the challenges associated with long-term crustal preservation. These considerations brought interest into Andean settings, causing Andean-type magmatism to be comparatively more studied than post-collisional magmas in current times. Due to their abundance, cordilleran rocks have received great attention and have been successfully identified in several places in the world, among which the largest examples can be found around Pacific ring of fire. The most notable include the Patagonian batholith (Herve et al., 2007; Pankhurst et al., 1999); the coast range batholith of Chile (Hervé et al., 1988; Parada et al., 1999); the coastal batholith of Peru (Atherton, 1990; Cobbing and Pitcher, 1972) and all the Andes volcanism as a whole; the Cordillera Central batholith of Colombia (Duque-Trujillo et al., 2019; Villagómez et al., 2011); Peninsular Ranges (Lee et al., 2007; Silver

and Chappell, 1988); the Cascades arc (Mullen et al., 2017; Walowski et al., 2016); Sierra Nevada (Bateman, 1992; Lackey et al., 2008) and the Guadalupe Igneous Complex (Best, 1963; Putirka et al., 2014); the Idaho Batholith (Gaschnig et al., 2011; Hyndman, 1983); the Coastal batholith through Canada to Alaska (Andronicos et al., 2003; Barker et al., 1986); and the Setouchi Volcanic belt (Tatsumi and Ishizaka, 1982, 1981), among others.

Cordilleran magmatism is characterised by silicic rocks, namely tonalites and granodiorites, comprising above 90% of the volume, and subordinate gabbroic and granitic (*sensu stricto*) intrusions. Monzonitic suites also appear scattered through large Andean-type batholiths, considered as the deepest melts from the subduction process (Pitcher, 1997; Rapela and Pankhurst, 1996). Similar to Caledonian-type magmas, these intrusions display relatively narrow major element ranges (SiO_2, 63–70 wt.%; FeO^T, 2–5 wt.%; MgO, 1–3 wt.%; CaO, 3–5 wt.%; Na_2O, 2–4 wt.%; and K_2O, 2–4 wt.%). Compared to the volcanic rocks, intrusive magmatism tends to show higher silica maxima, likely representing residual liquids crystallized in the magma chambers (Castro, 2020). Occasionally, high-Mg andesites can be found in the intrusions (Kelemen, 1995; Tatsumi and Ishizaka, 1982), showcasing similar Mg enrichment to that of the sanukitoid suite from post-collisional magmatism. Andean-type magmatism is widely known to display a typical trace element signature, with the first works on discrimination of tectonic setting of granitic rocks featuring criteria for arc volcanic rocks (Pearce et al., 1984; Pearce and Cann, 1973). These compositional features are well-established, remaining a reliable source of information as of today.

Many cordilleran magmatic batholiths feature a compositional gap in the intermediate terms, in which only the most mafic and differentiated compositions are represented. This geochemical feature is commonly known as the Bunsen-Daly gap (Bunsen, 1851; Daly, 1925), referring to two compositional groups (low silica and high silica) separated by a silica interval (55–60 wt.% SiO_2) with scarce representation in nature. Compositional gaps in igneous rocks have been widely discussed, leading to a reasonably accepted hypothesis. That is, compositional gaps are the results of large-scale differentiation processes in the magma chambers (Brophy, 1991; Reubi and Blundy, 2009). According to petrological experiments using basaltic starting material, the bimodal distribution is due to the shape of the magma crystallinity curve, sharply increasing at critical

temperatures (Melekhova et al., 2013). This steepness renders the intermediate compositions unlikely, causing the predominant representation of differentiates and differentiation cumulates. Interestingly, compositional gaps have not been described in Caledonian-type magmas, an observation that to this day remains unexplained (see references in section 2.2).

Extensive work has been carried out on the origin of cordilleran magmas. The classic hypotheses build upon the production of basaltic magmas in the peridotitic mantle (Hildreth, 1981). Considering that the average composition of continents is andesitic and so is the average arc magma, following process must account for the genesis of andesites. Consequently, this basaltic precursor has been hypothesized to generate andesites by a number of different processes. Cumulative underplating of basaltic magma into the lower crust is considered an effective advective process, progressively heating the lower crust. If sufficient temperature is reached, crustal-sourced felsic magmas of dacitic compositions can be generated (Huppert and Sparks, 1988). Solidification of basalt underplates is also proposed to exsolve water into the underlying crust, enhancing melting by water-flux (Collins et al., 2021, 2016). This scenario results in felsic crustal magmas, which can potentially hybridize with the underplated basalts to finally reproduce the andesites (Eichelberger, 1975; Pankhurst et al., 1988; Streck et al., 2007). This latest consideration is mainly constructed using isotopic and melt inclusion evidence, highlighting the high crustal affinity of intermediate magmas. Alternatively, a basaltic precursor has been proposed to reproduce the orogenic andesites through sheer differentiation, following a compositional evolution described by liquid line of descent according to petrological experiments (Lee et al., 2006; Lee and Bachmann, 2014; Ulmer et al., 2018).

However, the basaltic precursor suffers from similar drawbacks as the classic interpretation for the origin of post-collisional magmas. Large volumes of underplated basalt are needed to effectively rise the temperature of the lower crust above the solidus. Such volume of basalts is unaccounted for, with the average composition of the lower crust as predicted by xenoliths being residual (Rudnick and Fountain, 1995) and not matching a primary magma from a peridotitic source. Not to mention that the processes involving crustal melting that result in andesites are conspicuously complex,

invoking either the contrived concatenation of several independent processes or multi-stage differentiation (Hawkesworth and Kemp, 2006). Comparatively, differentiation of a basaltic precursor seems like a much more reasonable approach and is supported by thermodynamic constrains. Nevertheless, basalt differentiation inherently produces ultra-mafic cumulates that have not been observed in any exhumed lower crust terrain. Moreover, experimental liquids using a basaltic precursor do not accurately reproduce the compositional evolutionary trend of the real magmas (Castro, 2021, 2020).

Although the basalt input model is still favoured in plenty of works, an alternative has gained wide support and recognition in recent years. This model considers arc magmas to be sourced in silicic diapirs hosted in the mantle (Marschall and Schumacher, 2012), consequence of relaminated subducted materials represented by positively buoyant metasedimentary or metaigneous rocks (Hacker et al., 2011). Magmatism produced in these silicic diapirs is also silicic, potentially representing a direct mechanism for continental growth (Kelemen, 1995; Tatsumi and Ishizaka, 1981; Taylor, 1967). These considerations are supported by numerical models, in which relamination has proven a plausible mechanism to account for arc magmatism (Castro et al., 2013b; Maierová et al., 2018). Particularly, melange plumes are the most relevant when considering the oceanic stage of subduction (Maierová et al., 2018). Complementarily, petrological experiments simulating the hybrid melting of subducted melange and peridotite have been successful at reproducing the composition of arc magmatism (Codillo et al., 2018). Most notably, they have provided a sound justification for the well-known experimental alternative to the basaltic precursor. That is, an intermediate precursor has been widely studied as a potential parental composition for Andean-type magmas via petrological experiments (Alonso-Perez et al., 2009; Carroll and Wyllie, 1990; Castro, 2021; Grove et al., 1997; Patiño Douce, 2005, 1995; Qian and Hermann, 2013; Rapp and Watson, 1995; Sisson et al., 2005; Sisson and Grove, 1993).

However, even if petrological and numerical evidence seem to point in a clear direction, a natural example matching the intermediate parental models is yet to be found. Large-scale fractionation in cordilleran settings preclude the identification of pristine compositions, as suggested by the compositional gaps. Most interestingly, the experimental parental composition that accurately reproduces the Andean-type

magmas falls within the compositional gap typical of cordilleran magmas. Thus, identifying natural examples matching the model composition can be considered the next milestone in cordilleran magma petrogenesis. This task can be achieved by studying magma mingling zones, in which quenching is a widespread phenomenon, precluding differentiation.

3. Objectives

The evolution of the continental crust is a consequence of lithosphere dynamics and shall be described as an igneous process. The origin of the most voluminous type of magmatism, namely I-type magmas, represents the most immediate tracer for crustal evolution. However, the origins of I-type magmatism, the main source of new material for continental growth, remain a fundamental mystery in Earth Sciences. Existing models entail important drawbacks that remain unaddressed. Not only that, but also the attempts to solve their apparent flaws are usually built upon theoretical constructs that lack natural support.

This project aims at challenging the classic interpretations on the origin of I-type magmatism and its significance in the evolution of the crust and the lithosphere through geologic time. In a problem of such dimensions, a heuristic approach was selected as the main method for problem-solving, setting relatively close milestones to propel the research forward. Accordingly, big scope goals were deconstructed into smaller and achievable objectives. Natural evidence and common sense were the main drivers when formulating the work hypotheses. Method selection was deliberate to individual objectives, with a cautious awareness of the inherent limitations of each technique and emphasizing their complementary nature to strategically enrich each other. Each objective demanded the assessment of the state of the art relevant to the specific problem, ensuring different starting points for each challenge.

The resulting plan follows a hierarchical framework, in which priority objectives whose outcomes were potentially impactful for other interconnected objectives needed to be tackled first. Flexibility was a direct consequence of using this approach, given the need to adjust the plan to the obtained results.

The resulting plan can be found below, designed considering all the above described factors. Each objective encompasses a summary of the state of the art of each challenge, together with the logic behind its conception and the selected study method.

1) Determination of the origin of post-collisional magmatism. Assessing the limitations of the classic model based on a lower crustal source for post-collisional magmatism

is a top priority for discussing its role in crustal evolution. Although considered a minor contribution to crustal growth, important contradictions are found within this hypothesis. This objective can be broken down into the following more specific tasks:

a) Determination of the origin of the mafic-intermediate suite (i.e. sanukitoid series) and evaluating its role in post-collisional magmatism. Sanukitoid magmas are considered an exclusively mafic to intermediate series that represent the involvement of a modified lithospheric mantle in the orogenic process that underplates the lower crust, but their evolution during differentiation is not constrained. The crystallization sequence and potential cotectic behaviour of sanukitoid magmas driving sanukitoid granites can be studied through a meta-analysis of sanukitoid rocks and petrological experiments.

b) Determination of the origin of the silicic suite. Post-collisional silicic magmatism is considered to be crustal sourced after mafic mantle magma underplating, a model that entails several important drawbacks. The feasibility of the lower crust as a magmatic source and the parental magmas for post-collisional silicic magmas can also be tested through meta-analysis of post-collisional rocks and petrological experiments.

c) Determination of the origin of the mafic microgranular enclaves and evaluation of their relationship with the host silicic magmas. Inference highlights the potential value of enclaves as globules of quenched magma from the ascent conduits, thus potentially providing important insights into the petrogenetic process. An evaluation of their relationship with the host granites and their role in their petrogenesis can be carried out by field work and geochemical work (whole-rock major and trace elements and isotopes).

d) Determination of the thermal and water budget of the lower crust during collision. Lower crust melting models rely on both ultra-high temperatures and water contents, yet such explanations are not supported by natural observation, with natural plutonic rocks being relatively dry and yielding limited equilibrium temperatures. Numerical models are particularly instrumental in testing the evolution of intensive parameters in a geodynamical context.

2) Determination of the parental magmas to cordilleran magmatism. Strong inference provided by extensive petrological experiments and numerical models suggest that

the precursor to Andean-type magmatism is an intermediate magma sourced in a silicic diapir within the mantle lithosphere, but natural examples matching the model compositions are yet to be found. Exploring an Andean-type magma mingling zone by field and geochemical work can be particularly useful for this task.

3) Evaluation of the role of I-type magmatism in crustal evolution. The dynamic evolution of the lithosphere is the result of the superposition of crustal growth over crustal destruction events, each controlled by a vast number of natural processes. The ultimate goal of this PhD is to provide a conciliatory view between petrological and numerical evidence to the problem of crustal evolution.

4. Methodology

4.1 High-pressure high-temperature experiments

The characterisation of the phase relations and thermodynamic controls behind I-type magmatism was performed through high-pressure high-temperature experiments. Experimental runs were performed in a Boyd and England-type piston cylinder apparatus (Boyd and England, 1960), available at the Instituto Andaluz de Ciencias de la Tierra (Granada) and Museo Nacional de Ciencias Naturales (Madrid), both from the Consejo Superior de Investigaciones Científicas. The technique consists in simulating crustal and lithospheric conditions through submitting a small quantity of sample to controlled pressure and temperature.

Pressurization is achieved through hydraulic load inside a pressure vessel with a tungsten carbide (WC) core. The apparatus operates by applying mechanical force from two hydraulic ram pumps (Fig. 4.1). The upper ram applies a load pressure to the system, keeping all constituent parts of the apparatus assembled. The lower ram is then used to transmit force to a piston, which, in turn, compresses the experimental assembly loaded inside the pressure vessel through a pressure-transmitting medium (Fig. 4.1). Pressure is then monitored with two pressure sensors attached to the pressure circuit, one for the load ram and one for the piston ram.

The sample is heated by applying a regulated voltage to the experimental assembly. Temperature is monitored using a Pt_{100}-$Pt_{87}Rh_{13}$ type C thermocouple. This thermocouple is positioned near the experimental capsule using a sillimanite guide (Fig. 4.2). The other end of the thermocouple is wired to Eurotherm 808 controllers for temperature control and regulation. Potential overheating is controlled using a refrigeration system, with purified water pumped through the apparatus by an industrial chiller (Fig. 4.1). The implementation of the refrigeration system was different between the apparatus from the Instituto Andaluz de Ciencias de la Tierra and the Museo Nacional de Ciencias Naturales. In the former, water circulates above and below the pressure vessel through the refrigeration plate and the bridge (Fig. 4.1), while in the latter, water circulates inside the pressure vessel.

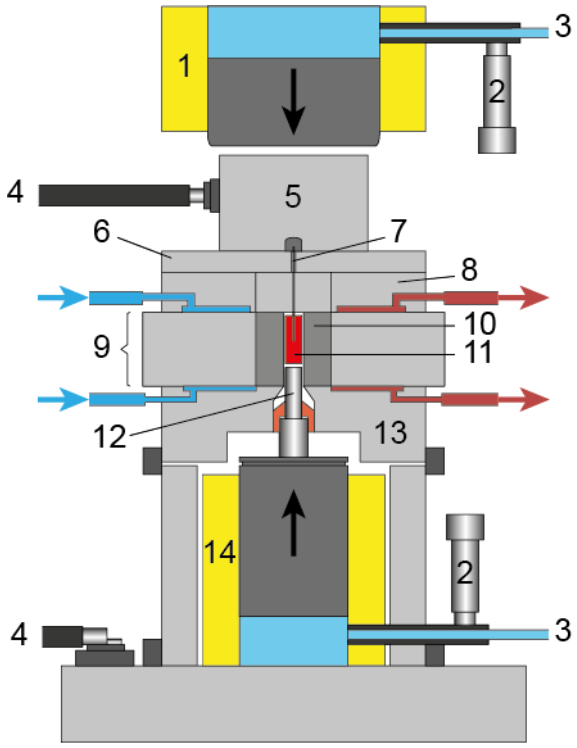

Figure 4.1: Schematic cartoon of the Boyd-England type piston cylinder apparatus. This configuration corresponds to that found in the Instituto Andaluz de Ciencias de la Tierra. 1: load hydraulic ram; 2: pressure sensor; 3: hydraulic oil; 4: energy connector; 5: energy connection plate; 6: load plate; 7: thermocouple; 8: refrigeration plate; 9: pressure vessel; 10: WC core; 11: experimental load; 12: piston; 13: bridge; 14: piston hydraulic ram.

Refrigeration induces a small uncertainty in the measured temperature, caused by the margins of the experimental assembly being slightly colder than the interior. This phenomenon has been widely studied (Pickering et al., 1998; Schilling and Wunder, 2004; Schmidt and Ulmer, 2004; Watson et al., 2002), resulting in a reasonable characterisation of the temperature confidence area around the thermocouple (Fig. 4.2). The presumed effect of the two refrigeration setups is different; water circulating below and atop of the pressure vessel exerts a vertical cooling effect over the experimental assembly, while water circulating inside the pressure vessel produces a horizontal cooling effect of the experimental assembly. This last case is expected to increase the vertical temperature confidence area, preventing temperature gradients in the experimental runs. Furthermore, to prevent the effect of vertical thermal gradients, capsules were handcrafted as tiny as possible and used precise placement near the

thermocouple. Additionally, water from refrigeration was kept at a relatively high temperature during the runs.

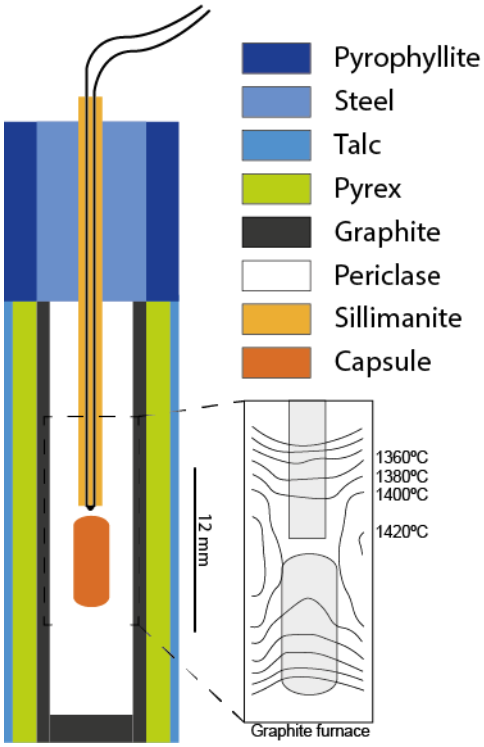

Figure 4.2: Schematic illustration of an experimental assembly. Temperature confidence intervals correspond to the refrigeration configuration depicted in figure 4.1.

The experimental assembly consists of half inch, talc-Pyrex-periclase cells inside which the capsule is loaded (Fig. 4.2). The material of the capsules depends on the goal temperature of the experimental runs. Experiments below 1050 ^{o}C used gold capsules, while in experiments above 1050 ^{o}C a Au–Pd alloy was used. Alloying of Au with Pd effectively rises the melting point of the capsule, with melting point increasing by increasing the Pd proportion in the alloy. However, although this process allows for experimentation at higher temperatures, it creates a rather important problem. That is, Au-Pd capsules subtract Fe from the experimental load, affecting the synthesized phases and their composition. Methods to counteract this effect include sample Fe pre-saturation (Brugier et al., 2015), experimental load isolation using Au inner capsule (Takahashi and Kushiro, 1983), experimentation on ultra-oxidizing conditions to reduce Fe exchange due to its dependency in fO_2 (Kawamoto and Hirose, 1994), or capsule Fe pre-saturation through the use of double capsules to saturate the inner Au-Pd capsule from the outside (e.g. Kägi et al., 2005; Kushiro, 1972). Among these, the double capsule

was the preferred method, given that using an out capsule filled with a Fe-rich sample has proven successful at minimizing Fe-loss and exert further control on the fO_2 of the experimental run. Hence, experiments using 2mm Au–Pd capsules were included in an outer 3mm Au–Pd capsule loaded with a QFM mix (Fig. 4.3), with oxygen fugacity expected to be buffered.

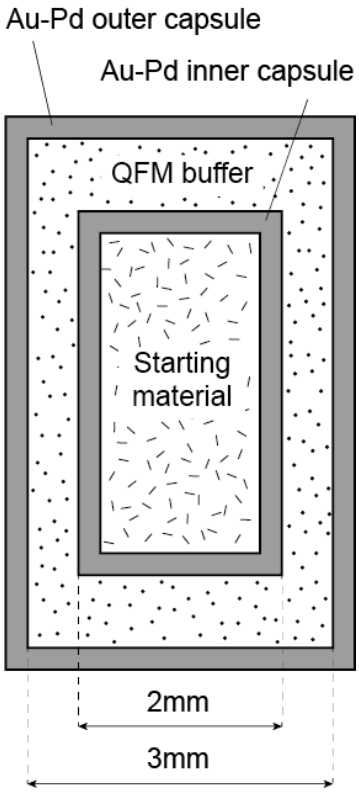

Figure 4.3: Representation of the double capsule technique used for some of the experimental runs. The starting material is loaded into the inner 2 mm capsule and is subsequently loaded into a 3 mm capsule together with QFM buffer mix or additional starting material.

An important consideration in petrological experiments is the attainment of equilibrium. This is achieved through a number of methods, such as homogenization of the samples in an agate mortar to prevent the existence of relict crystals, using synthetic glasses, and most importantly, selecting appropriate experiment duration.

Duration on the runs depends on a multitude of factors, such as the goal, composition and conditions of the experiments. Among them, the most influential is the composition of the starting material. Prior to experimentation, bulk compositions of the starting materials were determined by X-ray fluorescence using major pearls routine, analysing

SiO_2, TiO_2, Al_2O_3, $Fe_2O_3^T$, MnO, MgO, CaO, Na_2O, K_2O, P_2O_5 and LOI with a measurement accuracy superior to 0.2–0.3 wt% relative, in the Instituto Andaluz de Ciencias de la Tierra (University of Granada – Consejo Superior de Investigaciones Científicas). Experiments using natural rocks usually require longer times than those using synthetic glasses due to the presence of relic crystals. Similarly, experiments using a mix from two distinct rock compositions usually require higher homogenization times than those using a single composition, particularly when the two mixers are represented by two natural rocks. Moreover, temperature is almost as influential as the starting composition, given the intimate correlation between temperatures and chemical potential. As temperature rises chemical reactions occur at a faster rate due to the equally increased chemical kinetics, and so shorter durations are needed for attainment of equilibrium in the experimental run. For instance, experiments above 1200 ^oC with a mafic-intermediate starting material used shorter run times below 24 hours, also helping reduce the Fe-loss to the Au–Pd alloy. In contrast, experiments around 1000 ^oC were kept at the objective conditions for more than 48 hours. Once the experiment has run for the desired amount of time, the experiment is shut down by turning off the current, effectively quenching the experimental load. The capsule is then mounted in epoxy resin, polished and prepared for analysis of the results.

Analyses of the experimental results were performed with electron microprobe at the University of Huelva. Major elements of mineral phases and glasses were analysed with a JEOL JXA–8200 Superprobe equipped with four WDS spectrometers. Operation conditions were 15 kV for accelerating voltage and 20 nA for beam current. Calibration used a combination of silicates, oxides and pure metals and ZAF correction procedures (wollastonite for Ca and Si, jadeite for Na, orthoclase for K, corundum for Al, periclase for Mg, metallic Fe and Ti for Fe and Ti). A defocused beam 10 µm in diameter was used for glass analyses to minimize Na migration. Phase analyses were performed applying a smaller diameter beam when necessary (1–5 µm).

Petrological experiments were used to accomplish several objectives within the research plan. Each set used its own different starting materials and conditions after careful consideration. The conception and explicit methodology behind the experimental runs dedicated for objectives 1-a and 1-b is fully detailed in section 5.1.

4.2 Numerical modelling

4.2.1 Computational strategy

To constrain the viability of the classic post-orogenic magmatism models through the evolution of temperature, pressure and volatiles during collision, 2D high-resolution petrological-thermo-mechanical numerical experiments were performed. All numerical experiments used the I2VIS code (Gerya and Yuen, 2007, 2003) and were calculated on the cluster of ETH Zurich. The methodology is thoroughly explained in Gerya, 2019, and further references for all the concepts summarized in the following sections can be found therein.

The conceptual foundation of numerical experiments consists in three main partial differential equations (PDEs), which characterise the time-dependency of physical properties in a continuous medium. These are the continuity equation (conservation of mass), the momentum equation (conservation of momentum), the temperature equation (conservation of heat). The Poisson equation for gravity potential is also solved to account for the gravitational field. These PDEs are solved by conservative finite differences in a Eulerian reference frame, with physical properties being transported by Lagrangian markers by the marker-in-cell technique. Erosion, sedimentation, water transport and lithospheric mantle grainsize reduction are all accounted for in the calculations. The models use non-Newtonian visco–plastic rheologies to simulate multiphase flow and grainsize reduction (as described in Corradino et al., 2022) and are designed to study the dynamic and thermobarometric evolution of the lithosphere during continental collision.

The continuity equation

The continuity equation describes the conservation of mass during the displacement of a continuous medium. Its formulation depends on the observation point and can be either Eulerian when considering a fixed point in space, or Lagrangian for a moving point of reference. These are respectively expressed as

$$\frac{\partial \rho}{\partial t} + \mathrm{div}(\rho \vec{v}) = 0 \ (1.1)$$

$$\frac{D\rho}{Dt} + \rho \operatorname{div}(\vec{v}) = 0 \ (1.2)$$

where ρ is the local density in (kg/m^3), t is the time (s), v is the velocity (m/s), $\partial/\partial t$ is the Eulerian time derivative and D/Dt is the Lagrangian time derivative. The relationship between the Eulerian (1.1) and Lagrangian (1.2) continuity equations is the following:

$$\frac{D\rho}{Dt} = \frac{\partial \rho}{\partial t} + \vec{v} \operatorname{grad}(\rho) \ (1.3)$$

In this expression, term grad(ρ) represents the advective transport, which reflects changes in density in an immobile point due to the existence of density gradients.

The momentum equation

The momentum equation describes the conservation of momentum for a continuous medium in a gravity field. The respective Eulerian and Lagrangian expressions are as follows:

$$\frac{\partial \sigma_{ij}}{\partial x_j} + \rho g_j = \rho \left(\frac{\partial v_i}{\partial t} + v_j \frac{\partial v_i}{\partial x_j} \right) \ (1.4)$$

$$\frac{\partial \sigma_{ij}}{\partial x_j} + \rho g_j = \rho \frac{D v_i}{Dt} \ (1.5)$$

Where σ_{ij} is stress, ρ is density, g is gravity (m/s^2), and $\partial v_i/\partial t$ and Dv_i/Dt represent the time derivative of the velocity of the material passing through the reference point. These PDEs are solved under the assumption of incompressible materials. As in the continuity equation, the relationship between the Eulerian and Lagrangian expressions is the following:

$$\frac{D v_i}{Dt} = \frac{\partial v_i}{\partial t} + \vec{v} \operatorname{grad}(v_i) \ (1.6)$$

Adding a pressure gradient to the momentum equation using deviatoric stress relations results in the Navier-Stokes equation:

$$\frac{\partial \sigma'_{ij}}{\partial x_j} - \frac{\partial P}{\partial x_i} + \rho g_j = \rho \frac{D v_i}{Dt} \ (1.7)$$

Solving this equation for highly viscous flows means that term $\rho(Dv_i/Dt)$ is negligible compared to the value of the left-hand side of the equation, or what is the same, inertia is almost non-existent. Under such circumstances, this system can be described by the Stokes equation of slow creeping flow with position and time-dependent gravitational acceleration:

$$\frac{\partial \sigma'_{ij}}{\partial x_j} - \frac{\partial P}{\partial x_i} + \rho g_j = 0 \ (1.8)$$

The temperature equation

The temperature equation describes the heat conservation in a continuous medium. Changes in temperature of a given reference point or volume can occur in several forms, such as heat generation, heat consumption, heat advection or heat conduction. These are computed in the respective Eulerian and Lagrangian forms of the temperature equation:

$$\rho C_P \left(\frac{\partial T}{\partial t} + \vec{v} \, \mathrm{grad}(T) \right) = -\frac{\partial q_i}{\partial x_i} + H_r + H_s + H_a + H_L \ (1.9)$$

$$\rho C_P \left(\frac{DT}{Dt} \right) = -\frac{\partial q_i}{\partial x_i} + H_r + H_s + H_a + H_L \ (1.10)$$

In this expression C_P is the heat capacity (J), and the product ρC_P is the volumetric isobaric heat capacity (J/kg/m^3); q_i is the heat flux measured in the x_i direction (W/m^2); and H_r is the radiogenic heat from the disintegration of radioactive elements, H_s is the shear heat production, H_a is the adiabatic heat production, and H_L is the latent heat from phase transformation during rock formation, all together representing the volumetric heat production or consumption (W/m^3).

Heat flux can be described by Fourier's law of heat conduction:

$$q = -k \frac{\partial T}{\partial x} \ (1.11)$$

where k is the thermal conductivity (W/m/K) and is dependent on the rock type (Clauser and Huenges, 1995).

The shear heat production is related to the dissipation of mechanical energy and is defined as

$$H_s = \frac{1}{2\eta}\sigma'_{ij} \quad (1.12)$$

with η representing viscosity.

The adiabatic heat production is calculated after changes in pressure and can be calculated as

$$H_a = T\alpha\frac{DP}{Dt} \quad (1.13)$$

where *DP/Dt* is the time derivative of pressure and α is the thermal expansion. Adiabatic heat can be positive under compressional and negative under decompression.

Derivation of Eq. 1.10 using of the heat flux definition in Eq. 1.11 results in the following expression:

$$\rho C_P\left(\frac{DT}{Dt}\right) = k\frac{\partial^2 T}{\partial x^2} + H_r + H_s + H_a + H_L \quad (1.14)$$

The Poisson equation

The spatial changes in gravitational potential inside a self-gravitating continuum can be described by the Poisson equation:

$$\frac{\partial^2\Phi}{\partial x^2} + \frac{\partial^2\Phi}{\partial y^2} = 4K\gamma\pi\rho(P,T,c) \quad (1.15)$$

In this expression Φ is the gravitational potential, K is a variable that depends on the geometry of self-gravitating model in 2D, γ is the gravitational constant and ρ is density. The Poisson equation is solved to calculate the gravity potential that is subsequently used in eq. 1.8.

Eulerian frame of reference with Lagrangian markers: marker-in-cell method

In continuum mechanics and numerical modelling an important difference between Eulerian and Lagrangian reference frames must be made, as they condition the basis on

which the PDEs are solved, and the numerical grid is built upon. As previously mentioned, Eulerian refers to a fixed point of reference (or constant position), allowing the observation of the material or physical properties through those stationary points. Using a Eulerian reference frame (constructed using Eulerian points) grants a non-deforming grid for evaluating the time-dependant governing equations in which material properties change over time for each spatial location. In contrast, a Lagrangian approach tracks individual material particles carrying information of the physical properties as they move through space. Using a Lagrangian frame of reference (constructed using Lagrangian points) grants a moving grid that deforms with the material, changing its position over time while the physical properties measured in the moving point remain constant.

In numerical modelling advection of physical properties is a determining factor when configuring the numerical grid, particularly when considering non-diffusive properties such as lithology. Using Eulerian numerical methods to account for advection often leads to significant numerical diffusion. In contrast, using a Eulerian–Lagrangian algorithm prevents numerical diffusion in geodynamic modelling. That is, Lagrangian points or makers transport the physical properties and advect within an immobile, Eulerian grid (Fig. 4.4). This is called the marker-in-cell method. Properties are initially distributed in a vast number of markers and then advect according to the computed velocity field. After displacement the advected material properties are interpolated back from the markers to the Eulerian points or nodes using a weighted-distance average linear interpolation:

$$A_{i,j}^{t+\Delta t} = \frac{\sum_m A_m w_{m(i,j)}}{\sum_m w_{m(i,j)}}$$

$$w_{m(i,j)} = \left(1 - \frac{\Delta x_m}{\Delta x}\right) \times \left(1 - \frac{\Delta y_m}{\Delta y}\right)$$

In these expressions A represents the material property (density, viscosity…); $A_{i,j}^{t+\Delta t}$ is the value of the material property in the new time step at the considered Eulerian point or node; A_m is the value of the material property at the old time step on a Lagrangian point or marker; $w_m(i,j)$ is the weighted distance, calculated after Δx_m and Δy_m, which denote

the distance from the marker *m* to the *i,j* nodes, and *Δx* and *Δy*, which are the dimensions in 2D.

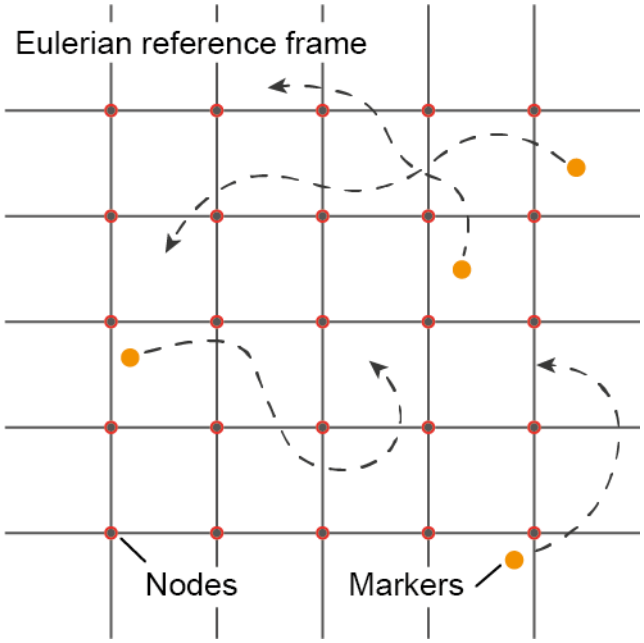

Figure 4.4: Simplified representation of a two-dimensional numerical grid. The reference frame is built using Eulerian points, also called nodes, thus being non-deformable and with a fixed position over time. The physical properties are transported using Lagrangian points, also called markers, and change their position with time.

Once the marker information is computed in the nodes, the subsequent step involves solving the governing equations of continuity, momentum, temperature and gravitational potential (eq. 1.1, 1.8, 1.14, 1.15). Since these are partial differential equations, discretization is necessary for their solution. Finite differences serve this purpose, and can be expressed in the next general form:

$$\frac{\partial A}{\partial x} = \frac{\Delta A}{\Delta x} = \frac{A_2 - A_1}{x_2 - x_1}$$

In this expression, the distance Δx between point x2 and x1 represents the resolution of the numerical grid. That is, the shorter the distance, the higher the resolution. Expressing the three governing equations using finite differences results in a number of linear equations that must be solved within each single point of the numerical grid. For 2D modelling, an accurate solution of the large system of equations is achieved by using

direct numerical methods such as Gaussian eliminations, only hampered by computational limitations.

Solution of the momentum equation provides updated values for the velocity field in the Eulerian nodes. Using this newly calculated velocity, subsequent displacement of the markers is achieved by interpolating the velocity field calculated in the nodes back to the markers. accurately calculated using a fourth order Rugne-Kutta advection scheme.

Erosion and sedimentation

Surface processes above the crust are implemented as internal free erosion/sedimentation surface by introducing a low density, low viscosity fluid layer above the crust. This free-surface boundary condition is implemented using a 12 km thick air/water layer with low density (1kg m^{-3} above 9 km, 1000 kg m^{-3} below 9 km) and viscosity (10^{17} Pa s). The surface of the lithosphere evolves due to erosion and sedimentation after the following Eulerian transport equation:

$$\frac{\partial y_{es}}{\partial t} = v_y - v_x \frac{\partial y_{es}}{\partial x} - v_s + v_e$$

Where y_{es} is a function of the horizontal distance x and defines the vertical position of the surface, v_y and v_x are the vertical and horizontal components of the material velocity field at the surface, v_s is the sedimentation rate, and v_e is the erosion rate. The sedimentation and erosion rates are used for air and water:

$$v_s = 0\ mm\ yr^{-1} \text{ and } v_e = 0.3\ mm\ yr^{-1} \text{ when } y < 9\ km$$

$$v_s = 0.03\ mm\ yr^{-1} \text{ and } v_e = 0\ mm\ yr^{-1} \text{ when } y > 9\ km$$

Water transport

The determination of magma forming conditions requires a fairly accurate estimation of the water contents in the source. Consequently, water is computed in the numerical model, either contained in pores at relatively low lithostatic pressures or in the structure of water-bearing phases. The implementation of this algorithm is detailed in Corradino et al., 2022.

An initial assumption establishes the decrease of pore water content from 2 wt.% to 0 wt.% at depth of 75 km due to compaction. This is formulated in the following equation:

$$x(wt.\%) = (1 - 0.013\Delta y)X_{H_2O}$$

In this expression, $X_{H_2O(p0)}$ is the free water content at surface, yielding a value of 2 wt.%, and Δy is the depth in km below the surface (0–75 km). Water released by dehydration reactions is determined by the assumption of thermodynamic equilibrium during the modelling time, with the stable water content for different lithologies corresponding to that determined by Gibbs free energy minimization as a function of pressure and temperature. Liberated water in the continuum moves upwards spontaneously until reaching a rock capable of assimilating additional amounts of water. This process is computed according to pressure gradients as:

$$v_{x(water)} = v_x - A\frac{\partial P}{\partial x}$$

$$v_{y(water)} = v_y - A\left(\frac{\partial P}{\partial x} - \rho_{fluid}g\right)$$

$$A = \frac{v_{percolation}}{g(\rho_{mantle} - \rho_{fluid})}$$

where v_x*(water)* and v_y*(water)* are the fluid vector velocities in *x* and *y* directions, v_x and v_y indicate the local velocity of the solid mantle, *A* is a water percolation constant, $v_{percolation}$ = 10 cm/yr, *g* is the gravitational acceleration, ρ_{mantle} and ρ_{fluid} are the density of the mantle and fluid, respectively.

4.2.2 Modelling initial setup

The computational domain covers a two-dimensional field of 4000 km wide by 1400 km deep (Fig. 4.5). The non-uniform rectangular grid consists of 1361 x 351 nodal points in which markers are randomly distributed, using a high-resolution scheme of 0.5 km x 0.5 km. All boundaries are free slip.

The continental crust has a total thickness of 35 km. It is subdivided into 20 km of upper continental crust with an average felsic composition, and 15 km of lower continental crust with an average mafic composition. The upper crust has a wet quartzite weak rheology and the lower crust has a plagioclase strong rheology (Ranalli, 1995). The rheology contrast within the crust often results in decoupling of upper and lower crust (Vogt et al., 2017). The underlying lithospheric mantle is 90 km thick, and uses a dry olivine rheology, same as the asthenosphere. The oceanic domain comprises an ocean plate with a variable length of 675 km or 400 km and equally variable thermal age of 90 Ma, 60 Ma and 40 Ma. The oceanic crust consists of 3 km of basalts over a 5 km gabbro layer for a total of 8 km. The thickness of the oceanic lithosphere is calculated as a function of the chosen initial age (homogeneous for the whole oceanic plate) and an oceanic geotherm, resulting in an oceanic lithosphere of simplified thermal structure.

To allow for subduction to initiate, an internal velocity field is prescribed within the lithosphere, with a variable symmetric convergence rate between the two colliding plates of 5 cm/y, 3 cm/y and 1 cm/y. The velocity field is maintained until collision, after which the model is driven exclusively by the slab pull. Subduction initiation is facilitated by setting up a weak zone with wet olivine rheology in the rightmost limit of the oceanic plate (Fig. 4.5).

Thermal boundaries are defined by an upper boundary with constant temperature of 0 ^{o}C, and no heat flux across the vertical boundaries. Natural inference of Moho temperatures displaying anomalous high temperatures during oceanic subduction up to 800–900 ^{o}C (Goes et al., 2020; Schutt et al., 2018). Moho temperatures were consequently raised to a conservative 660 ^{o}C in the upper plate. This temperature rise serves a dual purpose: on the one hand, it enhances magmatism during the collisional and post-collisional stage of the orogenic process; and on the other hand, it accounts for the inability of numerical models to model extensive oceans (>2000 km) that would

produce such temperature anomalies by pre-setting an already heated Moho. The rest of the model follows a thermal gradient of 6 ^{o}C/km until a temperature of 1330 ^{o}C, and a quasi-adiabatic 0.5 ^{o}C/km gradient for the asthenosphere. All material properties are summarised in Table 4.1.

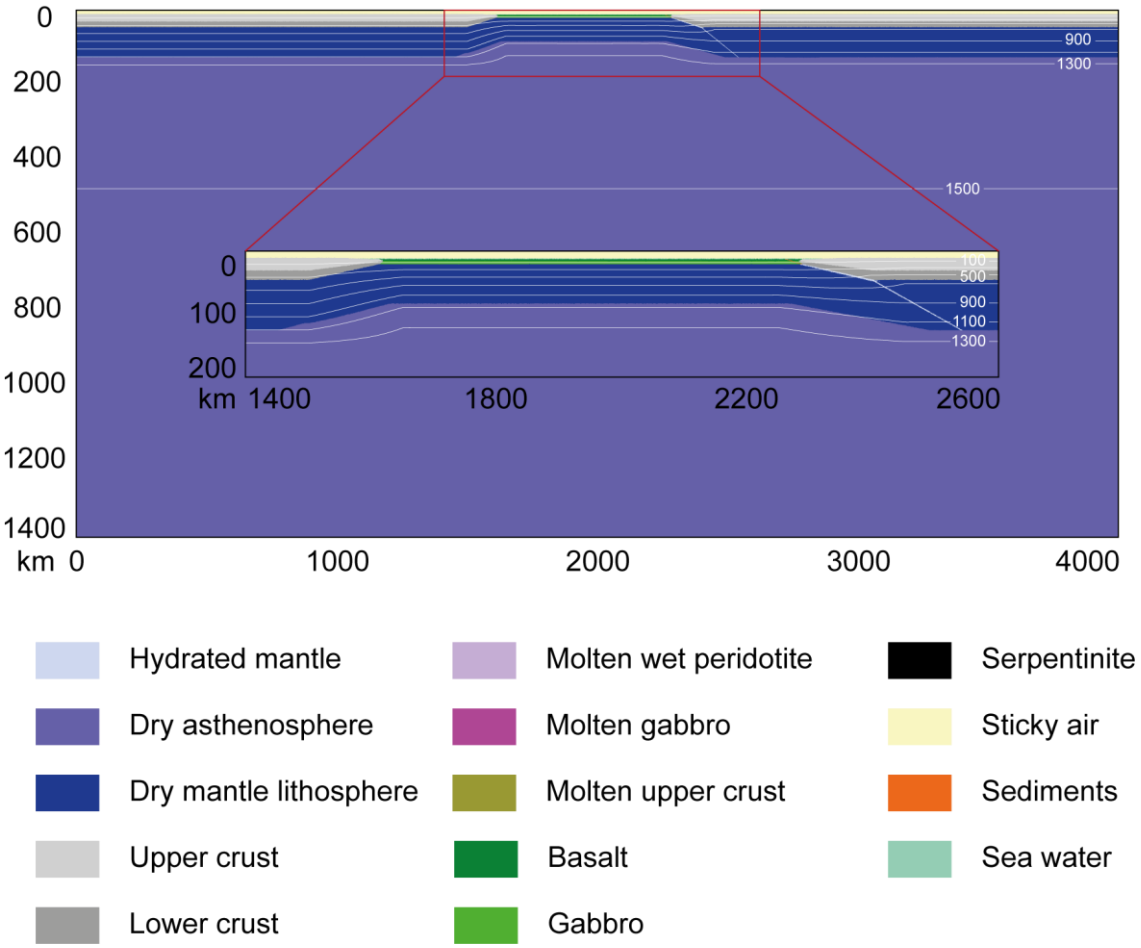

Figure 4.5. Cross section of the initial setup.

It is noteworthy that these numerical simulations cannot account for the complexity of natural collisional systems. Numerical models are not only hampered by the stability of the model and the consequent reliability of the results, but also by the irreproducibility of the heterogeneous rheology and lithology from nature. Likewise, the simulations use a constant velocity field, while in nature convergence velocity can erratically change over time, producing unpredictable results. All these factors must be taken into account when addressing the results of the models and their representativeness of natural orogens.

Properties	Upper cont. crust	Lower cont. crust	Mantle	Weak zone	Basalt
Flow law	Wet quartzite	Plagioclase (An75)	Dry olivine	Wet olivine	Wet quartzite
$1/A_D$ ($Pa^n s$)	1.97×10^{17}	4.80×10^{22}	3.98×10^{16}	3.98×10^{16}	1.97×10^{17}
n	2.3	3.2	3.5	2.3	2.3
Ea (kJ)	154	238	532	154	154
Va (J/bar)	0.3	0.8	2.6	1	0.8
sin(φ)	0.3 – 0.15	0.6 – 0.2	0.6 – 0.2	0.1 – 0.03	0.1 – 0.03
ρ (kg/m^3)	2700	2900	3300	3300	3000
Hr (muW/m^3)	1.8	0.18	0.022	0.022	0.022
k (W/m/K)	(0.64 + 807/A) × exp(B)	(1.18 + 474/A) × exp(B)	(0.73 + 1293/A) × exp(B)	(0.73 + 1293/A) × exp(B)	(1.18 + 474/A) × exp(B)

Table 4.1. Material properties. ρ is the initial density; A_D is the pre-exponential factor, n is the stress exponent, Ea is the activation energy, Va is the activation volume, φ is the friction angle, and Hr is the radioactive heat production. For all rocks: heat capacity Cp = 1000 J/K; coefficient of thermal expansion α = $3*10^{-5}$ 1/K; coefficient of thermal compressibility β = $1*10^{-5}$ 1/MPa; A = T(K) + 77; B = 0.00004 × P(MPa).

5. Results

5.1 Characterisation of I-type magmas

5.1.1

Sanukitoid crystallization relations at 1.0 and 0.3 GPa

Lithos, 2022

LITHOS 414-415 (2022) 106632

Contents lists available at ScienceDirect

LITHOS

journal homepage: www.elsevier.com/locate/lithos

Sanukitoid crystallization relations at 1.0 and 0.3 GPa

Daniel Gómez-Frutos *, Antonio Castro

Instituto Andaluz de Ciencias de la Tierra (CSIC – UGR), Avenida de las Palmeras 4, 18100 Armilla, Granada, Spain

ARTICLE INFO

Keywords:
High-Mg granitoid
Batholith
Differentiation series
Sanukitoid
Experimental petrology
Cotectic line

ABSTRACT

Sanukitoid (vaugnerites, appinites, durbachites) intrusions have been described in multiple locations around the world. Initially thought as an only basic-intermediate series, increasing interest in these rocks have pointed to the conclusion that they represent a whole differentiation series. A distinct geochemistry with high MgO, LILE and LREE (specially K, Ba and Sr) and depletion in CaO differentiates them from the standard calc-alkaline batholiths they appear associated with. While some of such features may be inherited from the metasomatized mantle source, no consistent explanation has been given for the singular geochemistry of the series. Accordingly, we propose two initial hypotheses: (1) the sanukitoid array is due to the existence of a cotectic line that determines the behaviour of the system; (2) the sanukitoid array does not represent a cotectic series, but the result of a ubiquitous process that deviates the rocks from their ideal differentiation trend. To test the thermodynamic behaviour of the system piston cylinder experiments were conducted at different temperatures in two pressure series appropriate for lower and upper crust differentiation (1.0, 0.3 GPa and 1100 °C, 1050 °C, 1000 °C, 900 °C). Two starting compositions are used: a sanukitoid enclave from Los Pedroches batholith (SW Spain) and a hydrous synthetic glass. Experimental results show that, while 1.0 GPa runs follow the calc-alkaline cotectic, 0.3 GPa runs follow a line that coincides with the sanukitoid series, proving the existence of a low pressure cotectic line. However, lack of cumulates at shallow depths and low water contents in the fractionated magmas (the granites) suggest that a complementary mechanism must be involved. The observed geochemical features may also be accounted for by contamination by entrainment of orthopyroxene from the source or early magmatic cumulates. This is supported by the showcased crystallization pattern, with orthopyroxene representing the liquidus phase, the presence of amphibole clots in these rocks, and the presence of autoliths with abundant orthopyroxene in sanukitoid intrusions. Additionally, the existence of a low pressure cotectic system induces the re-equilibration and digestion of such entrained orthopyroxene in the liquid when reaching shallow depths, leaving a seemingly homogeneous liquid. The two discussed mechanisms are valid, compatible, complementary and account for the geochemical trend shown by the series.

1. Introduction

Sanukitoid intrusions represent a volumetrically minor yet important series that has been recognized in multiple places all over the world (Fig. 1). This series was first described by Shirey and Hanson (1984) as a particular type of Archean intrusions linked to Tonalite-Trondhjemite-Granodiorite (TTG) magmatism, which closely resembled the high magnesium andesites of the Setouchi Volcanic Belt (Tatsumi and Ishizaka, 1982). Since then, they have been recognized as an important component in most Archean terrains (Martin et al., 2005). Common properties of the sanukitoid plutons include enrichment in compatible elements, such as Mg, Cr or Ni, the latest two signifying mantle affinity; and in large ion litophile elements (LILE), particularly Ba, Sr, K, and LREE elements (Shirey and Hanson, 1984). However, even if the exact geochemical definition has been changing throughout time (e.g. Heilimo et al., 2010; Shirey and Hanson, 1984; Stern et al., 1989), there is an increasing awareness that this magmatism may well represent a broader series (Heilimo et al., 2010; Martin et al., 2005; Stern and Hanson, 1991).

Similarly, although it was initially considered to be strictly restricted to Archean environments, recent works by Fowler and Rollinson (2012) demonstrated that the close similarities between Archean sanukitoid intrusions and Caledonian high Ba–Sr granites from the Scottish Caledonian province, denoting a link between Neoarchean sanukitoid magmatism and the beginning of Archean subduction. Likewise, López-Moro and López-Plaza (2004), Moyen et al. (2017) and Castro et al.

* Corresponding author.
E-mail address: daniel.gomez@csic.es (D. Gómez-Frutos).

https://doi.org/10.1016/j.lithos.2022.106632
Received 19 October 2021; Received in revised form 10 February 2022; Accepted 10 February 2022
Available online 14 February 2022

(2013) realized that sanukitic features were also widespread among monzonitic to ultrapotassic intrusions in the Iberian Variscan, the French Variscan and the Himalayas, respectively. These may embody the Phanerozoic analogous of the Archean sanukitoid magmatism and showcases a potential petrogenetic link with I-type batholiths.

Regarding its origins, it is widely accepted that the origin of these magmas entails a metasomatized lithospheric mantle probably enriched by a subducting basaltic slab and sediments (Lobach-Zhuchenko et al., 2008; Stern and Hanson, 1991). Lead and Nd isotopes are consistent with the involvement of a crustal component, suggesting that crustal recycling is a significative process in the generation of magmas (e.g. Halla, 2005; Heilimo et al., 2013; Stevenson et al., 1999). That is compatible with sanukitoid magmas being volatile-rich and acting as water donors for melting of the lower crust (Castro, 2020). The study of their petrogenesis has also been aborded by experimental petrology. The study of Archean sanukitoids has led to several experimental works (de Oliveira et al., 2010, and references therein). A phlogopite and pargasite bearing lherzolite has also successfully reproduced melt with shoshonitic affinity between 1 and 1.5 GPa and temperatures of 1050 to 1150 °C (Conceição and Green, 2004). Similarly, a harzburgitic source has been proposed as the cause of the characteristic high MgO and Mg# values from the Setouchi original sanukites (Wood and Turner, 2009). Nevertheless, there is still uncertainty about whether their origin is due to a single stage process, in which the melt acquires the sanukitoid signature in its way to the surface; or a two-stage process, with melting preceded by a metasomatic event (Martin et al., 2009, and references therein; Smithies and Champion, 2000).

Whatever the case, there is undeniable evidence that sanukitoids may represent a significant tracer in crustal recycling processes. Even if there are significant geological inferences of the importance of these series, the processes involving their differentiation remain poorly constrained. In this paper we show a meta-analysis of the world series and a set of experiments at 0.3 and 1.0 GPa, simulating upper and lower crust environments using sanukitoid-like starting materials. Our goal is to determine their crystallization patterns at different depths and the reasoning behind their differences with typical calc-alkaline trends.

2. The sanukitoid series

Although sanukitoids are often described as andesitic to dacitic intrusions (55–70 wt% SiO_2; Heilimo et al., 2010), the possibility that the 'sanukitoid suite' define a complete magmatic series was already proposed by Stern and Hanson (1991). Since then, these series have been described worldwide, yet received several local names. Rocks sharing the described geochemical properties are called either "sanukitoid" in the Archean shields, "vaugnerites" in the French Variscan, "durbachites" or "redwitzites" in the Bohemian Variscan, "appinites" or "high Sr-Ba granitoids" in the Scottish Caledonian (Moyen et al., 2017, and references therein).

Even if LILE and LREE signatures are important constraint regarding their origins, the likelihood of sanukitoids representing a magmatic differentiation series also must be evident in their major elements trend. To further explore this possibility, we elaborated a database from sanukitoids from all over the world. We included the most basic terms (<50 wt% SiO_2) matching the common geochemical signatures of sanukitoids (high Mg, K, LILE and LREE). However, there is a remarkable lack of felsic differentiated rocks in the bibliography since these series has historically been considered basic-intermediate. All things considered, we compiled a total of 2465 analyses. The bibliography used for the elaboration of such database is reported in the Supplementary Material S1.

Forasmuch as some of the most common referenced attributes of these magmas are their high Mg and K, it is expectable to find differences in these elements with respect to the calc-alkaline trend. Complementarily, while Ca was never a referenced characteristic of the sanukitoid magmas, we found it is most certainly depleted. Fig. 2 offers an illustration of these attributes using the CaO–MgO and the Or–An–En diagrams. The CaO–MgO diagram constitutes a proxy of phase equilibrium diagrams since these components are alkali-independent and represent the most outstanding changes in liquid compositions when decreasing temperature. Thus, this diagram offers a clear view of the deviation of the sanukitoid rocks, falling below the experimental, Andean-type calc-alkaline cotectic line (Castro, 2021). This is a consequence of both the high content in MgO and depletion in CaO. As mentioned before there is

Fig. 1. Global distribution of sanukitoid rocks from which geochemical data have been compiled (Supplementary Material S1). Map symbols represent geological domains in which sanukitoid rocks have been identified. Digital elevation model from Amante and Eakins (2009).

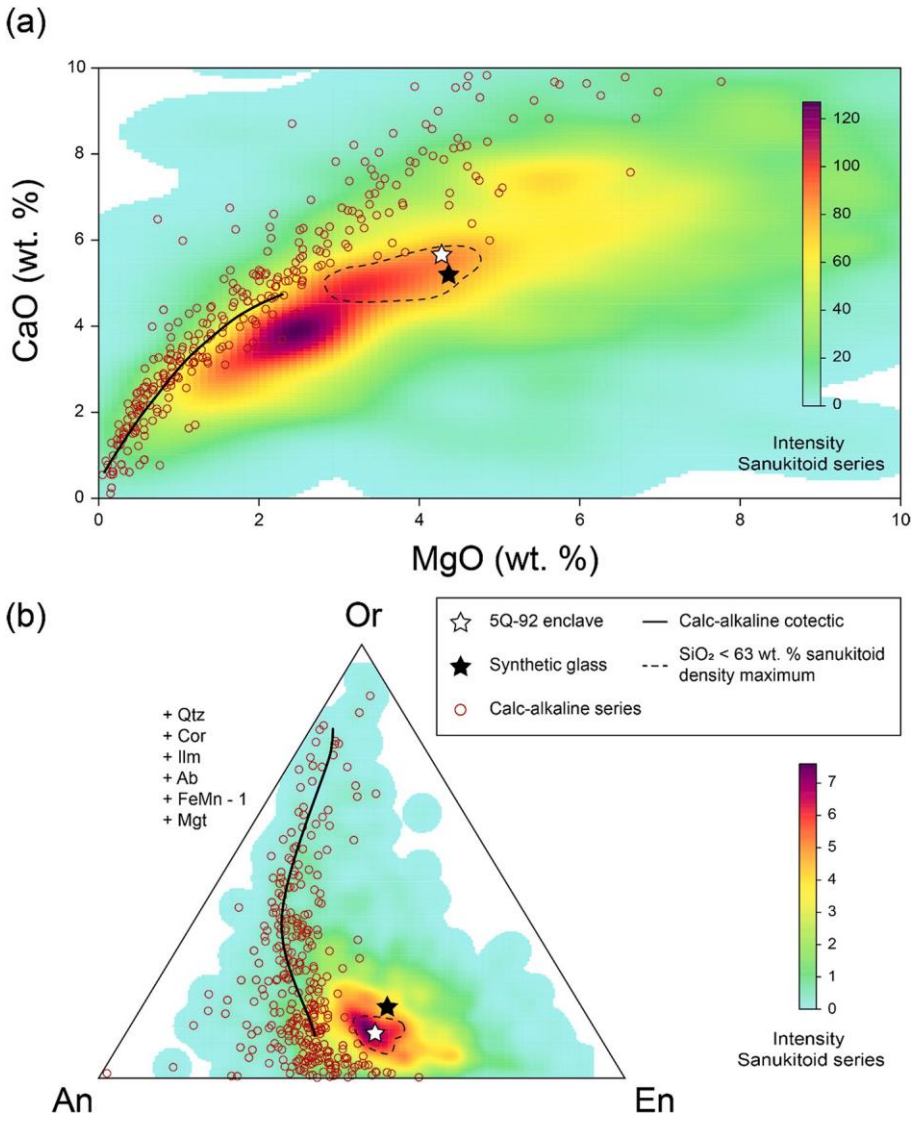

Fig. 2. Defining diagrams of the sanukitoid series (Kernel density contour plot) compared to the calc-alkaline series. Calc-alkaline series analyses from Sierra Nevada (Lackey et al., 2008) and Patagonia (Castro, 2020) batholiths. Calc-alkaline cotectic line experimentally determined by Castro (2021). Starting materials are normalised to sum 100. a) CaO–MgO diagram. b) Or–An–En diagram.

a lack of the most evolved terms, but the series show a tendency to evolve towards the granite minimum. Complementarily and offering a more complex view of the system, the Or–An–En diagram illustrates the same enrichment in Or and En and depletion in An component compared to Andean-type calc-alkaline magmatism. Overall, these two diagrams present a detailed view of the irrefutable differences between the sanukitoid series and the calc-alkaline series. But more interestingly, they highlight the heterogeneity of the sanukitoid series against the mostly homogenous calc-alkaline series. This fact offers interesting insights on the petrogenetic process of each system; sanukitoid magmas must generate in a highly variable source or by a complex, probably multivariate process that behaves like an open system, while calc-alkaline magmas have lower variability, and its behaviour is more similar to that of a closed system. Moreover, a world occurring series must inherently be a consequence of an intrinsic characteristic within the system, discarding local assimilation processes as the primary cause.

Once demonstrated that the sanukitoid series apparently do not follow the calc-alkaline trend, the question of the peculiar nature of the series becomes even more crucial. We contemplate two possibilities behind their geochemical signature: (1) The sanukitoid series follow their own cotectic line. Their differences with the calc-alkaline batholiths are not only superfluous, but a consequence of the existence of a yet undetermined thermal valley. This implies they describe a full series, meaning the existence of sanukitoid granites is theoretically possible. (2) The sanukitoid series follow the calc-alkaline cotectic, but a ubiquitous process deviates them from their ideal trend. While not as fancy as a new cotectic line, the thermodynamical implications of this possibility are equally huge. Essentially, alkaline series following the calc-alkaline cotectic, even having significantly different geochemistry, intrinsically imply the universality of the calc-alkaline cotectic. This means no matter the bulk composition of a rock is, its differentiated terms always follow the same differentiation path. An explanation for the deviated geochemical trend must be explored in this hypothesis. To assess the problematic of the cotectic or non-cotectic behaviour of the sanukitoid series, crystallization experiments were performed. The corresponding P and T values are permissible conditions at which the crystallization process might have taken place. This experimental work intends to constrain the differentiation processes, rather than their genesis.

3. Experimental set up

3.1. Experimental background

Crystallization of a high-Mg synthetic glass, close in composition to the high-Mg andesites from the Setouchi Volcanic Belt, in contact with a thin layer of San Carlos olivine orthopyroxene and olivine, was previously tested at 0.6 GPa (Wood and Turner, 2009). This work puts in value the crucial role of Mg-rich minerals (Ol, Opx) in high-Mg magmatism, which accounts for one of the key features of the sanukitoid magmas. It also proposes a potential harzburgitic nature as the source of high-Mg magmas, which enlightens one of the most debated topics regarding these magmas. However, differences of high-Mg and sanukitoid magmatism have been remarked (Smithies and Champion, 2000), being the latest geochemically closer to adakites. Volatiles are also known to play a major role in this system, with sanukitoid magmas bearing H_2O contents that may be around 3 wt%. Moreover, the influence of intensive parameters in the differentiation process of the series is yet to be tested. For these reasons a set of experiments using a hydrated starting materials was programmed to test the behaviour of the system at different temperature and pressure values.

3.2. Starting materials

The experimental runs used a sanukitoid enclave from the Pedroches batholith (Extremadura, Spain) and a hydrous mafic synthetic glass with 3 wt% H_2O. Although the two selected starting materials show differences in their SiO_2 and Al_2O_3 values, they share similar characteristic features of the sanukitoid magmas, namely high MgO and K_2O and low CaO. The bulk composition of the glass was assembled from high purity elemental oxides by repeated fusion at 1500 °C and atmospheric pressure in a vertical oven. An aliquot proportion of Al_2O_3 is added as $Al(OH)_3$ after melting to get the desired water content (3 wt%). The starting compositions were selected using field and meta-analytical criteria. The enclave is representative of a set of fine-grained sanukitoid enclaves from the Pedroches batholith, with modal plagioclase, amphibole, biotite and oxides, likely representing quenched melts of monzodioritic composition. Mafic synthetic glass was already used to successfully produce granodioritic melt in contact with a tonalitic layer (López et al., 2005). Both the enclave and the glass are close to classic sanukitoids from the Pilbara Craton and the Superior Province (Canada) and plot in the sanukitoid series field for all diagrams (Fig. 2), matching the composition of a hypothetical primary liquid. They also plot reasonably within the basic-intermediate density maximum of the series in the CaO–MgO and Or–An–En diagrams, calculated by excluding all analyses with $SiO_2 < 63$ wt%. Particularly, in the Or–An–En diagram a density maximum that reaches higher MgO concentrations for the basic-intermediate terms of the series. More mafic compositions were rejected due to the possibility of representing cumulates.

3.3. Experimental procedures and analytical techniques

Double capsule experiments were performed to minimize Fe loss and to constrain oxygen fugacity. Inner 2 mm $Au_{75}Pd_{25}$ capsules contain 5 mg of sample, and outer 3 mm Pt or $Au_{75}Pd_{25}$ buffer capsules are loaded with 10 mg of a magnetite, fayalite and silicic glass mix and 1 μL of water added with a mycrosyringe. Capsules were filled, sealed by pressure folding and introduced in a MgO (crushable magnesia) pressure container. Experiments were conducted in a Boyd-England piston-cylinder apparatus at Instituto Andaluz de Ciencias de la Tierra (CSIC – UGR) using half inch, talc-Pyrex assemblies. Each experimental cell was loaded with two capsules, each filled with a different starting material. For this reason, each experiment will be named Gl for the synthetic glass and E for the 5Q-92 enclave. Temperatures were measured and controlled using Pt_{100}-$Pt_{87}Rh_{13}$ thermocouples wired to Eurotherm 808 controllers. Two pressure series were carried out to 0.3 GPa and 1.0 GPa. 0.3 GPa runs were performed at temperatures of 1050 °C, 1000 °C and 900 °C, while 1.0 GPa runs reached 1100 °C and 900 °C. All assemblies were initially pressurized to the objective P and 1200 °C and held for 3 h. Higher homogenization times were not considered to prevent Fe loss. Once that time had passed the experiments were cooled to the objective T at 10 °C/h, although D21–3 run used a faster 30 °C/h cooling ramp. Experiments were held for up to 41 h at the final temperature and then quenched by switching off the power. A complete list of run conditions and experimental results is reported in Table 2.

Analyses of major elements of mineral phases and glasses of experimental capsules were performed with a JEOL JXA–8200 Superprobe equipped with 4 spectrometer WDS at the University of Huelva. Operation conditions were 15 kV for accelerating voltage and 20 nA for beam current. A combination of silicates, oxides and pure metals were used for calibration and ZAF correction procedures (wollastonite for Ca and Si, jadeite for Na, orthoclase for K, corundum for Al, periclase for Mg, metallic Fe and Ti for Fe and Ti). A defocused beam 10 μm diameter was used for glass analyses to minimize Na migration. Phase analyses were performed applying a smaller diameter beam when necessary (1–5 μm). Bulk compositions of the starting materials (Table 1) were determined by XRF using major pearls routine, analysing SiO_2, TiO_2, Al_2O_3, $Fe_2O_3^T$, MnO, MgO, CaO, Na_2O, K_2O, P_2O_5 and LOI with a measurement accuracy superior to 0.2–0.3 wt% relative.

4. Experimental results

4.1. Attainment of equilibrium

When performing experiments to test the thermodynamic behaviour of a system the attainment or close approach to equilibrium is an evident prerequisite. Samples were heated to near-liquidus temperatures and held for 3 h to homogenize the melt and eliminate relict crystals of the 5Q-92 enclave. The method was mostly successful except for very few and small (<10 μm) relict plagioclase cores in D20–8 enclave experiment and some corundum cores in experiments with the synthetic glass. In addition, even if reversal experiments were not performed, there is evidence that suggest equilibrium was attained. Most of the experiments have a large proportion of liquid (up to 80% in the highest temperature runs) and show a positive corelation between fraction of liquid and temperature. The evolution of major elements is consistent with varying intensive parameters, resembling a differentiation trend. In the whole set of runs silica increases when decreasing temperature, while #Mg and Ca steadily decrease when decreasing temperature (Fig. 3). Phases are usually euhedral and manifest well developed mineral faces. They also showcase standard deviations of less than 2% relative for all the major

Table 1
Composition of the starting materials.

	Starting materials		Model compositions	
	Synthetic glass	5Q-92	Pilbara Suite[1]	Superior Province[2]
SiO_2	54.71	60.36	61.86	58.95
TiO_2	1.35	0.88	0.51	0.54
Al_2O_3	20.57	15.59	14.48	17.79
FeOt	7.27	6.03	5.64	5.22
MgO	4.38	4.30	4.17	4.58
MnO	0	0.13	0.08	0.10
CaO	4.85	5.34	4.67	4.94
Na_2O	3.28	3.97	3.91	4.21
K_2O	3.60	2.17	1.8	3.1
P_2O_5	0	0.52	0.24	0.30
LOI	–	0.7	2	–
Total	100	100	97.36	99.73

Composition recalculated to an anhydrous base. Synthetic glass starting material contains 3 wt% H_2O as $Al_2(OH)_3$. Total iron as FeO.

[1] Pilbara suite sanukitoid; Smithies and Champion (2000).

[2] Roaring River Valley Complex. Canadian Superior Province; Stern et al. (1989).

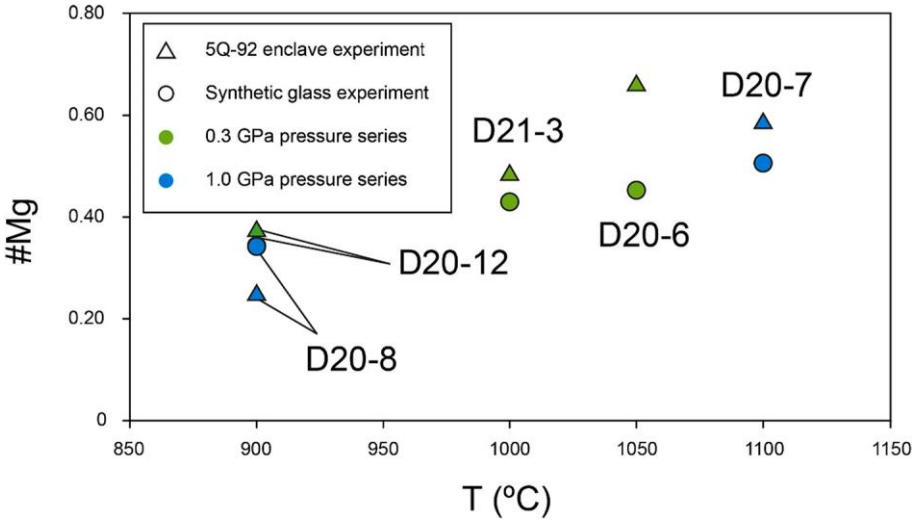

Fig. 3. Variation of the #Mg [= molar MgO/(MgO + FeO^T)] with temperature of experimental runs. Regular decrease in #Mg when decreasing T indicates that thermodynamic equilibrium was achieved. The phase contributing to the increase in #Mg as melting progresses is essentially orthopyroxene.

components and less than 10% for the accessory phases (except D21-3 run, see Section 4.2). As an additional test, experimental conditions were calculated with orthopyroxene-liquid thermometry (Putirka, 2008). Calculated conditions using this method were accurate, with temperatures within a range of ±10 ˚C and pressures of ±0.1 GPa. Likewise, we used the same approach to test the existence of thermal gradients in some experiments by using Opx–liquid pairs of each end of the capsule. A maximum of 20 ˚C difference was revealed, which is negligible for the purpose of testing the cotectic behaviour of a system, but enough to justify the small variations in the thermo-barometric calculations. Since double capsule experiments were performed using QFM buffer, oxygen fugacity was measured at about ΔQFM ±1 using the Mgt-liquid equilibrium (Arató and Audétat, 2017), excepting for D20–12 that showcases an fO_2 of nearly ~QFM +3 (Table 2).

Nevertheless, even if there are strong inferences to assume equilibrium was attained, there are some other considerations worth mentioning. Clinopyroxene tend to nucleate around orthopyroxene with 5Q-92 starting composition, resulting in mixed pyroxene aggregates (Fig. 4). However, most crystals are still euhedral to subhedral, and glass compositions are consistent with their synthetic glass starting material counterparts, which never show this kind of crystal zoning. It is also worth noting this kind of peritectic reaction is also observed in rocks, where orthopyroxene is commonly being consumed to form clinopyroxene around it. For these reasons, it is unlikely that this phenomenon has had any significant effect on the phase equilibria.

4.2. Experimental results

Synthesized products consist of mostly homogenous glass and mineral assemblages that include plagioclase and orthopyroxene as ubiquitous phases, and varying proportions of clinopyroxene, biotite, olivine, magnetite, ilmenite, spinel and apatite (Table 2). Relic corundum left after the addition of $Al(OH)_3$ as water carrier was observed in all the synthetic glass runs. However, its proportions are always lower than 1% and its effects on the bulk composition of the system may be negligible. Glass and phase proportions were determined by least-square multiple regression, balancing the bulk chemical composition of the sample with the optimal proportions of the run products (Fig. 5). Calculations were performed using the Solver tool of the Microsoft Excel® spreadsheet MINSQ (Herrmann and Berry, 2002). For some of the runs, image analysis was the preferred method due to better accuracy of the modal estimations. Compositional images (back scattered electron images) and ImageJ software (Rasband, 1997-2018) were used in the latest case, followed by a final mass balance adjustment. Reliability of the results is supported by standard deviations lower than unity for most of the product glass compositions for key elements

Table 2
Experimental conditions and assemblages.

Run	P (GPa)	T (˚C)	Duration (h)	Cooling ramp (˚C/h)	Starting material	log fO_2 (±ΔQFM)	Phase assemblage and proportions (wt%)
D21-3	0.3	1050	13	30	5Q-92 Enclave	−0.4	Gl (68) + Opx (5) + Cpx (6) + Pl (17) + Ap (<1) Mgt[3] (4)[2]
					Synthetic glass	−0.8	Gl (68) + Opx (6) + Ol (2) + Pl (19) + Ilm (1) + Mgt[3] (4)[2]
D20-6	0.3	1000	29	10	5Q-92 Enclave	+0.8	Gl (58) + Opx (9) + Cpx (10) + Pl (23) + Ap (<1) + Mgt[3] (4)[2]
					Synthetic glass	+0.1	Gl (65) + Opx (11) + Pl (18) + Sp (3) + Ilm (3)[1]
D20-12	0.3	900	29	10	5Q-92 Enclave	+2.9[4]	Gl (46) + Opx (6) + Cpx (10) + Ol (2) + Pl (32) + Mgt (3)[1]
					Synthetic glass	+2.7[4]	Gl (43) + Opx (2) + Ol (8) + Pl (39) + Mgt (3) + Sp (5)[1]
D20-7	1.0	1100	28	10	5Q-92 Enclave	+0.9	Gl (71) + Opx (7) + Cpx (6) + Pl (13) + Ap (<1) + Mgt (3)[2]
					Synthetic glass	−0.4	Gl (81) + Opx (3) + Ol (1) + Amp (4) + Bt (3) + Pl (5) + Sp (2) + Ilm (1)[2]
D20-8	1.0	900	41	10	5Q-92 Enclave	+0.3	Gl (44) + Opx (8) + Cpx (10) + Pl (34) + Mgt (4)[2]
					Synthetic glass	−0.5	Gl (39) + Opx (6) + Bt (14) + Pl (36) + Mgt (5) + Sp (<1)[1]

Phase abbreviations are as follows: Gl, glass; Opx, orthopyroxene; Cpx, clinopyroxene; Ol, olivine; Pl, plagioclase; Mgt, magnetite; Sp, spinel; Ilm, ilmenite; Ap, apatite.

[1] Modal proportion obtained by image analysis via ImageJ software.

[2] Modal proportions obtained by MINSQ spreadsheet (Herrmann and Berry, 2002).

[3] Fictive magnetite added using the analysis of a magnetite of the other starting material that may be either non-observed magnetite, Fe loss or both. Available magnetite of closest experiment using the same starting material was used for each case (e.g. fictive Mgt of D21-3E run used D20-12E Mgt).

[4] Glass measurements for fO_2 estimation performed in small pools, probably causing the analysis to be contaminated by the surrounding phases.

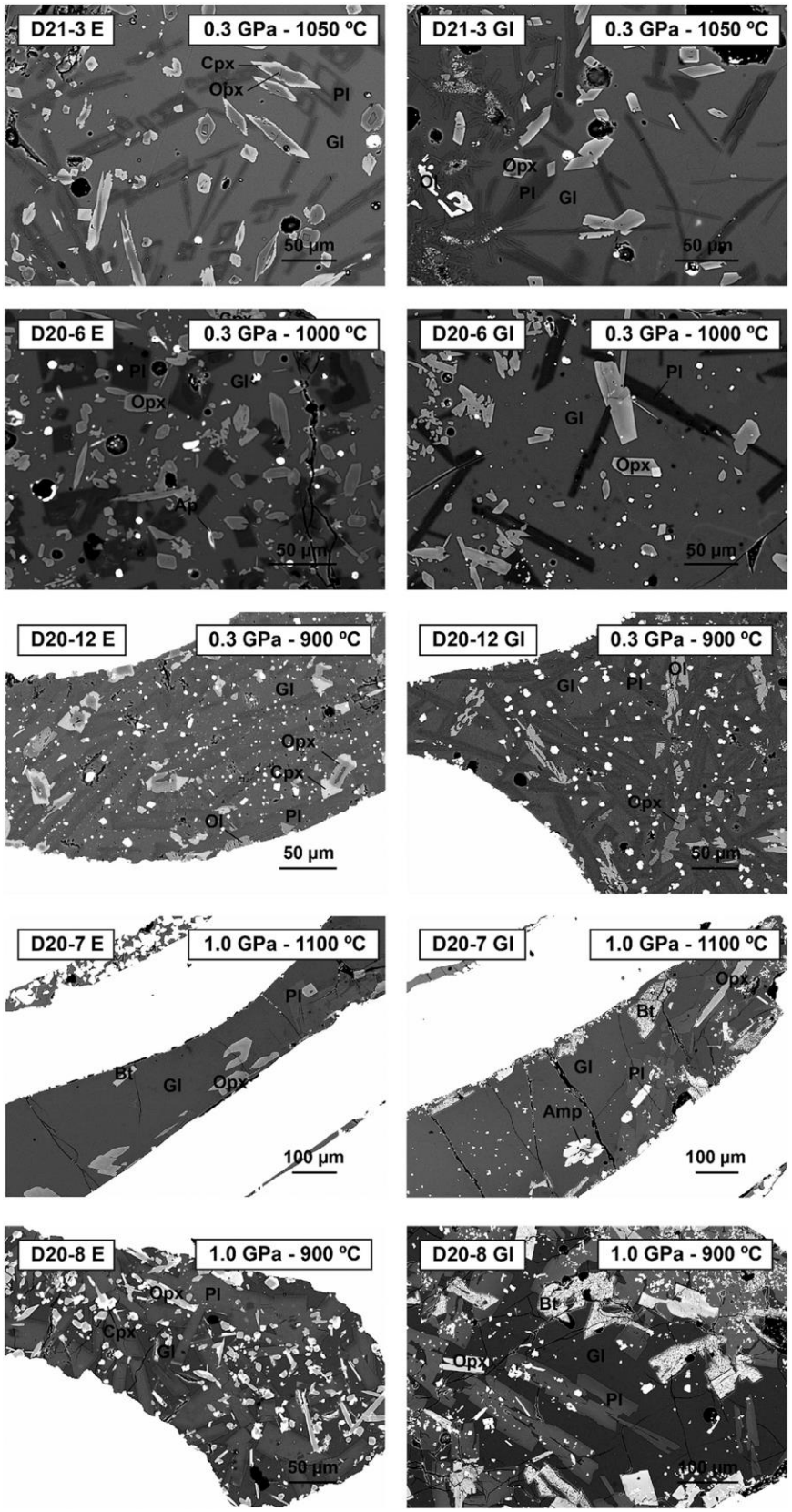

Fig. 4. Backscattered electron images of representative sections of each experimental run. Each image is labelled with run number, starting material (E, 5Q-92 enclave; Gl, synthetic glass) and temperature. Phase abbreviations are as follows: Gl, glass; Opx, orthopyroxene; Cpx, clinopyroxene; Ol, olivine; Amp, amphi- bole; Bt, biotite; Pl, plagioclase.

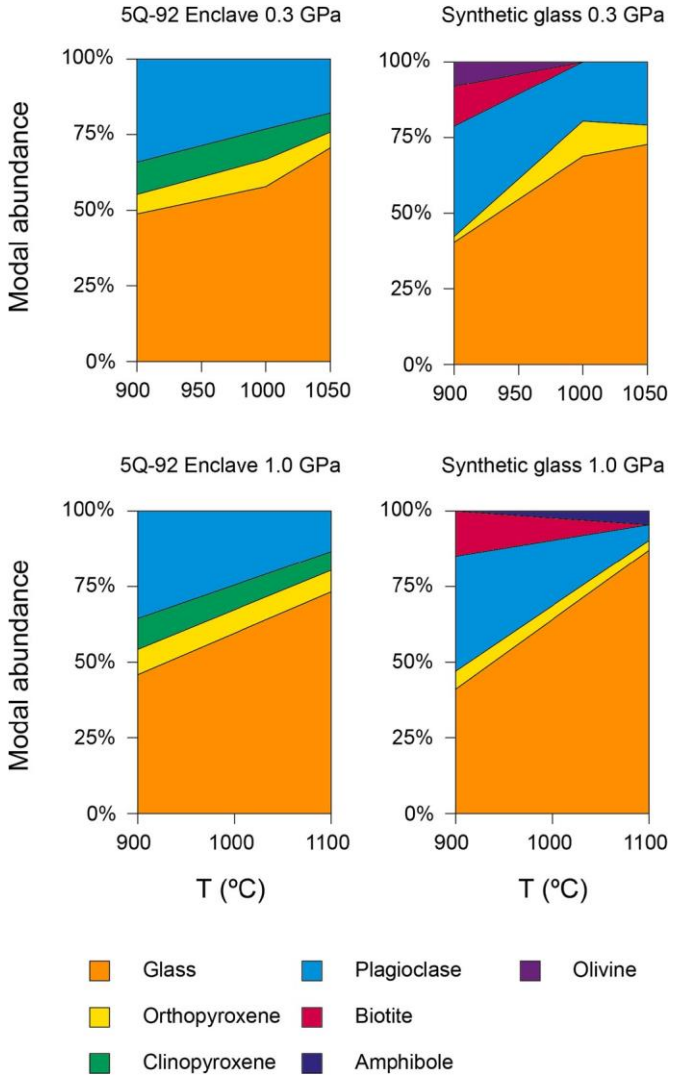

Fig. 5. Variations in modal proportions with temperature in the experimental runs.

such as Ca, Mg or K. Higher standard deviations are an exception for some of the glasses and mineral phases, and particularly D21-3, which shows the largest deviations (slightly above 1%). These are the consequence of the existence of a thermal gradient inside the long, double capsule assemblies. It is worth mentioning that all the measured glass compositions for each capsule follow a linear trend which resembles a differentiation trend following the sanukitoid array density maxima (Fig. 6). Since this experimental work is oriented to determine the composition of cotectic liquids, the existence of such small thermal gradient do not invalidate the results, but further support the idea that the obtained liquids follow a cotectic array. Exact temperature measurement is irrelevant since the purpose is to see whether the quenched liquids follow a sanukitoid cotectic array or not. The fact that these variations are systematic with a temperature gradient in a linear path and the coherence of the most variable results within the whole context supports the reliability of D21-3. Furthermore, the latest being the experiment with the largest variability and gradient, and still in agreement with the rest of the results, further supports the consistency of the experimental results. Extrapolation of the linear trend displayed by the experimental glasses also intersect the starting materials (Fig. 6). Regarding mineral phases, most of them are also homogeneous. Higher standard deviations for oxides are due to analytical uncertainties given the small size of the crystals. The high Al_2O_3 of orthopyroxene can be partially explained by the high alumina content of the starting materials, particularly the synthetic glass (similar to that of a high alumina basalt), and partially explained by heterogeneous nucleation of orthopyroxene over high-Al spinel. Nevertheless, differences in the alumina content do not affect the orthopyroxene/liquid Fe/Mg partitioning, evidenced by the constant #Mg of the orthopyroxene when comparing runs at the same temperature (compare for instance Opx of D20-8; Fig. 3).

Due to the presence of magnetite in some of the experiments, precise calculations using mass balance is not a reliable method for estimating the exact Fe loss. Mass balance using magnetite cannot differentiate Fe redox state. Since ±1% of modal magnetite has an amount of Fe equal to a hypothetical ±10 wt% relative of Fe loss, mass balance can overestimate magnetite to compensate the actual Fe loss. Contrarily, calculations with experiments with no observed magnetite may result in Fe loss maximums of ~30 wt% relative that partially can be unobserved magnetite. Excluding a few cases, mass balance calculations improve when a fictive magnetite is added, including elements that are not present in the magnetite, leading to residuals near unity. For this reason, a fictive magnetite phase using the composition of the closest temperature run using the same starting material is utilized for the mass balance calculations in experiments that lack such phase and show such Fe loss maximums, regardless of it being non-observed magnetite, Fe loss or both. This uncertainty cannot be quantitatively solved. However, experiments with analysed magnetite suggest that, even if part of that low percentage was Fe loss, it would not exceed ~15 wt% relative. It is only expectable that the rest of the experiments using the same methodology will have roughly similar Fe loss. Moreover, preventive methods were performed to minimize Fe loss. For these reasons, inferences suggest Fe loss was not significant regarding phase equilibria.

Major element compositions of the experimental glasses and phases are given in Table 3. Modifying temperature only induces different melt compositions along the cotectic line. However, differences between the two pressure series products are more remarkable. 1.0 GPa pressure series perfectly fall in the calc-alkaline experimental cotectic, but more interestingly, all experimental liquids from 0.3 GPa pressure series fit into a logarithmic curve that represents the main sanukitoid cotectic array in the CaO–MgO diagram (Fig. 6). 0.3 GPa experimental liquids fall within the ranges of sanukitoid series density maximum for CaO–MgO diagram, and follow their tendency shown in the Or–An–En diagram. D20–12 is the lowest temperature experiment, and thus produced a granitic melt (SiO_2 > 63 wt%) which is distant from the density maximum but follow the sanukitoid array. The rest of the melts for the 0.3 GPa pressure series are mostly andesitic (SiO_2 = ~60%) but show some variation due to the temperature gradient in the assemblies. It is also worth noting that the adjusted logarithmic curve perfectly follows the density maximum in the CaO–MgO diagram for the whole world series.

5. Discussion

Results from this study put in value the role of pressure in the thermodynamic behaviour of the sanukitoid system. 1.0 GPa pressures, proxying the conditions of the lower crust, produce standard, Andean-type calc-alkaline differentiates. However, 0.3 GPa runs provide undeniable evidence of the existence of a low pressure sanukitoid cotectic liquid line of descent. Relatively similar experimental compositions between 1000 °C and 1050 °C are coherent with the crystallinity curve of the system, with a drastic increase in crystallinity of >20% below 1000 °C. Likewise, crystallization of clinopyroxene at expense of orthopyroxene not only is not a sign of disequilibrium, but an observed common feature of sanukitoid rocks. Orthopyroxene-clinopyroxene peritectic reaction likely starts at 1100 °C, nearly 100 °C below the estimated liquidus of the system. Clinopyroxene has crystallized only in experiments using 5Q-92 enclave, probably due to the higher proportion of CaO compared to that in the synthetic glass. Instead, biotite is only present in the 1.0 GPa synthetic glass runs. An explanation may be

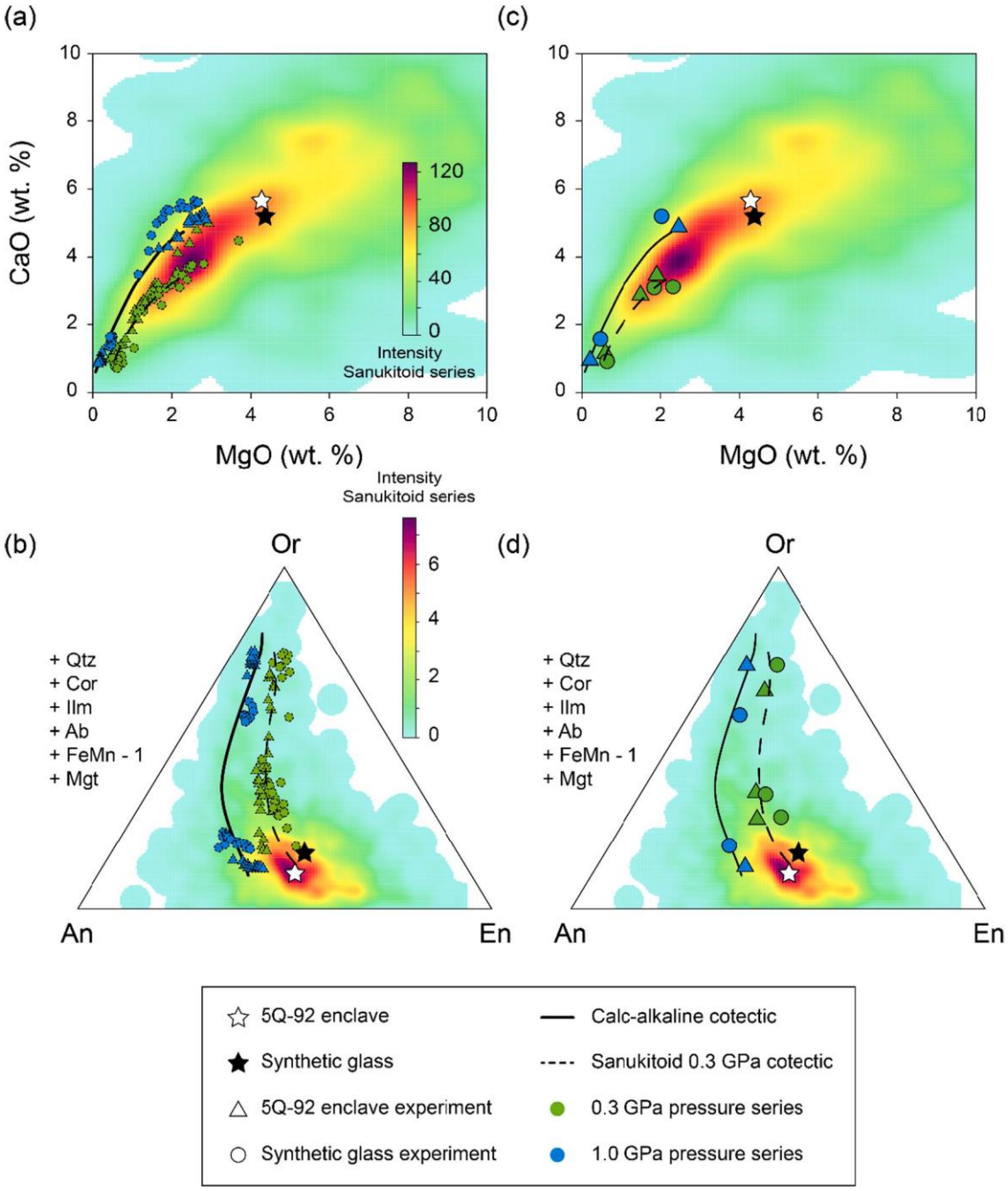

Fig. 6. Comparison of sanukitoids and Andean-type calc-alkaline series with experimental liquids. a) and b) individual glass measurements; c) and d) average for each temperature run. Dashed line represents the tendency curve of the glasses fitted to a logarithmic fit. Note the curve follows the maxima of the sanukitoid Kernel density diagram (background). Extrapolation of the tendency curve also intersect the starting materials.

synthetic glass has higher abundance of FeO and Al_2O_3, and its experiments are characterized by higher Al_2O_3 contents in all phases regardless of the pressure, the only exception being D20-7 E, that also displays high Al_2O_3.

Initially, two hypotheses were established concerning the sanukitoid distinct series geochemistry. The series may either be the result of (1) cotectic differentiation or (2) calc-alkaline differentiation deviated by a ubiquitous process. Since low pressure differentiation has been proved to consistently segregate high-Mg and low-Ca sanukitoid-type melts, it can be in principle assumed that this as a potential cause for such geochemical features. However, even if the results seem to point in a single direction, shallow emplacement and differentiation, as the only mechanism responsible for the sanukitoid series, has some drawbacks worth discussing. For this reason, both initial hypotheses will be reviewed in the following lines.

5.1. *Hypothesis 1: differentiation at low pressure*

The first possibility for sanukitoid signature is also the most immediate regarding the results of the experiments, in which, sanukitoid series are controlled by low-pressure differentiation. That is, the behaviour of the system is thermodynamically fixed by a cotectic liquid line of descent (Fig. 7). Moreover, obtained granitic melt from D20–12 run provides significant evidence that the series can produce granites. This is of special value considering that a mantle-derived andesitic system can be responsible for the generation of volumetrically

Table 3
Electron microprobe analyses of the experimental products.

Run	P (GPa)	T (°C)	Phase	n	SiO_2	TiO_2	Al_2O_3	FeO^T	MnO	MgO	CaO	Na_2O	K_2O	P_2O_5	F/LOI	Total	#Mg
5Q-92 Enclave																	
21-3 E	0.3	1050	Gl	10	63.12	1.17	16.42	1.68	0.09	1.82	3.36	4.22	3.60	0.61		96.23	0.66
					2.58	*0.16*	*0.52*	*1.00*	*0.04*	*0.78*	*1.33*	*0.14*	*0.55*	*0.25*		*0.52*	
			Opx	11	55.71	0.35	2.93	6.36	0.36	31.68	2.20					99.59	0.90
					0.69	*0.06*	*0.76*	*0.24*	*0.04*	*1.02*	*0.54*					*0.46*	
			Cpx	9	51.89	1.10	4.20	4.04	0.33	18.42	19.37	0.34		0.11		99.98	0.89
					1.19	*0.40*	*1.27*	*0.53*	*0.03*	*1.34*	*1.44*	*0.04*		*0.07*		*0.46*	
			Ol	1	39.25	0.03	0.08	10.28	0.33	48.34	0.17		0.03	1.24		99.84	0.89
			Pl	6	56.91	0.13	27.35	0.29	0.02	0.13	9.50	5.63	0.49	0.09		100.75	0.44
					0.51	*0.03*	*0.37*	*0.03*	*0.01*	*0.04*	*0.36*	*0.28*	*0.04*	*0.04*		*0.46*	
			Ap	2	29.26	0.54	7.71	0.63	0.06	0.94	31.71	0.57	1.17	24.78	2.87	99.05	0.72
					6.69	*0.08*	*1.99*	*0.09*	*0.02*	*0.01*	*6.00*	*0.21*	*0.19*	*4.51*	*0.08*	*1.33*	
20-6 E	0.3	1000	Gl	13	61.29	1.66	16.46	2.67	0.09	1.41	2.73	3.69	4.11			94.57	0.48
					1.04	*0.20*	*0.45*	*0.52*	*0.02*	*0.33*	*0.39*	*0.12*	*0.08*			*0.51*	
			Opx	12	52.88	0.43	2.36	13.82	0.42	26.94	2.20					99.07	0.78
					0.71	*0.11*	*0.52*	*0.98*	*0.04*	*0.60*	*0.48*					*0.84*	
			Cpx	2	51.82	0.49	2.92	6.80	0.38	19.81	15.32	0.52				98.06	0.84
					0.17	*0.08*	*0.22*	*0.80*	*0.01*	*0.06*	*1.23*	*0.05*				*0.30*	
			Pl	9	56.74	0.07	26.34	0.21			7.73	6.31	0.77			98.15	0.00
					1.26	*0.03*	*0.87*	*0.08*			*0.89*	*0.47*	*0.31*			*0.32*	
			Ap	3	0.47	0.07	0.04	0.35	0.06	0.08	54.79	0.07	0.11	40.91	4.53	99.57	0.28
					0.08	*0.04*	*0.02*	*0.13*	*0.01*	*0.05*	*0.86*	*0.02*	*0.05*	*0.26*	*1.09*	*0.89*	
20-12 E	0.3	900	Gl	8	69.08	1.12	14.25	1.70	0.05	0.57	1.14	3.54	5.72	0.41		97.90	0.37
					0.42	*0.07*	*0.13*	*0.13*	*0.02*	*0.12*	*0.18*	*0.38*	*0.09*	*0.10*		*0.51*	
			Opx	6	53.35	0.41	3.60	10.86	0.42	29.48	1.98					100.11	0.83
					0.94	*0.09*	*1.01*	*0.78*	*0.11*	*0.70*	*0.30*					*0.60*	
			Cpx	13	48.43	1.46	5.42	9.07	0.36	15.37	18.80	0.47		0.15		99.54	0.75
					1.05	*0.32*	*1.01*	*0.34*	*0.07*	*1.07*	*1.08*	*0.05*		*0.07*		*0.24*	
			Ol	10	39.17	0.02	0.06	14.72	0.52	44.83	0.16			0.68		100.15	0.84
					0.27	*0.01*	*0.02*	*0.45*	*0.08*	*0.39*	*0.01*			*0.16*		*0.41*	
			Pl	9	57.29	0.12	26.18	1.16			9.00	5.90	0.63	0.06	0.02	100.35	0.00
					0.49	*0.03*	*0.37*	*0.09*			*0.48*	*0.20*	*0.05*	*0.01*		*0.33*	
			Mgt	7	0.22	8.42	2.47	73.28	0.82	5.21	0.12	0.04	0.08	0.02	0.04	91.10	0.11
					0.10	*0.43*	*0.13*	*0.65*	*0.12*	*0.18*	*0.03*	*0.05*	*0.01*	*0.02*	*0.04*	*0.80*	
D20-7 E	1.0	1100	Glass	17	56.51	1.02	19.82	2.79	0.11	2.24	4.50	2.44	1.81			91.25	0.59
					0.77	*0.09*	*0.58*	*0.08*	*0.03*	*0.33*	*0.33*	*0.14*	*0.11*			*0.76*	
			Opx	9	49.70	0.61	10.12	9.33	0.33	28.46	0.81					99.36	0.84
					0.87	*0.07*	*1.03*	*0.44*	*0.04*	*0.62*	*0.14*					*0.71*	
			Bt	5	36.92	4.32	16.83	7.23	0.06	19.45	0.06	1.07	8.07			94.01	0.83
					1.35	*0.38*	*0.59*	*0.62*	*0.03*	*1.05*	*0.02*	*0.08*	*0.46*			*1.10*	
			Pl	8	53.11	0.06	29.65	0.25			10.94	4.82	0.34			99.17	0.00
					0.52	*0.04*	*0.18*	*0.05*			*0.42*	*0.23*	*0.03*			*0.41*	
			Ilm	2	20.91	64.32	7.53	1.68	0.04	0.52	1.61	0.72	0.38			97.71	0.36
					8.62	*14.61*	*1.84*	*0.24*	*0.01*	*0.24*	*0.07*	*0.26*	*0.12*			*3.73*	
			Sp	2	3.97	0.35	53.02	15.11	0.24	16.32	0.53	0.12	0.17			97.35	0.66
					4.25	*0.12*	*3.01*	*0.26*	*0.01*	*2.29*	*0.69*	*0.14*	*0.22*			*5.23*	
D20-8 E	1.0	900	Glass	11	68.67	0.20	13.33	1.10	0.07	0.18	0.90	2.56	5.03			92.16	0.22
					0.59	*0.02*	*0.32*	*0.07*	*0.02*	*0.03*	*0.08*	*0.13*	*0.16*			*0.43*	
			Opx	10	51.58	0.35	3.79	13.04	0.39	27.12	2.04					98.30	0.79
					0.93	*0.08*	*0.82*	*1.57*	*0.07*	*1.04*	*0.27*					*1.20*	
			Cpx	9	49.99	0.72	3.86	9.26	0.40	16.69	16.74	0.53	0.05			98.33	0.76
					0.83	*0.19*	*0.87*	*0.52*	*0.04*	*1.23*	*0.93*	*0.06*	*0.02*			*0.63*	
			Pl	20	56.15	0.06	26.86	0.41			8.23	6.12	0.77			98.60	0.00
					2.05	*0.04*	*1.11*	*0.14*			*1.33*	*0.65*	*0.26*			*0.66*	
			Mgt	5	0.77	29.85	0.59	60.36	0.58	1.27	0.38	0.04	0.13			93.99	0.04
					0.48	*1.77*	*0.07*	*1.50*	*0.08*	*0.21*	*0.41*	*0.02*	*0.02*			*0.43*	
Synthetic glass																	
21-3 Gl	0.3	1050	Gl	7	60.10	1.24	17.42	4.75		2.20	2.83	2.71	4.47			95.83	0.45
					3.30	*0.30*	*0.62*	*1.43*		*0.79*	*1.02*	*0.15*	*0.73*			*0.46*	
			Opx	11	49.30	0.90	9.63	14.11		25.52	0.67	0.09	0.06			100.36	0.76
					0.67	*0.19*	*0.95*	*1.12*		*0.95*	*0.10*	*0.15*	*0.05*			*0.33*	
			Ol	4	38.01	0.06	0.07	22.55		39.28	0.12					100.09	0.76
					0.43	*0.02*	*0.05*	*0.86*		*0.60*	*0.02*					*0.68*	
			Pl	7	51.31	0.13	30.80	0.84		0.18	12.96	3.52	0.54			100.00	0.41
					0.45	*0.07*	*0.36*	*0.11*		*0.10*	*0.62*	*0.08*	*0.11*			*0.63*	
			Ilm	2	6.34	48.39	2.58	34.60		7.51	0.42	0.27	0.49			100.67	0.27
					2.09	*0.92*	*0.18*	*4.74*		*2.03*	*0.013*	*0.20*	*0.15*			*0.92*	
20-6 Gl	0.3	1000	Glass	18	58.15	1.38	18.82	4.11		1.73	2.91	2.85	4.53			94.47	0.43
					1.50	*0.42*	*0.43*	*0.35*		*0.45*	*0.48*	*0.07*	*0.12*			*0.58*	
			Opx	12	49.01	0.60	8.72	13.23		26.92	0.92					99.40	0.78
					1.43	*0.15*	*2.03*	*0.97*		*1.08*	*0.21*					*0.60*	
			Pl	8	52.02	0.08	29.38	0.45			11.33	4.30	0.77			98.33	0.00
					0.57	*0.02*	*0.50*	*0.07*			*0.37*	*0.28*	*0.08*			*0.27*	

(*continued on next page*)

Table 3 (*continued*)

Run	P (GPa)	T (°C)	Phase	n	SiO_2	TiO_2	Al_2O_3	FeO^T	MnO	MgO	CaO	Na_2O	K_2O	P_2O_5	F/LOI	Total	#Mg
			Ilm	1	1.62	43.93	1.90	40.49		5.70	0.38	0.09	0.32			94.43	0.20
			Sp	2	0.75	0.50	59.21	21.47		16.23	0.09	0.05	0.09			98.39	0.57
					0.59	*0.05*	*0.33*	*0.75*		*0.22*	*0.01*	*0.05*	*0.02*			*0.24*	
20-12 Gl	0.3	900	Gl	9	67.66	1.09	16.02	2.09		0.62	0.89	3.04	7.32			98.72	0.34
					0.94	*0.18*	*0.40*	*0.20*		*0.08*	*0.12*	*0.09*	*0.16*			*0.42*	
			Opx	5	48.89	0.89	8.70	13.99		26.43	0.68					99.58	0.77
					0.50	*0.20*	*0.33*	*1.07*		*0.51*	*0.07*					*0.47*	
			Ol	9	37.93	0.09	0.19	23.86		38.32	0.13					100.52	0.74
					0.57	*0.09*	*0.12*	*0.45*		*0.79*	*0.02*					*0.52*	
			Pl	7	53.68	0.12	28.69	0.67			11.20	4.52	0.88			99.76	0.00
					1.02	*0.02*	*1.08*	*0.07*			*1.04*	*0.44*	*0.23*			*0.45*	
			Sp	4	0.84	2.20	43.68	36.42		12.42	0.08	0.03	0.08			95.74	0.38
					0.89	*0.56*	*4.18*	*4.48*		*1.99*	*0.03*	*0.01*	*0.04*			*1.34*	
			Mgt	8	0.56	10.48	11.41	64.81		5.69	0.13	0.05	0.12		0.07	93.23	0.14
					0.46	*2.11*	*3.59*	*5.73*		*0.96*	*0.09*	*0.05*	*0.03*		*0.03*	*1.82*	
D20-7 Gl	1.0	1100	Glass	17	56.10	1.06	19.47	3.36		1.88	4.82	3.12	3.07			92.87	0.50
					1.37	*0.20*	*0.38*	*0.19*		*0.44*	*0.56*	*0.34*	*0.41*			*0.78*	
			Opx	8	49.21	0.80	9.13	11.49		27.11	1.26					98.99	0.81
					0.50	*0.16*	*0.71*	*0.65*		*0.79*	*0.36*					*0.47*	
			Ol	3	38.79	0.03	0.05	16.45		44.54	0.11					99.96	0.83
					0.63	*0.02*	*0.01*	*1.18*		*0.16*	*0.00*					*0.53*	
			Amp	8	39.68	3.63	16.58	9.81		13.30	10.73	2.15	1.16			97.05	0.71
					0.66	*0.59*	*0.59*	*0.62*		*0.41*	*0.36*	*0.10*	*0.17*			*0.60*	
			Bt	10	36.81	4.83	17.79	9.13		16.76	0.10	0.83	9.01			95.26	0.77
					0.98	*0.48*	*0.46*	*1.46*		*1.25*	*0.12*	*0.10*	*0.29*			*0.86*	
			Pl	10	55.01	0.05	28.28	0.46			10.33	5.11	0.58			99.82	0.00
					0.67	*0.03*	*0.51*	*0.03*			*0.26*	*0.18*	*0.05*			*0.43*	
			Sp	7	0.18	0.37	62.17	15.51		19.43	0.06	0.02	0.03			97.75	0.69
					0.08	*0.04*	*2.01*	*0.75*		*0.78*	*0.02*	*0.01*	*0.01*			*2.07*	
			Ilm	1	4.11	48.40	1.98	36.53		7.22	0.47	0.20	0.24			99.17	0.26
D20-8 Gl	1.0	900	Glass	10	64.38	0.20	14.97	1.41		0.41	1.41	3.08	4.36			90.21	0.34
					1.06	*0.09*	*0.45*	*0.08*		*0.03*	*0.11*	*0.11*	*0.07*			*0.64*	
			Opx	9	48.10	0.67	9.76	13.16		26.62	1.15					99.46	0.78
					0.70	*0.09*	*0.92*	*0.27*		*0.48*	*0.20*					*0.41*	
			Bt	12	36.23	5.04	17.12	11.13		16.37	0.04	0.66	9.17			95.76	0.72
					0.37	*0.59*	*0.65*	*0.72*		*0.58*	*0.03*	*0.03*	*0.15*			*0.48*	
			Pl	10	53.36	0.07	28.98	0.49			10.52	4.89	0.68			98.99	0.00
					1.17	*0.03*	*0.67*	*0.08*			*0.83*	*0.51*	*0.06*			*0.29*	
			Mgt	7	0.37	15.50	5.47	70.16		2.12	0.15	0.07	0.07			93.88	0.05
					0.32	*11.49*	*4.40*	*6.75*		*1.19*	*0.11*	*0.07*	*0.02*			*0.77*	
			Sp	1	0.47	0.54	53.92	32.17		10.92	0.05	0.03	0.08			99.27	0.38

n, number of analyses. Numbers in italics below each wt% are standard deviations. Higher standard deviations in oxides are due to the small size of the crystals.

meaningful granitic bodies. Considering the tendency shown by the experiments we can also assume the series will match the granite minimum at lower temperatures, sharing a eutectic composition with calc-alkaline batholiths. A eutectic fixed composition for the differentiation products of two different parental magmas implies well-known granites may have resulted from either of them. Further criteria must be developed to distinguish between calc-alkaline granites and sanukitoid granites.

Nevertheless, while shallow depth differentiation will most likely account for some of the cases, there are strong arguments against this being the principal cause of the whole series. Even where large intrusions are described (e.g. those in the Karelian province, the Caledonian province or the French Massif Central), ultra-mafic rocks potentially representing cumulates are scarce. Only a few local ultra-mafic dikes and small plutons are described in some specific places, such as the Karelian province in the Baltic Shield (Lobach-Zhuchenko et al., 2005, 2008), Caledonian province (Fortey et al., 1994) and the Iberian Massif of Spain (Galán and Suárez, 1989). They are referenced to as 'cortlandtites' (Bender et al., 1982), and are described as olivine, orthopyroxene and amphibole-rich rocks, with little to no plagioclase. Note that the occurrence of these ultra-mafic bodies is anecdotic compared to the volume of sanukitoid plutons, and the latest being a consequence of low-pressure differentiation inherently implies more abundant cumulates. Moreover, since residues are colinear with the differentiation path, a Ca-richer composition is invoked for the cumulates (see 0.3 GPa experimental residues having CaO ≈ 10 wt% in CaO – MgO diagram in Fig. 7). Cortlandtites are mainly constituted by Mg-rich minerals and have plagioclase in accessory proportions at best, not matching this hypothetical composition.

Another fundamental problem with differentiation of sanukitoids to produce granites is their initial water contents. Intermediate rocks are a common feature in Andean-type batholiths, mostly characterized by having euhedral amphibole. This denotes high initial water contents for the parental magma of these rocks of up to 6 wt%, as such is required for a near-liquidus precipitation of amphibole. Fractionation of such parental magma implies that the produced granodiorite, tonalites or granites must showcase water contents higher than 10 wt%, which is totally unrealistic (Castro, 2020).

For these reasons, even if thermodynamics supports the sanukitoid series being the result of differentiation, including granitic terms, there is a severe lack of natural inferences for this hypothesis to be single-handedly responsible for most of the series.

5.2. *Hypothesis 2: restite/cumulate self-contamination*

The second hypothesis explores the sanukitoid series being the result of contamination of magmas that initially had standard calc-alkaline features. There are two considerations to be made in this regard. First, since a local assimilation process cannot account for a homogeneous and worldwide occurring series, a potential contamination process must be a consequence of an intrinsic characteristic of the sanukitoid system. Thus, contamination with cogenetic solid material (cumulates or restites) can be responsible of the observed geochemical variations. And second, the abundance of cumulates from the sanukitoid array at

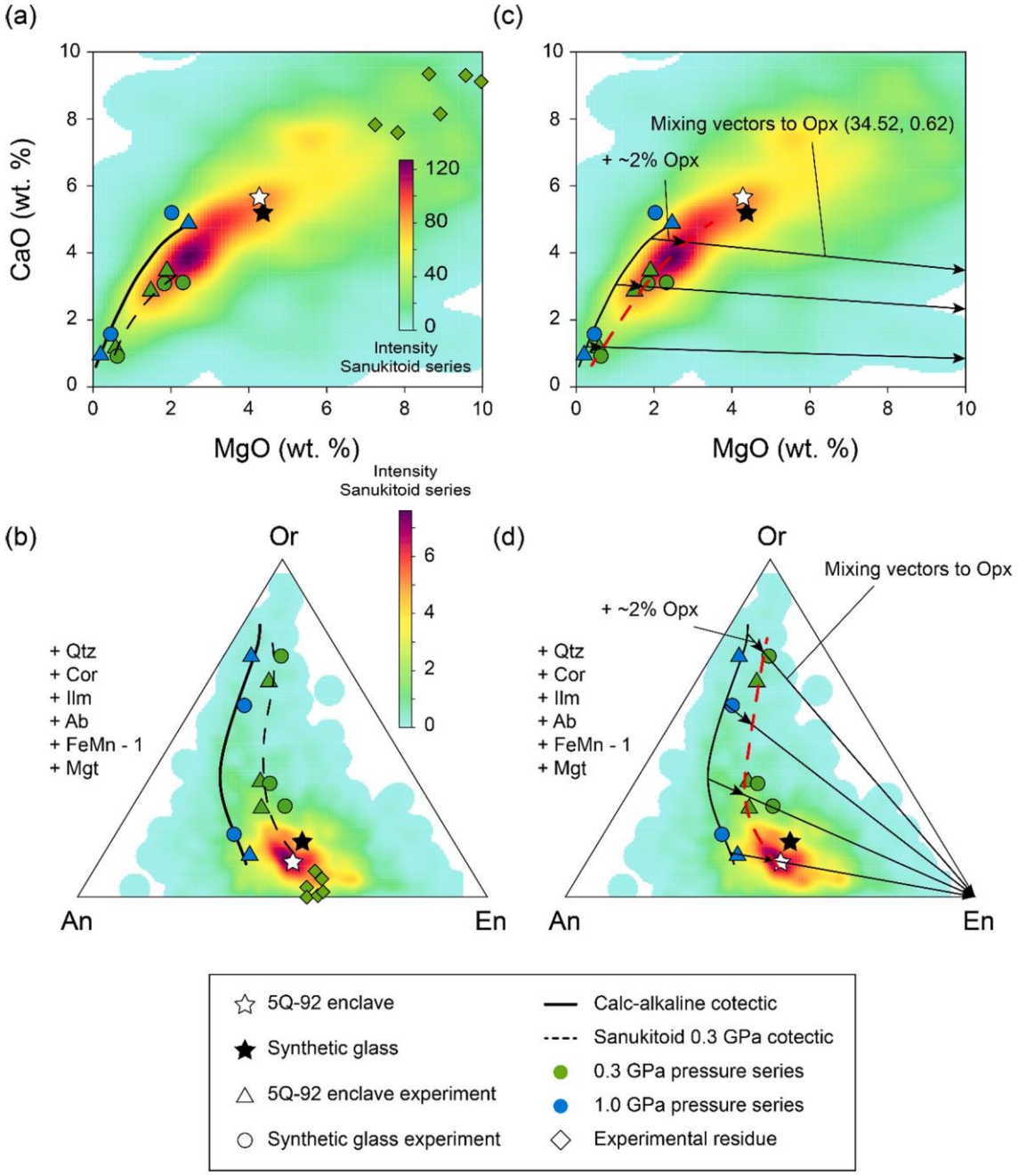

Fig. 7. Comparison diagrams used to illustrate the two discussed hypotheses to explain the sanukitoid geochemistry. a) and b) low-pressure differentiation of a sanukitoid parental magma. Experimental residues fall reasonably well in the sanukitoid field but have up to almost 10 wt% CaO. c) and d) orthopyroxene restite contamination model. Dashed line in red represents the model line obtained by adding 2% Opx to the calc-alkaline cotectic. Tie lines represent the contamination with pure Opx from either an ultramafic source or cumulate. (For interpretation of the references to colour in this figure legend, the reader is referred to the web version of this article.)

shallow depth is trivial compared to the volume of the batholiths or even the sanukitoid plutons, hence the contamination must occur well before the emplacement of the melt. Experimental results proved that a sanukitoid system produce calc-alkaline differentiates at 1.0 GPa. Differentiation of andesitic mantle magmas at such pressure leaves a refractory residue in the lower crust, which is supported by the mafic nature of the lower crust. This also contributes to the CaO depletion of the series via plagioclase fractionation, since granulitic lower crust is mostly CaO enriched. All in all, these factors lead to a unique conclusion: the hypothetical contamination takes place in the source of the melt before and/or during extraction.

When discussing the material that the contamination process took place with, varied accidental rocks from the lower crust are discarded due to the worldwide common and homogeneous features of the series. The only non-variable, intrinsic process to the series that may account for the observed trend is self-contamination. The initially calc-alkaline-like magma mixes with a Mg-rich, Ca-poor material at the early stages of differentiation. Calc-alkaline differentiation residues are colinear with their products as shown by Castro (2021). Thus, mixing lines between calc-alkaline magmas and their residues should follow the calc-alkaline cotectic and cannot account for the trend observed in the sanukitoid series. Given these considerations we find two possibilities for the nature of the contaminating agent.

Assuming a classic model of lower crust melting (Annen et al., 2006),

a melt generated in the lower crust can contaminate with the sanukitoid parental magma to produce high-Mg melts. A potential mix of end members, one being the sanukitoid parental magma and the other being an intermediate melt that falls in the granite minimum, lead to sanukitoid-like compositions. Different proportions between the two may lead to the variability observed in the series. Nevertheless, that hypothetical crustal melt must be at temperatures of around 800 °C to have granitic composition in this system. Assuming a contamination with a sanukitoid parental magma, it must have occurred at the early stages of magma generation since that is the only stage in which the availability of such magma is abundant. In the early stages of magma segregation within this context, temperatures of 800 °C are unlikely to produce a significant volume of crustal melt in the absence of unrealistically high amounts of water. If such proportions of volatiles reached the lower crust and melt it, there will be evidence of euhedral amphibole in rocks from the lower crust and differentiates may be even more water-rich than the parental magma. Contrary to that, most batholiths register low water contents. Thermo-mechanical behaviour of two magma bodies with contrasting temperatures (crustal magma at ~800 °C, sanukitoid magma at ~1150 °C) also stands out as a problem for this model. Thermal diffusion is significantly higher than ionic diffusion (Sparks and Marshall, 1986), and if the two mentioned magmas are in contact sanukitoid may quickly suffer undercooling and drastically rise its crystallinity degree, experimentally proved to happen between 1100 and 1000 °C. This leads to ineffective magma mixing, and magma mingling relations will be abundant. However, evidence point to an effective process, with a variable series that ranges from the most basic terms to the most acid.

According to experimental results and thermodynamic criteria, orthopyroxene is likely the liquidus phase in the sanukitoid system. Experiments have also proved that it is the only ever-present mafic phase. It is plausible to assume that the residues from earliest stages of differentiation are mainly constituted by orthopyroxene, and their abundancy in the lower crust must be high since there is little evidence of them in shallow depths. The already proposed harzburgitic source (Wood and Turner, 2009) further supports the idea of a Mg-rich environment for the early differentiation of this system and is also consistent with the observed CaO depletion of the series. High availability of Mg in the source, especially in the form of orthopyroxene-rich cumulates, is coherent with a self-contamination leading to an apparently Mg-rich liquid line of descent. Concisely, the parental magma carries orthopyroxene cumulates via self-contamination before it even starts to differentiate, geochemically conditioning the future differentiation from the very beginning. Another possibility is the contamination with biotite, an also Mg-rich phase present in metasomatized mantle sources. The efficiency of this contamination process may be quantitatively tested in comparison with that of the orthopyroxene. Using a model composition following calc-alkaline cotectic (e.g. D20-7 Gl run liquid), a contamination with ~10% of average biotite (~13 wt% MgO) is required for the initial composition to move into the sanukitoid cotectic array. More phlogopitic compositions would lead to more efficient reproduction of the high-Mg series with less amount but would also produce excess K_2O. The same operation may be performed using the average composition of experimental orthopyroxene obtained in this work (~28 wt% MgO), testing this way the self-contamination process with residues of the own system. Unsurprisingly this calculation leads to a significantly more efficient contamination process, only requiring a ~ 2% of average orthopyroxene to reproduce the high-Mg signature (Fig. 7). For these reasons, while the contamination with biotite is most certainly occurring given the K_2O abundancy of the series, we find orthopyroxene contamination to be the most efficient process to account for the high-Mg signature. Petrography observations also support this interpretation. Most sanukitoid rocks exhibit abundant amphibole clots (Castro and Stephens, 1992) that likely were initially orthopyroxene aggregates. Likewise, orthopyroxene-rich autoliths abundance agrees with these considerations, being the non-digested remanent of the initial contaminating agent and having the same composition as the sanukitoid magmas.

5.3. Compatibility of the models

The above-discussed hypotheses are by no means incompatible since experimental results prove that fractional crystallization of a sanukitoid mafic magma segregates high-Mg differentiates which follow a cotectic path. The mixing proportion with cumulates determines the degree of deviation of the melt from the Andean-type, calc-alkaline trend. Furthermore, if a fast extraction of a nearly uncontaminated melt takes place and it evolves in shallower depths, the apparent trend observed would be the same as a cumulate contaminated sanukitoid melt, although the main cause of its geochemistry would be drastically different.

The thermodynamic value of a low-pressure cotectic line is beyond the origin of the sanukitoid series. This experimental work puts in value the importance of low-pressure cotectic systems as re-equilibration agents during magma emplacement. When a supposedly restite contaminated magma from a metasomatized mantle reaches shallow depths, no matter how much excess MgO in the form of orthopyroxene it brings from the source, the low-pressure system will re-equilibrate the liquid into a Mg-rich cotectic composition, thus dissolving all restitic phases into the liquid. Note this process is not utterly efficient since it would take ideal emplacement conditions and a long period of time to wholly homogenize such melt. It is only expectable for it to have remnant restitic orthopyroxene, which will constitute the amphibole clots in the future. Such incongruent process would produce observable geochemical variations in the emplaced magma. This, together with the already highly variable restite contamination process ultimately accounts for the high heterogeneity of the series. The significant aspect of this argumentation is an initially heterogenous melt is capable of ideally re-homogenize and re-equilibrate in shallow depth during magma emplacement due to the existence of the low-pressure sanukitoid cotectic system.

6. Concluding remarks

Experiments with sanukitoid-like starting materials undeniably prove the cotectic behaviour of the sanukitoid system at 0.3 GPa, successfully reproducing high-Mg and low-CaO differentiates. Products obtained in the experimental runs are mostly homogenous, with ubiquitous orthopyroxene, plagioclase and oxides across all the experiments, but differences in the rest of the solid assemblages with the two starting materials proves the high sensibility of the system to composition.

Shallow depth emplacement and differentiation can account for local sanukitoid plutons in which cumulates are observed, but lack of cumulates in most of the sanukitoid batholiths evidences this process cannot explain the series alone. An alternative, complementary process is required to account for the volume of sanukitoid bodies described, and the worldwide occurrence of the series immediately excludes any process linked to any kind local assimilation. The explanation must involve an intrinsic feature of the magmatic system. We find this characteristic to be either one of the next two possibilities: (1) a relatively low temperature, granitic, crustal melt mixes with sanukitoid parental magma. However, we find this possibility unlikely due to the difference in temperatures between the two mixing components and the water required to generate a significant amount of melt to satisfy the process. (2) Sanukitoid self-contamination with orthopyroxene-rich cumulates from the earliest stages of differentiation, that likely remains in the lower crust after only a small portion of the sanukitoid melt have extracted. This agrees with field observations and is compatible with low-pressure differentiation. For these reasons this is the most plausible explanation for a significant volume of the series.

Experimental work performed here shows two compatible ways in which, the abundant sanukitoid intrusions may develop their

characteristic geochemical affinity, one being low pressure differentiation and the other one orthopyroxene-rich restite contamination. Both models explain the high-Mg content observed in the series, even if one of them is clearly favoured to be the most efficient one. Regarding the low CaO and high K_2O tendency shown by the series, the role of a metasomatized mantle source of harzburgitic nature has already been put in value by previous works. Plagioclase fractionation in the lower crust may complementarily contribute to the CaO depletion. Moreover, the existence of a low-pressure cotectic sanukitoid system conditions the re-equilibration of previously heterogeneous melts during emplacement. New experiments will be proposed to further tie in the insights of a series closely linked to crustal recycling processes.

Declaration of Competing Interest

The authors declare that they have no known competing financial interests or personal relationships that could have appeared to influence the work reported in this paper.

Acknowledgements

This work was supported through the Spanish Research Agency (AEI) Grant N° PGC2018-096534-B-I00 (Proyecto IBERCRUST). We are particularly grateful to Hugh Rollinson for his constructive criticism. We also want to thank an anonymous reviewer for the kind comments provided.

Appendix A. Supplementary data

Supplementary data to this article can be found online at https://doi.org/10.1016/j.lithos.2022.106632.

References

Amante, C., Eakins, B.W., 2009. ETOPO1 Arc-minute Global Relief Model: Procedures, Data Sources and Analysis.

Annen, C., Blundy, J.D., Sparks, R.S.J., 2006. The genesis of intermediate and silicic magmas in deep crustal hot zones. J. Petrol. 47 (3), 505–539.

Arató, R., Audétat, A., 2017. FeTiMM - a new oxybarometer for mafic to felsic magmas. Geochem. Perspect. Lett. 5, 19–23.

Bender, J.F., Hanson, G.N., Bence, A.E., 1982. The Cortlandt complex: evidence for large-scale liquid immiscibility involving granodiorite and diorite magmas. Earth Planet. Sci. Lett. 58 (3), 330–344.

Castro, A., 2020. The dual origin of I-type granites: the contribution from experiments. Geol. Soc. Lond., Spec. Publ. 491 (1), 101–145.

Castro, A., 2021. A non-basaltic experimental cotectic array for calc-alkaline batholiths. Lithos 382, 105929.

Castro, A., Stephens, W.E., 1992. Amphibole-rich polycrystalline clots in calc-alkaline granitic rocks and their enclaves. Can. Mineral. 30 (4), 1093–1112.

Castro, A., Aghazadeh, M., Badrzadeh, Z., Chichorro, M., 2013. Late Eocene–Oligocene post-collisional monzonitic intrusions from the Alborz magmatic belt, NW Iran. An example of monzonite magma generation from a metasomatized mantle source. Lithos 180, 109–127.

Conceiç˜ao, R.V., Green, D.H., 2004. Derivation of potassic (shoshonitic) magmas by decompression melting of phlogopite + pargasite lherzolite. Lithos 72 (3–4), 209–229.

de Oliveira, M.A., Dall'Agnol, R., Scaillet, B., 2010. Petrological constraints on crystallization conditions of Mesoarchean sanukitoid rocks, Southeastern Amazonian Craton, Brazil. J. Petrol. 51 (10), 2121–2148.

Fortey, N.J., Cooper, A.H., Henney, P.J., Colman, T., Nancarrow, P.H.A., 1994. Appinitic intrusions in the English Lake district. Mineral. Petrol. 51 (2–4), 355–375.

Fowler, M., Rollinson, H., 2012. Phanerozoic sanukitoids from Caledonian Scotland: implications for Archean subduction. Geology 40 (12), 1079–1082.

Galán, G., Suárez, O., 1989. Cortlandtitic enclaves associated with calc-alkaline granites from Tapia-Asturias (Hercynian Belt, northwestern Spain). Lithos 23 (4), 233–245.

Halla, J., 2005. Late Archean high-Mg granitoids (sanukitoids) in the southern Karelian domain, eastern Finland: Pb and Nd isotopic constraints on crust- mantle interactions. Lithos 79 (1–2), 161–178.

Heilimo, E., Halla, J., Ho¨ltt¨a, P., 2010. Discrimination and origin of the sanukitoid series: geochemical constraints from the Neoarchean western Karelian Province (Finland). Lithos 115 (1–4), 27–39.

Heilimo, E., Halla, J., Andersen, T., Huhma, H., 2013. Neoarchean crustal recycling and mantle metasomatism: Hf–Nd–Pb–O isotope evidence from sanukitoids of the Fennoscandian shield. Precambrian Res. 228, 250–266.

Herrmann, W., Berry, R.F., 2002. MINSQ–a least squares spreadsheet method for calculating mineral proportions from whole rock major element analyses. Geochemistry 2 (4), 361–368.

Lackey, J.S., Valley, J.W., Chen, J.H., Stockli, D.F., 2008. Dynamic magma systems, crustal recycling, and alteration in the central Sierra Nevada batholith: the oxygen isotope record. J. Petrol. 49 (7), 1397–1426.

Lobach-Zhuchenko, S.B., Rollinson, H.R., Chekulaev, V.P., Arestova, N.A., Kovalenko, A. V., Ivanikov, V.V., Guseva, N.S., Sergeev, S.A., Matukov, D.I., Jarvis, K.E., 2005. The Archaean sanukitoid series of the Baltic Shield: geological setting, geochemical characteristics and implications for their origin. Lithos 79 (1–2), 107–128.

Lobach-Zhuchenko, S.B., Rollinson, H., Chekulaev, V.P., Savatenkov, V.M., Kovalenko, A.V., Martin, H., Guseva, N.S., Arestova, N.A., 2008. Petrology of a Late Archaean, highly potassic, sanukitoid pluton from the Baltic Shield: insights into Late Archaean mantle metasomatism. J. Petrol. 49 (3), 393–420.

López, S., Castro, A., García-Casco, A., 2005. Production of granodiorite melt by interaction between hydrous mafic magma and tonalitic crust. Experimental constraints and implications for the generation of Archaean TTG complexes. Lithos 79 (1–2), 229–250.

López-Moro, F.J., Lo´pez-Plaza, M., 2004. Monzonitic series from the Variscan Tormes Dome (Central Iberian Zone): petrogenetic evolution from monzogabbro to granite magmas. Lithos 72 (1–2), 19–44.

Martin, H., Smithies, R.H., Rapp, R., Moyen, J.F., Champion, D., 2005. An overview of adakite, tonalite–trondhjemite–granodiorite (TTG), and sanukitoid: relationships and some implications for crustal evolution. Lithos 79 (1–2), 1–24.

Martin, H., Moyen, J.F., Rapp, R., 2009. The sanukitoid series: magmatism at the Archaean–Proterozoic transition. Earth Environ. Sci. Trans. R. Soc. Edinburgh 100 (1–2), 15–33.

Moyen, J.F., Laurent, O., Chelle-Michou, C., Couzini´e, S., Vanderhaeghe, O., Zeh, A., Villaros, A., Gardien, V., 2017. Collision vs. subduction-related magmatism: two contrasting ways of granite formation and implications for crustal growth. Lithos 277, 154–177.

Putirka, K.D., 2008. Thermometers and barometers for volcanic systems. Rev. Mineral. Geochem. 69 (1), 61–120.

Rasband, W.S., 1997-2018. ImageJ. U. S. National Institutes of Health, Bethesda, Maryland, USA. https://imagej.nih.gov/ij/.

Shirey, S.B., Hanson, G.N., 1984. Mantle-derived Archaean monzodiorites and trachyandesites. Nature 310 (5974), 222–224.

Smithies, R.H., Champion, D.C., 2000. The Archaean high-Mg diorite suite: links to tonalite–trondhjemite–granodiorite magmatism and implications for early Archaean crustal growth. J. Petrol. 41 (12), 1653–1671.

Sparks, R.S.J., Marshall, L.A., 1986. Thermal and mechanical constraints on mixing between mafic and silicic magmas. J. Volcanol. Geotherm. Res. 29 (1–4), 99–124.

Stern, R.A., Hanson, G.N., 1991. Archean high-Mg granodiorite: a derivative of light rare earth element-enriched monzodiorite of mantle origin. J. Petrol. 32 (1), 201–238.

Stern, R.A., Hanson, G.N., Shirey, S.B., 1989. Petrogenesis of mantle-derived, LILE-enriched Archean monzodiorites and trachyandesites (sanukitoids) in southwestern Superior Province. Can. J. Earth Sci. 26 (9), 1688–1712.

Stevenson, R., Henry, P., Garí epy, C., 1999. Assimilation–fractional crystallization origin of Archean sanukitoid suites: western Superior Province, Canada. Precambr. Res. 96 (1–2), 83–99.

Tatsumi, Y., Ishizaka, K., 1982. Origin of high-magnesian andesites in the Setouchi volcanic belt, southwest Japan, I. Petrographical and chemical characteristics. Earth Planet. Sci. Lett. 60 (2), 293–304.

Wood, B.J., Turner, S.P., 2009. Origin of primitive high-Mg andesite: constraints from natural examples and experiments. Earth Planet. Sci. Lett. 283 (1–4), 59–66.

5.1.2

Post-collisional batholiths do contribute to crustal growth

Earth and Planetary Science Letters, 2023

Earth and Planetary Science Letters 603 (2023) 117978

Contents lists available at ScienceDirect

Earth and Planetary Science Letters

journal homepage: www.elsevier.com/locate/epsl

Post-collisional batholiths do contribute to continental growth

Daniel Gómez-Frutos [a,b,*], Antonio Castro [a,b], Gabriel Gutiérrez-Alonso [c]

[a] Museo Nacional de Ciencias Naturales (MNCN), Consejo Superior de Investigaciones Científicas (CSIC), C. José Gutiérrez Abascal 2, 28006 Madrid, Spain
[b] Instituto Andaluz de Ciencias de la Tierra (CSIC - UGR), 18110 Granada, Spain
[c] Departamento de Geología, Universidad de Salamanca, Salamanca 37008, Spain

article info

Article history:
Received 1 September 2022
Received in revised form 7 December 2022
Accepted 23 December 2022
Available online xxxx
Editor: R. Hickey-Vargas

Keywords:
crustal growth
continental crust
post-collisional magmatism
metasomatized mantle
tectonics
batholith

abstract

Post-collisional voluminous silicic magmatism is represented in most orogens across the world in the form of large granodiorite batholiths and minor intermediate and mafic intrusions, postdating 5-30 Ma the age of the collisional paroxysm responsible of the main mountain building events. Post-collisional mafic intrusions are acknowledged as a mechanism that contributes to long-term yet minor continental growth. The silicic magmas forming the large batholiths, however, have been dismissed from the crustal growth discussion due to bias in the conception that they always generate by recycling older lower crustal igneous rocks. Contrary to this, geochemical and isotopic relations together with new experimental data provided in this paper suggest that the post-collisional signature can be reproduced without the implication of a crustal component, supporting a potential common origin for the two suites, intermediate and silicic. That is, both suites can be derived from a metasomatized mantle source, thus representing the injection of largely juvenile material to produce new continental crust. This inference is contextualized within the supercontinent cycle, showing that the timing of post-collisional magmatism accounts for the generation and preservation rates predicted by the existing models, since both reach maximum values in the amalgamation-collisional stage of the supercontinent cycle, rather than in the subduction stage. All together these inferences lead to think that post-Archean, post-collisional magmatism has been significantly underestimated when computing continental crustal growth through time.

1. Introduction

The existence of continental crust is one of the main differences in the evolution of the geosphere of the Earth, contrasting other planets in the Solar system. Its formation and evolution remain a fundamental discussion topic in Earth Sciences, leading to several attempts to constrain the main continental crust formation mechanisms (e.g. Arndt and Goldstein, 1987; Arndt, 2013; Condie et al., 2011; Hawkesworth et al., 2010; Rudnick, 1995). When stablishing the mechanisms by which crustal growth takes place, three requisites must be satisfied regardless of the geological setting: (1) the segregation and differentiation of igneous material from the mantle, (2) the incorporation of such material into pre-existing continental crust, and (3) its preservation in the form of large igneous bodies (Condie et al., 2011; Couzinié et al., 2016; Hawkesworth et al., 2009). Thus, since crustal growth can be fully understood by an igneous process it is safe to assert that igneous rocks constitute the best tracers to understand the processes involved in crustal growth.

The recent advance of new microanalytical techniques has allowed the development of models based on zircon isotopic composition. Particularly, Lu-Hf isotopes in zircon crystals have significantly different behaviour during partial melting in the mantle (Lu tends to concentrate in the mantle, producing higher $^{176}Hf/^{177}Hf$ ratios than those present in zircon crystals of a crustal source), and this system has been the most successful approach to discern crustal and mantle sources (e.g. Griffin et al., 2000; Kemp et al., 2006). Measurements in single zircon grains by in-situ analytical techniques (SIMS and LA-(MC)ICP-MS) have led to the elaboration of large datasets that illustrate the age when the igneous protolith separated from the mantle (Payne et al., 2016). As a result, this method has enabled the elaboration of several crustal growth models that constitute an essential contribution to the understanding of crustal growth over time (Cawood et al., 2013; Dhuime et al., 2011; Hawkesworth et al., 2010, 2019).

However, some limitations on the use of this technique have been recently pointed out. Model ages using Lu-Hf systematics suffer from similar problems to Sm-Nd system (Arndt and Goldstein,

* Corresponding author.
E-mail address: daniel.gomez@csic.es (D. Gómez-Frutos).

https://doi.org/10.1016/j.epsl.2022.117978

1987), being affected by entrainment of magmas from different sources and thus representing a hybrid age (Belousova et al., 2010; Payne et al., 2016; Roberts and Spencer, 2015). While this may be partially compensated by comparison with O isotopes, this problem is further aggravated by the reliance of these models on the number of sampled zircon grains (Hawkesworth et al., 2019; Voice et al., 2011), potentially producing fictitious density maxima, and their representativity of periods of enhanced preservation rather than crystallization (Arndt, 2013; Condie et al., 2011). Moreover, Lu-Hf systematics are unable to discriminate between largely recy- cled magmas from juvenile post-collisional magmatism, with the later representing the addition of new continental crust yet being invisible in the zircon record (Couzinié et al., 2016). Due to these limitations, the crustal growth estimations obtained through the use of Lu-Hf isotope systematics entail an important paradox: for being the continental crust destruction rates significantly higher in post-Archean (< 3 Ga) times due to the creation of active mar- gins, zircon-based models predict stable low continental growth rates and low net growth (e.g. Dhuime et al., 2012, 2018; Voice et al., 2011). Furthermore, all the mentioned models rely on the equilibrium between net continental crustal growth based in crust generation in subduction related magmatic arcs and arc destruction through tectonic erosion, being the latter significantly higher in oceanic arcs than in continental arcs (Spencer et al., 2017). These models only consider collision related magmatism as a minor crustal input. That is, it is generally considered that collisional and post-collisional magmatism only recycles former igneous rocks without adding new material to the crustal budget or adding little amounts which are prone to be subsequently volumetrically compensated through lithospheric delamination and/or dripping. These observations point to a mass deficit in the continental crust that is among the most important unresolved facts in Earth Sciences.

An interesting approach to this problem that is often overlooked is the study of magmas themselves. The Earth's continents are mostly composed of igneous and meta-igneous rocks, with a bulk composition that is andesitic on average and hence classically associated with subduction (e.g. Dewey and Windley, 1981; Rudnick and Fountain, 1995). That is, continents are on average more silicic and less magnesian than basalts (SiO_2 = 65.2 wt.%; MgO = 2.5%), representing a system that is not in equilibrium with the peridotite mantle (Hacker et al., 2011; Rudnick and Fountain, 1995; Rudnick et al., 2003). The discussion about their origins has been historically focussed on the magmatic processes directly related to the subduction setting. In this regard, the most voluminous type of granite magmatism, namely I-type (Chappell and White, 2001; Pitcher, 1987), has been accountable for continental crust generation (Jagoutz and Kelemen, 2015; Rudnick and Fountain, 1995). Particularly, the subduction related I-type magmas, also named Cordilleran-type or Andean-type, are thought to be the main source of new continental crust (Barth et al., 2000; Dewey and Windley, 1981). This widely accepted statement has led to neglect the role of the more voluminous Caledonian I-type batholiths, generated in collisional orogens, especially during the post-collisional stages (Barbarin, 1999; Fowler and Henney, 1996; Pitcher, 1987), and their role in continental growth.

In this work we review the role of post-collisional magmatism as a potential continental growth mechanism using the magmas as the starting point, and not only models based in zircon crystals. We consider post-collisional batholiths as those large igneous silicic bodies emplaced substantially later (5-30 Ma) than the aftermath of the orogenic edifice building and its subsequent collapse. Analyses of published geochemical data are used to establish key differences between subduction-related (Andean-type) and post-collisional (Caledonian-type) batholiths, providing evidence that the latter have a distinct geochemical signature that departs from the subduction process. This geochemistry is put in contrast with isotopic ratios and new experimental data to unravel the controversy around the origin of post-collisional batholiths, pointing to the conclusion that crustal growth via post-collisional magmatism may have been severely underestimated. How the provided data and arguments affect the existing models or crustal growth rate estimations is out of the scope of this paper, being rather focused on the process itself.

2. The duality of I-type batholiths

The formation of I-type batholiths is known to involve crustal scale processes in two main and contrasting tectonic environments, namely subduction zones at active continental margins and post-collisional orogens in supercontinent forming orogenic belts. While the former is believed to supply enough igneous material to account for the continental growth according to volume balance (Jagoutz and Kelemen, 2015), inference based on present day outcropping magmatic rocks highlights the potential relevance of the also abundant post-collisional magmas. These are widely represented in orogenic collisional belts that have led to the amalgamation of the last four known supercontinents happening in post-Archean times, namely Nuna-Columbia, Rodinia, Pannotia and Pangea (Fig. 1).

Regarding their composition, an intriguing observation is the subtle differences between post-collisional and Andean-type magmas (Castro, 2020), even if most of these batholiths share roughly similar major oxides concentrations (SiO_2, 63–70 wt.%; FeO^T, 2–5 wt.%; MgO, 1–3 wt.%; CaO, 3–5 wt.%; Na_2O, 2–4 wt.%; and K_2O, 2–4 wt.%). This is an interesting fact considering their sources are believed to be so different, specifically partial melting of mantle-derived underplated basalts with contribution from oceanic crust in the case of Andean-type, and partial melting of old igneous lower crust with a small contribution from the mantle in the case of post-collisional type (Pitcher, 1987). Hence, it is expectable that such different settings leave a rather distinct geochemical fingerprint in the magmas.

To identify the post-collisional geochemical signature a preliminary discrimination must be made between their two characteristic suites: (1) a metaluminous (ASI<1) to slightly peraluminous silicic suite (ASI$\geq$1.0) [ASI (Alumina Saturation Index) = molar $Al_2O_3/Na_2O+K_2O+(CaO-3.3*P_2O_5)$], mostly represented by granodiorites and the volumetrically largest of the two; and (2) a metaluminous high-K calc-alkaline suite that ranges from mafic to felsic, and is embodied by smaller intrusions (Bonin, 2004; Moyen et al., 2017). While the mafic suite has been the subject of varied studies (e.g. Couzinié et al., 2016; Fowler and Rollinson, 2012; Orejana et al., 2009), revealing particularities that will be discussed ahead, the silicic suite has historically received less attention. In this sense, we compiled a total of 2552 major element analyses that belong to the silicic suite from the most studied and well known post-collisional batholiths in the world, namely (1) the Caledonian batholiths in the northern British Isles (ca. 400 Ma), (2) the European Variscan belt, including the Iberian Massif, the French Massif Central and the Bohemian Massif (ca. 300 Ma), and (3) the Central Asian Orogenic Belt (CAOB; ca. 550-150 Ma) (Fig. 1). Compared to Andean-type rocks, post-collisional granites (*s.l.*) are always enriched in MgO and K_2O and depleted in CaO. Anomalous enrichment in MgO is mainly displayed by the most mafic terms of the series, while the high K_2O and low CaO values are widespread among the whole series. Trace elements also show an enriched signature in LILE and LREE compared to Andean-type batholiths, particularly Sr and Ba, making these rocks known as high Ba-Sr granitoids in the Caledonian belt (Fowler and Henney, 1996; Fowler and Rollinson, 2012). Nevertheless, even if trace elements provide useful information regarding the source due to its enriched nature, the systematic distinction of two magmatic se-

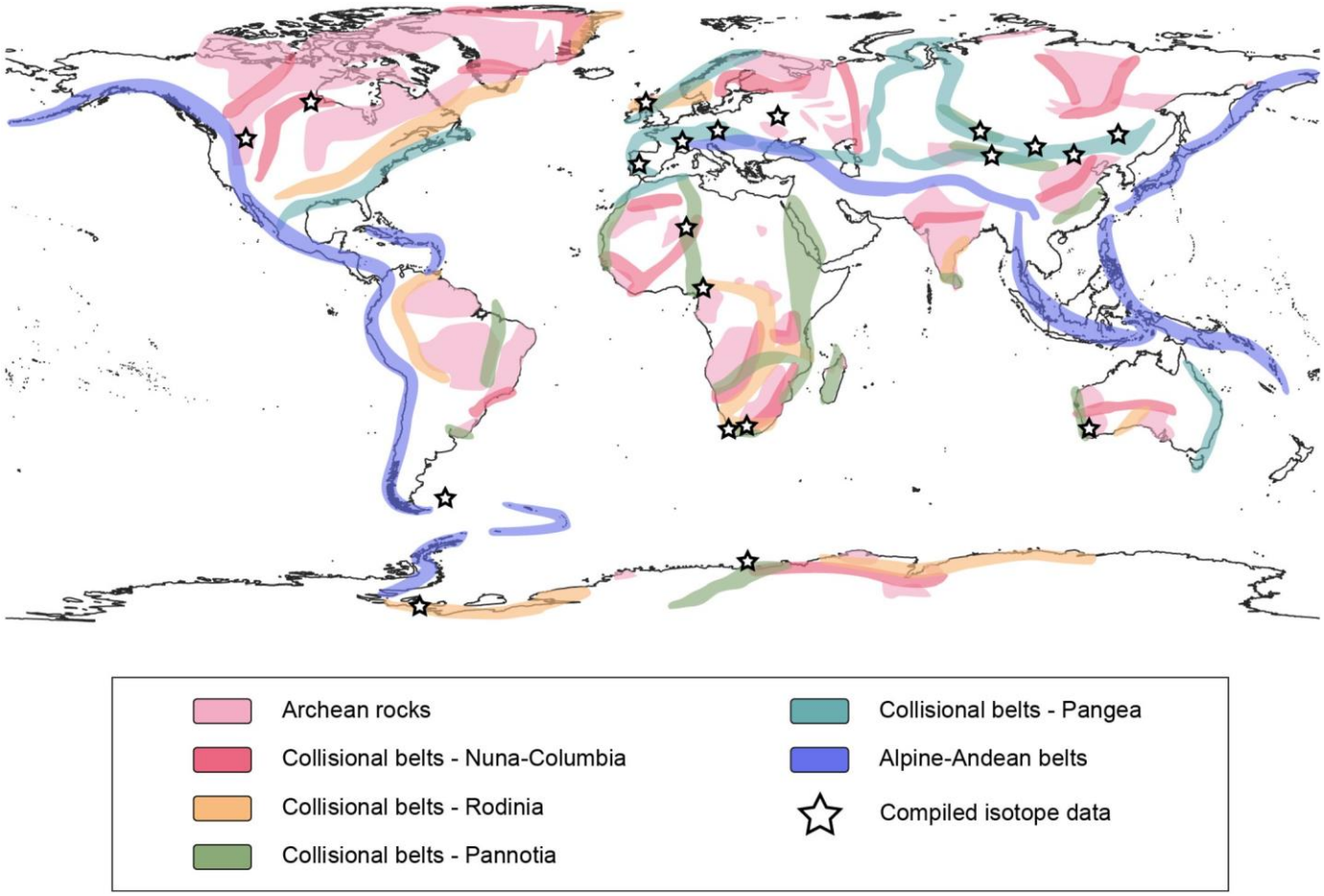

Fig. 1. Collisional belt schematic world map. Most of these collisional belts are characterized by the presence of post-collisional I-type batholiths, independently of their age. Present-day subduction related orogenic belts and recent collisional belts are also represented, in which in some cases no post-collisional batholiths are present (either they have not formed yet, or the erosion level is not deep enough yet). Compiled isotopic data locations are marked (see Fig. 3 for further details). Colour contours represent Nuna-Columbia (2.0 – 1.5 Ga), Rodinia (1.3 – 1.0 Ga); Pannotia (0.7 – 0.54 Ga); Pangea, including Caledonian, Variscan-Appalachian, Uralian and part of the Central AsianOrogenic Belt (0.4 – 0.25 Ga); and Archean. References used to the elaboration of this map can be found in the Supplementary Material 6.

ries must be established using major elements, as they record melt compositions and potential phase equilibria at the source.

The key geochemical features of post-collisional magmas may be found in Fig. 2. Samples from the characteristic Andean batholiths of Sierra Nevada and Patagonia are also plotted for comparison, showcasing the differences between the two types of I-type magmatism. The selected diagrams are the CaO–MgO plot and the Or–An–En projected space. The CaO–MgO diagram constitutes a proxy of phase equilibria since both CaO and MgO represent the most outstanding changes in liquid composition in equilibrium with a solid saturation assemblage of orthopyroxene ± clinopyroxene ± plagioclase ± amphibole, when decreasing temperature in calc-alkaline systems. This diagram shows the deviation of post-collisional batholiths, represented by Kernel density contour plots, with the three sample groups (Fig. 2a, 2b and 2c) falling underneath the plot of the Sierra Nevada and Patagonia batholiths and the Andean-type experimental cotectic line (Castro, 2021). This is due to both their depletion in CaO and enrichment in MgO. The Variscan group shows two different trends due to higher MgO values found in the French Massif Central data. Complementarily, Or–An–En diagram is a more complex representation of the system. In this diagram differences can be found in the three sample groups; Caledonian and CAOB series show density maxima towards a more intermediate composition (comparatively higher MgO), while European Variscan showcase higher K_2O concentrations. Likewise, Iberian, Bohemian and French massifs display differences, with the latter having higher MgO. Nevertheless, the most relevant aspect illustrated by this diagram is that although the composition of post-collisional batholiths is heterogeneous, there is a systematic difference respecting to Andean-type batholiths. Additional Harker diagrams can be found in Supplementary Material 1. The compiled data can be found in Supplementary Material 2.

Another key feature of post-collisional magmas is the ubiquitous occurrence of small mafic intrusions scattered around the extensive granodioritic bodies, representing the mafic end member of the high-K calc-alkaline post-collisional suite. These are usually volumetrically small compared to the large granodioritic bodies they are associated with. Due to their singular geochemistry, they have historically received several names, such as sanukitoids, vaugnerites, appinites, durbachites… (e.g. Fowler and Henney, 1996; Fowler and Rollinson, 2012; Shirey and Hanson, 1984; Smithies and Champion, 2000). This post-collisional mafic magmatism will be referred to as sanukitoids in this paper. Sanukitoids have a particular geochemical signature that sets them apart from calc-alkaline mafic magmas related with subduction settings. That is, they are enriched in MgO and K_2O and depleted in CaO compared to Andean-type magmas. Interestingly, such features are coincident with the geochemical signature displayed by the granitic terms of post-collisional batholiths. This suggests that the two suites may be related by magmatic differentiation from a common mafic magma (Fowler et al., 2001, 2008; Gómez-Frutos and Castro, 2022; Moyen et al., 2017).

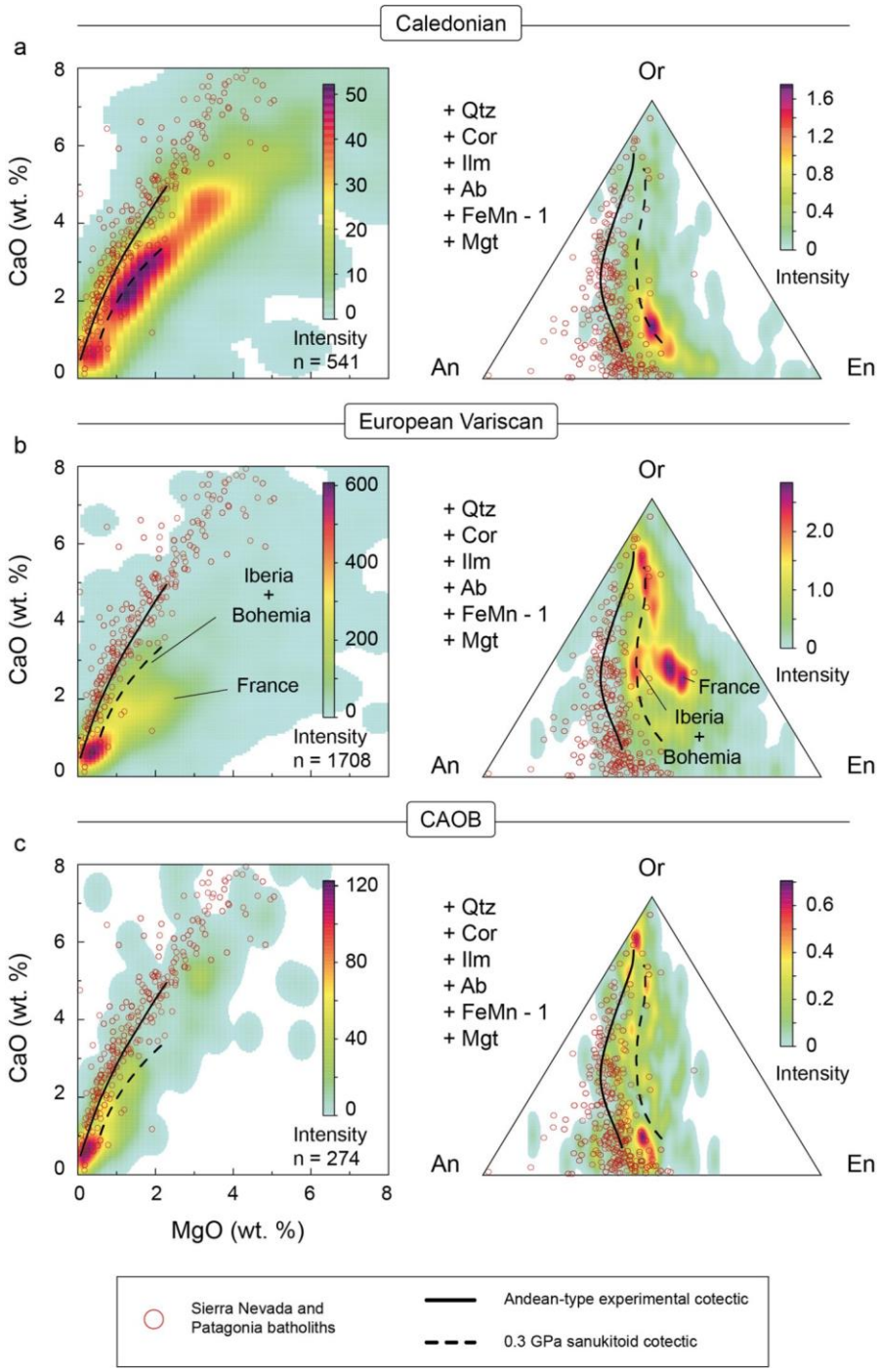

Fig. 2. Geochemical diagrams comparing three representative series of post-collisional magmatism (Kernel density contour plot) and Andean-type magmatism (red circles). (a) Caledonian series, (b) European Variscan, (c) Central Asian Orogenic Belt (CAOB). CaO–MgO diagram: post-collisional magmas are both more magnesian and less calcic than Andean-type magma. Variscan data group shows two different trends; for similar CaO values French Massif Central data are more magnesian than Iberia and Bohemia data. Or–An–En diagram: post-collisional magmas fall to the right of the Andean-type experimental cotectic array due to their Ca depletion and Mg and K enrichment. Again, by being more magnesian French Massif Central plots closer to the En pole. Andean-type data is from Sierra Nevada and Patagonia. Post-collisional magmatism and Andean-type compiled data can be found in Supplementary Material 2. Andean-type experimental cotectic line determined by Castro (2021). (For interpretation of the colours in the figure(s), the reader is referred to the web version of this article.)

The close geochemical similarity between the peraluminous silicic suite and the sanukitoids is twofold: on one hand the distinction between the two suites becomes arbitrary when exploring the geochemistry of the full series, and on the other hand, the petrogenetic relationship between the felsic and mafic endmember is conspicuous. Since the mafic endmember is widely accepted to be sourced from a metasomatized mantle source, a felsic endmember that shares most of its geochemical features must be related to that same metasomatized mantle source in some way. This observation is central to this paper.

3. The recycled isotopic signatures

The study of radiogenic isotopes systematics has provided important observations to the crustal growth discussion and granite *sensu lato* petrogenesis. Most recent studies used Hf-O systemat-

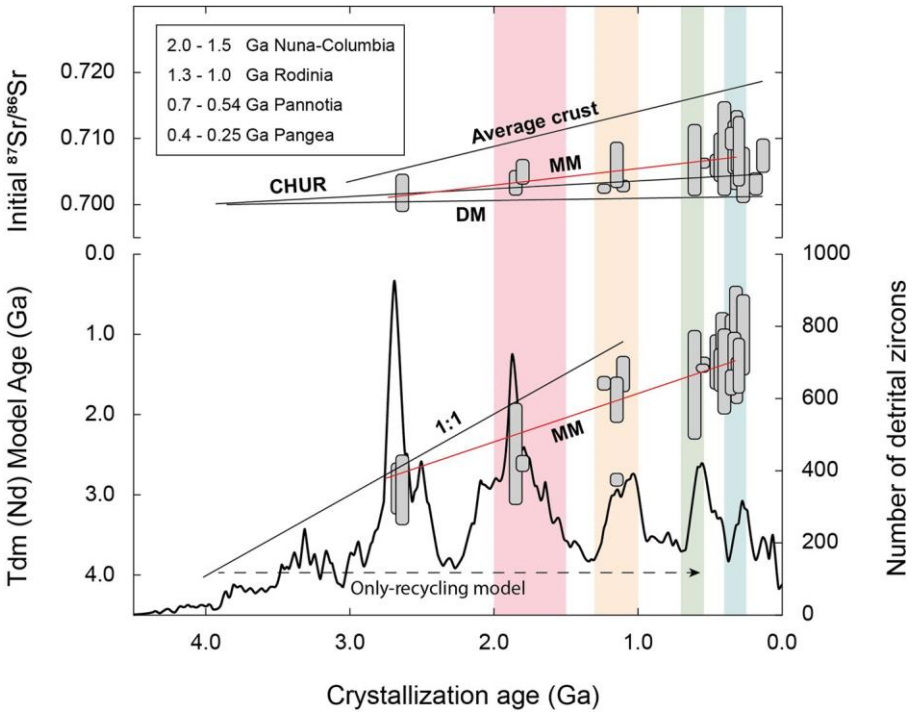

Fig. 3. Initial Sr and Nd model age against crystallization age diagrams. Detrital zircon numbers represented for comparison (Condie, 2014), providing a correlation between crustal growth predicted by number of detrital zircons and the age of the post-collisional batholiths. Initial Sr diagram shows post-collisional batholiths plot below the average crust model and towards the CHUR/DM model, suggesting a juvenile (mantle) component even when only considering granitic magmas. Model ages diagram shows that the batholiths plot following neither an only-recycling model nor an only-growth model represented by the 1:1 line. In both diagrams, the batholiths fit perfectly to the metasomatized mantle (MM) model line, pointing to a roughly similar source for both granites and mafic magmas. The MM line a linear regression of sanukitoid rocks around the world (Pearson correlation coefficient = −0.82; r^2 = 0.67). Abbreviations are as follows: CAOB, Central Asian Orogenic Belt; CHUR, Chondritic Uniform Reservoir; DM, Depleted Mantle; MM, Metasomatized Mantle. The compiled isotope data can be found in Supplementary Material 3.

ics to discuss crustal growth and estimate crustal growth rates (see references above). But even if these studies are of special use for a global approach to the problematic, the compilations are often referred to detrital zircon grains. This implies an inherent assumption that these zircon grains are sourced from weathering and transport of previously formed igneous rocks, and it is difficult to know for certain if the magmatic rocks that produced those detrital zircon grains were granitic or not. In contrast, the use of whole-rock isotopic ratios from granitic rocks is more informative about the processes of new crust generation and/or recycling, complimenting the existing Hf-O data.

When discussing post-collisional batholiths one of the most observed facts is that they always display older Sm-Nd model ages than their crystallization ages, classically interpreted to be caused by the presence of an old crust recycled component. However, it remains unclear whether the involvement of such old crust took place during mantle metasomatism, by assimilation of continental rocks during ascent or by direct batch melting of the crust to produce the magmas. In order to set this problem, we have compiled a database (768 Nd and 633 Sr analyses) of whole rock isotope data from post-collisional batholiths around the world. Pericratonic batholiths formed at the end of the Archean are also included. The compilation can be found in Supplementary Material 3.

The compiled isotope data are represented in Fig. 3. Sr initial ratios against crystallization time diagram shows that the former increase over time for post-collisional granite batholiths. These increasing ratios do not follow the 'average crustal ratio', which is otherwise followed by a fully recycled crustal material. Interestingly, most batholiths plot between the two main models, the average crust and the mantle (CHUR), implying that significant juvenile material is being supplied to generate the post-collisional magmatism, even when only granitic magmas are considered. In other words, based in the Sr isotopic signature, post-collisional granites contain a mantle (juvenile) component. On the other hand, Nd model ages plotted against crystallization time (Fig. 3) indicate that model ages (age of lithospheric residence) also increase with time. This increase has, however, a shallower slope than the depleted mantle model, implying that the model age of the batholiths is older than their age of generation. That is, a recycled (crustal and/or lithospheric mantle) component is present in the magmas. This means that part of the mass of the magmas was residing in the crust either in the form of sediments or older granitic rocks and was incorporated to the source of batholiths when they were generated at a given time, or that they represent melting of the subcontinental lithospheric mantle. These observations limit the viability of two models: (1) if granites formed following an 'only-recycling model' that affects a primitive (Archean) granitic crust, they must follow a flat time evolution with a constant model age through time. (2) If, by contrast, granite magmatism represents a net addition of magma to the crust from a depleted sublithospheric mantle, the batholiths will plot on the 1:1 line, representing an 'only-growth model', since model ages and crystallization ages should be identical. None of these models are satisfied due to the mixed signature displayed by the Sm-Nd data from post-collisional batholiths.

Nevertheless, a third possibility is that the magmas originate in a metasomatized mantle source. By being sourced in an enriched mantle, the batholiths will plot along an intermediate line. A model line of metasomatized mantle post-collisional magmatism is plotted for comparison. This line is a linear regression of sanukitoid data (rocks with mafic-intermediate compositions, SiO_2 < 63 wt.%) from several different batholiths (Supplementary Material 3). Interestingly, the model line overlaps the trend of the studied batholiths. This observation tallies with the common ma-

jor element signature displayed by post-collisional granites (*s.l.*) and associated sanukitoids, and it can only be explained if the two types of magmas originate in closely similar processes. This is of special interest when considering the controversial origin of the post-collisional magmatism.

4. Origin of post-collisional batholiths

Holding post-collisional magmatism responsible for the generation of new continental crust implies a deep understanding of the origin of such magmas, since crustal growth entails the entrainment of juvenile mantle material to the continental crust. While some existing models do propose a mantle origin for post-collisional batholiths (Fowler and Henney, 1996; Fowler et al., 2001; Hildebrand and Whalen, 2017), several other models to explain the origin of these magmas are based on the initial premise that significant volumes of magma are produced by lower crust melting (e.g. Annen et al., 2006; Aranovich et al., 2014; Petford and Gallagher, 2001). However, there are significant variables that are commonly dismissed in the continental crust melting models:

(1) The lower crust is mafic on average (Rudnick and Fountain, 1995). A hypothetical basalt precursor in the lower crust for the batholiths entails the need for the elimination of an ultramafic residue from the lower crust in order to produce the observed bulk composition. In contrast, implication of an already fractionated andesitic precursor will provide the needed composition to form the continental crust skipping the problem of a missing ultramafic residue.
(2) The lower crust is essentially depleted. Simple melting of the lower crust cannot reproduce the enriched signature of post-collisional batholiths. An additional element in the process needs to be involved.
(3) The crust showcases unrealistically high solidus temperatures (>850°C) that are incapable of producing significant amounts of liquids even when periodic influx of mafic magma is invoked (Bonin, 2004). Thus, water is a necessary addition to lower the solidus even more (e.g. Aranovich et al., 2014; Castro, 2020; Collins et al., 2016; Weinberg and Hasalová, 2015).
(4) However, this consideration entails yet another problem, since even with the most conservative estimation of 4 wt.% H_2O dissolved in the parental magma (Plank et al., 2013) the water content in a residual granitic liquid that represents a 0.2 melt fraction will have ~20 wt.% H_2O. This water amount in residual liquid is unrealistic and is not supported neither by the observed igneous textures in the rocks nor by the scarcity of pegmatitic dykes in the plutons.
(5) Fully recycled lower crust inherently implies a recycled isotopic signature. Nevertheless, as shown in the previous epigraph the rocks show an important mantle component in their Sr and Nd isotopes.

While these issues represent an ongoing debate, they have highlighted the importance of sanukitoid as heat and water donors for water-fluxed melting. Additionally, they are also capable of resupplying incompatible elements to the lower crust, particularly K_2O, Sr and Ba (Smithies et al., 2021). In summary, all the aforementioned arguments are consistent with a petrogenetic relationship between metasomatized mantle magma and post-collisional granites. Accidental phenomena such as magma mixing and/or crustal assimilation cannot account for the world-wide uniform geochemistry, the cotectic patterns followed by the rock series and the trends displayed by their isotopic signatures.

Taking sanukitoid rocks into account, previous experiments have attempted to constrain their role in the process. Results provide key insights on the topic, such as the importance of a dominant harzburgitic source (Wood and Turner, 2009), and the inability to reproduce the post-collisional signature by melting of a mixed sanukitoid and granulitic compound representative of the lower crust (Castro, 2020) or by sheer differentiation (Gómez-Frutos and Castro, 2022), with the latest work providing evidence that differentiation at shallow depth do reproduce the post-collisional geochemical signature, and that lower crustal pressures (c.a. >1.0 GPa) produces Ca-depleted melts. With this background and following the common conception that the crust is involved in the process, we performed a new set of experiments to test the importance of varying sanukitoid-crust proportions and its impact on the liquid composition. Selected pressures were 1.0 GPa and 0.5 GPa to simulate differentiation at the crust-lithospheric mantle boundary and at emplacement level.

Table 1
Composition of the starting materials.

	Starting materials		Model compositions		
	A208-22	5Q-92	Middle crust average[1]	Pilbara Suite[2]	Superior Province[3]
SiO_2	70.22	60.36	69.4	61.86	58.95
TiO_2	0.44	0.88	0.33	0.51	0.54
Al_2O_3	15.15	15.59	16.21	14.48	17.79
FeOt	3.11	6.03	2.72	5.64	5.22
MgO	1.00	4.30	1.27	4.17	4.58
MnO	0.07	0.13	0.03	0.08	0.10
CaO	3.17	5.34	2.96	4.67	4.94
Na_2O	3.42	3.97	3.55	3.91	4.21
K_2O	2.39	2.18	3.36	1.8	3.1
P_2O_5	0.13	0.52	0.15	0.24	0.30
LOI	0.91	0.7	-	2	-
Total	100	100	99.98	97.36	99.73

Composition recalculated to an anhydrous base. Total iron as FeO.
[1] Middle crust average; Rudnick et al. (2003).
[2] Pilbara suite sanukitoid; Smithies and Champion (2000).
[3] Roaring River Valley Complex sanukitoid. Canadian Superior Province; Stern et al. (1989).

4.1 Experimental approach

The process was tested using representative compositions for both components (Table 1), namely a mafic enclave (5Q-92) from Los Pedroches batholith in the Variscan complex Iberian Massif in SW Iberia as the sanukitoid component, and a granodiorite (A208-22) from the Andes volcanic arc that also resembles the av- erage composition of the middle crust (Rudnick et al., 2003). 5Q-92 mafic enclave was already used in former experimental work and is already justified to be representative of the common nature of sanukitoids after comparing it with the sanukitoid world series (Gómez-Frutos and Castro, 2022). A208-22 granodiorite exhaustive description can be found in previous works (Castro et al., 2011).

Prior to the interaction experiments the mafic enclave was hydrated with 3 wt.% H_2O and melted at 1200°C to produce a natural glass and minimize the existence of relict crystals. The resulting hydrated glass was grounded to a fine powder and mixed with the A208-22 granodiorite into different proportions 1:1, 1:3, 3:1. The mixtures were milled and homogenized to enhance the process by simulating grain-to-grain interactions, and then used for six experimental runs. Additionally, four more runs were performed only with the granodiorite, two of them with an additional 3 wt.% H_2O (experiments are labelled as w, standing for water-bearing; and nw, standing for no water in Table 2). Sanukitoid-only experiments were also performed, in this case with a varying range of temperature due to the system being mafic-intermediate and thus having higher liquidus temperatures. Granodiorite and mixtures runs were carried to temperatures of 1000°C and pressures of 1.0 GPa and 0.5 GPa. Correspondingly, the three runs using only sanukitoid were carried to 1000, 1050 and 1100°C and 1.0 GPa.

Table 2
Experimental glasses.

Run	Duration (hours)	Mix (A208-22:5Q-92)	T (°C)	P (GPa)	*n*	SiO_2	TiO_2	Al_2O_3	FeO^T	MgO	MnO	CaO	Na_2O	K_2O	P_2O_5	*F*	Total
D21-19	50	1:3	1000	1.0	14	65.41	0.57	14.90	2.47	0.95	0.07	2.57	2.82	2.94	0.32	0.28	93.13
						1.42	*0.05*	*0.40*	*0.22*	*0.19*	*0.02*	*0.31*	*0.27*	*0.30*	*0.11*	*0.12*	*0.60*
D21-19	50	1:1	1000	1.0	13	67.82	0.46	13.63	2.01	0.72	0.07	1.98	2.83	3.30	0.29	0.18	93.14
						0.97	*0.06*	*0.61*	*0.11*	*0.22*	*0.02*	*0.46*	*0.28*	*0.19*	*0.13*	*0.12*	*0.53*
D21-19	50	3:1	1000	1.0	14	69.20	0.42	13.09	1.70	0.47	0.05	1.41	2.78	3.57	0.19	0.13	92.90
						0.75	*0.10*	*0.31*	*0.07*	*0.03*	*0.02*	*0.05*	*0.19*	*0.15*	*0.12*	*0.07*	*0.84*
D21-20	95	1:3	1000	0.5	5	66.12	0.65	15.05	2.45	1.29	0.09	2.90	2.69	2.71	0.44	0.20	94.41
						0.46	*0.07*	*0.40*	*0.09*	*0.04*	*0.02*	*0.06*	*0.47*	*0.30*	*0.09*	*0.02*	*0.39*
D21-20	95	1:1	1000	0.5	11	70.11	0.55	13.94	2.10	0.70	0.05	1.87	3.05	3.47	0.28	0.10	96.09
						0.66	*0.05*	*0.31*	*0.15*	*0.05*	*0.02*	*0.09*	*0.22*	*0.09*	*0.14*	*0.03*	*0.64*
D21-20	95	3:1	1000	0.5	3	72.96	0.80	12.75	2.11	0.38	0.03	0.59	2.72	3.75	0.29	0.07	96.30
						1.11	*0.03*	*0.55*	*0.05*	*0.04*	*0.01*	*0.06*	*0.35*	*0.55*	*0.14*	*0.02*	*0.64*
D21-23w	69	1:0	1000	1.0	5	66.55	0.33	14.35	1.58	1.03	0.07	2.35	3.19	2.19	0.06	0.14	91.78
						0.97	*0.03*	*0.45*	*0.11*	*0.09*	*0.03*	*0.14*	*0.41*	*0.05*	*0.02*	*0.03*	*0.69*
D21-23nw	69	1:0	1000	1.0	5	69.13	0.37	13.10	1.28	0.42	0.05	0.91	2.72	4.00	0.18	0.08	92.15
						0.38	*0.02*	*0.23*	*0.06*	*0.02*	*0.01*	*0.02*	*0.12*	*0.05*	*0.12*	*0.04*	*0.63*
D21-24w	50	1:0	1000	0.5	6	66.05	0.41	14.82	1.89	1.08	0.06	2.44	3.41	2.23	0.12	0.12	92.55
						1.40	*0.05*	*0.77*	*0.25*	*0.19*	*0.01*	*0.34*	*0.07*	*0.08*	*0.06*	*0.04*	*0.46*
D21-24nw	50	1:0	1000	0.5	5	69.82	0.38	12.96	1.43	0.43	0.05	0.88	3.40	3.90	0.13	0.08	93.40
						0.71	*0.08*	*0.33*	*0.17*	*0.06*	*0.02*	*0.14*	*0.04*	*0.08*	*0.05*	*0.02*	*0.53*
D22-1	70	0:1	1000	1.0	21	66.71	0.58	15.16	2.31	0.72	0.06	1.77	3.15	4.6	0.14	0.29	95.22
						1.06	*0.08*	*0.41*	*0.16*	*0.10*	*0.02*	*0.20*	*0.33*	*0.35*	*0.02*	*0.03*	*0.69*
D22-2	50	0:1	1050	1.0	7	65.03	0.80	16.33	3.77	0.94	0.09	2.37	3.17	3.40	0.23	0.27	96.13
						0.66	*0.08*	*0.53*	*0.24*	*0.16*	*0.03*	*0.18*	*0.22*	*0.34*	*0.04*	*0.02*	*0.71*
D22-10	44	0:1	1100	1.0	11	59.66	1.25	17.07	3.43	2.23	0.10	4.18	3.90	3.19	0.63	0.17	95.65
						1.43	*0.17*	*0.55*	*0.34*	*0.43*	*0.02*	*0.56*	*0.25*	*0.16*	*0.15*	*0.02*	*0.70*

n, number of analyses. Numbers in italics below each wt.% are standard deviations.

A total of thirteen experimental runs were performed. Run durations exceeded two days in most cases and are reported in Table 2. Results will allow to compare liquid compositions in four case scenarios: (1) heat triggered melting of the granodiorite, (2) fluid-fluxed melting when water is added directly into the granodiorite, (3) fluid-fluxed melting when water is supplied by a mafic magma, and (4) sanukitoid only melting. A detailed description of the experimental and analytical techniques can be found in Supplementary Material 4.

4.2 Experimental results

Synthesized products consist of homogeneous glass and mineral assemblages. Glass major element measurements display standard deviations lower than unity. Solid phases are mostly constituted by variable proportions of orthopyroxene, clinopyroxene, amphibole, plagioclase and quartz as the main phases, and magnetite and apatite as common accessory phases. Relict crystal prevention with the formerly described method was mostly successful, with the exception of traces of relict albite-rich plagioclase cores that may be found in the assemblages. Modal proportion calculations performed with MINSQ spreadsheet (Herrmann and Berry, 2002) result in residual values lower than two. Additionally, glass modal proportion and Mg# [=molar MgO/(MgO+FeO^T)] increases with increasing the fraction of 5Q-92 in the mixtures (Fig. 4). All these considerations together suggest that equilibrium was successfully attained. It is also worth noting that sanukitoid only run at 1050° C (D22-2) display anomalously high FeO contents in the synthesized glass in comparison with the 1000° C and 1100° C runs (D22-1 and D22-10, respectively).

Glass measurements for all experimental runs with their respective standard deviations are displayed in Table 2. Major element and glass modal abundance are plotted in comparison with post-collisional granodiorites (63 < SiO_2 < 70; Fig. 4). The silica interval is restricted after the natural observation that granodiorites embody the largest volumes of intrusive rocks within post-collisional batholiths. The plotted experimental glasses suggest that increasing Andean-type component (A208-22) deviates the composition from the observed natural trend, the only exception being K_2O. The synthesized glasses are also plotted in the two selected classification diagrams and additional Harker diagrams (Fig. 5). Regardless of the mix proportions all synthesized glasses using A208-22 (crustal component) fall within the error intervals of the Andean experimental cotectic line (Castro, 2021), and on top of the Andean-type calc-alkaline array. Increasing proportions in the mafic component when the crustal component is present only pushes the resulting liquid into a more mafic yet typical Andean-type composition. Granodiorite-only runs also fall in the same area, with the water-bearing runs being constituted mainly by liquid and thus falling near the starting material composition. Comparatively, runs using only sanukitoid successfully reproduce the post-collisional geochemical signature, being depleted in CaO, enriched in K_2O and within the expected MgO density range for their respective silica values. Phase analyses and modal proportions can be found in Supplementary Material 5.

5. Discussion

5.1 Continental crust melting

The classical works on I-type magmatism defined the origin of post-collisional magmas as 'infracrustal', or 'below the crust' (Chappell and Stephens, 1988). Contrarily to this genetical definition, several works containing the term 'infracrustal' have attempted to unravel the crustal source of post-collisional batholiths (e.g. Bonin, 2004; Pitcher, 1987). This is paradoxical considering the several problems entailed by lower crust melting models (see above). And more importantly, they are contrary to the insights provided by the experimental results.

First, the most important implication of our experimental results is that the post-collisional geochemical signature can be reproduced by using only sanukitoid (metasomatized mantle) starting material (Fig. 5). Contrarily, experimental runs using a crustal component depart from the post-collisional signature, suggesting that the geochemical features of the melts are fully controlled by the Andean liquid line of descent rather than by the varying proportion of mafic mantle magma supplied to the crust. In other words, melting of an Andean-type granodioritic source and further contamination with a mafic end-member push the magma towards

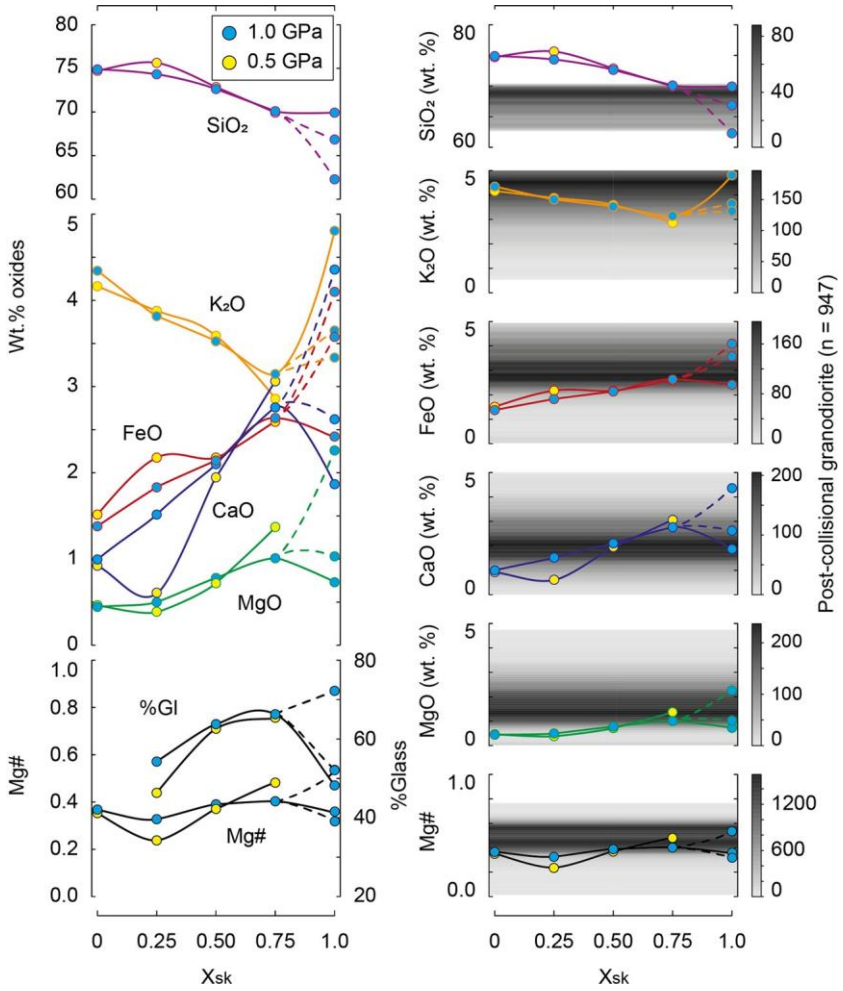

Fig. 4. Sanukitoid (sk = 5Q-92) mixture proportion against major element concentrations in experimental glass and modal glass fraction. Each circle represents an experimental run. Experimental glasses using 100% sanukitoid at 1000°C, 1050°C and 1100°C show coherent major element patters, increasing MgO and CaO and decreasing K_2O and SiO_2 when increasing temperature. Run at 1050° C show anomalously high FeO content and low Mg#. Kernel density plots post-collisional granodiorites ($63 < SiO_2 < 70$) for comparison. Restricted silica interval is selected after natural inference of the most voluminous bodies found in post-collisional batholiths being granodioritic. Major elements of experimental glass suggest that increasing the Andean-type component (A208-22) deviates the composition from the observed natural trend, the only exception being K_2O. Both glass proportion and Mg# increase with increasing sanukitoid component in the mix runs (and thus the H_2O content). Sanukitoid only runs show a decrease in glass proportion, coherent with a fully intermediate-mafic system having higher liquidus temperatures. Pressure does not seem to have a significant effect on neither of the parameters represented.

more mafic compositions (black circles, Fig. 5), but does not reproduce the low Ca and high Mg and K contents of post-collisional batholiths. Previous experimental studies performed with granulitic starting materials resembling a mafic lower crust have not successfully reproduced the post-collisional geochemical signature either (Castro, 2020).

The inherent implication of these observations is that the major element geochemistry of post-collisional batholiths is satisfied only when the crust is excluded from the process, thus granitic (*s.l.*) magmas representing fractionates from an intermediate magma that generated in a metasomatized mantle source (Fig. 6). This conclusion eliminates several problems entailed by the lower crust melting model. By coming from the mantle, temperature and water are no longer a limitation when considering the high solidus of this system. Moreover, the solid residue of the sanukitoid system is mainly constituted of plagioclase and pyroxene, and thus is compatible with the noritic composition of the lower continental crust (Meissner et al., 1986).

Besides, the hypothesis that a trachiandesitic (sanukitoid) magma from a metasomatized mantle source is the precursor of the granitic batholiths is also supported by the isotopic arguments provided in this paper (Fig. 3). Whole-rock isotopes show not only that the batholiths do not follow an only-crustal array, but also the exact overlap between isotopes from sanukitoid and granitic rocks, the former represented by the metasomatized-mantle (MM) model line. The fact that evolved isotopic signatures are present in the more mafic terms of the series makes crustal processes of contamination and magma mixing unlikely, since no correlation is observed with characteristic crustal contaminants such as Si and K. Hence, the only plausible explanation that satisfies all observations is that the recycled signature was already present in a mantle source.

Nevertheless, even if all collected evidence points to a mantle source for the post-collisional magmatism, some drawbacks of the model must be addressed. Previous experimental results using sanukitoid-only starting material (5Q-92) at 0.3 GPa provide interesting insights on the problem. While the geochemical signature is indeed reproduced by 0.3 GPa differentiation of a sanukitoid parental magma (0.3 GPa sanukitoid experimental cotectic, Fig. 5), shallow depth differentiation for the mantle magmas implies the generation of a solid residue that is absent in the batholiths at the level of final emplacement and crystallization. On the other hand, 1.0 GPa differentiation eliminates the problem of the shallow residue, since it stays in the lower crust and accounts for its gran-

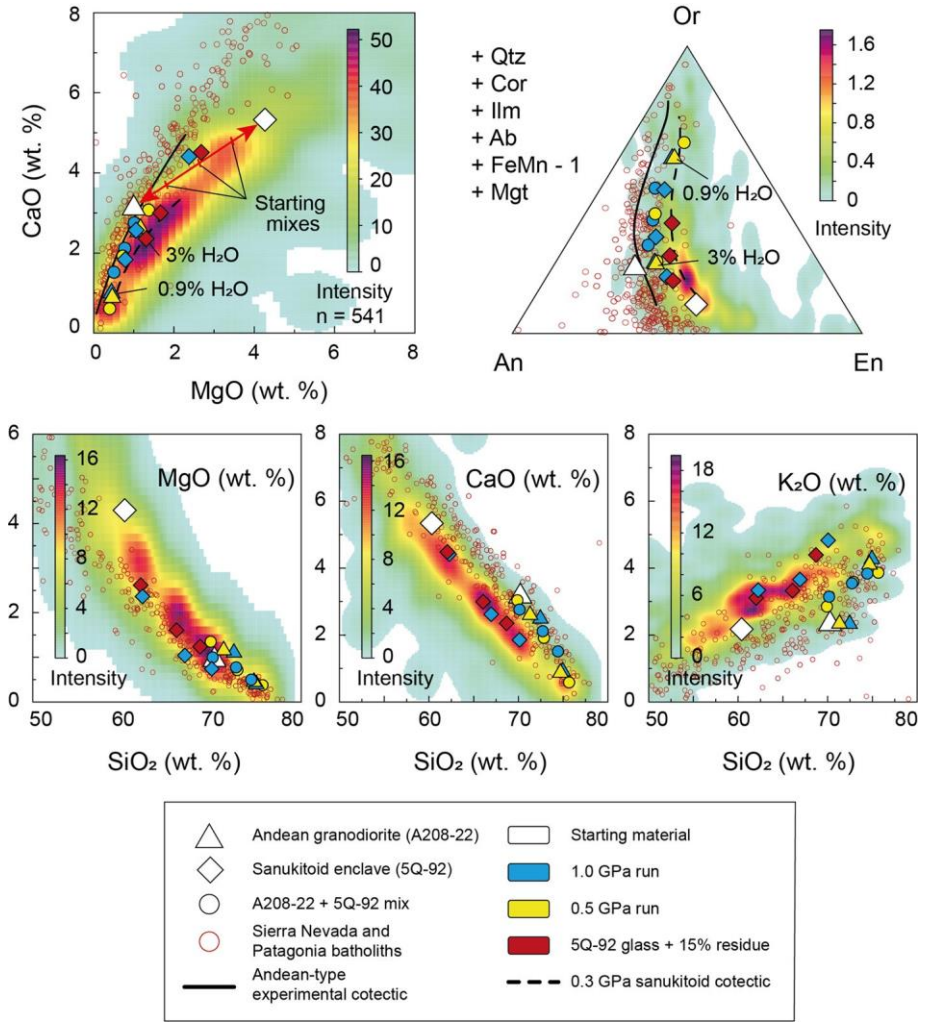

Fig. 5. Selected diagrams and additional Harker diagrams with the experimental liquids plotted. For the runs using mixes higher CaO and MgO equals to higher mafic component in the mix. The Kernel density plot represents the British Caledonian batholith. The experimental liquids from mixes follow the Andean-type cotectic array, showing no deviation towards post-collisional signature when increasing the mafic component. Liquids from using only Andean granodiorite (A208-22) also have Andean-type geochemistry, regardless of the water content. Sanukitoid (5Q-92) only runs have post-collisional geochemical signature, following the post-collisional density maxima in CaO and K_2O Harker diagrams. Mixing of sanukitoid liquids with 15% of the experimental solid residue improves the MgO values, resulting in a composition that fully matches the post-collisional geochemical signature.

ulitic nature (Fig. 6), but slightly higher MgO values are observed in the rocks than in the synthesized products (blue squares, Fig. 5). Further explanations must be provided to account for this ambiguity. In this regard, we find of special interest the widespread presence of amphibole aggregates (clots) that represent relic pyroxene crystals (Stephens, 2001), together with relic plagioclase cores, in many post-collisional plutons. These observations point to the conclusion that the rocks represent a system that was not 100% liquid, with the magmas most likely dragging suspended solid material either from the source or from a putative magma chamber. Experimental results suggest that the incorporation of crustal material (granite) pushes the composition towards Andean-type affinity, thus excluding the interaction with a crustal contaminant as the cause of post-collisional magmatism. Moreover, to account for a ubiquitous feature of magmas, namely the off-Andean post-collisional array (Fig. 2), the incorporated material must be available regardless of the specific setting. This is only explained if the contaminant is an intrinsic characteristic of the system and not an accidental contaminant. We propose that mafic contaminants are represented by minerals as pyroxene or amphibole entrained within the magmas as either early crystalized cumulates or restitic phases from a mantle ultramafic source (Fig. 6). To test this hypothesis, the sanukitoid experimental liquids were mixed with 15% of the experimental residue. This value is calculated after checking different mix proportions and testing which one satisfies the post-collisional geochemistry best. Interestingly, the resulting composition falls in the post-collisional array (red squares, Fig. 5). This estimation is also supported by the relatively common reaction textures that are observed on the rocks. Specifically, relict cores of anortite-rich plagioclase are common in granodiorites and enclaves. Also, amphibole clots are widely present in the rocks of the series. This can be explained by shallow depth re-equilibration of the liquids, as shown by the 0.3 GPa sanukitoid experimental cotectic (Gómez-Frutos and Castro, 2022). Furthermore, a geochemical signature partially caused by a variable self-contamination process that behaves like an open system is coherent with the heterogeneity displayed by post-collisional rocks. While this contamination mechanism can also occur in the Andean-type system, the scarcity of orthopyroxene causes the whole composition of the residue to be colinear with the cotectic. Thus, the contaminated liquids are displaced along mixing lines close to the cotectic line (Castro, 2021, his Fig. 3). Furthermore, a high residence time in the crust while slowly cooling is expected to re-equilibrate the mag-

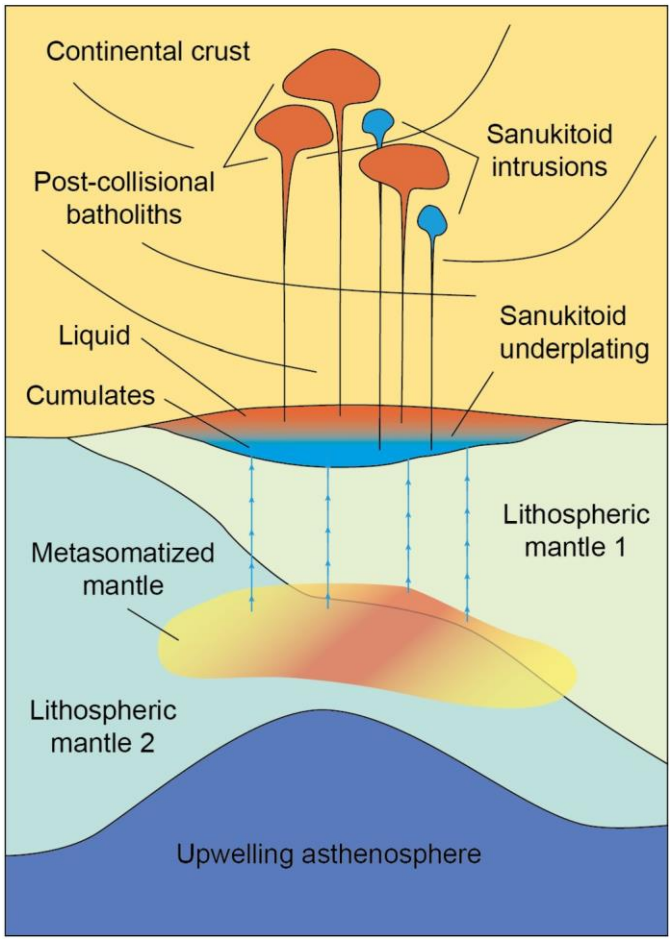

Fig. 6. Schematic petrogenetic model for post-collisional magmatism. Asthenosphere upwelling heats the pre-existing metasomatized mantle, potentially triggering melting. Subsequent sanukitoid melts ascend and underplate in the high rheology contrast surface between the crust and the lithospheric mantle. Due to density contrast differentiated liquids rise and cumulates sink. Extracted melts drag cumulate phases due to their high availability, resulting in the heterogeneous geochemistry displayed by post-collisional batholiths. After all melt extraction has occurred leftover cumulate material joins the lower crust, accounting for its depleted nature. This whole process represents the addition of a considerable amount of igneous material to the continental crust from the underlying metasomatized mantle.

mas into the low-Ca and high-Mg observed signature, erasing any former evidence of disequilibrium.

In summary, our experimental results support an origin of post-collisional batholiths in which the continental crust is not involved directly in the process. This consideration, together with the isotopic and physical evidence, points to the conclusion that the post-collisional granites share a common source with the mafic magmas they appear associated with. That is, they both come from a metasomatized mantle source.

On a final note, the origin of this metasomatized mantle and geodynamic processes leading to mantle melting and post-collisional magma generation are a topic that need of further discussion. It has been argued in arc related environments that melts and/or fluids from a subducted slab are unable to transport the trace element budget that characterize intermediate magmatism, being necessary the whole material present in subducted mélanges of oceanic crust sediments (Castro et al., 2013; Nielsen and Marschall, 2017). This metasomatism may be the result of multiple subduction events, and not only the most recent one, as shown by the wide range of model ages in post-collisional magmas (Fig. 3). Moreover, the preferred mechanism to trigger melting is a combination of decompression and heating due to mantle upwelling (Fig. 6). This is a plausible scenario according to thermomechanical models in collisional orogens (e.g. Faccenda et al., 2008; Ueda et al., 2012). Although post-collisional magmatism differs from arc magmatism (see above), the interaction between mantle and subducted materials is needed in both cases. However, note that these considerations are merely speculative and depicting an accurate model is beyond the scope of this paper. Hence, this topic should and will be the subject of future works, most preferably combining the information given by new experiments and thermomechanical models.

5.2 Implications for crustal growth

Data provided in the former epigraphs aimed to unravel the origin of the batholiths, pointing to the conclusion that they were originated in the mantle. This premise has direct consequences in the crustal growth discussion in several different aspects. Evidence of granodioritic magmas sourced in the mantle represents a major issue when addressing the origin of continents, since thepost-Archean continental crust is estimated to be constituted by andesites or granitoids of granodioritic affinity (Hacker et al., 2011; Rudnick et al., 2003). Crustal growth for a given time interval is calculated by the volume of continental crust generated from the mantle minus the amount immersed and assimilated back into the mantle (Condie and Aster, 2010). In other words, two main points must be addressed when discussing crustal growth over a given process, namely generation of the magmas and preservation rates. In this regard, the timing of the magmatic process is of special relevance, since it has a direct impact on both aforementioned fac- tors.

Work on zircon large datasets has recently been the focus of crustal growth studies, allowing for a global view of the supercontinent cycle and crustal growth intervals (Dhuime et al., 2018). While Hf-O systematics have limitations, specifically when used on detrital zircon grains for petrogenetic purposes, they trace the occurrence of big magmatic events and their timing within the supercontinent cycle. If post-collisional magmatism produces new continental crust, the assembly of supercontinents and their related orogenic process must be correlated with maxima in the continental crust production. In this regard, accretionary orogens have been active continuously throughout a major part of the Earth history and constitute major sites of continental growth (Cawood et al., 2006). Accordingly, the peak of crustal growth for each supercontinent cycle is coincident with the post-collisional stage (Condie and Aster, 2010; Hawkesworth et al., 2010; Hildebrand and Whalen, 2017). This observation makes no sense other than the batholiths representing juvenile injections to the continental crust.

Equally important, preservation is widely known to be a key factor when considering the net growth of the continental crust. Not only that, but recent work has also even considered that preservation is more relevant than magma generation for crustal net growth, with peaks in crystallization ages reflecting biases in preservation rather than magma production (Hawkesworth et al., 2009). Appropriately, the estimated preservation rates agree with the post-collisional batholiths playing a major role in crustal growth, since the preservation potential of new igneous rocks reaches a maximum in the post-collisional stage of the supercontinent cycle (Condie et al., 2011; Hawkesworth et al., 2009). This enhanced preservation potential is due to the rocks being shielded in the new orogens produced in each supercontinent cycle and mostly located towards its core. This results in an important contribution to the creation of long-term lived continental crust (Couzinié et al., 2016; Hawkesworth et al., 2010).

The two described factors support the role of post-collisional magmatism as a crustal growth mechanism. Both the generation

and preservation rates are explained by holding post-collisional magmas partially responsible for crustal growth. Additionally, natural evidence provided by outcropping rocks shows that this magmatism has been present throughout most of the history of the planet, associated with large scale orogenic process and supercontinent assembly. However, it has been particularly abundant in post-Archean times, producing a significant magmatic input during the most recent supercontinents formation. If this magma is mantle derived the stablished crustal growth paradigms must be revised, since the crustal growth associated with it may have been severely underestimated.

6. Conclusions

While the post-collisional mafic suite has recently been demonstrated to be a limited crustal growth mechanism, the more voluminous silicic suite has historically been dismissed in the crustal growth discussion due to bias imposed by the notion that it derives from a mostly recycled crustal source. However, the data presented in this paper points to the different conclusion that post-collisional granitic magmas indeed represent crustal growth.

If the post-collisional magmas come from a fully recycled crustal source, they should display crustal isotopic signatures. However, provided data shows that all the presented batholiths have a significant mantle component, coincident with a metasomatized mantle model line calculated using the mafic magma associated to these intrusions. Furthermore, experimental data provides a mechanism for the generation of the granitic suites and reproduction of the post-collisional geochemical signature (high MgO and K_2O, low CaO, and high LILE and LREE) by only using a mantle derived parental magma. That is, differentiation from a sanukitoid (post-collisional mafic magma) parental magma reproduces the post-collisional geochemical signature, with additional contamination with its own residue further enhancing the high-Mg signature and accounting for the heterogeneity of the series. Therefore, the crustal component is ultimately not necessary for the reproduction of the post-collisional granitic batholiths during batholith generation and emplacement, being the continental-like signature already present in the mantle source. This petrological argument points to the conclusion that post-collisional magmas represent the addition of juvenile material to the continental crust.

The generation of continental crust by post-collisional magmatism is also coherent with the observed generation and preservation rates within each supercontinent cycle. The existing models reveal the overlap between peaks in the continental crust production and orogenic to post-orogenic processes, correlating the post-collisional stage with the largest mantle derived magmatic input to the crust. Additionally, the preservation rates of magmas also reach maxima in the post-collisional stage, with the magmas shielded in the core of the orogens that amalgamated the supercontinents.

All presented arguments stablish a mechanism that can generate new continental crust in the most appropriate moment to allow its long-term preservation. Existing models must be revisited considering the given evidence, since post-Archean crustal growth may have been severely underestimated.

CRediT authorship contribution statement

Daniel Gómez-Frutos: Conceptualization, Data curation, Formal analysis, Investigation, Methodology, Validation, Visualization, Writing – original draft, Writing – review & editing. **Antonio Castro:** Conceptualization, Funding acquisition, Investigation, Methodology, Project administration, Supervision, Validation, Writing – review & editing. **Gabriel Gutiérrez-Alonso:** Conceptualization, Funding acquisition, Supervision, Writing – review & editing.

Declaration of competing interest

The authors declare that they have no known competing financial interests or personal relationships that could have appeared to influence the work reported in this paper.

Data availability

The compiled and experimental data is available in the online Supplementary Material.

Acknowledgements

This work was supported through the Spanish Research Agency (AEI) Grant N° PGC2018-096534-B-I00 (Proyecto IBERCRUST). We acknowledge the support received from the Instituto Andaluz de Ciencias de la Tierra (CSIC - UGR) and its staff for the installation of a high-pressure laboratory. We are particularly grateful to Taras Gerya and Mike Fowler for their positive and constructive feedback. We also want to thank Rosemary Hickey-Vargas for her handling of this manuscript.

Appendix A. Supplementary material

Supplementary material related to this article can be found online at https://doi.org/10.1016/j.epsl.2022.117978.

References

Annen, C., Blundy, J.D., Sparks, R.S.J., 2006. The genesis of intermediate and silicic magmas in deep crustal hot zones. J. Petrol. 47 (3), 505–539. https://doi.org/10.1093/petrology/egi084.

Aranovich, L.Y., Makhluf, A.R., Manning, C.E., Newton, R.C., 2014. Dehydration melting and the relationship between granites and granulites. Precambrian Res. 253, 26–37. https://doi.org/10.1016/j.precamres.2014.07.004.

Arndt, N.T., Goldstein, S.L., 1987. Use and abuse of crust-formation ages. Geology 15 (10), 893–895. https://doi.org/10.1130/0091-7613(1987)15<893:UAAOCA>2.0.CO;2.

Arndt, N.T., 2013. The formation and evolution of the continental crust. Geochem. Perspect. 2 (3), 405.

Barbarin, B., 1999. A review of the relationships between granitoid types, their origins and their geodynamic environments. Lithos 46 (3), 605–626. https://doi.org/10.1016/S0024-4937(98)00085-1.

Barth, M.G., McDonough, W.F., Rudnick, R.L., 2000. Tracking the budget of Nb and Ta in the continental crust. Chem. Geol. 165 (3–4), 197–213. https://doi.org/10.1016/S0009-2541(99)00173-4.

Belousova, E.A., Kostitsyn, Y.A., Griffin, W.L., Begg, G.C., O'Reilly, S.Y., Pearson, N.J., 2010. The growth of the continental crust: constraints from zircon Hf-isotope data. Lithos 119 (3–4), 457–466. https://doi.org/10.1016/j.lithos.2010.07.024.

Bonin, B., 2004. Do coeval mafic and felsic magmas in post-collisional to within-plate regimes necessarily imply two contrasting, mantle and crustal, sources? A review. Lithos 78 (1–2), 1–24. https://doi.org/10.1016/j.lithos.2004.04.042.

Castro, A., Moreno-Ventas, I., Fernández, C., Vujovich, G., Gallastegui, G., Heredia, N., Martino, R.D., Becchio, R., Corretgé, L.G., Díaz-Alvarado, J., Such, P., García-Arias, M., Liu, D.Y., 2011. Petrology and SHRIMP U–Pb zircon geochronology of Cordilleran granitoids of the Bariloche area, Argentina. J. South Am. Earth Sci. 32 (4), 508–530. https://doi.org/10.1016/j.jsames.2011.03.011.

Castro, A., Vogt, K., Gerya, T., 2013. Generation of new continental crust by sublithospheric silicic-magma relamination in arcs: a test of Taylor's andesite model. Gondwana Res. 23 (4), 1554–1566. https://doi.org/10.1016/j.gr.2012.07.004.

Castro, A., 2020. The dual origin of I-type granites: the contribution from experiments. Geol. Soc. (Lond.) Spec. Publ. 491 (1), 101–145. https://doi.org/10.1144/SP491-2018-110.

Castro, A., 2021. A non-basaltic experimental cotectic array for calc-alkaline batholiths. Lithos 382, 105929. https://doi.org/10.1016/j.lithos.2020.105929.

Cawood, P.A., Kroner, A., Pisarevsky, S., 2006. Precambrian plate tectonics: criteria and evidence. GSA Today 16 (7), 4. https://doi.org/10.1130/GSAT01607.1.

Cawood, P.A., Hawkesworth, C.J., Dhuime, B., 2013. The continental record and the generation of continental crust. GSA Bull. 125 (1–2), 14–32. https://doi.org/10.1130/B30722.1.

Chappell, B.W., Stephens, W.E., 1988. Origin of infracrustal (I-type) granite magmas. Earth Environ. Sci. Trans. R. Soc. Edinb. 79 (2–3), 71–86. https://doi.org/10.1017/S0263593300014139.

Chappell, B.W., White, A.J., 2001. Two contrasting granite types: 25 years later. Aust. J. Earth Sci. 48 (4), 489–499. https://doi.org/10.1046/j.1440-0952.2001.00882.x.

Collins, W.J., Huang, H.Q., Jiang, X., 2016. Water-fluxed crustal melting produces Cordilleran batholiths. Geology 44 (2), 143–146. https://doi.org/10.1130/G37398.1.

Condie, K.C., Aster, R.C., 2010. Episodic zircon age spectra of orogenic granitoids: the supercontinent connection and continental growth. Precambrian Res. 180 (3–4), 227–236. https://doi.org/10.1016/j.precamres.2010.03.008.

Condie, K.C., Bickford, M.E., Aster, R.C., Belousova, E., Scholl, D.W., 2011. Episodic zircon ages, Hf isotopic composition, and the preservation rate of continental crust. GSA Bull. 123 (5–6), 951–957. https://doi.org/10.1130/B30344.1.

Condie, K.C., 2014. Growth of continental crust: a balance between preservation and recycling. Mineral. Mag. 78 (3), 623–637. https://doi.org/10.1180/minmag.2014.078.3.11.

Couzinié, S., Laurent, O., Moyen, J.F., Zeh, A., Bouilhol, P., Villaros, A., 2016. Post-collisional magmatism: crustal growth not identified by zircon Hf–O isotopes. Earth Planet. Sci. Lett. 456, 182–195. https://doi.org/10.1016/j.epsl.2016.09.033.

Dewey, J.F., Windley, B.F., 1981. Growth and differentiation of the continental crust. Philos. Trans. R. Soc. Lond. Ser. A, Math. Phys. Sci. 301 (1461), 189–206. https://doi.org/10.1098/rsta.1981.0105.

Dhuime, B., Hawkesworth, C., Cawood, P., 2011. When continents formed. Science 331 (6014), 154–155. https://doi.org/10.1126/science.1201245.

Dhuime, B., Hawkesworth, C.J., Cawood, P.A., Storey, C.D., 2012. A change in the geodynamics of continental growth 3 billion years ago. Science 335 (6074), 1334–1336. https://doi.org/10.1126/science.1216066.

Dhuime, B., Hawkesworth, C.J., Delavault, H., Cawood, P.A., 2018. Rates of generation and destruction of the continental crust: implications for continental growth. Philos. Trans. R. Soc. A, Math. Phys. Eng. Sci. 376 (2132), 20170403. https://doi.org/10.1098/rsta.2017.0403.

Faccenda, M., Gerya, T.V., Chakraborty, S., 2008. Styles of post-subduction collisional orogeny: influence of convergence velocity, crustal rheology and radiogenic heat production. Lithos 103 (1–2), 257–287. https://doi.org/10.1016/j.lithos.2007.09.009.

Fowler, M.B., Henney, P.J., 1996. Mixed Caledonian appinite magmas: implications for lamprophyre fractionation and high Ba-Sr granite genesis. Contrib. Mineral. Petrol. 126 (1), 199–215. https://doi.org/10.1007/s004100050244.

Fowler, M.B., Henney, P.J., Darbyshire, D.P.F., Greenwood, P.B., 2001. Petrogenesis of high Ba–Sr granites: the Rogart pluton, Sutherland. J. Geol. Soc. 158 (3), 521–534. https://doi.org/10.1144/jgs.158.3.52.

Fowler, M.B., Kocks, H., Darbyshire, D.P.F., Greenwood, P.B., 2008. Petrogenesis of high Ba–Sr plutons from the northern highlands Terrane of the British Caledonian Province. Lithos 105 (1–2), 129–148. https://doi.org/10.1016/j.lithos.2008.03.003.

Fowler, M., Rollinson, H., 2012. Phanerozoic sanukitoids from Caledonian Scotland: implications for Archean subduction. Geology 40 (12), 1079–1082. https://doi.org/10.1130/G33371.1.

Gómez-Frutos, D., Castro, A., 2022. Sanukitoid crystallization relations at 1.0 and 0.3 GPa. Lithos 414, 106632. https://doi.org/10.1016/j.lithos.2022.106632.

Griffin, W.L., Pearson, N.J., Belousova, E., Jackson, S.E., van Achterbergh, E., O'Reilly, S.Y., Shee, S.R., 2000. The Hf isotope composition of cratonic mantle: LAM- MC-ICPMS analysis of zircon megacrysts in kimberlites. Geochim. Cosmochim. Acta 64, 133–147. https://doi.org/10.1016/S0016-7037(99)00343-9.

Hacker, B.R., Kelemen, P.B., Behn, M.D., 2011. Differentiation of the continental crust by relamination. Earth Planet. Sci. Lett. 307 (3–4), 501–516. https://doi.org/10.1016/j.epsl.2011.05.024.

Hawkesworth, C., Cawood, P., Kemp, T., Storey, C., Dhuime, B., 2009. A matter of preservation. Science 323 (5910), 49–50. https://doi.org/10.1126/science.1168549.

Hawkesworth, C.J., Dhuime, B., Pietranik, A.B., Cawood, P.A., Kemp, A.I., Storey, C.D., 2010. The generation and evolution of the continental crust. J. Geol. Soc. 167 (2), 229–248.

Hawkesworth, C., Cawood, P.A., Dhuime, B., 2019. Rates of generation and growth of the continental crust. Geosci. Front. 10 (1), 165–173. https://doi.org/10.1016/j.gsf.2018.02.004.

Herrmann, W., Berry, R.F., 2002. MINSQ–a least squares spreadsheet method for calculating mineral proportions from whole rock major element analyses. Geochem., Explor. Environ. Anal. 2 (4), 361–368. https://doi.org/10.1144/1467-787302-010.

Hildebrand, R.S., Whalen, J.B., 2017. The Tectonic Setting and Origin of Cretaceous Batholiths Within the North American Cordillera: the Case for Slab Failure Magmatism and Its Significance for Crustal Growth, vol. 532. Geological Society of America.

Jagoutz, O., Kelemen, P.B., 2015. Role of arc processes in the formation of continental crust. Annu. Rev. Earth Planet. Sci. 43, 363–404. https://doi.org/10.1146/annurev-earth-040809-152345.

Kemp, A.I.S., Hawkesworth, C.J., Paterson, B.A., Kinny, P.D., 2006. Episodic growth of the Gondwana supercontinent from hafnium and oxygen isotopes in zircon. Nature 439, 580–583. https://doi.org/10.1038/nature04505.

Meissner, R., Marshall, J., Plumb, R.A., 1986. The Continental Crust: a Geophysical Approach, vol. 34. Academic Press.

Moyen, J.F., Laurent, O., Chelle-Michou, C., Couzinié, S., Vanderhaeghe, O., Zeh, A., Villaros, A., Gardien, V., 2017. Collision vs. subduction-related magmatism: two contrasting ways of granite formation and implications for crustal growth. Lithos 277, 154–177. https://doi.org/10.1016/j.lithos.2016.09.018.

Nielsen, S.G., Marschall, H.R., 2017. Geochemical evidence for mélange melting in global arcs. Sci. Adv. 3 (4), e1602402. https://doi.org/10.1126/sciadv.1602402.

Orejana, D., Villaseca, C., Pérez-Soba, C., López-García, J.A., Billström, K., 2009. The Variscan gabbros from the Spanish Central System: a case for crustal recycling in the sub-continental lithospheric mantle? Lithos 110 (1–4), 262–276. https://doi.org/10.1016/j.lithos.2009.01.003.

Payne, J.L., McInerney, D.J., Barovich, K.M., Kirkland, C.L., Pearson, N.J., Hand, M., 2016. Strengths and limitations of zircon Lu-Hf and O isotopes in modelling crustal growth. Lithos 248, 175–192. https://doi.org/10.1016/j.lithos.2015.12.015.

Petford, N., Gallagher, K., 2001. Partial melting of mafic (amphibolitic) lower crust by periodic influx of basaltic magma. Earth Planet. Sci. Lett. 193 (3–4), 483–499. https://doi.org/10.1016/S0012-821X(01)00481-2.

Pitcher, W.S., 1987. Granites and yet more granites forty years on. Geol. Rundsch. 76 (1), 51–79. https://doi.org/10.1007/BF01820573.

Plank, T., Kelley, K.A., Zimmer, M.M., Hauri, E.H., Wallace, P.J., 2013. Why do mafic arc magmas contain 4 wt% water on average? Earth Planet. Sci. Lett. 364, 168–179. https://doi.org/10.1016/j.epsl.2012.11.044.

Roberts, N.M., Spencer, C.J., 2015. The zircon archive of continent formation through time. Geol. Soc. (Lond.) Spec. Publ. 389 (1), 197–225. https://doi.org/10.1144/SP389.14.

Rudnick, R.L., 1995. Making continental crust. Nature 378 (6557), 571–578. https://doi.org/10.1038/378571a0.

Rudnick, R.L., Fountain, D.M., 1995. Nature and composition of the continental crust: a lower crustal perspective. Rev. Geophys. 33 (3), 267–309. https://doi.org/10.1029/95RG01302.

Rudnick, R.L., Gao, S., Holland, H.D., Turekian, K.K., 2003. Composition of the continental crust. The Crust 3, 1–64.

Shirey, S.B., Hanson, G.N., 1984. Mantle-derived Archaean monozodiorites and trachyandesites. Nature 310 (5974), 222–224. https://doi.org/10.1038/310222a0.

Smithies, R.H., Champion, D.C., 2000. The Archaean high-Mg diorite suite: links to tonalite–trondhjemite–granodiorite magmatism and implications for early Archaean crustal growth. J. Petrol. 41 (12), 1653–1671. https://doi.org/10.1093/petrology/41.12.1653.

Smithies, R.H., Lu, Y., Kirkland, C.L., Johnson, T.E., Mole, D.R., Champion, D.C., Martin, L., Jeon, H., Michael, T.D., Johnson, S.P., 2021. Oxygen isotopes trace the origins of Earth's earliest continental crust. Nature 592 (7852), 70–75. https://doi.org/10.1038/s41586-021-03337-1.

Spencer, C.J., Roberts, N.M.W., Santosh, M., 2017. Growth, destruction, and preservation of Earth's continental crust. Earth-Sci. Rev. 172, 87–106. https://doi.org/10.1016/j.earscirev.2017.07.013.

Stephens, W.E., 2001. Polycrystalline amphibole aggregates (clots) in granites as potential I-type restite: an ion microprobe study of rare-Earth distributions. Aust. J. Earth Sci. 48 (4), 591–601. https://doi.org/10.1046/j.1440-0952.2001.00880.x.

Stern, R.A., Hanson, G.N., Shirey, S.B., 1989. Petrogenesis of mantle-derived, LILE-enriched Archean monzodiorites and trachyandesites (sanukitoids) in southwestern Superior Province. Can. J. Earth Sci. 26 (9), 1688–1712. https://doi.org/10.1139/e89-145.

Ueda, K., Gerya, T.V., Burg, J.P., 2012. Delamination in collisional orogens: thermomechanical modeling. J. Geophys. Res., Solid Earth 117 (B8). https://doi.org/10.1029/2012JB009144.

Voice, P.J., Kowalewski, M., Eriksson, K.A., 2011. Quantifying the timing and rate of crustal evolution: global compilation of radiometrically dated detrital zircon grains. J. Geol. 119 (2), 109–126. https://doi.org/10.1086/658295.

Weinberg, R.F., Hasalová, P., 2015. Water-fluxed melting of the continental crust: a review. Lithos 212, 158–188. https://doi.org/10.1016/j.lithos.2014.08.021.

Wood, B.J., Turner, S.P., 2009. Origin of primitive high-Mg andesite: constraints from natural examples and experiments. Earth Planet. Sci. Lett. 283 (1–4), 59–66. https://doi.org/10.1016/j.epsl.2009.03.032.

5.1.3

Mafic microgranular enclaves (MMEs) trace the origin of post-collisional magmas

Geology, 2023

GEOLOGY | THE GEOLOGICAL SOCIETY OF AMERICA®

https://doi.org/10.1130/G51248.1

Manuscript received 21 March 2023
Revised manuscript received 3 May 2023
Manuscript accepted 16 May 2023

Published online 1 June 2023

Mafic microgranular enclaves (MMEs) trace the origin of post-collisional magmas

Daniel Gómez-Frutos* and Antonio Castro
Museo Nacional de Ciencias Naturales (MNCN), Consejo Superior de Investigaciones Científicas (CSIC), C. José Gutiérrez Abascal 2, 28006 Madrid, Spain

ABSTRACT

Mafic microgranular enclaves (MMEs) are a ubiquitous feature of post-collisional magmatism, receiving much attention among earth scientists over the last decades. While recent advances point to the large-scale involvement of the lithospheric mantle in granite petrogenesis, MMEs have received less attention in such discussion. Because MMEs are commonly acknowledged to represent the mafic end member with a mantle affinity that is related to early-stage batholith petrogenesis, they constitute a good proxy for the mantle role in the process. Using MME data from Los Pedroches batholith in southwestern Iberia, we conduct a geochemical comparative study between MMEs and the mafic-intermediate (sanukitoid) suite of post-collisional batholiths. An accurate overlap between the two groups is revealed, implying a potential genetic link between MMEs and the sanukitoid suite. Together with evidence from experimental cotectic liquids, the link between the high-Mg signature of post-collisional magmas and the predominance of amphibole in the studied MME samples is used to account for the composition of post-collisional magmatism. Implications for post-collisional batholith petrogenesis is then discussed in a qualitative manner, suggesting a heterogeneous yet common two-stage origin for all post-collisional magmatism in which the relationship between MMEs, sanukitoid, and the host felsic magmas is a differentiation process, thus representing a major input of juvenile magma into the crust.

INTRODUCTION

Fine-grained and dark mafic microgranular enclaves (MMEs) are a characteristic feature of post-collisional granodiorites and granites, together with the characteristic mafic-intermediate and felsic suites of post-collisional magmatism (e.g., Couzinié et al., 2016; Gómez-Frutos et al., 2023; Moyen et al., 2017). Although they share many geochemical features with their host granitic magmas, MMEs have a stronger mantle affinity (Clemens et al., 2017; Holden et al., 1987), implying extensive mantle-crust interaction in the petrogenesis of the granite magmas. However, even though the petrogenetic significance of MMEs has been studied for several decades (e.g., Barbarin, 2005; Barbarin and Didier, 1992; Paterson et al., 2004; Vernon, 1984; Wiebe, 2016), a satisfactory explanation that meets all observations for such mantle-crust interaction and for their relationship with host granites remains elusive (see Clemens et al., 2017, for a review). While different interpretations for the petrogenesis of MMEs exist (Barbey et al., 2008; Rodríguez and Castro, 2019; Vernon et al., 1988; Žák and Paterson, 2010), it is widely accepted that MMEs were involved in the earliest stages of magma generation, constituting direct evidence of the mechanism that formed the batholiths. Moreover, if MMEs represent melt generated in the mantle as commonly inferred, exploring their relationship with the modified mantle-sourced mafic-intermediate suite, also called sanukitoid, can provide useful insights. Sanukitoid magmas (including appinites and vaugnerites) have been described all around the world as minor mafic-intermediate intrusions associated with post-collisional granite batholiths, displaying a heterogeneous yet consistent geochemistry (e.g., Fowler and Rollinson, 2012; Heilimo et al., 2010). In this paper, we investigate the genetic link between post-collisional MMEs and host granitic rocks by comparing new data from the Los Pedroches batholith (southwestern Iberia) with a large sanukitoid magma database and existing experimental data. The potential significance of MMEs regarding the origin of post-collisional batholiths as fractionated liquids from an intermediate parental magma is established.

MMES FROM LOS PEDROCHES

The Los Pedroches batholith is an aligned group of intrusions located in the southernmost sector of the Central Iberian Zone in the Iberian Massif. It is hosted mainly by low-grade Carboniferous strata, with only the northern part of the batholith intruding older metapelites of early Cambrian to Neoproterozoic age. The batholith comprises two large groups of intrusions (Fig. 1): (1) an elongated massif referred to as Los Pedroches granodiorite, in which abundant MMEs can be found, and (2) a peraluminous monzogranitic unit, occurring as small discontinuous intrusions that crosscut the granodioritic massif and are much scarcer in MMEs (Carracedo et al., 2009). The current study is focused on the granodiorite suite, which shows evidence of limited assimilation of crustal material during emplacement given the scarcity of host xenoliths, low values in alumina saturation index (ASI), and the isotopic equilibrium between the studied MMEs. A representative number of new enclaves was collected for this study and complemented with existing data from the bibliography (for further details see Table S1 in the Supplemental Material[1]).

The collected MME samples display variations in grain size, texture, and modal abundance but have a consistent assemblage of plagioclase (Pl), biotite (Bt), amphibole (Amp), quartz (Qz), and K-feldspar (Kfs) with accessory apatite,

Daniel Gómez-Frutos https://orcid.org/0000-0001-7057-1210
*daniel.gomez@csic.es

[1]Supplemental Material. Rock analyses, sample photographs, sampling and analytical methods, additional Harker diagrams, and extended discussion for geochemical modeling. Please visit https://doi.org/10.1130/GEOL.S.23063099 to access the supplemental material, and contact editing@geosociety.org with any questions.

CITATION: Gómez-Frutos, D., and Castro, A., 2023, Mafic microgranular enclaves (MMEs) trace the origin of post-collisional magmas: Geology, v. 51, p. 743–747, https://doi.org/10.1130/G51248.1

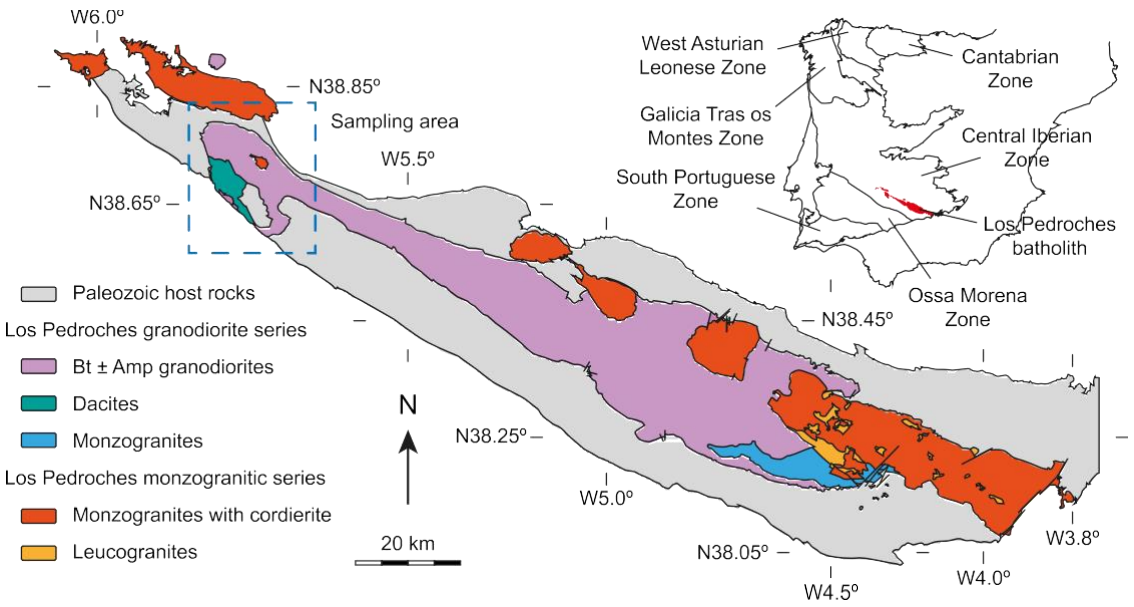

Figure 1. Geological setting of the study area. Los Pedroches batholith is in the Central Iberian Zone, in the Iberian Massif. Surrounding rocks are mainly Carboniferous metasediments. Bt—biotite; Amp—amphibole. Map modified from Instituto Geológico y Minero de España, cartografía geológica digital continua (http://info.igme.es/cartografiadigital/geologica/geodezona.aspx?Id=Z2500).

allanite, zircon, titanite, and oxides, the same assemblage as the host granodiorite. Moreover, MMEs are devoid of chilled margins but show magmatic quenching textures affecting the whole enclaves and no evidence of reaction with the host granodiorite (Castro and Stephens, 1992; Fig. S2). Because mingling between two magmas results in chilled margins, these observations are explained only if MMEs and host rocks are two systems in chemical equilibrium, with MMEs being autoliths (Rodríguez and Castro, 2019). Two types of MMEs are distinguished: MME1 and MME2. Mesocratic and porphyritic textures characterize MME1, with phenocrysts of Pl and Amp clots as much as 5 mm in length, enclosed in a fine-grained groundmass of Pl, Qz, Kfs, Bt, and Amp. By contrast, MME2 is rich in Amp and shows varied textures from equigranular hypidiomorphic to porphyritic, with phenocrysts of Pl and Amp aggregates (clots). Transitional enclaves between the two groups are common. Amphibole (hornblende to locally subsolidus actinolite) clots are the most outstanding feature of both groups, a characteristic that is also common in post-collisional Caledonian-type plutons (Castro and Stephens, 1992). Considering their potential relevance as possible remnants of an ultramafic end member or magmatic cumulates, sampling focused on collecting enclaves containing variable amounts of Amp clots. Collected samples were analyzed for major and trace elements. A selected group was analyzed for isotopic ratios of the Sr and Nd systematics (rock analyses and analytical methods can be found in Table S1 and Supplemental Text S3 [see footnote 1]).

COMPARATIVE PETROLOGY

Comparative classification diagrams for the Los Pedroches MMEs, their granodiorite host, and sanukitoid series are represented in Figure 2. World sanukitoid series are represented in a kernel density diagram (Figs. 2A–2D) and an average line (Fig. 2E) incorporating a database of 2557 analyses. In most diagrams, a clear overlap between all Los Pedroches samples and the maximum density areas of the sanukitoid series is evident. Compared to the Sierra Nevada (western USA) and Patagonian Andean-type batholiths (dashed red line and gray circles; compilations are available in Gómez-Frutos et al., 2023), significant differences can be observed in the geochemistry of MMEs and host granodiorites. A high-Mg# (Mg# = molar MgO/[MgO + FeO_T], where T indicates total iron) signature is evident in the Fe*-silica diagram (Fe* = wt% FeO_T/[FeO_T + MgO]) (Fig. 2A), a common feature of the sanukitoid series. The ASI (ASI = Al_2O_3/[Na_2O + K_2O + {CaO − 3.3 × P_2O_5}]) diagram shows an overlap in the metaluminous field between all the plotted series (Fig. 2B). Most interestingly, a consistently depleted CaO but enriched K_2O and MgO signature in all plotted groups of the the MME-granodiorite association and the sanukitoid series is evidenced in the modified alkali-lime index (MALI = wt% [Na2O + K2O − CaO]) (Fig. 2C) and CaO-MgO diagrams (Fig. 2D), coherent with the post-collisional geochemical signature (Gómez-Frutos et al., 2023). Furthermore, Los Pedroches MMEs also display the characteristic trace element enrichment of sanukitoid magmas, namely in Cr and Ni, and in contents of large-ion lithophile elements (LILEs), such as Rb, Sr, and Ba (Fig. 2E). Major and trace element resemblance between MMEs and sanukitoid series supports that the two groups are analogous, implying that they share a common origin and that a modified mantle played an essential role in the origin of MMEs. See Figure S4 (see footnote 1) for additional Harker diagrams.

COMPARISON WITH EXPERIMENTAL COTECTIC LIQUIDS

If derivation from a modified mantle accounts for the origin of the sanukitoid suite (Rapp et al., 2010), conditions during three stages in the evolution of the magmas will be the most influential in constraining magma crystallization conditions: (1) conditions in the mantle during segregation, (2) conditions at boundaries with large rheology contrasts (Moho), and (3) conditions at the final emplacement level. Among them, residence time in the Moho and at emplacement level is expected to be substantially higher than in the source, being the most significant when addressing crystallization conditions. Consequently, pressures of ~1.0 and 0.3 GPa have the most compositional effect in the magmas (de Oliveira et al., 2010). Previous experimental work using Los Pedroches MMEs as a starting material attempted to constrain the geochemical evolution of the sanukitoid series (Gómez-Frutos and Castro, 2022; Gómez-Frutos et al., 2023). Experimental liquids at 1.0 and 0.3 GPa follow a cotectic linear path in the CaO-MgO diagram (Fig. 2D), different from that followed by Andean-type batholiths (Castro, 2021). The implication of the existence of a common cotectic trend is that the composition of both sanukitoids and MMEs is thermodynamically constrained instead of resulting from magma mixing processes. Furthermore, their compositional similarity supports that they share the same origin and are controlled by a common thermodynamic system, following the same liquid line of descent (LLD). In other words, altogether, MMEs and sanukitoid represent the mantle component in post-collisional magma generation.

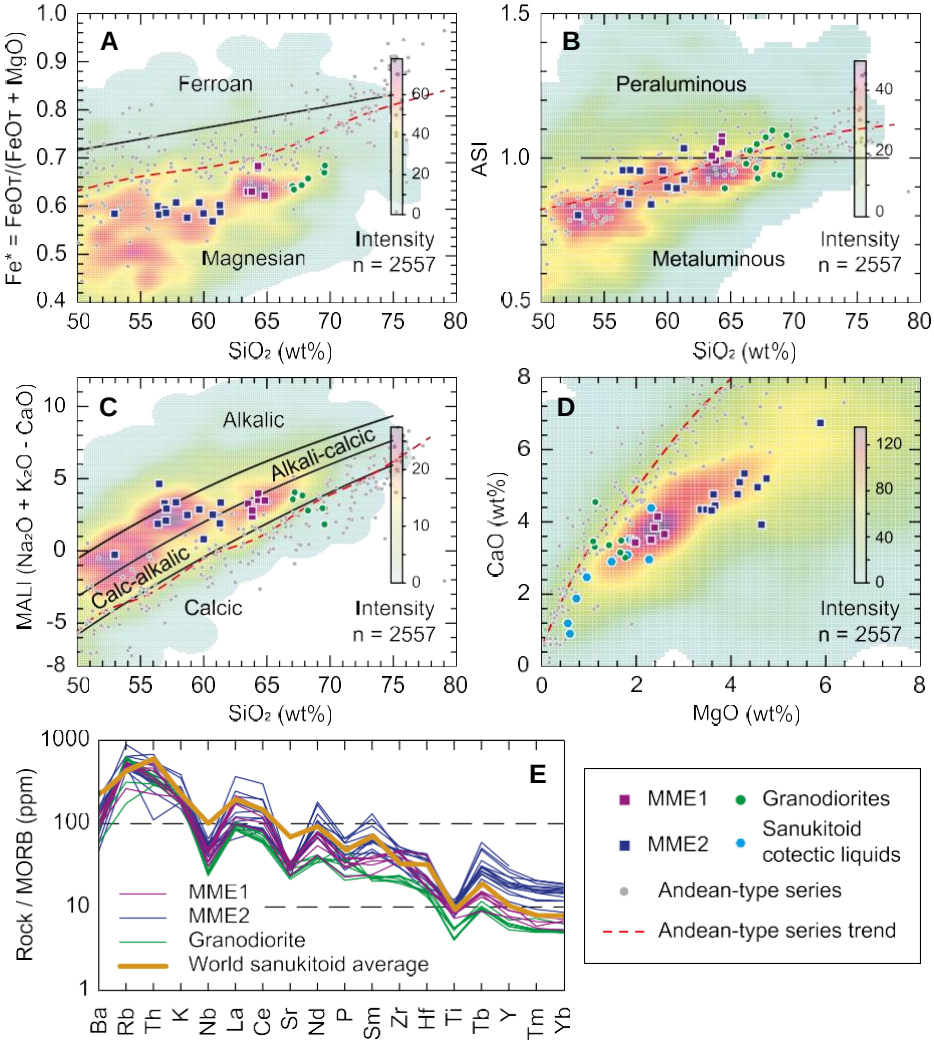

Figure 2. Classification diagrams for post-collisional Los Pedroches batholith samples showing an overlap between mafic microgranular enclaves (MMEs), host rocks, and sanukitoid series (kernel contour plot and average line). (A) Fe* versus SiO_2 diagram. T indicates total iron. (B) Alumina saturation index (ASI = $Al_2O_3/[Na_2O + K_2O + \{CaO - 3.3 \times P_2O_5\}]$) versus SiO_2 diagram. (C) Modified alkali-lime index (MALI) versus SiO_2 diagram. A–C are from Frost et al. (2001). (D) CaO versus MgO diagram. (E) Primitive mantle–normalized trace element spider diagram. Data sources: comparative Andean-type and sanukitoid series from compilation in Gómez-Frutos et al., 2023; cotectic experimental liquids from Gómez-Frutos and Castro, 2022; sources from Los Pedroches data available in Table S1 (see text footnote 1).

MMES AND THE ROLE OF ORTHOPYROXENE IN THE POST-COLLISIONAL SIGNATURE

Cotectic differentiated liquids reproduce most of the geochemical features of granitic (sensu lato) post-collisional magmas (Fig. 2). Nevertheless, they do not fully reproduce the high MgO contents of the series. While Mg# is indeed enriched compared to that of Andean-type rocks, experimental liquids still have slightly lower MgO contents than typical post-collisional rocks. We attribute MgO enrichment to the entrainment of ultramafic material, also likely related to the heterogeneity of the series. However, MgO enrichment is a ubiquitous feature of the magmas, with previous work concluding MMEs obtained their geochemical signature at depth, prior to being incorporated into their host magmas (Clemens et al., 2017, and references therein). Moreover, Sm-Nd isotopes from Los Pedroches batholith indicate that MMEs, sanukitoids, and granites (sensu lato) originated from a common parental magma and that they evolved along a LLD in a mostly closed system where crustal contamination was limited. These considerations exclude contamination during ascent as a potential mechanism to account for the high-MgO signature, suggesting that, instead, it is an intrinsic characteristic of the system.

Experimental evidence highlights how the products from melting of a metasomatized mantle are subjected to the nature of the pre-metasomatism mantle (Rapp et al., 2010), pointing to a dominantly harzburgitic mantle when addressing the high-Mg signature (Wood and Turner, 2009). More specifically, orthopyroxene (Opx) was identified as the liquidus phase of the sanukitoid system (Gómez-Frutos and Castro, 2022). Orthopyroxene constitutes both an available phase in the source and a potential cumulate in a putative crustal magma chamber. Moreover, entrainment of residual Opx in the magmas can account for the high-Mg signature and does not modify the apparently closed system Sm-Nd signature. These inferences point directly to the Amp clots, assumed to come from Opx alteration by rehydration during crystallization (Beard et al., 2005). In Los Pedroches MMEs, the most mafic type (MME2) has the largest abundance of Amp clots and plots toward the Mg pole in the CaO-MgO diagram, showcasing the largest scatter and accounting for the high-Mg signature (Fig. 2D). Textural variations in MME2 are representative of such self-contamination process, with the most equigranular enclaves resembling cumulates and the most porphyritic resembling parental liquids. Together with Opx, crystal accumulation of accessory phases is also plausible, accounting for the observed deviations in Los Pedroches MMEs compared to the sanukitoid array (e.g., accumulation of titanite produces excess of TiO_2). Potential resulting disequilibrium textures are likely masked by the magmas re-equilibrating during emplacement, as given by the low-pressure cotectic predicted in the experiments.

RELATIONSHIP BETWEEN MMES AND THE HOST MAGMAS

On the relationship between MMEs and host magmas, the most common explanation is that MMEs are the result of hybridization between a mantle-sourced material and melt generated by heating of the lower crust during magma emplacement (e.g., Barbey et al., 2008; Perugini et al., 2003). This hybridization model, however, cannot explain the lack of compositional modifications in the host granitic rocks due to the presence of MMEs, field relationships pointing to independent petrogenetic processes between MMEs and their granitic hosts (Clemens et al., 2017), equilibrium textures between systems that presumably come from two contrasting sources (mantle and crust), or the clear resemblance in major and trace elements between MMEs and mantle magmatism revealed by this study. If instead differentiation is invoked, most of these contradictions are immediately discarded. Inferences from other post-collisional batholiths have already pointed to a common origin for the mafic and felsic magmas (Fowler et al., 2008; Fowler and Henney, 1996; Moyen et al., 2017). Experimental cotectic liquids and the geochemical link between all post-collisional rocks (Figs. 2 and 3) provide consistent evidence that a mantle-

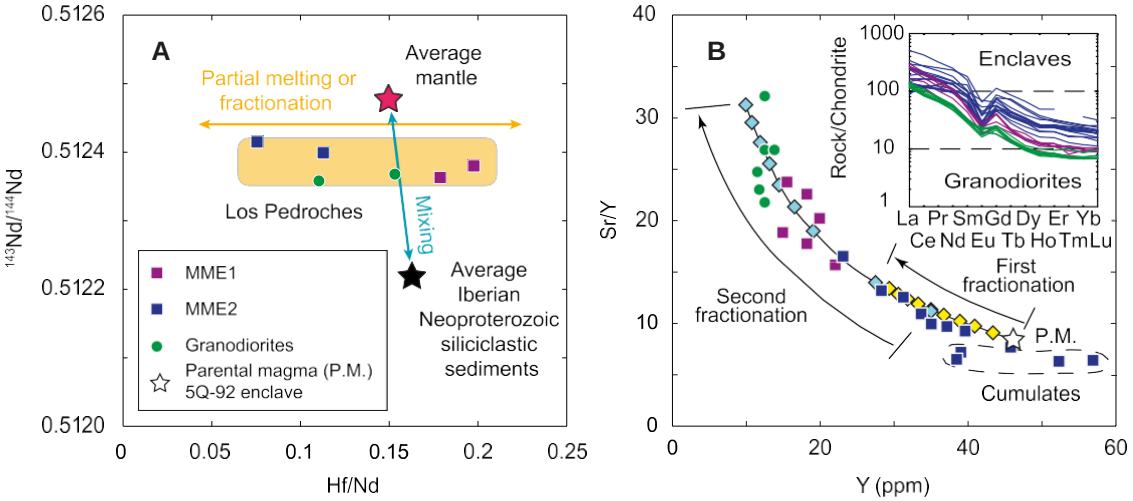

Figure 3. (A) $^{143}Nd/^{144}Nd$ compared to Hf/Nd (Nielsen and Marschall, 2017). Plotted samples from Los Pedroches batholith follow a horizontal trend, characteristic of partial melting and/or differentiation. Mantle and sediment models are calculated using an average from pre-collisional gabbros (Orejana et al., 2017) and abundant sediments (Fernández et al., 2008) in the Iberian pre-Variscan crust. (B) Projection of Los Pedroches samples and model lines of fractionated liquids (see Supplemental Text S5 for details [see text footnote 1]). They were calculated by batch equilibrium at steps of 0.1 liquid fraction from a parental magma (5Q-92 enclave; Gómez-Frutos and Castro, 2022) in a first instance (yellow diamonds) and using 0.5 liquid fraction as parental liquid of a second stage (blue diamonds). In absence of garnet in the source (La/Yb remains almost constant among the series; inset shows chondrite-normalized plot for comparison; normalization after Nakamura, 1974), a process in two stages is necessary to produce the high Sr/Y ratio of granodiorites.

derived parental magma can differentiate granodiorites, excluding both the crust in the process and the two-end-member model. This interpretation is supported by horizontal patterns in the $^{143}Nd/^{144}Nd$–Hf/Nd diagram, indicating partial melting followed by magmatic differentiation (Fig. 3A), whereas mixing between two different end members would result in vertical patterns (Nielsen and Marschall, 2017). Close similarities for all samples in Nd and Sr initial isotopic ratios (Donaire et al., 1999) support the idea that these magmas are part of the same system, regardless of the whole-rock composition. Minor differences in Sr_i (where i means initial) are due to local assimilation processes that have been previously described for the Scottish Caledonian (Holden et al., 1987, 1991). Further evidence provided by Sr/Y-Y relations support a two-stage magma fractionation model (Fig. 3B), likely resembling source and lower crust underplating conditions (Fig. 4). Quenching textures in MMEs and MMEs representing fragments of ascent conduits support such conclusions, given that mafic-intermediate magma is the first to rise due to density contrast and lower viscosity and undercooling is expected to happen during ascent (Rodríguez and Castro, 2019), resulting in the observed quenching textures. Quenching also precludes contamination in the enclaves, pointing to pristine trace elements and isotopic relations. Subsequent pulses of more differentiated magma (the granodiorites) are then able to extract fragments from the ascent conduit during ascent, transporting them in suspension and ultimately resulting in the observed autolithic MMEs (Fig. 4). In conclusion, based on the studied MMEs from Los Pedroches batholith, we propose that post-collisional granite petrogenesis can be explained by partial melting and/or differentiation from an intermediate parental magma sourced in the lithospheric mantle, excluding the crust as a potential source.

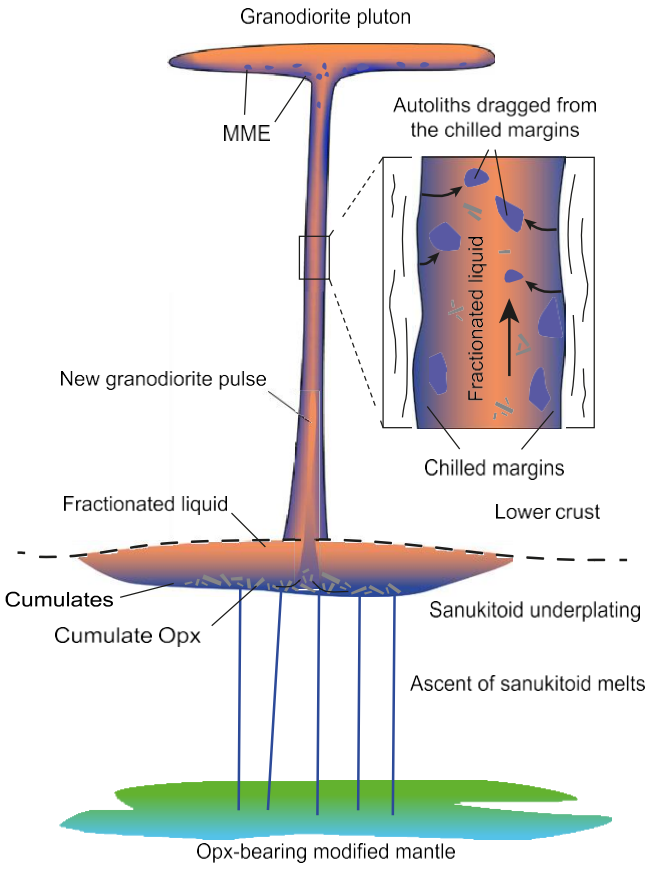

Figure 4. Petrogenetic model for post-collisional magmatism. Ascended liquids from orthopyroxene (Opx)–bearing modified mantle underplate lower crust. Differentiation produces solid phases (mainly the liquidus phase of the system—Opx), and some of them are dragged by fractionated liquid during ascent. First pulse is mafic and generates chilled margins, accounting for quenching textures. Further pulses of more differentiated liquids drag even more cumulate material and fragments of ascent conduit, resulting in mafic microgranular enclaves (MMEs) and amphibole clots.

ACKNOWLEDGMENTS

This work was supported through the Spanish Research Agency (AEI) grant IBERCRUST II/PID2021-126347NB-I00/AEI/10.13039/501100011033/FEDER,UE. We want to thank Rob Strachan for his handling of this manuscript, and Brendan Murphy and Mike Fowler for their constructive feedback.

REFERENCES CITED

Barbarin, B., 2005, Mafic magmatic enclaves and mafic rocks associated with some granitoids of the central Sierra Nevada batholith, California: Nature, origin, and relations with the hosts: Lithos, v. 80, p. 155–177, https://doi.org/10.1016/j.lithos.2004.05.010.

Barbarin, B., and Didier, J., 1992, Genesis and evolution of mafic microgranular enclaves through various types of interaction between coexisting felsic and mafic magmas: Earth and Environmental Science Transactions of the Royal Society of Edinburgh, v. 83, p. 145–153, https://doi.org/10.1017/S0263593300007835.

Barbey, P., Gasquet, D., Pin, C., and Bourgeix, A.L., 2008, Igneous banding, schlieren and mafic enclaves in calc-alkaline granites: The Budduso pluton (Sardinia): Lithos, v. 104, p. 147–163, https://doi.org/10.1016/j.lithos.2007.12.004.

Beard, J.S., Ragland, P.C., and Crawford, M.L., 2005, Using incongruent equilibrium hydration reactions to model latter-stage crystallization in plutons: Examples from the Bell Island tonalite, Alaska: The Journal of Geology, v. 113, p. 589–599, https://doi.org/10.1086/431911.

Carracedo, M., Paquette, J.L., Alonso Olazabal, A., Santos Zalduegui, J.F., de García de Madinabeitia, S., Tiepolo, M., Gil Ibarguchi, J.I., 2009, U-Pb dating of granodiorite and granite units of the Los Pedroches batholith. Implications for geodynamic models of the southern Central Iberian Zone (Iberian Massif). International Journal of Earth Sciences, v. 98, p. 1609–1624, https://doi.org/10.1007/s00531-008-0317-0.

Castro, A., 2021, A non-basaltic experimental cotectic array for calc-alkaline batholiths: Lithos, v. 382–383, 105929, https://doi.org/10.1016/j.lithos.2020.105929.

Castro, A., and Stephens, W.E., 1992, Amphibole-rich polycrystalline clots in calc-alkaline granitic rocks and their enclaves: Canadian Mineralogist, v. 30, p. 1093–1112.

Clemens, J.D., Elburg, M.A., and Harris, C., 2017, Origins of igneous microgranular enclaves in granites: The example of Central Victoria, Australia: Contributions to Mineralogy and Petrology, v. 172, 88, https://doi.org/10.1007/s00410-017-1409-2.

Couzinié, S., Laurent, O., Moyen, J.-F., Zeh, A., Bouilhol, P., and Villaros, A., 2016, Post-collisional magmatism: Crustal growth not identified by zircon Hf–O isotopes: Earth and Planetary Science Letters, v. 456, p. 182–195, https://doi.org/10.1016/j.epsl.2016.09.033.

de Oliveira, M.A., Dall'Agnol, R., and Scaillet, B., 2010, Petrological constraints on crystallization conditions of Mesoarchean sanukitoid rocks, southeastern Amazonian craton, Brazil: Journal of Petrology, v. 51, p. 2121–2148, https://doi.org/10.1093/petrology/egq051.

Donaire, T., Pascual, E., Pin, C., and Duthou, J.-L., 1999, Two-stage granitoid-forming event from an isotopically homogeneous crustal source: The Los Pedroches batholith, Iberian Massif, Spain: Geological Society of America Bulletin, v. 111, p. 1897–1906, https://doi.org/10.1130/0016-7606(1999)111<1897:TSGFEF>2.3.CO;2.

Fernández, C., Becchio, R., Castro, A., Viramonte, J.M., Moreno-Ventas, I., and Corretgé, L.G., 2008, Massive generation of atypical ferrosilicic magmas along the Gondwana active margin: Implications for cold plumes and back-arc magma generation: Gondwana Research, v. 14, p. 451–473, https://doi.org/10.1016/j.gr.2008.04.001.

Fowler, M.B., and Henney, P.J., 1996, Mixed Caledonian appinite magmas: Implications for lamprophyre fractionation and high Ba-Sr granite genesis: Contributions to Mineralogy and Petrology, v. 126, p. 199–215, https://doi.org/10.1007/s004100050244.

Fowler, M., and Rollinson, H., 2012, Phanerozoic sanukitoids from Caledonian Scotland: Implications for Archean subduction: Geology, v. 40, p. 1079–1082, https://doi.org/10.1130/G33371.1.

Fowler, M.B., Kocks, H., Darbyshire, D.P.F., and Greenwood, P.B., 2008, Petrogenesis of high Ba–Sr plutons from the Northern Highlands Terrane of the British Caledonian Province: Lithos, v. 105, p. 129–148, https://doi.org/10.1016/j.lithos.2008.03.003.

Frost, B.R., Barnes, C.G., Collins, W.J., Arculus, R.J., Ellis, D.J., and Frost, C.D., 2001, A geochemical classification for granitic rocks: Journal of Petrology, v. 42, p. 2033–2048, https://doi.org/10.1093/petrology/42.11.2033.

Gómez-Frutos, D., and Castro, A., 2022, Sanukitoid crystallization relations at 1.0 and 0.3 GPa: Lithos, v. 414–415, https://doi.org/10.1016/j.lithos.2022.106632.

Gómez-Frutos, D., Castro, A., and Gutiérrez-Alonso, G., 2023, Post-collisional batholiths do contribute to continental growth: Earth and Planetary Science Letters, v. 603, 117978, https://doi.org/10.1016/j.epsl.2022.117978.

Heilimo, E., Halla, J., and Hölttä, P., 2010, Discrimination and origin of the sanukitoid series: Geochemical constraints from the Neoarchean western Karelian Province (Finland): Lithos, v. 115, p. 27–39, https://doi.org/10.1016/j.lithos.2009.11.001.

Holden, P., Halliday, A.N., and Stephens, W.E., 1987, Neodymium and strontium isotope content of microdiorite enclaves points to mantle input to granitoid production: Nature, v. 330, p. 53–56, https://doi.org/10.1038/330053a0.

Holden, P., Halliday, A.N., Stephens, W.E., and Henney, P.J., 1991, Chemical and isotopic evidence for major mass transfer between mafic enclaves and felsic magma: Chemical Geology, v. 92, p. 135–152, https://doi.org/10.1016/0009-2541(91)90053-T.

Moyen, J.-F., Laurent, O., Chelle-Michou, C., Couzinié, S., Vanderhaeghe, O., Zeh, A., Villaros, A., and Gardien, V., 2017, Collision vs. subduction-related magmatism: Two contrasting ways of granite formation and implications for crustal growth: Lithos, v. 277, p. 154–177, https://doi.org/10.1016/j.lithos.2016.09.018.

Nakamura, N., 1974, Determination of REE, Ba, Fe, Mg, Na and K in carbonaceous and ordinary chondrites: Geochimica et Cosmochimica Acta, v. 38, p. 757–775, https://doi.org/10.1016/0016-7037(74)90149-5.

Nielsen, S.G., and Marschall, H.R., 2017, Geochemical evidence for mélange melting in global arcs: Science Advances, v. 3, e1602402, https://doi.org/10.1126/sciadv.1602402.

Orejana, D., Villaseca, C., and Martínez, E.M., 2017, Basic Ordovician magmatism of the Spanish Central System: Constraints on the source and geodynamic setting: Lithos, v. 284–285, p. 608–624, https://doi.org/10.1016/j.lithos.2017.05.012.

Paterson, S.R., Pignotta, G.S., and Vernon, R.H., 2004, The significance of microgranitoid enclave shapes and orientations: Journal of Structural Geology, v. 26, p. 1465–1481, https://doi.org/10.1016/j.jsg.2003.08.013.

Perugini, D., Poli, G., Christofides, G., and Eleftheriadis, G., 2003, Magma mixing in the Sithonia Plutonic Complex, Greece: Evidence from mafic microgranular enclaves: Mineralogy and Petrology, v. 78, p. 173–200, https://doi.org/10.1007/s00710-002-0225-0.

Rapp, R.P., Norman, M.D., Laporte, D., Yaxley, G.M., Martin, H., and Foley, S.F., 2010, Continent formation in the Archean and chemical evolution of the cratonic lithosphere: Melt–rock reaction experiments at 3–4 GPa and petrogenesis of Archean Mg-diorites (sanukitoids): Journal of Petrology, v. 51, p. 1237–1266, https://doi.org/10.1093/petrology/egq017.

Rodríguez, C., and Castro, A., 2019, Origins of mafic microgranular enclaves and enclave swarms in granites: Field and geochemical relations: Geological Society of America Bulletin, v. 131, p. 635–660, https://doi.org/10.1130/B32028.1.

Vernon, R.H., 1984, Microgranitoid enclaves in granites—Globules of hybrid magma quenched in a plutonic environment: Nature, v. 309, p. 438–439, https://doi.org/10.1038/309438a0.

Vernon, R.H., Etheridge, M.A., and Wall, V.J., 1988, Shape and microstructure of microgranitoid enclaves: Indicators of magma mingling and flow: Lithos, v. 22, p. 1–11, https://doi.org/10.1016/0024-4937(88)90024-2.

Wiebe, R.A., 2016, Mafic replenishments into floored silicic magma chambers: American Mineralogist, v. 101, p. 297–310, https://doi.org/10.2138/am-2016-5429.

Wood, B.J., and Turner, S.P., 2009, Origin of primitive high-Mg andesite: Constraints from natural examples and experiments: Earth and Planetary Science Letters, v. 283, p. 59–66, https://doi.org/10.1016/j.epsl.2009.03.032.

Žák, J., and Paterson, S.R., 2010, Magmatic erosion of the solidification front during reintrusion: The eastern margin of the Tuolumne batholith, Sierra Nevada, California: International Journal of Earth Sciences, v. 99, p. 801–812, https://doi.org/10.1007/s00531-009-0423-7.

Printed in USA

5.1.4

The pristine precursor of Andean-type magmas preserved in magma mingling zones

Scientific Reports, 2024

www.nature.com/scientificreports

scientific reports

Check for updates

OPEN

The pristine precursor of Andean-type magmatism preserved in magma mingling zones

Daniel Gómez-Frutos[1]✉, Antonio Castro[1] & Jesús de la Rosa[2]

Intermediate magma compositions have been postulated to be parental to Andean-type magmatism in the recent years. Geochemical and experimental methods have allowed the modelling of a hypothetical parental composition that accounts for the major element trends displayed by Andean-type batholiths. However, natural plutonic examples matching the modelled composition remain lacking, likely due to the predominance of fractionated liquids and cumulates in the batholiths after protracted and large-scale differentiation. Contrary to this, magma mingling zones, a common feature in Andean-type batholiths, are characterised by quenching phenomena, minimising differentiation. In this paper, we present data from intermediate magmatism in the world-class Gerena magma mingling zone in the Seville Sierra Norte batholith (southern Iberia), compositionally equivalent to Andean-type magmatic series. Geochemical data from quenched dark globules of variable scale and the corresponding host granodiorites are contrasted with the bimodal trends displayed by the host batholith. Results suggest that the smaller-scale dark globules have not undergone any significant fractionation. Furthermore, after conducting geochemical modelling we conclude the dark globules represent a composition that could be parental to Andean-type magmas. We propose that magma mingling zones are an optimal place to probe for parental magmas of Andean-type magmatism, particularly those represented in pristine melanocratic, intermediate globules.

Intermediate composition volcanic rocks and magmas are volumetrically dominant over basalts in active continental margins[1]. Similarly, diorites and Qz-diorites, the plutonic equivalents of erupted andesites, dominate over gabbros. Intermediate magma compositions (SiO_2 = 53–63 wt%; MgO = 2–8 wt%) have been extensively used as parental magma systems for experimental modelling of the compositional trends of batholiths[2–11]. However, unambiguous identification of intermediate plutonic rocks matching the model compositions remains elusive.

This problem relates to one of the main features displayed by Andean-type batholiths, namely the existence of compositional gaps[12,13]. Commonly known as the Bunsen-Daly gap[14,15], these refer to two compositional groups (low silica and high silica) separated by a silica interval (around 55–60 wt% SiO_2) with scarce representation from natural samples. Different plausible explanations include that compositional gaps result when a hot, mantle-sourced basalt intrudes the lower crust and partially melts it to produce a silicic magma[14,16,17]; large-scale magma immiscibility[18]; or continuous differentiation that gives rise to cumulates and fractionated liquids[19]. Whatever the case, these processes preclude the identification of rocks as parental magmas, highlighting the relevance of identifying zones where fractionation was limited or non-existent. Moreover, all these models entail the coexistence of different magma types in the same chamber, producing local yet pervasive mingling phenomena in the batholiths[20,21].

In this sense, magma mingling zones (MMZ), a common feature of Andean-type batholiths, drew the attention of volcanologists because they represent snapshots of the complex dynamic processes that occurred in response to magma chamber replenishment[22]. Quenching phenomena, a characteristic feature of MMZ due to the thermal contrast between different types of magmas, minimise magmatic differentiation, mixing and contamination with the host crust. Thus, quenching maintains almost intact the pristine composition of the magmas invading shallow felsic magma chambers by replenishment. Building on this foundation, we conducted a geochemical study of mingled Andean-type intermediate magmas in the world-class example of Gerena MMZ

[1]Museo Nacional de Ciencias Naturales (MNCN), Consejo Superior de Investigaciones Científicas (CSIC), C. José Gutiérrez Abascal 2, 28006 Madrid, Spain. [2]Centro de Investigación CIQSO, Universidad de Huelva, Huelva, Spain. ✉email: daniel.gomez@csic.es

(Seville Sierra Norte batholith, Southern Spain), where details of magma mingling were reported years ago[23]. A preliminary comparison between Gerena, the Variscan Seville Sierra Norte batholith and the Jurassic Guadalupe Igneous Complex (California) is used to establish the Andean-type affinity of Gerena MMZ. Subsequent geochemical criteria are then used for the identification of samples with limited fractionation. After geochemical modelling comprising existing data from the Seville Sierra Norte batholith, the results will provide insights into the identification of pristine, parental intermediate magmatism in Andean-type settings. Although this work is referred to plutonic systems, the geochemical equivalence between arc plutonic and volcanic rocks has been vastly addressed in the existing literature[24,25], thus making the results of this work applicable to volcanic settings. We contend that the application of the same criteria to other MMZs around the world could be relevant in addressing petrogenetic studies of batholiths and silicic volcanism.

Geological setting, field relations and sampling

The Gerena MMZ is part of a major intrusive body of the Seville Sierra Norte batholith, emplaced during the Lower Carboniferous at the South Portuguese zone of the Iberian massif (Fig. 1). The Seville Sierra Norte batholith was emplaced at ca. 340 Ma[26] into a low-grade metasedimentary pile formed by Devonian siliciclastic metasediments and metavolcanics and Lower Carboniferous volcano-clastic successions of the Iberian Pyrite belt. The whole batholith has been interpreted as Andean-type in terms of rock compositions, resulting by subduction and further oblique collision of the Laurussia and Gondwana supercontinents during the Carboniferous[27]. The Gerena MMZ is exceptionally exposed at the Guadalquivir fault, containing well preserved relations of magma-in-magma injections and quenching. Two main types of magmatism can be found, namely net-veined felsic complexes that intruded a consolidated tonalite, and intermediate globular intrusions and synplutonic dykes that intruded a felsic magma chamber[23]. A representative number of samples were collected from both the felsic complexes and the intermediate globules. However, since the felsic complexes expectedly represent differentiated magma, the present study mainly revolves around the melanocratic, intermediate globules.

Diorites and Qz-diorites manifest as distinct, dark fine-grained globules that exhibit diverse sizes and shapes, spanning from a few centimetres to several meters. These globules can display angular or rounded forms and are readily identifiable by their overall fine-grained textures, occasionally porphyritic, and non-crenulated contacts. They are found within a matrix of medium-grained biotite-granodiorite (Fig. 2a,b). Dark globules occasionally display discrete and discontinuous chilled margins with finer grain size than the core, and lobate contacts against the host granodiorite (Fig. 2c). Some dark globules contain pegmatitic ocelli aligned in bands parallel to the chilled margins (Fig. 2d) and represent fragments from the external rigid carapace of magma injections. Larger dark globules also found in the Gerena MMZ appear as meter-sized dismembered bodies, displaying a

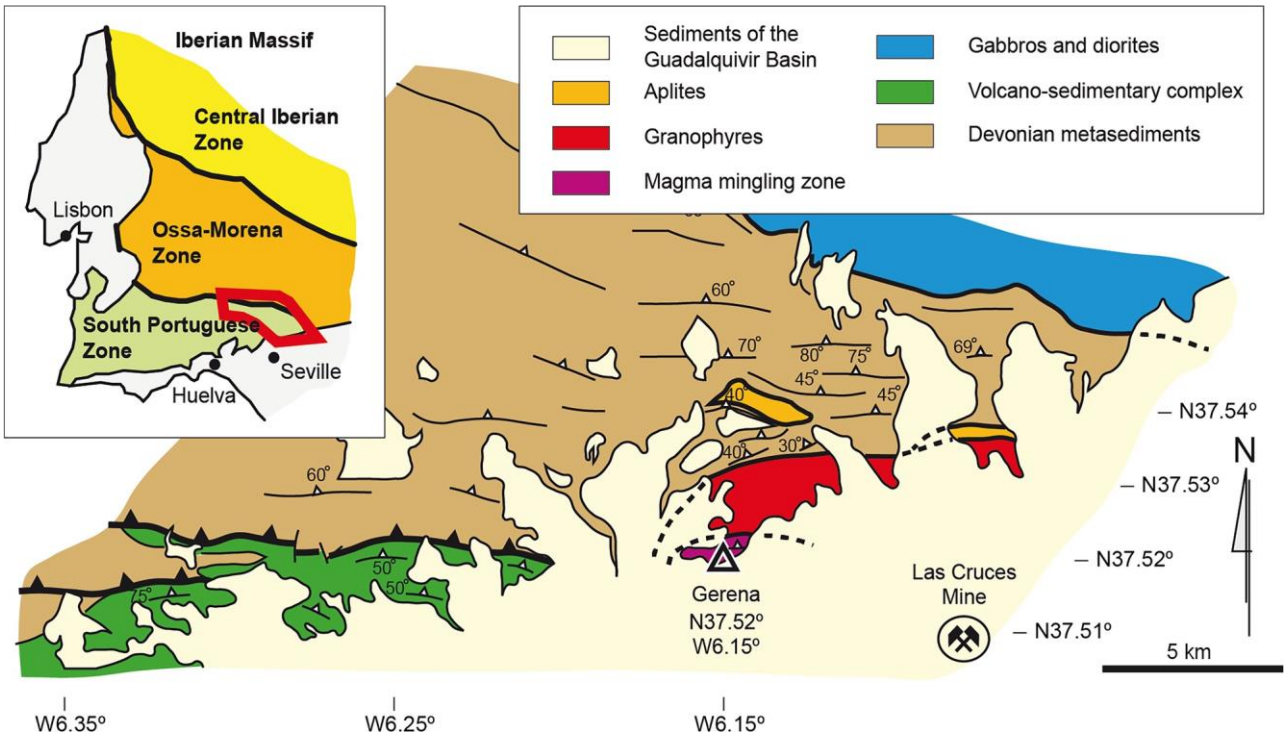

Figure 1. Geological map of the Seville Sierra Norte batholith showing the location of the Gerena magma mingling zone. Map modified from Instituto Geológico y Minero de España, mapa geológico digital continuo GEODE (accessed in 2023, available for public access in http://info.igme.es/cartografiadigital/geologica/geodezona.aspx?Id=Z1500). The map and the rest of the figures were created using Adobe Illustrator 27.9 under a license from the Museo Nacional de Ciencias Naturales (Consejo Superior de Investigaciones Científicas).

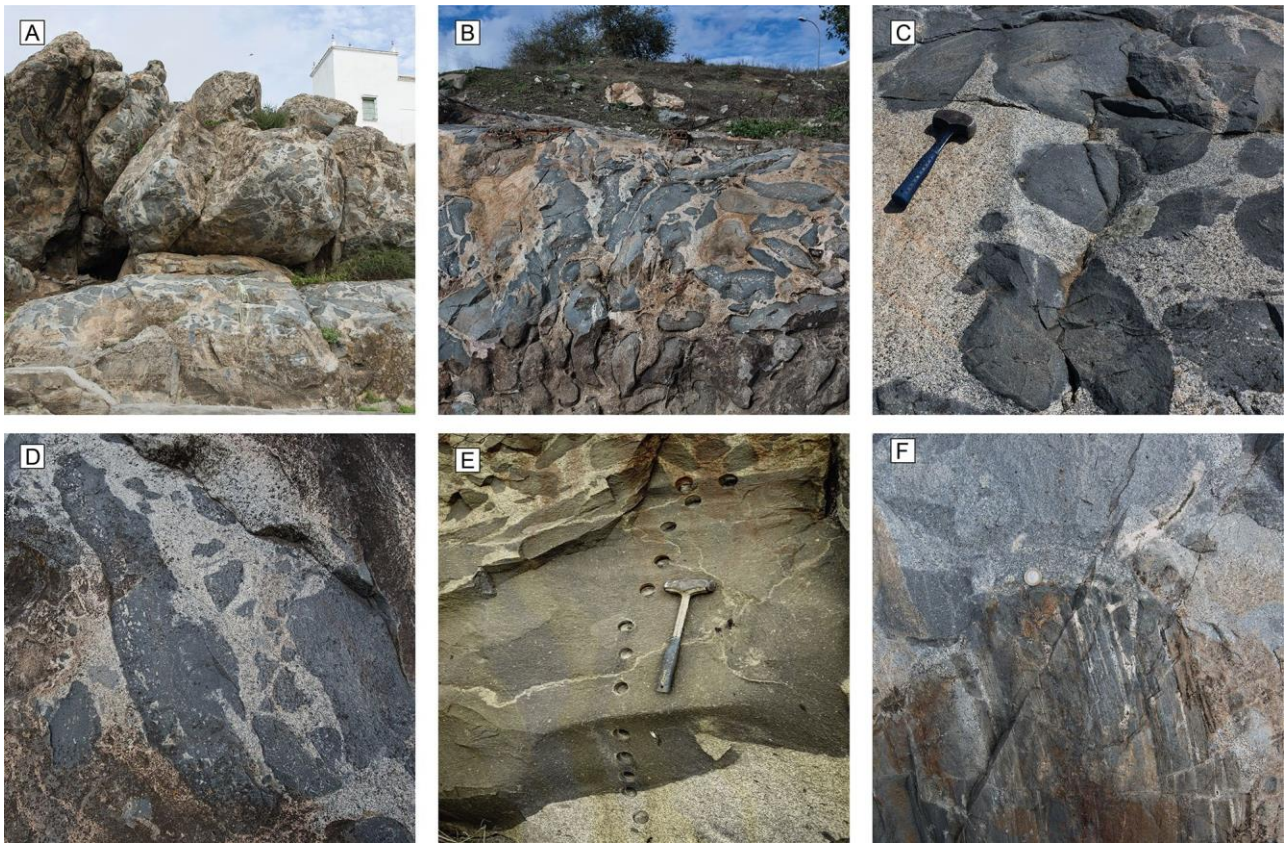

Figure 2. Representative field relations of dark globules and synplutonic dykes of the Gerena magma mingling zone. (**A, B**) General view of one of the breccia-like zones with dark magmatic globules of variable shape and size enclosed in a medium-grained biotite granodiorite. (**C**) Details of homogeneous dark globules with rounded shapes and devoid of continuous chilled margins. (**D**) Large and elongated globule showing pegmatitic vesicles concentrated along a zone close to the chilled margin on one side. The other side shows irregular contacts with dispersed fragments around. (**E**) Transversal section of a large dark globule from the chilled margin to the interior. Fragments from the chilled margin are observed as inclusions (autoliths) in the interior of the globule. (**F**) Partially molten hornfels xenolith from metasedimentary country rocks. These xenoliths supply evidence for local contamination of the host granodiorite.

tabular geometry and chilled margins (Fig. 2e). Hornfels xenoliths from the host rocks are found scattered in the granodiorites, showing small degree of migmatization (Fig. 2f).

Short-range differentiation by in-situ crystallization, in conjunction with the formation of chilled margins in ascent conduits and dykes[28], may imply small variations in silica ranges in larger dark globules. Thus, in order to identify undifferentiated magma compositions, we test the presence of minor variations in globules of variable scale. A set of samples was collected across a large dark globule showing a chilled margin at one of the sides (Fig. 2e). Other samples were collected from smaller dark globules. A few samples from the host granodiorites were also collected for reference. The dark globules appear as fine-grained, slightly porphyritic rocks constituted by plagioclase, amphibole and quartz as the main phases, and biotite, apatite, K-feldspar, titanite, zircon and opaque minerals as accessory phases. On the other hand, the host granodiorites are characterised by a medium-grain, locally granophyric texture, and are mainly composed of quartz, K-feldspar and plagioclase, and allanite, apatite, hornblende, and zircon as common accessory minerals. An exhaustive description of the Gerena rocks and mineral compositions can be found in previous works[23].

Samples were crushed, milled, and analysed for major and trace elements using standard XRF and ICP-MS techniques, respectively. A selection of samples from dark globules were analysed for trace elements and Sr and Nd isotopes. The complete set of results can be found in the Supplementary Material S1, and the analytical details are given in the Supplementary Material S2.

Whole rock geochemistry

Comparative classification diagrams for Gerena MMZ samples, the Sevilla Sierra Norte batholith and experimental cotectic liquids are available in Figs. 3 and 4. Data from previous studies in the Gerena MMZ[23] and the GAP model for Andean-type magmas parental[4] were also plotted in the figures. A database from the Guadalupe Igneous Complex[29] was represented for comparative purposes as a reference of a well-known Andean-type batholith (kernel density plot, Figs. 3, 4). Composition of the average bulk continental crust is available for further reference[30]. The exact overlap between the Sevilla Sierra Norte batholith and the Guadalupe Igneous

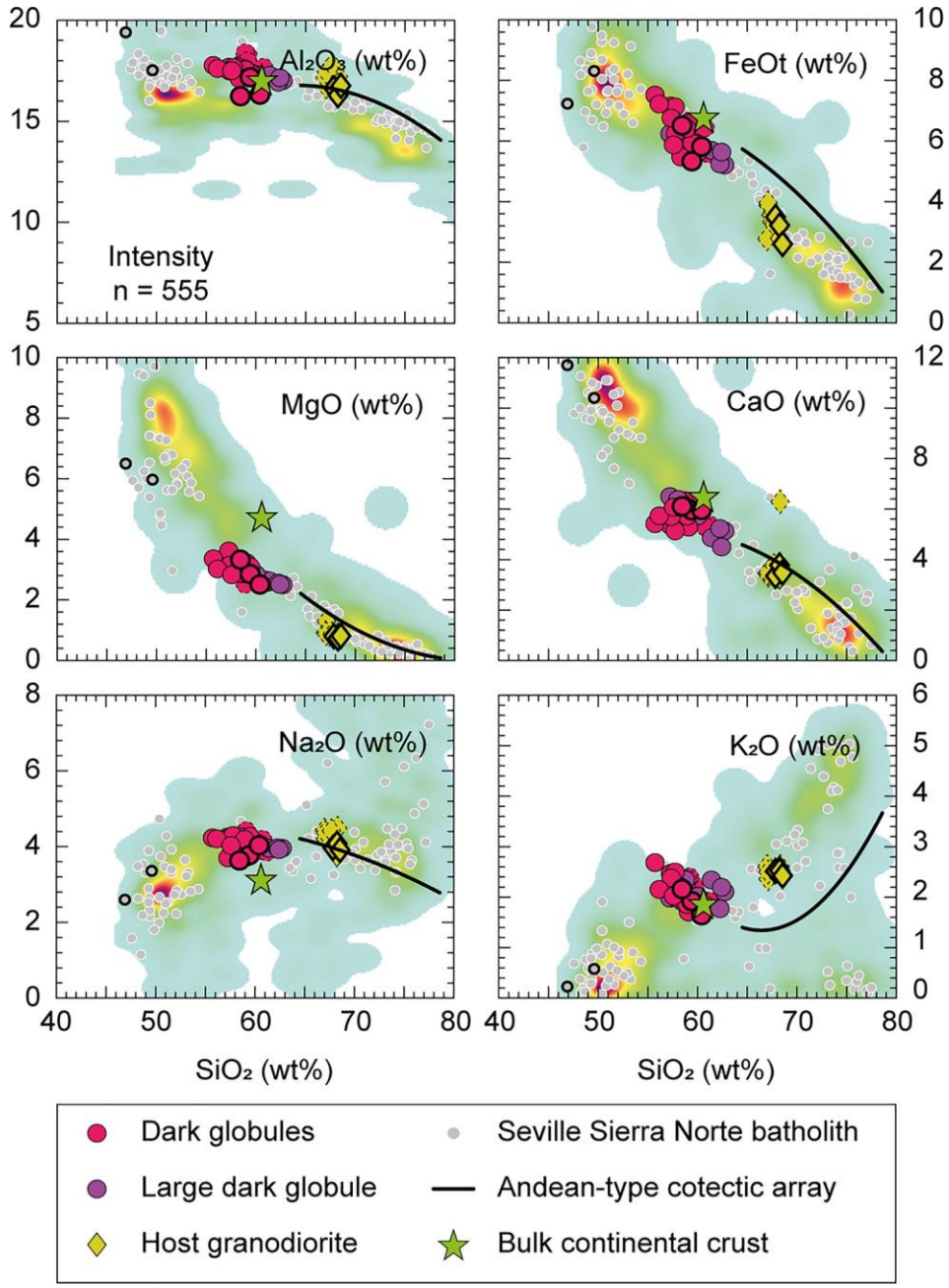

Figure 3. Harker diagrams for the Gerena samples. Comparative series from Sevilla Sierra Norte batholith[27] and Guadalupe Igneous Complex[29]. Dashed points are additional Gerena analyses reported years ago[23], from which the dark globules show an exact overlap with the new analyses. Points with thicker contours represent the compositions used for geochemical model in Fig. 6.

Complex provides an immediate depiction of the Andean-type affinity of Gerena MMZ. Consistent with this pattern, all Gerena samples follow the trend displayed by the Guadalupe Igneous Complex in Harker diagrams, only diverging with slightly smaller CaO and MgO, and larger Al_2O_3 contents for their respective silica values (Fig. 3). Noticeable differences are observed between the dark globules and the larger dark globule, with the former clustering within a narrow silica interval (56–60 wt% SiO_2) compared to the linear trend displayed by large dark globule. In the CaO–MgO (Fig. 4a), despite their lower CaO and MgO respective to silica contents, Gerena samples follow the experimental cotectic path of calc-alkaline rocks[4], coherent with the patterns of Andean-type batholiths[24]. The A–B diagram (A = molar [Al–Na–K-2 × Ca] × 1000; B = molar [Fe + Mg + Ti] × 1000) presents a similar situation, although the large dark globule exhibit a scattered distribution instead of a linear pattern (Fig. 4b). Notably, the average bulk continental crust composition matches the dark globules from Gerena MMZ, with the only deviations found in MgO contents (Figs. 3, 4). Moreover, major element patterns in Figs. 3 and 4 showcase Gerena samples falling in the compositional gap of the Seville Sierra Norte batholith.

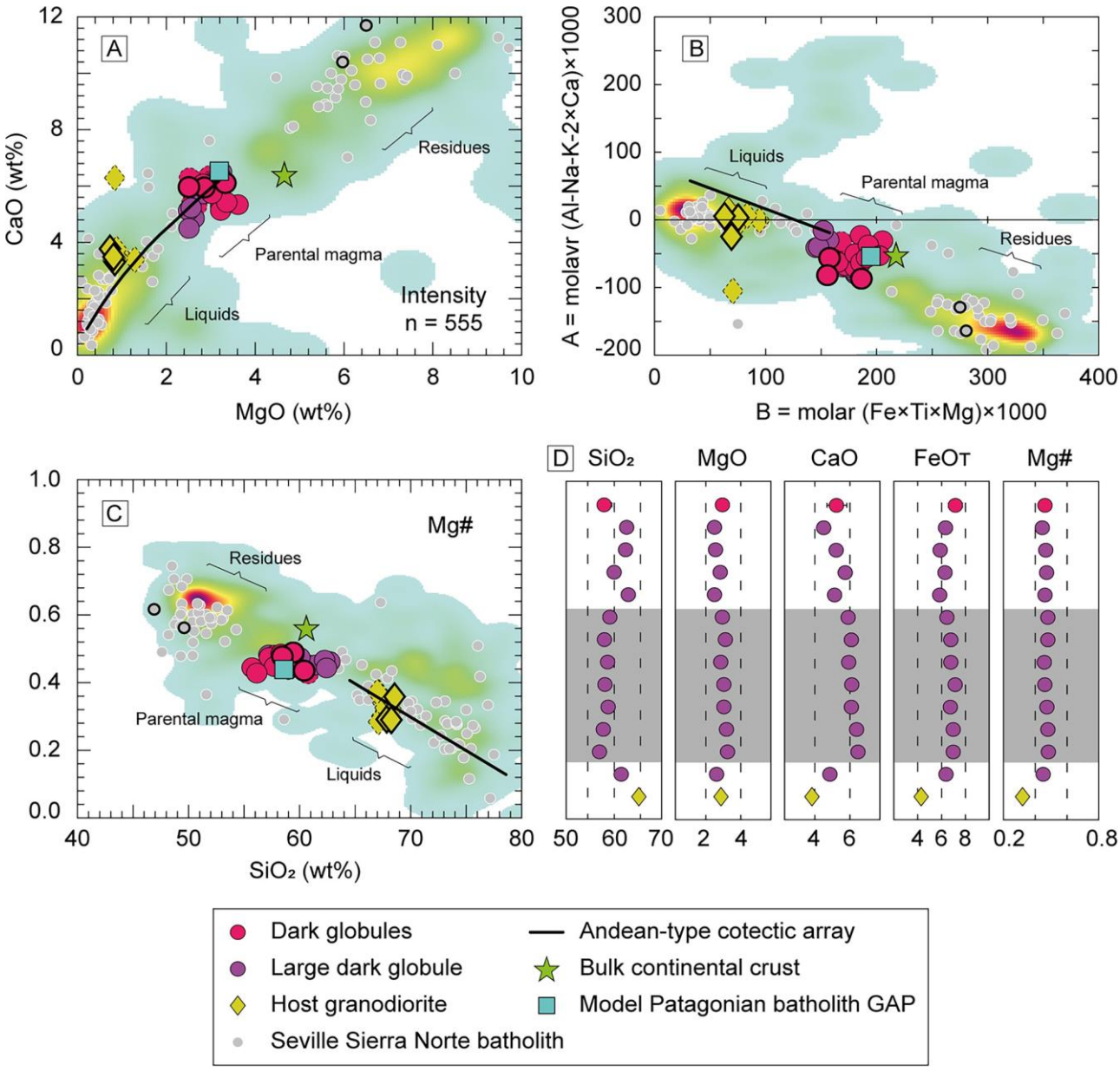

Figure 4. Classification diagrams for the Gerena samples and geochemical profile of the large dark globule. Reference GAP model is added for comparison[4]. Comparative series and colour codes are the same as in Fig. 3. (**A**) CaO–MgO diagram. All collected samples fall in the gap between liquids and residues. Most fractionated samples follow the trend displayed by the Andean main cotectic array (black line[4]). (**B**) A–B diagram. (**C**) Mg# against SiO_2 diagram. (**D**) Compositional profile across the dyke shows the variations in major elements (numbers are wt%) resulting from differentiation by in-situ crystallization from the walls to inside. Shaded area represents samples matching the composition of the average of dark globules.

A geochemical profile of the large dark globule is shown in Fig. 4d, offering an enhanced visualization of the inner compositional zoning of the meter-sized dark globule. The average composition of the smaller dark globules is offered for comparison. Enrichment in SiO_2 and depletions in FeO, MgO and CaO are observed in the edges of the profile. Contamination with the host granodiorite (yellow diamonds, Fig. 4d) is observed near the contact. However, composition remains unmodified over a wide zone of large globule (grey zone, Fig. 4d), most prominently showed by the constant Mg#, and close to the average composition of smaller dark globules (purple squares, Fig. 4d). Such geochemical homogeneity strongly suggests that there is no significant differentiation among the globules, with only small variations found in the rims. Plagioclase phenocrysts are mostly concentrated at the central part of the globule, giving rise to Ca and Al enrichment with respect to the chilled margins. Samples from the central zone overlap the composition of the smaller dark globules.

Regarding trace elements, all analysed samples show relatively similar patterns, with typical arc signatures. Notably, dark globules exhibit roughly similar patterns to those from the host granodiorites (Fig. 5a,b). Whole

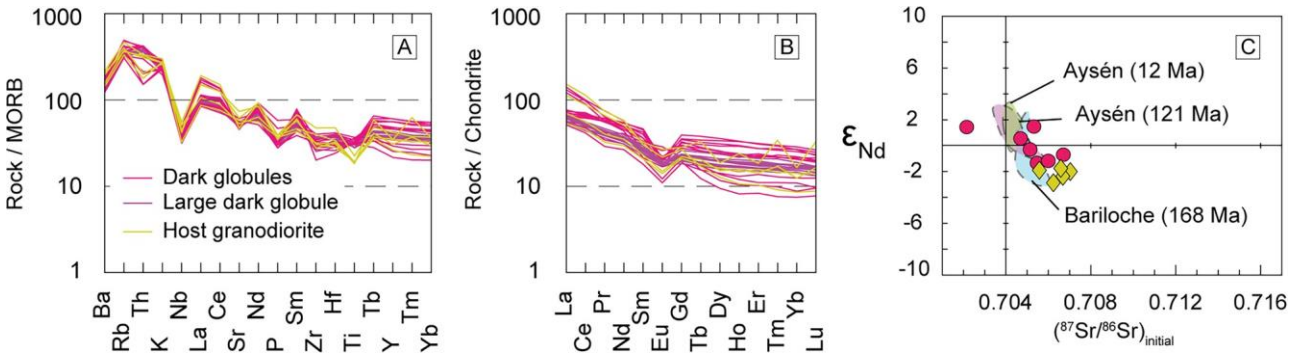

Figure 5. Trace element and isotopic diagrams from the Gerena samples. (**A**) Mid ocean ridge basalt-normalised trace element spider diagram[52], and (**B**) chondrite-normalized diagram[58]; all groups showcase relatively similar patterns with typical arc signature. (**C**) ℇNd compared to initial $^{87}Sr/^{86}Sr$ calculated for 340 Ma. The Gerena rocks exhibit a similar tendency to those found in Aysén and Bariloche from the Patagonian batholith[31]. Granodiorites show a stronger crustal affinity than dark globules, suggesting assimilation of metapelitic host rocks.

rock Sr and Nd isotopes were determined in a selected range of representative samples from both the dark globules and host granodiorites (Fig. 5c). A majority of the examined samples exhibit a consistent pattern, with the host granodiorites displaying higher crustal affinity. Only one of them (A423-18) stands apart from the rest, showing a stronger mantle affinity. The trend followed by the Gerena samples parallels that seen in the North Patagonian batholith, exemplified by Aysén and Bariloche[31], and further highlighting the similitudes between the Gerena MMZ and other Andean-type batholiths.

Discussion

Unfractionated magmatism in the Gerena magma mingling zone

Intermediate magmatism from the Gerena MMZ showcases a compositional range between larger and smaller dark globules. Samples from the central part of the large dark globule overlap the composition of the smaller dark globules, while the geochemical patterns displayed by the edges of the large dark globule are more similar to the granodiorite (Fig. 2f). Observed differences within the large dark globule are coherent with those predicted experimentally by in-situ crystallization at the sidewalls of magma channels[28]. These differences are due to fractional crystallization occurring in the edges caused by temperature contrast with the host, further physically enhanced by the more viscous mushes accumulating towards the edges. Given these considerations it can be argued that larger globules are suboptimal places to sample unfractionated rocks, due to the small variations at the rims of the globules after intrinsic in-situ crystallization.

Although fractionation is possible at the level of emplacement, as it was identified in the large dark globule, the composition of dark globules remains almost identical among varied shapes, pointing to negligible fractionation. Dark globules are comparable in textures and compositions to mafic microgranular enclaves (MMEs), a ubiquitous feature of granite batholiths in Andean-type settings[32]. Mafic microgranular enclaves have been interpreted as fragments of synplutonic magma injections or to represent the input of mafic magma from the mantle that triggered crustal melting and granite melt generation[33,34]. Nevertheless, dark globules display clear differences with larger dark globules that could represent magma injections found in Gerena MMZ, the latter characterised by angular edges and size of meters. Only a narrow range of variation is found in Sr and Nd isotopes, in which the granodiorite samples are richer in evolved components. This points to a possible crustal contaminant, enriched in radiogenic Sr and depleted in radiogenic Nd (Fig. 5c). The implication is that dark globules, on being cogenetic with the host granodiorites, were protected of contamination by their solid state and the surrounding felsic granodiorite during ascent and cooling. Thus, the evolved geochemical features such as the high silica content, low-MgO or isotopic values that characterise dark globules can be considered inherited from the source. However, it is noteworthy that trace element patterns (Fig. 5a,b) show clear similarities between dark globules and the comparatively more evolved granites. This observation is apparently contradictory when considering the differences in major elements between the two groups and can only be explained by the strong control imposed by accessory phases in granitic systems. Such issue is well-documented in granite petrogenesis, where processes like entrainment, fractionation or dissolution of common accessory phases such as zircon, monazite and apatite, can exert a strong influence on the resulting trace element signature[35,36]. These phenomena are rather unpredictable, hindering the use of trace element for petrogenetic interpretations in the Gerena MMZ. For this reason, we rely on the other evidence, namely the overlap between the Gerena dark globules, the parental experimental models and the compositional gap, and conclude that dark globules (or the equivalent MMEs) from MMZ are optimal places to probe for magmas with limited fractionation.

Relationship with the Seville Sierra Norte batholith

Once the dark globules have been identified as undifferentiated magma, the next logical step is to test their genetic relationship with the granites and mafic rocks of the Seville Sierra Norte batholith. For this purpose, a binary difference test was conducted to assess the reproducibility of a parental composition from its respective

differentiate and residue. In other words, this method conducts a regression model through binary differences to test the likelihood of two selected compositions, representing a fractionated rock and a differentiation residue, resulting from fractionating a parental composition. The regression accuracy is represented by R-squared values and embodies the likelihood of the three chosen compositions being related by differentiation (details on this method can be found in the Data Repository). Three representative dark globule and granite pairs were selected for geochemical modelling (points with thicker contours in Figs. 3, 4). These samples were intendedly collected in adjacent areas for this specific purpose. Regarding the residue, it is important to note that while the use of granite compositions for this purpose is relatively straightforward given their relative homogeneity due to their cotectic behaviour, the use of residue compositions is more challenging. This is mainly because the geochemistry of cumulate rocks, which likely result from multiple differentiation processes, is practically undistinguishable from that of differentiation residues. Additionally, olivine-rich cumulate rocks may be present in the Seville Sierra Norte batholith as a result of minor basaltic intrusions[27]. Since this model aims for a composition in equilibrium with a dioritic precursor represented by the dark globules (i.e., compositions resulting from a single differentiation process), selecting an accurate cumulate composition is a critical prerequisite. Taking these factors into account, we selected a composition that is coherent with the rest of the Seville Sierra Norte data, and close to the density maxima from the comparative series after the Guadalupe Igneous Complex in most of the diagrams. For comparison purposes, we also tested a reported cumulate from the literature[26] (Figs. 3, 4, grey points with black contours).

Results of the modelling are available in Fig. 6. Regardless of the used compositions, all tests yielded an excellent correlation with R-squared values of > 0.96. Tests using cumulate composition yields worse correlations for Fe and Al (Fig. 6a–c), likely due to accumulation of spinel. This can also be explained by small degrees of assimilation of host hornfels, supported by the presence of migmatization (Fig. 2f) and the slightly higher crustal affinity displayed by the granodiorites (Fig. 5c). Comparatively, a small improvement is observed in the selected residue composition (Fig. 6d–f). This observation is coherent with a parental melt of circa 60 wt% SiO_2 resulting in a residue with basaltic-like composition ($SiO_2 \approx 50$ wt%). Moreover, variations among residual compositions having effect in the order of centesimals supports the strong genetic relation between the dark globules and the granodiorites. Although this test can be applied to trace element values, results may be unreliable for the reasons exposed above. Furthermore, while assimilation of small batches of host rocks may not have a significant effect in major elements (Figs. 3, 4), trace element and isotopes are a lot more sensible, with the latter showcasing slight deviations that are coherent with a contaminant (Fig. 4d).

An intermediate precursor to Andean-type magmatism

Arc magmatism generation has been classically associated with basalt production from the peridotite mantle[37,38], resulting in the felsic arc rocks by a number of processes, such as magma mixing and contamination[39] or differentiation from a hydrous basaltic parental[40,41]. These models, however, entail important drawbacks that limit their viability, such as the elimination of an unseen ultramafic residue from the continents[38,42], or their inability to account for the andesitic average composition of the continental crust[30] without invoking complex multistage differentiation processes[37]. Not only that, but previous experimental work has also evidenced the inability to differentiate andesites from primary basalts, leading to inaccurate differentiate compositions[4]. Contrary to this, the use of an intermediate parental composition offers a solution to most of these challenges that, on top of it, is supported by existing experimental work (see references above). In this sense, dark globules from magma mingling zones can represent natural rocks matching the intermediate experimental models.

Even so, since a purely peridotitic mantle source is unable to produce intermediate magmatism[38,43], a modification by either magma mixing or assimilation and fractional crystallization must be assumed[40]. Accordingly, pristine magmas of andesitic composition can be generated by melting of silicic diapirs coming from subducted mélanges of oceanic crust and sediments[44–46] and their reaction with the peridotite mantle[47–50]. This consideration agrees with the data set showing the participation of evolved components even in the dark globules, a characteristic feature shared with diorites and granodiorites of various ages. Notably, similar patterns can be observed in Aysén and Bariloche in the North Patagonian batholith[31], which were interpreted as resulting from melting of subducted mélanges incorporated by subduction and diapiric upwelling to hot zones of the suprasubduction mantle wedge. Consequently, major element geochemical trends of Andean-type batholiths follow cotectic lines that are reproduced experimentally by using a non-basaltic, dioritic (= andesitic) starting composition[4]. For those experiments, the composition of the parental diorite was modelled after the composition of the gap observed between granodiorites and diorites in the Patagonian batholith, following inference that large-scale fractionation is the cause of the gap[29,51]. Large-scale fractionation causes the parental magma to be the less represented by rocks, as these are mostly fractionated into liquids and residues. The same gap is observed in the whole Seville Sierra Norte batholith, in which dark globules represent the less abundant rocks of a general bimodal distribution (Fig. 3a,b), uncoincidentally plotting in the compositional gap between residues and differentiates. Note this is a common feature displayed by Andean-type magmatism, as shown by the comparative series (Fig. 3). Moreover, alternatives like magma mixing are unlikely due to the non-linear trends displayed by the Seville Sierra Norte batholith (Fig. 3). In contrast, differentiation is supported by the compositional correlation between the residues and differentiates and the dark globules as the potential parental magma (Fig. 6). These observations are further supported by the close match between the dark globules and the average bulk continental crust in most available diagrams (Figs. 3, 4), reinforcing the notion of continental growth in active margins through intermediate magmatism[49,52].

A cogenetic relation between enclaves and host granodiorites (sensu lato) in Andean-type and post-collisional batholiths around the world is widely accepted[29,53,54]. The lack of reaction rims around MMEs, the compatibility of mineral assemblages between enclaves and host and the geochemical and isotopic similarities[55,56] support a

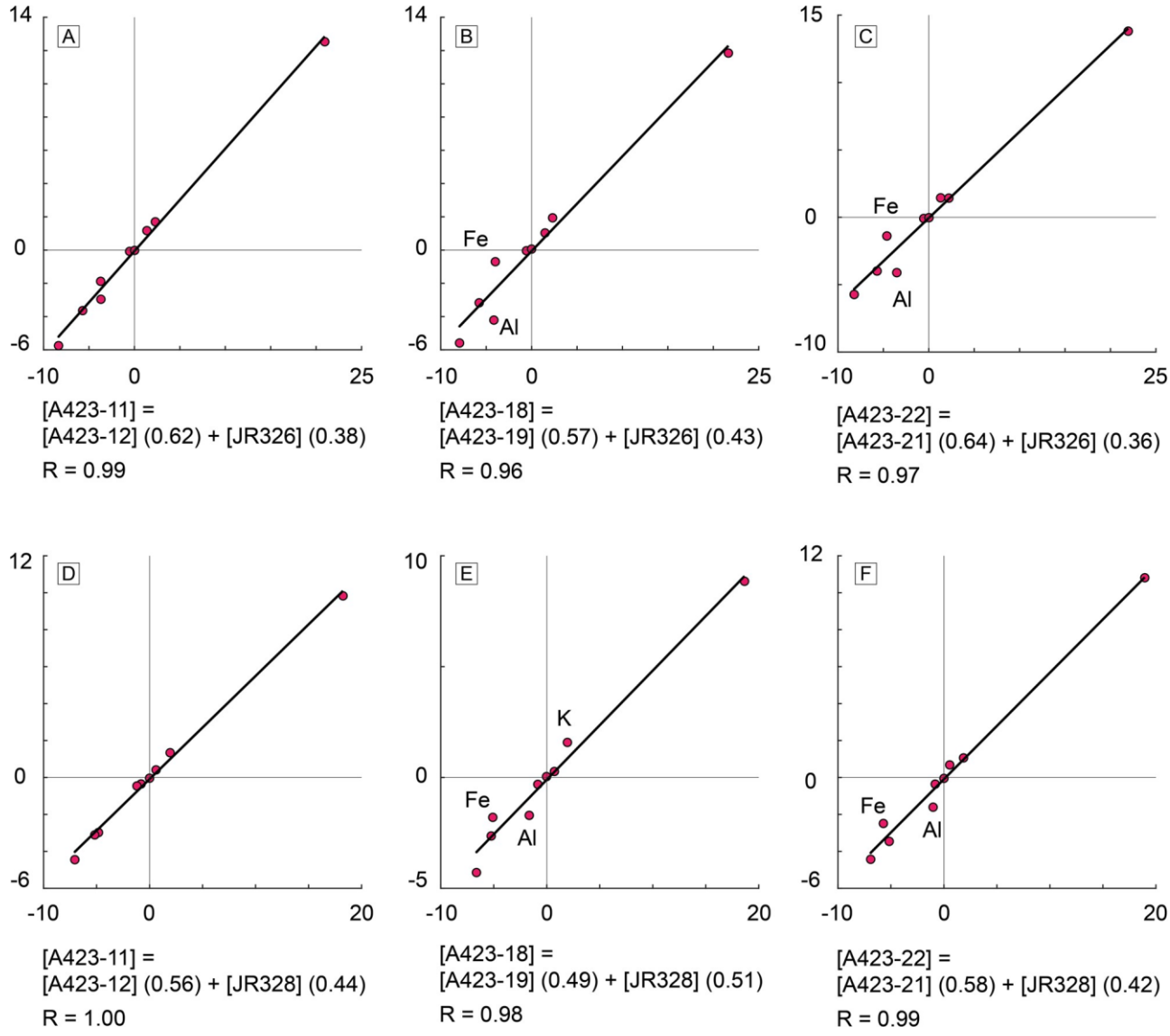

Figure 6. Binary difference test between the Gerena dark globules, differentiates and residual rocks from the Seville Sierra Norte batholith. Selected samples for each test are available in each diagram. Tests (**A–C**) are conducted with a cumulate composition, while tests (**D–F**) are conducted with a residual composition presumably with less cumulate affinity. All tests yield excellent correlations between the selected samples, implying that the dark globules can reproduce the fractionated and residual compositions through differentiation.

common magmatic origin. On top of that, most recent work on post-collisional MMEs show that enclaves may indeed represent the quenched parental magma of granite batholiths[56]. However, when probing for pristine parental magma in MMEs it is important to note that not all of them represent parental magmas. A study of mineral relations and whole chemical compositions of enclaves from the Tuolumne intrusive complex concluded that the most mafic MMEs represent cumulates that lost up to 50% liquid, yielding an estimated dioritic composition for the parental magmas of $SiO_2 = 60–62$ wt%; CaO ≈ 5.2 wt%[32]. Such values are almost coincident with the model diorite composition (GAP model in Fig. 4) and the average values of the Gerena dark globules. Furthermore, the comparison with the diorites of the Kuna Crest lobe that represent the initiation of the Tuolumne batholith in Sierra Nevada (California) and, hence, the less fractionated pulse of magma[57]. In particular, the Zone I of the zoned lobe is the most primitive in terms of Sr–Nd isotopic ratios and has a major element composition that fairly matches that of the Gerena dark globules. Implication of these inferences is that mingling zones are a result of new pulses of parental magma intruding their own differentiates and residues.

Concluding remarks

The Gerena magma mingling zone, located in the Sevilla Sierra Norte batholith, constitutes a world-class example featuring all typical characteristics of Andean-type magmatism. The host granodiorite is intruded by abundant intermediate magmas that appear in the form of dark globules of variable size. While larger dark globules hint

to have undergone local fractionation, inference suggest that dark globules represent pristine magmas that have not undergone any significant differentiation. After modelling their correlation with differentiated rocks and cumulates from the Seville Sierra Norte batholith, further comparison with experimental and geochemical evidence suggests that these commonly occurring dark globules are, in turn, the parental to Andean-type batholiths. Altogether, we conclude that magma mingling zones and microgranular enclaves, both typical features of Andean-type batholiths, constitute optimal settings to probe for the unfractionated magmas, in which a pristine diorite (or andesite) composition can be identified as the parental magma of the system.

Data availability

All data generated or analysed during this study are included in this published article, available in its Supplementary Files.

Received: 21 October 2023; Accepted: 27 February 2024
Published online: 29 February 2024

References

1. Gill, J. B. Bulk chemical composition of orogenic andesites. In *Orogenic Andesites and Plate Tectonics* (ed. Gill, J. B.) 97–167 (Springer, 1981).
2. Alonso-Perez, R., Müntener, O. & Ulmer, P. Igneous garnet and amphibole fractionation in the roots of island arcs: Experimental constraints on andesitic liquids. *Contrib. Mineral. Petrol.* **157**, 541–558 (2009).
3. Carroll, M. R. & Wyllie, P. J. The system tonalite-H2O at 15 kbar and the genesis of calc-alkaline magmas. *Am. Mineral.* **75**, 345–357 (1990).
4. Castro, A. A non-basaltic experimental cotectic array for calc-alkaline batholiths. *Lithos* **382**, 105929 (2021).
5. Grove, T. L., Donnelly-Nolan, J. M. & Housh, T. Magmatic processes that generated the rhyolite of Glass Mountain, Medicine Lake volcano, N. California. *Contrib. Mineral. Petrol.* **127**, 205–223 (1997).
6. Patiño Douce, A. E. Experimental generation of hybrid silicic melts by reaction of high-Al basalt with metamorphic rocks. *J. Geophys. Res. Solid Earth* **100**, 15623–15639 (1995).
7. Patiño Douce, A. E. Vapor-absent melting of tonalite at 15–32 kbar. *J. Petrol.* **46**, 275–290 (2005).
8. Qian, Q. & Hermann, J. Partial melting of lower crust at 10–15 kbar: Constraints on adakite and TTG formation. *Contrib. Mineral. Petrol.* **165**, 1195–1224 (2013).
9. Rapp, R. P. & Watson, E. B. Dehydration melting of metabasalt at 8–32 kbar: Implications for continental growth and crust-mantle recycling. *J. Petrol.* **36**, 891–931 (1995).
10. Sisson, T. & Grove, T. Temperatures and H2O contents of low-MgO high-alumina basalts. *Contrib. Mineral. Petrol.* **113**, 167–184 (1993).
11. Sisson, T., Ratajeski, K., Hankins, W. & Glazner, A. F. Voluminous granitic magmas from common basaltic sources. *Contrib. Mineral. Petrol.* **148**, 635–661 (2005).
12. Brophy, J. G. Composition gaps, critical crystallinity, and fractional crystallization in orogenic (calc-alkaline) magmatic systems. *Contrib. Mineral. Petrol.* **109**, 173–182 (1991).
13. Bachmann, O. & Huber, C. Silicic magma reservoirs in the Earth's crust. *Am. Mineral.* **101**, 2377–2404 (2016).
14. Bunsen, R. Ueber die Processe der vulkanischen Gesteinsbildungen Islands. *Ann. Phys.* **159**, 197–272 (1851).
15. Daly, R. A. *The Geology of Ascension Island* Vol. 60, 3–80 (JSTOR, 1925).
16. Chayes, F. Relative abundance of intermediate members of the oceanic basalt-trachyte association. *J. Geophys. Res.* **68**, 1519–1534 (1963).
17. Reubi, O. & Blundy, J. A dearth of intermediate melts at subduction zone volcanoes and the petrogenesis of arc andesites. *Nature* **461**, 1269–1273 (2009).
18. Charlier, B. *et al.* Large-scale silicate liquid immiscibility during differentiation of tholeiitic basalt to granite and the origin of the Daly gap. *Geology* **39**, 907–910 (2011).
19. Grove, T. & Donnelly-Nolan, J. The evolution of young silicic lavas at Medicine Lake Volcano, California: Implications for the origin of compositional gaps in calc-alkaline series lavas. *Contrib. Mineral. Petrol.* **92**, 281–302 (1986).
20. Frost, T. P. & Mahood, G. A. Field, chemical, and physical constraints on mafic-felsic magma interaction in the Lamarck Granodiorite, Sierra Nevada, California. *Geol. Soc. Am. Bull.* **99**, 272–291 (1987).
21. Žák, J. & Paterson, S. R. Characteristics of internal contacts in the Tuolumne Batholith, central Sierra Nevada, California (USA): Implications for episodic emplacement and physical processes in a continental arc magma chamber. *Geol. Soc. Am. Bull.* **117**, 1242–1255 (2005).
22. Eichelberger, J. Vesiculation of mafic magma during replenishment of silicic magma reservoirs. *Nature* **288**, 446–450 (1980).
23. Castro, A., de La Rosa, J. D. & Stephens, W. E. Magma mixing in the subvolcanic environment: Petrology of the Gerena interaction zone near Seville, Spain. *Contrib. Mineral. Petrol.* **106**, 9–26 (1990).
24. Castro, A. The dual origin of I-type granites: The contribution from experiments. *Geol. Soc. Lond. Spl. Publ.* **491**, 101–145 (2020).
25. Kelemen, P., Hanghøj, K. & Greene, A. One view of the geochemistry of subduction-related magmatic arcs, with an emphasis on primitive andesite and lower crust. *Treat. Geochem.* **3**, 659 (2003).
26. de la Rosa Díaz, J., Rogers, G. & Dorado, A. C. Relaciones 87Sr/86Sr de rocas básicas y granitoides del batolito de la Sierra Norte de Sevilla. *Rev. Soc. Geol. España* **6**, 141–149 (1993).
27. De la Rosa, J. *Petrología de las rocas básicas y granitoides del batolito de la Sierra Norte de Sevilla, Zona Surportuguesa, Macizo Ibérico*. Unpublished Doctoral Thesis, Univ. of Sevilla (1992).
28. Rodríguez, C. & Castro, A. Silicic magma differentiation in ascent conduits. Experimental constraints. *Lithos* **272**, 261–277 (2017).
29. Putirka, K. D. *et al.* Pluton assembly and the genesis of granitic magmas: Insights from the GIC pluton in cross section, Sierra Nevada Batholith, California. *Am. Mineral.* **99**, 1284–1303 (2014).
30. Rudnick, R. L. & Gao, S. Composition of the continental crust. In *The Crust* (eds Rudnick, R. L. & Gao, S.) (Elsevier-Pergamon, 2003).
31. Castro, A. *et al.* Secular variations of magma source compositions in the North Patagonian batholith from the Jurassic to Tertiary: Was mélange melting involved? *Geosphere* **17**, 766–785 (2021).
32. Barnes, C., Werts, K., Memeti, V., Paterson, S. & Bremer, R. A tale of five enclaves: Mineral perspectives on origins of mafic enclaves in the Tuolumne Intrusive Complex. *Geosphere* **17**, 352–374 (2021).
33. Holden, P., Halliday, A. & Stephens, W. Neodymium and strontium isotope content of microdiorite enclaves points to mantle input to granitoid production. *Nature* **330**, 53–56 (1987).
34. Tobisch, O., McNulty, B. & Vernon, R. Microgranitoid enclave swarms in granitic plutons, central Sierra Nevada, California. *Lithos* **40**, 321–339 (1997).

1. Bea, F. & Montero, P. Behavior of accessory phases and redistribution of Zr, REE, Y, Th, and U during metamorphism and partial melting of metapelites in the lower crust: An example from the Kinzigite formation of Ivrea-Verbano, NW Italy. *Geochim. Cosmochim. Acta* **63**, 1133–1153 (1999).
2. Watt, G. & Harley, S. Accessory phase controls on the geochemistry of crustal melts and restites produced during water-undersaturated partial melting. *Contrib. Mineral. Petrol.* **114**, 550–566 (1993).
3. Hawkesworth, C. J. & Kemp, A. Evolution of the continental crust. *Nature* **443**, 811–817 (2006).
4. Kay, R. W. & Kay, S. M. Delamination and delamination magmatism. *Tectonophysics* **219**, 177–189 (1993).
5. Streck, M. J., Leeman, W. P. & Chesley, J. High-magnesian andesite from Mount Shasta: A product of magma mixing and contamination, not a primitive mantle melt. *Geology* **35**, 351–354 (2007).
6. Lee, C.-T.A., Cheng, X. & Horodyskyj, U. The development and refinement of continental arcs by primary basaltic magmatism, garnet pyroxenite accumulation, basaltic recharge and delamination: Insights from the Sierra Nevada, California. *Contrib. Mineral. Petrol.* **151**, 222–242 (2006).
7. Ulmer, P., Kaegi, R. & Müntener, O. Experimentally derived intermediate to silica-rich arc magmas by fractional and equilibrium crystallization at 1.0 GPa: An evaluation of phase relationships, compositions, liquid lines of descent and oxygen fugacity. *J. Petrol.* **59**, 11–58 (2018).
8. Arndt, N. T. & Goldstein, S. L. An open boundary between lower continental crust and mantle: Its role in crust formation and crustal recycling. *Tectonophysics* **161**, 201–212 (1989).
9. Rudnick, R. L. Making continental crust. *Nature* **378**, 571–578 (1995).
10. Marschall, H. R. & Schumacher, J. C. Arc magmas sourced from mélange diapirs in subduction zones. *Nat. Geosci.* **5**, 862–867 (2012).
11. Gerya, T. V., Yuen, D. A. & Sevre, E. O. D. Dynamical causes for incipient magma chambers above slabs. *Geology* **32**, 89–92 (2004).
12. Cruz-Uribe, A. M., Marschall, H. R., Gaetani, G. A. & Le Roux, V. Generation of alkaline magmas in subduction zones by partial melting of mélange diapirs—An experimental study. *Geology* **46**, 343–346 (2018).
13. Castro, A. *et al.* Melting relations of MORB-sediment mélanges in underplated mantle wedge plumes; implications for the origin of Cordilleran-type batholiths. *J. Petrol.* **51**, 1267–1295 (2010).
14. Codillo, E., Le Roux, V. & Marschall, H. Arc-like magmas generated by mélange-peridotite interaction in the mantle wedge. *Nat. Commun.* **9**, 2864 (2018).
15. Castro, A., Vogt, K. & Gerya, T. Generation of new continental crust by sublithospheric silicic-magma relamination in arcs: A test of Taylor's andesite model. *Gondwana Res.* **23**, 1554–1566 (2013).
16. Straub, S. M., Gómez-Tuena, A. & Vannucchi, P. Subduction erosion and arc volcanism. *Nat. Rev. Earth Environ.* **1**, 574–589 (2020).
17. Melekhova, E., Annen, C. & Blundy, J. Compositional gaps in igneous rock suites controlled by magma system heat and water content. *Nat. Geosci.* **6**, 385–390 (2013).
18. Taylor, S. R. & McLennan, S. M. *The Continental Crust: Its Composition and Evolution* (Blackwell Scientific Publications, 1985).
19. Barbarin, B. Mafic magmatic enclaves and mafic rocks associated with some granitoids of the central Sierra Nevada batholith, California: Nature, origin, and relations with the hosts. *Lithos* **80**, 155–177 (2005).
20. Barbey, P., Gasquet, D., Pin, C. & Bourgeix, A. Igneous banding, schlieren and mafic enclaves in calc-alkaline granites: The Budduso pluton (Sardinia). *Lithos* **104**, 147–163 (2008).
21. Vernon, R. Microgranitoid enclaves in granites—Globules of hybrid magma quenched in a plutonic environment. *Nature* **309**, 438–439 (1984).
22. Gómez-Frutos, D. & Castro, A. Mafic microgranular enclaves (MMEs) trace the origin of post-collisional magmas. *Geology* **51**, 743–747 (2023).
23. Memeti, V., Paterson, S. R. & Mundil, R. Coupled magmatic and host rock processes during the initiation of the tuolumne intrusive complex, Sierra Nevada, California, USA: A transition from ephemeral sheets to long-lived, active magma mushes. *Bulletin* **134**, 1347–1374 (2022).
24. Nakamura, N. Determination of REE, Ba, Fe, Mg, Na and K in carbonaceous and ordinary chondrites. *Geochim. Cosmochim. Acta* **38**, 757–775 (1974).

Acknowledgements

This work was supported through the Spanish Research Agency (AEI) IBERCRUST II/PID2021-126347NB-I00/AEI/10.13039/501100011033/FEDER,UE. The authors want to thank Gary S. Michelfelder, Adam Curry and two anonymous reviewers for their constructive criticism that helped improve this manuscript.

Author contributions

D.G.F. and A.C. were responsible for the conceptualization and preparation of the manuscript. J.D.L.R. carried the analyses and provided additional information from his PhD thesis. All authors contributed to sampling and data curation.

Competing interests

The authors declare no competing interests.

Additional information

Supplementary Information The online version contains supplementary material available at https://doi.org/10.1038/s41598-024-55699-x.

Correspondence and requests for materials should be addressed to D.G.-F.

5.2 Numerical modelling

A total of eighteen numerical experiments were performed to investigate the dynamics and evolution of physical parameters such as temperature, pressure and water during subduction and collision, as well as the potential sources for melting. For this purpose, a sensitivity study was performed covering a range of different parameters, such as the length of the oceanic plate (400 – 675 km), the thermal age of the oceanic crust (40 Myr, 60 Myr, 90 Myr) and the convergence rate of the continental plates (1 cm/yr, 3 cm/yr and 5 cm/yr). Results from the numerical models are summarised in figure 5.1 and table 5.1.

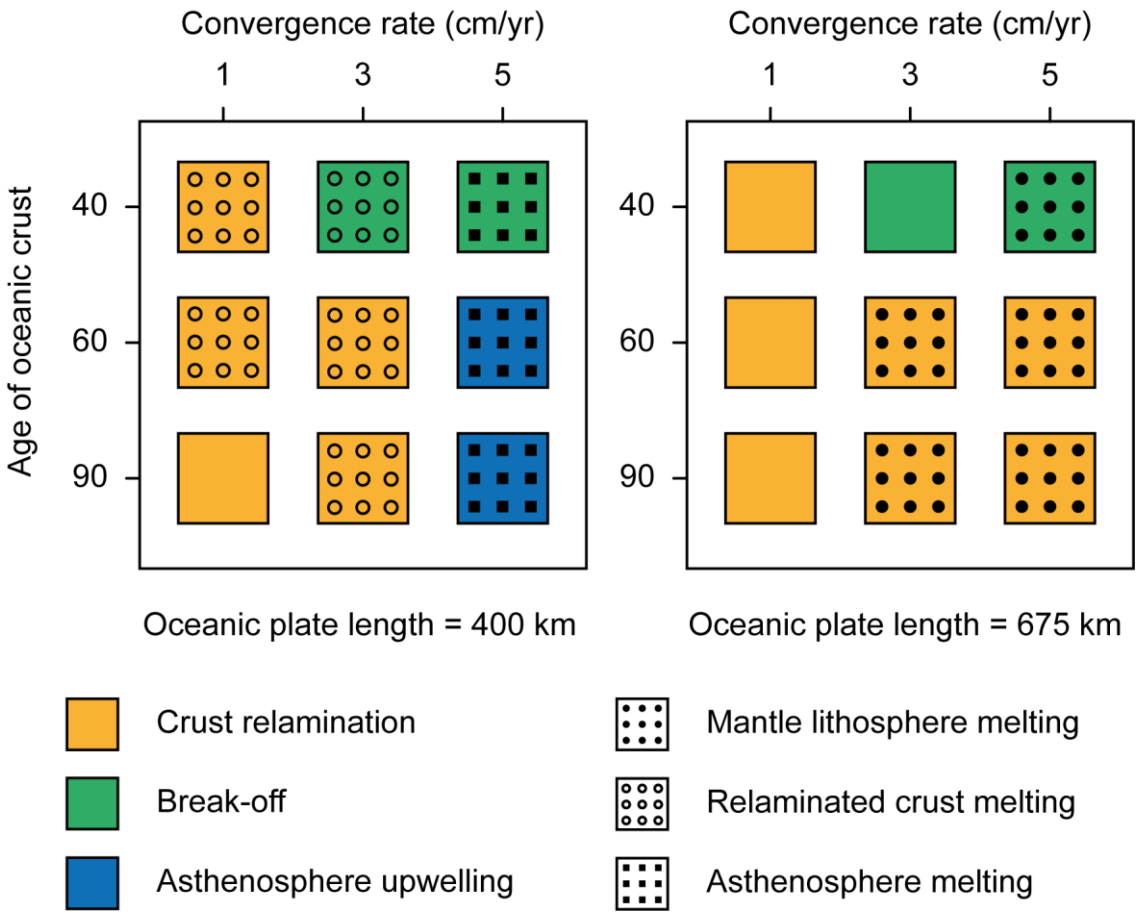

Figure 5.1. Parameters and results of conducted numerical experiments. Sources of melting represent both the initial and predominant source of magmatism in the model. All mantle magmatism occurs as a consequence of hydration from the subducting slab. Each studied parameter exerts a strong control over the dynamic and magmatic regime of the model: the oceanic plate length conditions the dominance of lithospheric mantle

or relaminated crust magmas; the age of the oceanic crust influences the likelihood of slab break-off; and the convergence rate the duration and volume of magmatism.

Three major regimes of long-term development post-dating collision can be identified within the results, namely (1) subducted continental crust relamination, (2) slab break-off, and (3) asthenosphere upwelling. Among them, continental crust relamination is the most widespread result of the numerical study, with slab break-off occurring only in experiments using the youngest oceanic crust and asthenosphere upwelling in experiments using a shorter oceanic plate and high convergence velocities.

A majority of the numerical experiments resulted in significant magmatism during the collisional and post-collisional stages. Two main sources of magmas can be identified: (1) the mantle lithosphere from the upper plate, melting as a result of hydration from the oceanic plate and post-collisional extension; and (2) the relaminated crust from the subducting plate, melting after relamination and subsequent intrusion of the relaminated crust in the upper plate lithospheric mantle. These two melting endmembers usually occur at different stages within the orogenic process, causing transitional scenarios to be the most common. It is noteworthy that the occurrence of each type of magma is highly dependent on the length of the oceanic plate, with lithospheric mantle magmatism being favoured by a larger ocean and relaminated crust magmatism being favoured by a shorter ocean. Besides, lack of magmatism is characteristic of subduction with slower convergence velocities, particularly when using a larger oceanic plate.

To properly constrain the controls on magmatism during collision, model 1 was chosen for reference as the most observed scenario within the experimental results. This reference model shows the development of the physical controls on magmatic sources during collision and registers a change in magma sources, from an initial syn-collisional to early post-collisional stage featuring lithospheric mantle magmatism, to a fully post-collisional stage characterised by relaminated crust magmatism after relamination initiation. Furthermore, models 6 and 26 were chosen to be representative of the two end-member settings for magmatism, dominated respectively by lithospheric mantle magmatism and relaminated crust magmatism respectively. All the models follow very similar dynamics prior to continental collision: the oceanic subduction takes place and is

followed by slab roll back. Continental subduction then begins, with a progressive yet sharp decrease in the subduction velocity, after which the evolution of the models starts to differ. No arc magmatism was registered in any of the tested numerical models.

Model	Length of the oceanic crust (km)	Convergence rate cm/yr	Age of the oceanic crust (Myr)	Result	Melting
1	675	3	60	Relamination	Mantle lithosphere
2	675	5	60	Relamination	Mantle lithosphere
3	675	3	40	Break-off	No melting
4	675	5	40	Break-off	Mantle lithosphere
5	675	3	90	Relamination	Mantle lithosphere
6	675	5	90	Relamination	Mantle lithosphere
13	400	3	60	Relamination	Relaminated crust
14	400	5	60	Asthenosphere upwelling	Asthenosphere
15	400	3	40	Break-off	Relaminated crust
16	400	5	40	Break-off	Asthenosphere
17	400	3	90	Relamination	Relaminated crust
18	400	5	90	Relamination	Asthenosphere
25	400	1	60	Relamination	Relaminated crust
26	400	1	40	Relamination	Relaminated crust
27	400	1	90	Relamination	No melting
31	675	1	60	Relamination	No melting
32	675	1	40	Relamination	No melting
33	675	1	90	Relamination	No melting

Table 5.1. Summary of the parameters and results from the numerical experiments. Although most models present magmatism from different sources, melting column refers to the dominating source within each model.

5.2.1 Reference model

The reference model (model 1, Table 5.1) features a symmetrical convergence rate of 3 cm/y between two identical continental lithospheres, separated by a 60 Myr old and 675 km wide ocean. Available figures show the evolution of lithology (Fig. 5.2), temperature (Fig. 5.3), pressure (Fig. 5.4), second strain rate invariant and velocity field (Fig. 5.5) and water contents (Fig. 5.6).

During the oceanic subduction dehydration from the subducted ocean ascends through the asthenosphere, and an incipient thermal anomaly is formed in the mantle wedge.

Once the ocean is closed and collision begins after ca. 10 Myr, mantle velocity field starts pushing the mantle towards the subducting plate, initiating a small upwelling and slowing the subducting plate, which in turn is now exclusively driven by the slab pull. During this stage, deformation is characterised by the development of faulting in the overriding plate as a result of the compression stress, mainly located near the foreland basin (Fig. 5.5).

Oceanic subduction is followed by continental subduction, with the entrainment of the lower plate into the asthenosphere. Continental subduction enhances mantle flow in the wedge, causing more intense deformation in the foreland and a progressively larger thermal anomaly. The gradual heating and hydration of the lithospheric mantle from the overriding plate triggers magmatism after ca. 17 Myr (Fig. 5.2 and 5.3). During this stage, the leading edge of the subducting plate reaches the transition zone at 660 km and becomes positively buoyant, ultimately ceasing continental subduction.

During the following 10 Myr in the evolution of the model the mantle wedge continues to increase its thermal anomaly and the intensity of the mantle velocity. These factors facilitate the weakening of the subducting continental crust, resulting in the detachment of the upper crust and relamination initiation. At ca. 28 Myr a significant portion of the subducted upper crust has relaminated. At this point in the evolution of the model, the strong vertical component in the mantle velocity field and rollback force causes the incorporation of the relaminated upper continental crust into the overriding plate lithospheric mantle. By ca. 34 Myr the relaminated crust interacts with the hydrated lithospheric mantle, initiating partial melting of the relaminated crust. At this stage, the overriding plate undergoes post-collisional extension, which conditions the appearance of normal faults throughout the continental crust. Nevertheless, most of the deformation is accommodated in the plates interface through the formation of new structures verging to the subducting plate after the large volume of relaminated upper crust.

Pullback forces continue in the following million years, ending in the relamination of a minor volume of lower continental crust that is incorporated to the mantle wedge. In this case, the temperature regime is insufficient to trigger magmatism from such a mafic

source. Throughout the whole model evolution the pressure regime (Fig. 5.4) registers variations of ±5 kbar in the lithospheric mantle.

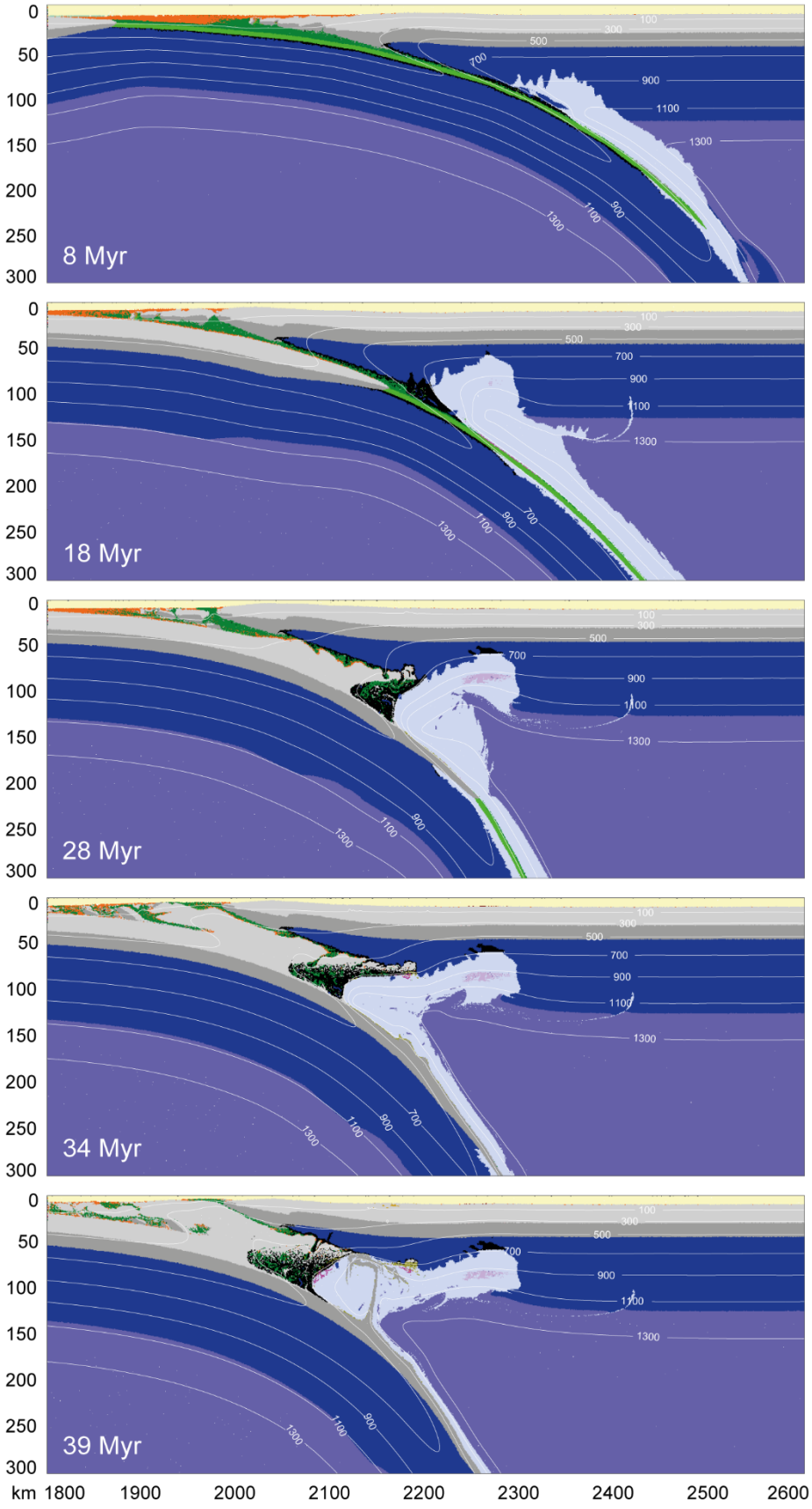

Figure 5.2. Development of the reference model (model 1, Table 5.1). Colour scheme is the same as in fig. 4.5.

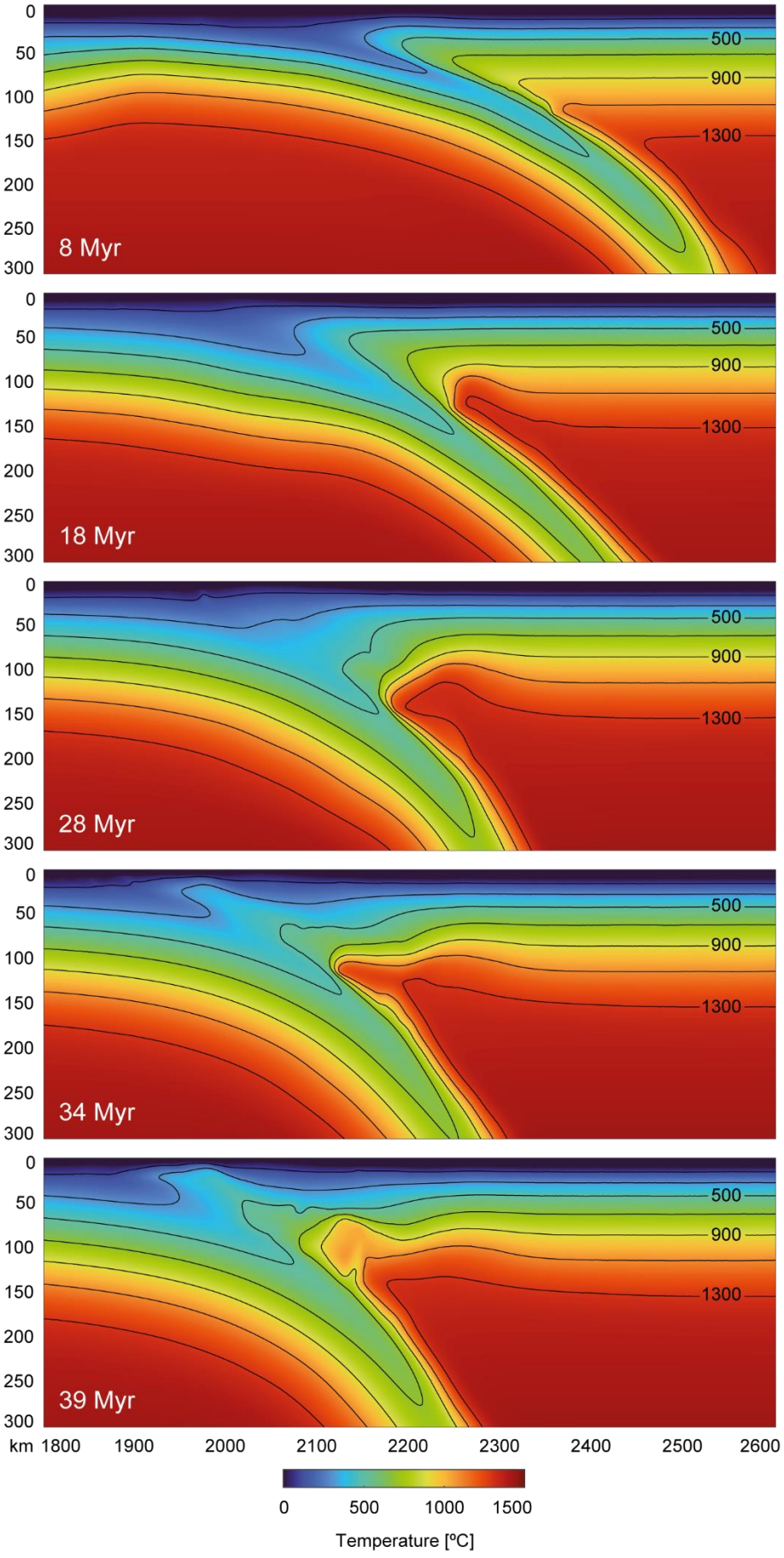

Figure 5.3. Temperature evolution of the reference model (model 1, Table 5.1).

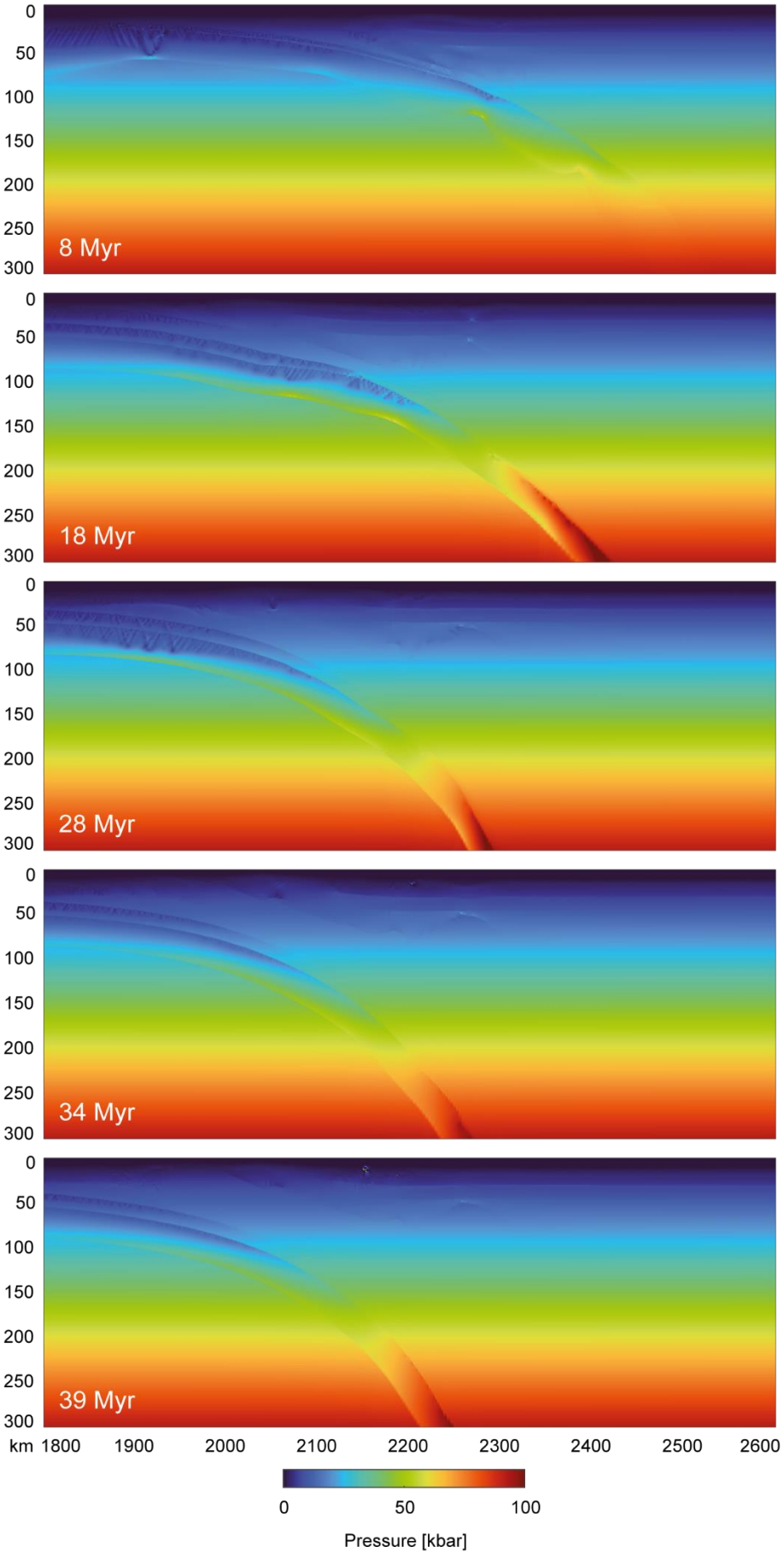

Figure 5.4. Pressure evolution of the reference model (model 1, Table 5.1).

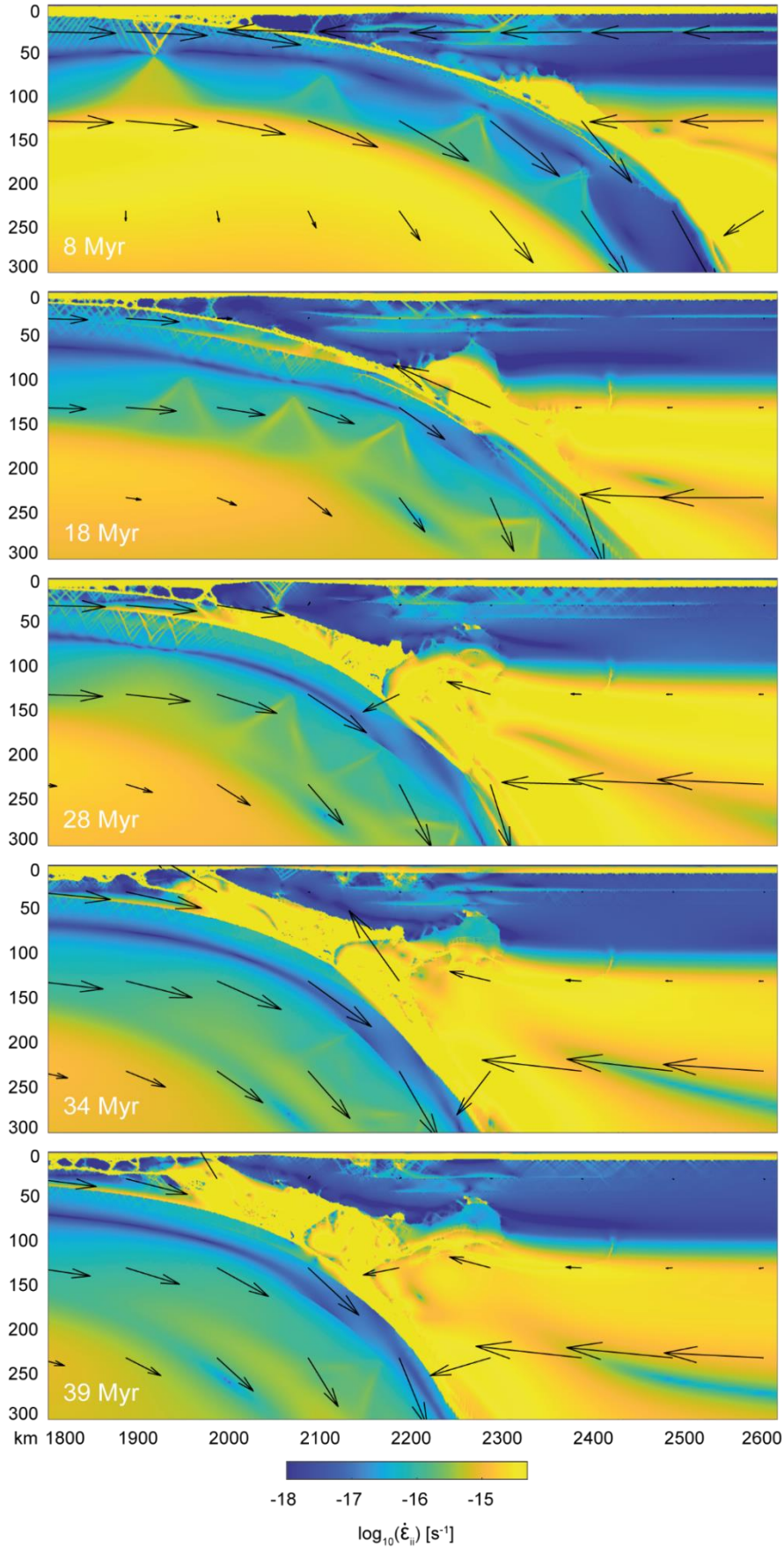

Figure 5.5. Evolution of the second strain rate invariant of the reference model (model 1, Table 5.1). Arrows represent the velocity field at each given timestep.

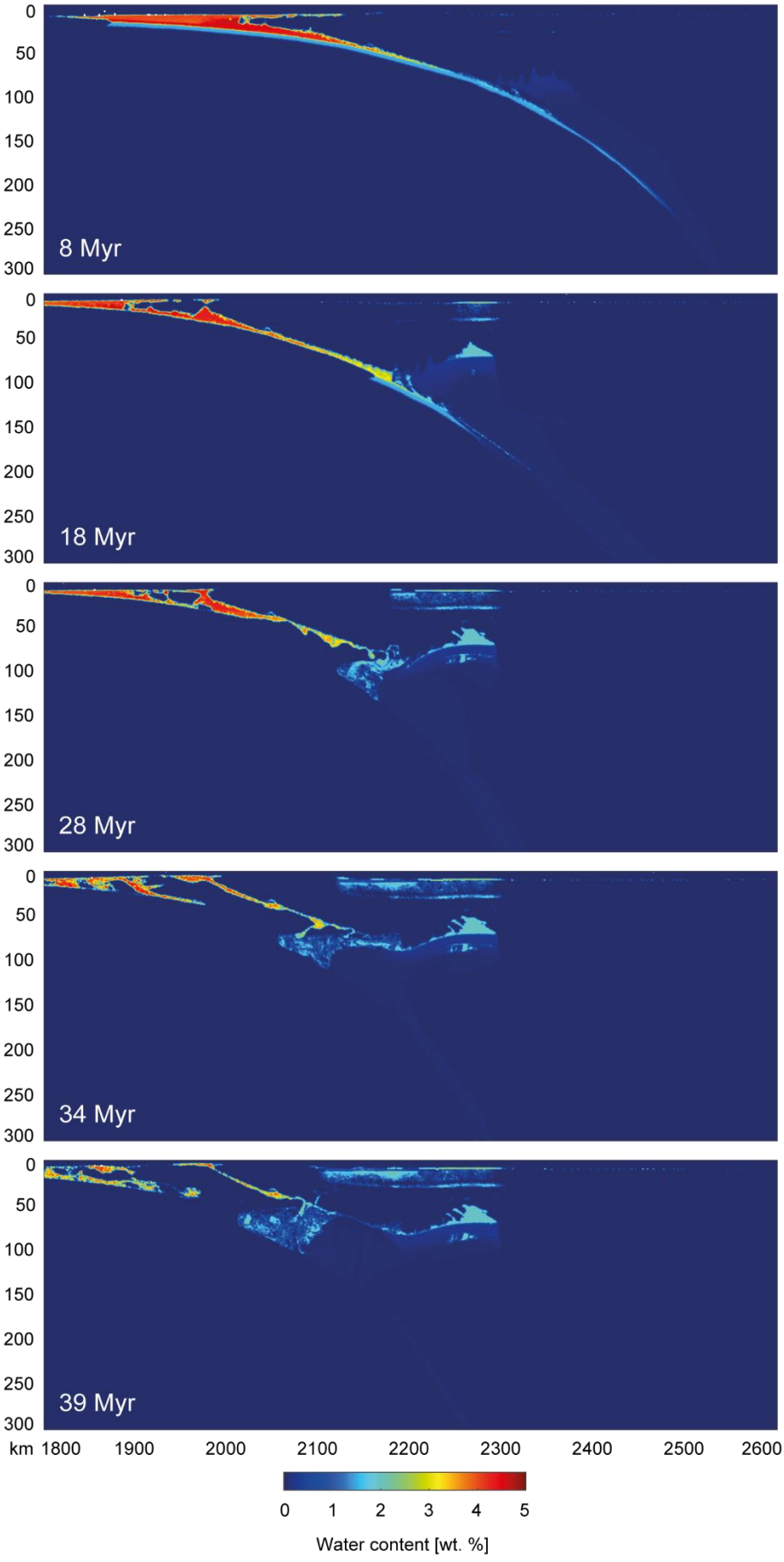

Figure 5.6. Water content evolution of the reference model (model 1, Table 5.1)

5.2.2 Comparison with the magmatic endmember models

The endmember for lithospheric mantle magmatism features a higher convergence rate than the reference model with 5 cm/y, with an ocean length of 675 km and 90 Myr age. Alternatively, the endmember for relaminated crust magmatism uses a slower convergence rate of 1 cm/y and a shorter ocean of 400 km and 60 Myr age. The two endmember models for magmatism share roughly similar geodynamic evolution with the reference model, as both are dominated by crustal relamination (Fig. 5.1, Table 5.1).

The endmember for lithospheric mantle magmatism is characterised by more prominent partial melting from the hydrated lithosphere. Available figures show the evolution of lithology (Fig. 5.7), temperature and pressure (Fig. 5.8), and second strain rate invariant, velocity field and water contents (Fig. 5.9). The higher convergence velocity (5 cm/y compared to 3 cm/y from the reference model) leads to a more intense mantle flux, facilitating an equally more intense thermal anomaly in the mantle wedge, and to the subducting slab reaching the transition zone after 9 Myr. Similarly, the comparatively increased convergence rate produces a more intense deformation during oceanic subduction, with the development of faulting systems associated to compressive forces in the upper plate.

The endmember for relaminated crust magmatism features a more volumetrically significant partial melting from the relaminated crust. Relevant figures show the evolution of lithology (Fig. 5.10), temperature and pressure (Fig. 5.11), and second strain rate invariant, velocity field and water contents (Fig. 5.12). Mantle velocities in the mantle wedge have a more notable vertical component in the mantle wedge, facilitating relamination and the introduction of the relaminated material in the lithosphere. Hydration is comparatively less effective due to the shorter ocean, reaching the lithosphere after a significant volume of continental crust has already been relaminated. The shorter ocean also allows for a slightly steeper subduction, with the subducting slab reaching the transition zone at 36 Myr.

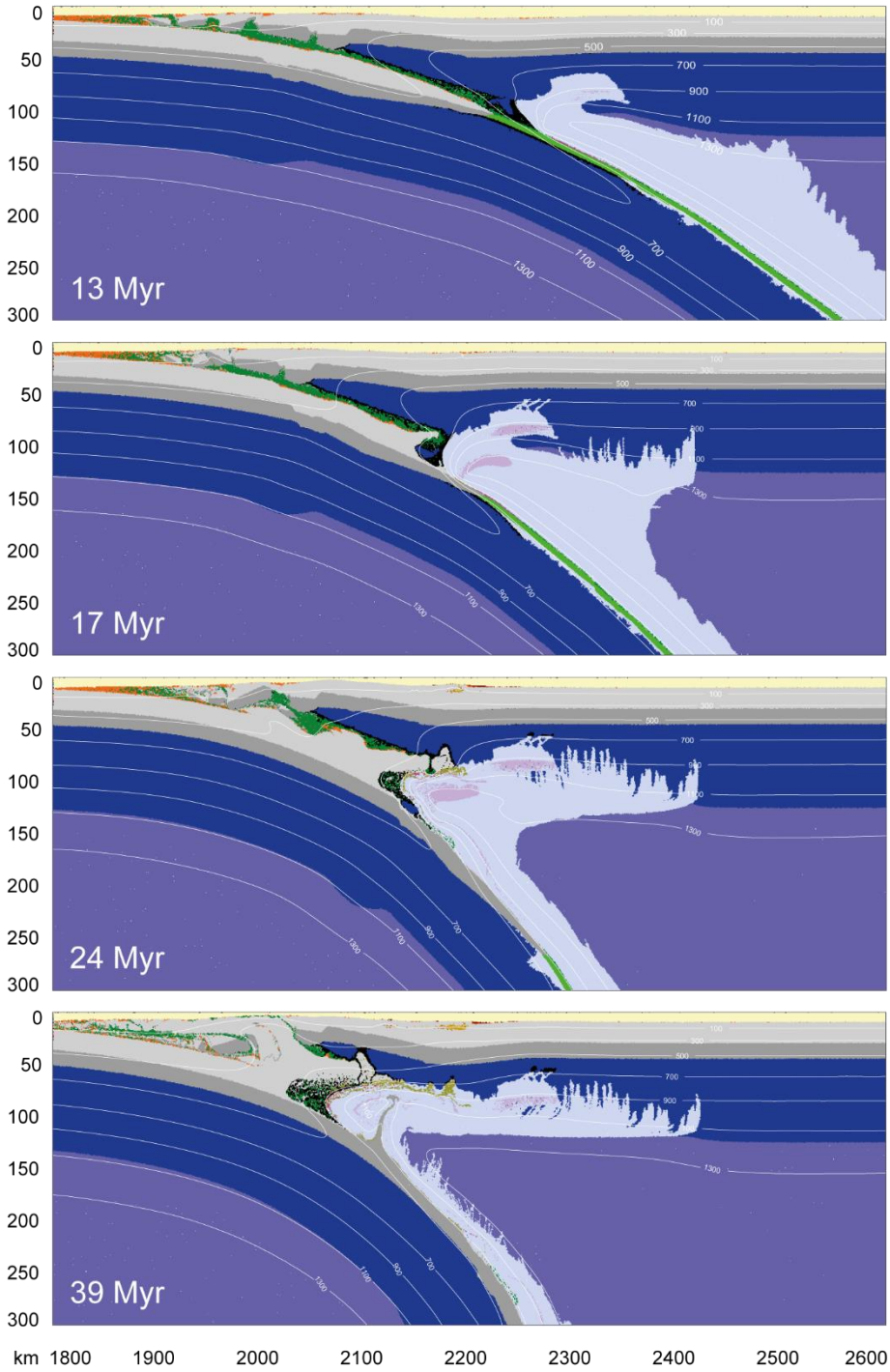

Figure 5.7. Development of the end-member model for lithospheric mantle dominated magmatism (model 6, Table 5.1). Colour scheme is the same as in fig. 4.5.

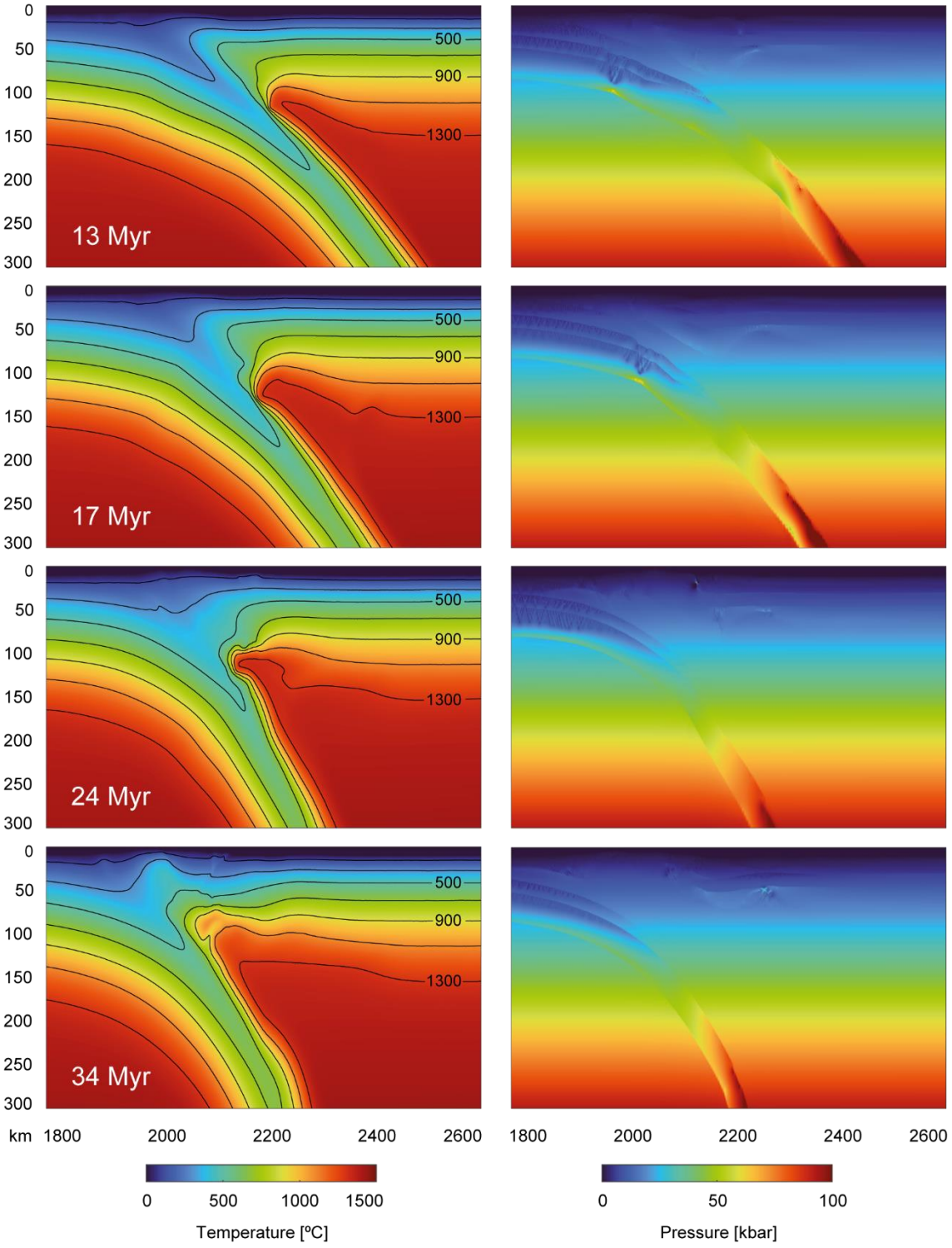

Figure 5.8. Temperature and pressure evolution of the end-member model for lithospheric mantle dominated magmatism (model 6, Table 5.1).

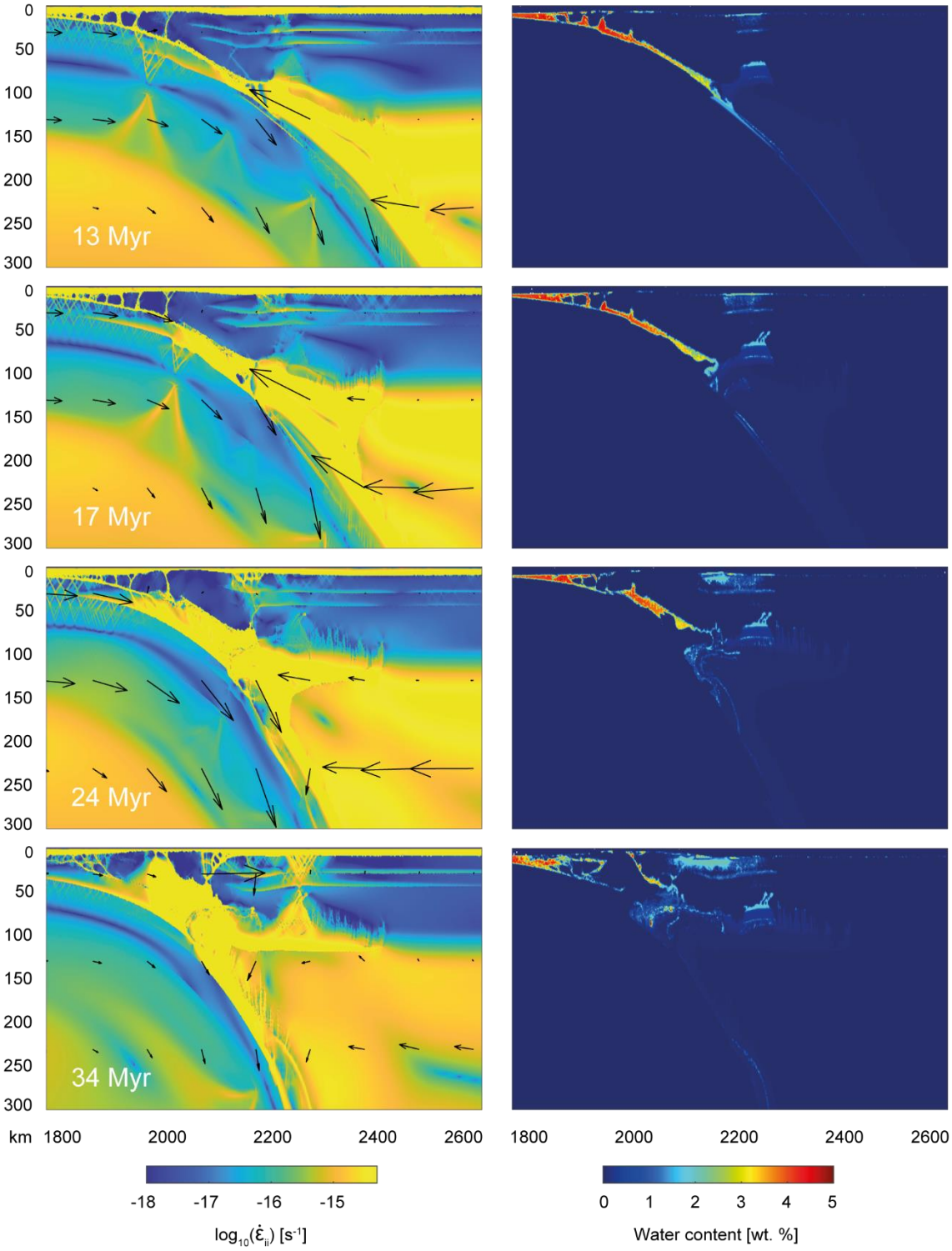

Figure 5.9. Second strain rate invariant and water content evolution of the end-member model for lithospheric mantle dominated magmatism (model 6, Table 5.1). Arrows represent the velocity field at each given timestep.

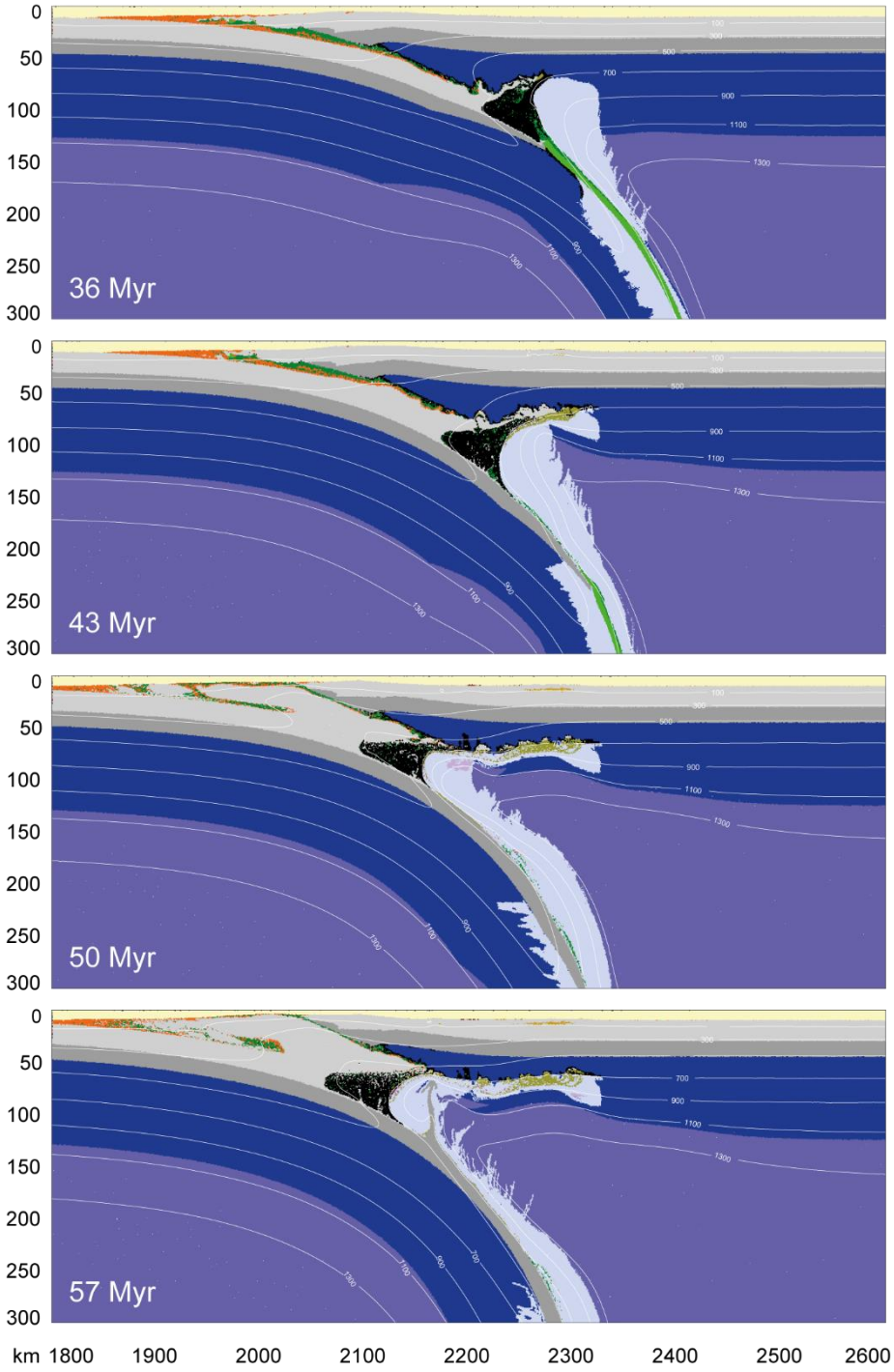

Figure 5.10. Development of the end-member model for relaminated crust dominated magmatism (model 26, Table 5.1). Colour scheme is the same as in fig. 4.5.

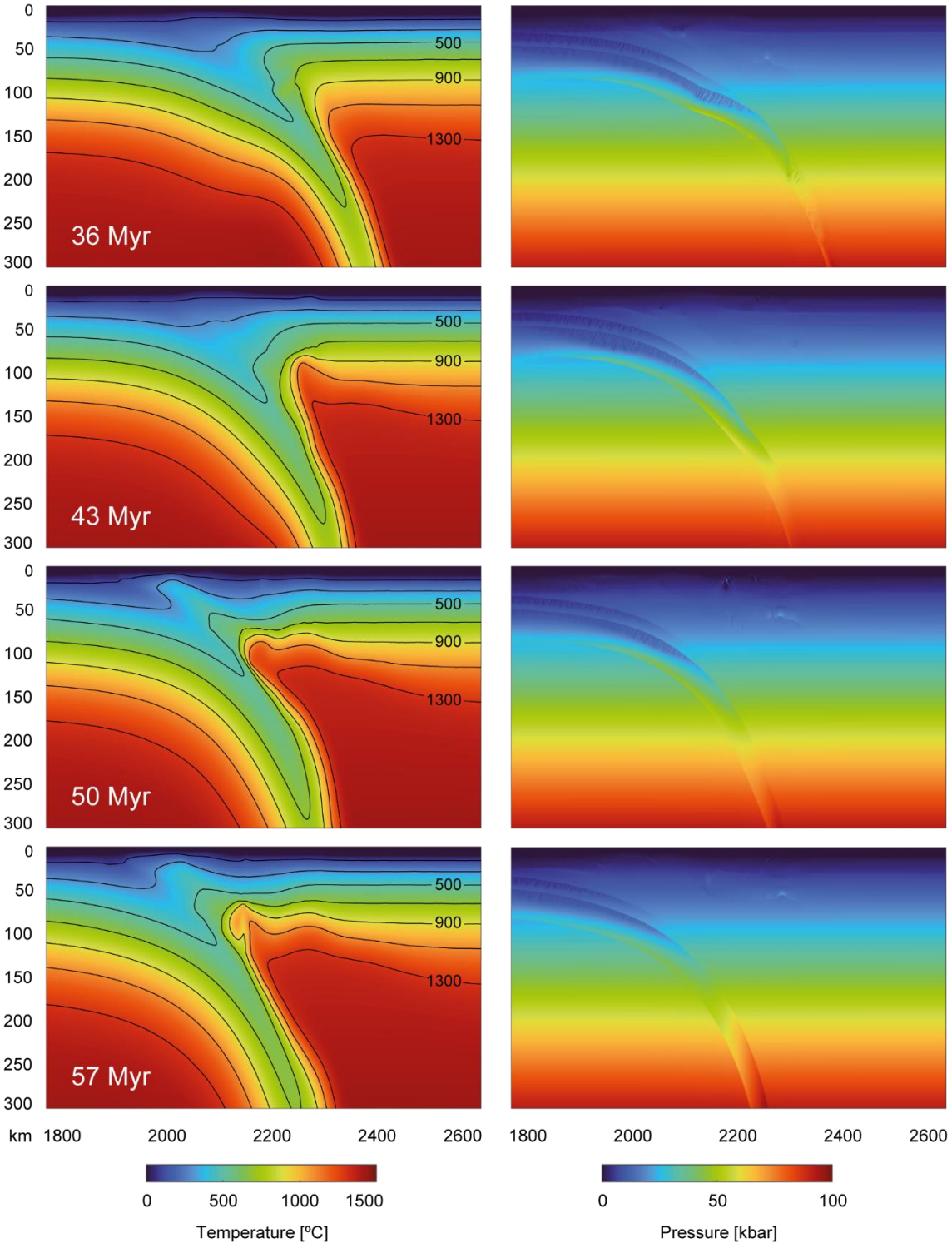

Figure 5.11. Temperature and pressure evolution of the end-member model for lithospheric mantle dominated magmatism (model 6, Table 5.1).

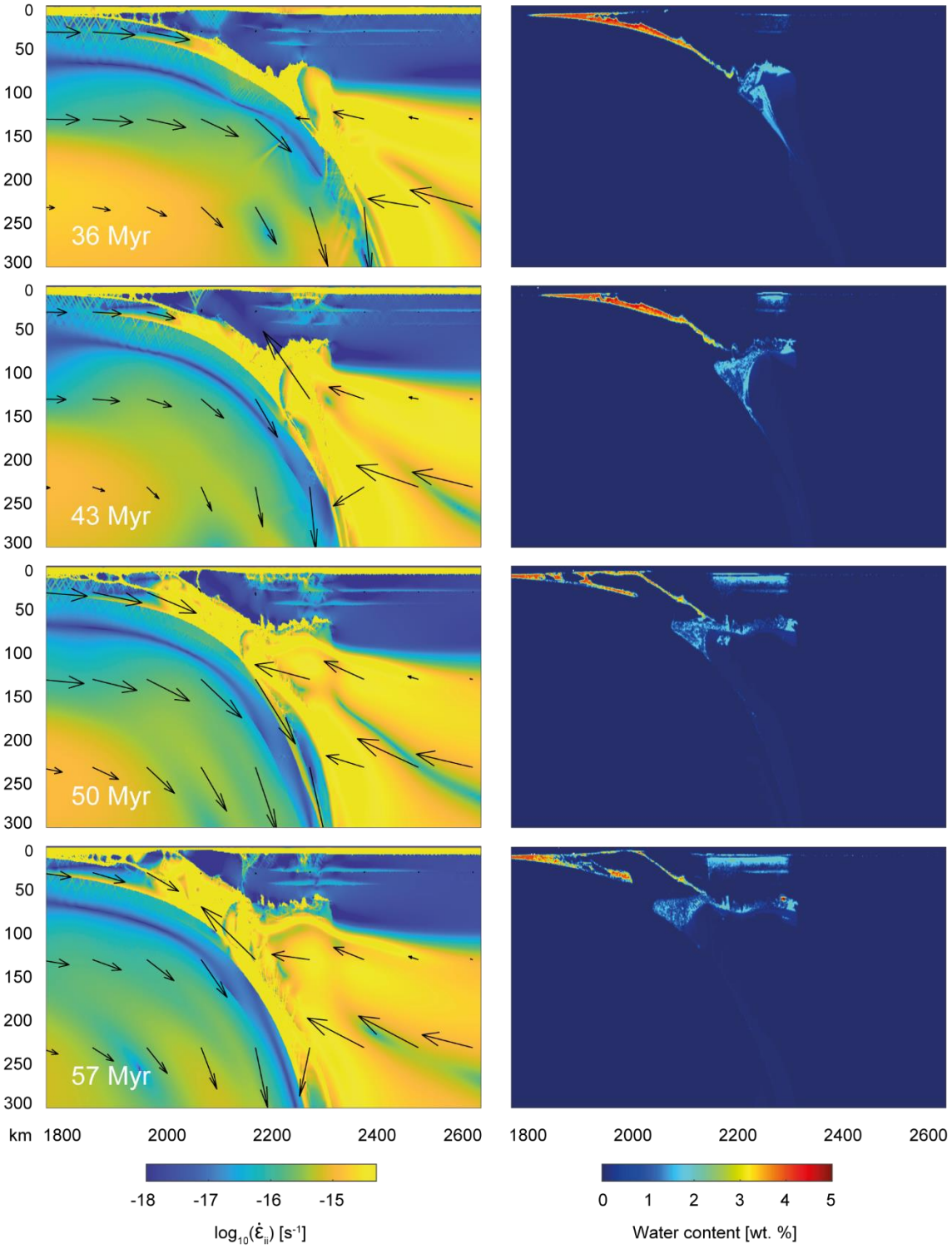

Figure 5.12. Second strain rate invariant and water content evolution of the end-member model for lithospheric mantle dominated magmatism (model 6, Table 5.1). Arrows represent the velocity field at each given timestep.

6. Discussion

6.1 Evidence from numerical models

6.1.1 Sensitivity to model parameters

The experimental results from the numerical study suggest that the convergence rate, length and thermal age of the oceanic crust exert a strong control over the geodynamic regime of subduction and subsequent collision. Among them, the length of the oceanic plate is the most influential in the style of magmatism during collision. Nevertheless, physical parameters of particular petrological relevance such as temperature, pressure and water content remain notably similar regardless of the varying model parameters. The numerical models show a consistent variety of magmatic sources in a limited range of geodynamic settings, potentially highlighting the robustness of the initial setup and selected model parameters.

6.1.1.1 Influence of the length of the oceanic lithosphere

The ocean width has been recognised as a significant variable in determining the different variations in orogenic style (Andrić et al., 2018; Dymkova et al., 2016). Shorter oceans facilitate a more efficient migration of deformation towards the foreland, resulting not only in more intense deformation (Fig. 5.12), but also in larger volumes of relamination from the subducted continental crust (Fig. 5.10). This geodynamic constrain makes the width of the oceanic lithosphere the most influential parameter in determining the style of magmatism. Specifically, numerical experiments using a longer oceanic plate allow for more prolonged and consequently larger thermal anomaly in the lithospheric mantle. A larger thermal anomaly allows for a comparatively more prominent activation of the mantle lithosphere as a magmatic source.

Besides, the length of the oceanic lithosphere dictates the order of activation for each magmatic source. A larger (675 km) ocean enables the production of lithospheric magmatism before crustal relamination initiation. In contrast, experiments using a shorter ocean tend to generate smaller batches of lithospheric mantle magmas, compared to the earlier and larger production of magmatism from the relaminated continental crust.

6.2.1.2 Influence of the convergence rate

Convergence rate has proven to be one of the most influential parameters in the style of post-subduction collisional orogeny, having a direct effect in the rheological coupling of the lithosphere (Faccenda et al., 2008) and the efficiency of slab dehydration (Dymkova et al., 2016). Notably, the newly obtained numerical models do not show significant variations among different convergence velocities in the rheological coupling of the lithosphere (Figs. 5.2, 5.7, 5.10). Upper crust consistently decouples from the lower crust after relamination initiation, suggesting that decoupling is a result of the rheological contrast between the weak upper crust (wet quartzite flow law) and strong lower crust (plagioclase An_{75} flow law). Likewise, no significant differences are found in the hydration and resulting water content of the lithospheric mantle from the overriding plate among the models. Water contents reach a consistent maximum of 2-3 wt. % in the hydrated upper plate regardless of the convergence velocity (Figs. 5.6, 5.9, 5.12).

Nevertheless, convergence velocity has a direct impact on the magmatism style of the numerical models. Particularly, in experiments using a larger (675 km) ocean higher convergence velocities appear to be favourable for a higher mantle flux and thermal anomaly in the mantle wedge, enhancing magmatic production from the lithospheric mantle. The opposite is also true, with slower convergence velocities precluding this phenomenon and limiting magmatism from the hydrated lithosphere. Instead, slow convergence velocities facilitate the gradual entrainment of larger portions of relaminated crust in the lithosphere, allowing for a more effective hybridisation. Comparatively, models using a shorter (400 km) oceanic plate and high (5 cm/yr) convergence velocity were the only resulting in a high thermal anomaly in the mantle wedge and subsequent melting of the asthenosphere.

6.1.1.3 Influence of the age of the oceanic lithosphere

The age of the oceanic lithosphere defines both the temperature distribution within the slab as well as its density (Turcotte and Schubert, 2002). The temperature distribution of the subducting ocean has a direct effect both on the geodynamic and magmatic regime of the model. Experiments using a younger (40 Myr) ocean use a weaker oceanic crust, being a lot more sensible to grainsize reduction and commonly resulting in detachment (Fig. 5.1). Likewise, a younger ocean is hotter and less negatively buoyant, resulting in a

weaker slab pull and ultimately favouring slab failure once the initial imposed convergence velocity disappears. Comparatively, an older and denser ocean favours the subducting lithosphere to sink into the asthenosphere, precluding slab detachment. In combination with faster convergence rates, experiments using an older oceanic plate favoured trench retreat and extension in the overriding plate, allowing for a larger production of magmatism. This model parameter is however influential only when considered in conjunction with the width of the oceanic plate and convergence rate.

6.1.2 Constrains from numerical models to post-collisional magmas

Magma production is dominated by the progressive modification of the magmatic source, most commonly caused by crustal relamination (Fig. 6.1). Subduction is ultimately the main driver of magmatism, causing an increasingly larger thermal anomaly in the mantle lithosphere. The gradual entrainment of oceanic crust into the asthenosphere liberates water to enhance melting, and further mantle lithosphere modification is driven after collision by fragments of relaminated crust. However, the influence of the width of the oceanic lithosphere has proven to be an important factor in determining vastly different styles of magmatism. The resemblance with nature of each endmember and transitional scenarios must be addressed prior to further discussion.

An important constrain arising from post-collisional magmas is the age distribution from different intrusions within the same batholith. More specifically, the age differences between felsic and mafic intrusions have been commonly overlooked due to the biased interpretation of a dual origin for post-collisional magmas. That is, a crustal and mantle origin for the felsic and mafic-intermediate suites, respectively. According to the previously presented results, the felsic magmatism results from differentiation of mantle-derived mafic to intermediate magmas (Gómez-Frutos et al., 2023; Gómez-Frutos and Castro, 2023, 2022), implying that the age differences can be representative of the petrogenetic process. Appropriately, mafic rocks consistently yield older ages than the more differentiated granitic intrusions in places where ages from both types have been calculated (e.g. Carracedo et al., 2009; Couzinié et al., 2016; Williamson et al., 1992).

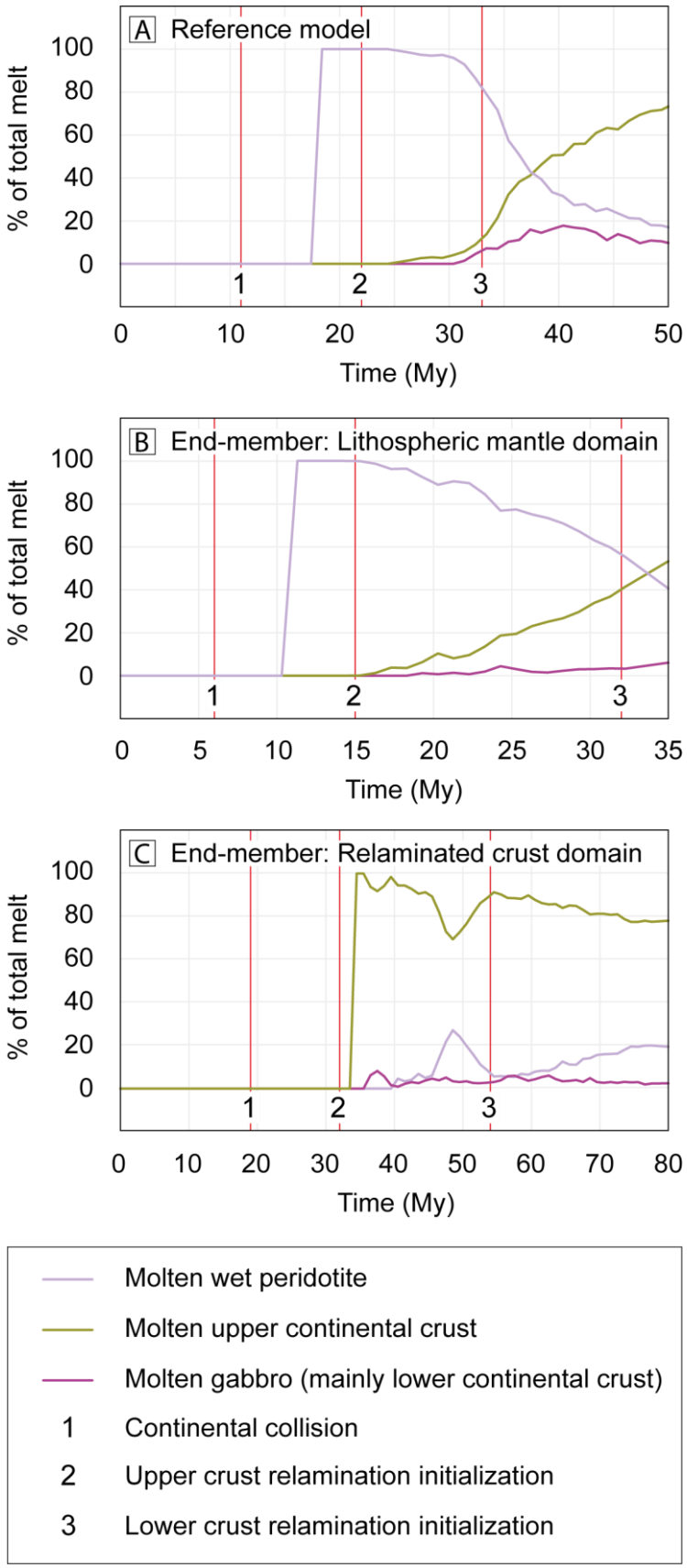

Figure 6.1. Magmatic source evolution throughout the reference and two end-member models. Continental subduction and crustal relamination causes a progressive source modification.

Although these observations can be considered preliminary and should be the focus of future works, they help to constrain the numerical results. Models featuring a larger ocean produce juvenile lithospheric mantle magmatism prior to the recycled magmas from the relaminated crust, expected to produce mafic and more felsic magmas, respectively. Furthermore, models using a short ocean and high convergence velocities (models 14, 16 and 18, Table 5.1) resulted in significant asthenosphere melting. As already noted, the subsequent large volumes of mantle picrites are unaccounted for in natural orogens. Although these observations are a simplification since they do not account for different degrees of partial melting, inference suggest that the use of larger oceans reproduce a scenario more similar to nature. These inferences suggest that models using shorter oceanic lithosphere are not a reliable source of information for magmatism in collisional settings.

Collision allows for an appropriate scenario for partial melting, producing a considerable thermal anomaly in the mantle. However, shortening is mostly accommodated along the weak plate interface, resulting in minor deformation in the upper plate, with the early development of fault systems due to compression (Fig. 5.5, 5.9, 5.12). The thermal anomaly neither affects the lower crust from the upper plate nor the Moho temperatures in any of the obtained numerical models. Upwelling scenarios only cause isotherms to tighten near the Moho, resulting in significantly increased temperature gradients in the mantle lithosphere. In contrast, the overlying continental crust remains at relatively constant temperatures (Fig. 5.3, 5.8, 5.11). That is, the mantle thermal anomaly never affects the continental crust, and collision have a limited effect on the thermal budget of the lower crust.

These considerations serve as another significant limitation to the deep crustal hot zone model for post-collisional magma generation (Annen et al., 2008, 2006; Hawkesworth and Kemp, 2006; Solano et al., 2012), previously addressed through petrological experiments (Gómez-Frutos et al., 2023). The resulting Moho conditions yield a limited range of 700 – 800 ^{o}C for partial melting of the lower crust. Existing numerical models suggest that thinner and weaker overriding plates enhance mantle flow and produce comparatively larger thermal anomalies (Hertgen et al., 2020). However, the resulting temperatures are in any case insufficient to produce voluminous magmatism from a

granulitic source (Castro, 2020; Patiño Douce, 1999). Although periodic influx of basaltic magma from the mantle is usually invoked to justify a sufficient thermal anomaly in the lower crust for magma generation (Annen et al., 2006), the abundant magmatism from the mantle obtained in the numerical results is expected to have a much larger volume expression that any potential crustal partial melt. For these reasons, numerical modelling evidence matches petrological evidence at dismissing the lower crust as an unlikely source for the main granite (*s.l.*) post-collisional batholiths.

On the potential source conditions for post-collisional magmas, the numerical models yield consistent values for temperature and pressure in molten areas. The thermal budget for such process is limited to a range of c.a. 1000 – 1200 ^{o}C (Fig. 5.3, 5.8, 5.11), and pressures of 15 – 25 kbar (Fig. 5.4, 5.8, 5.11). These conditions are supported by petrological experiments, in which a hybrid peridotite – silicic contaminant source has successfully reproduced liquids with I-type affinity under such conditions (Codillo et al., 2018). Moreover, numerical works on arc settings are in agreement with the obtained temperature and pressure ranges, resulting in significant partial melting of the contaminated lithospheric mantle (Castro et al., 2013b; Vogt et al., 2012). All these factors not only support the reliability of the numerical results, but also further depict a limited range for the conditions of post-collisional magma production.

The water content is another important issue when discussing the source for post-collisional magmas. Numerical models estimate around 2 wt. % H_2O in molten hydrated mantle and relaminated crust (Fig. 5.6, 5.9, 5.12), a significantly lower amount than previous estimations. Existing estimations of water contents in I-type magmas offer vastly different ranges, with the most conservative estimations pointing to an average of 4 wt. % H_2O in mafic magmas (Plank et al., 2013), water-rich silicic magma reservoirs bearing 6 – 12 wt. % H_2O (Collins et al., 2021, and references therein), and up to 16 – 20 wt. % H_2O in super-hydrous arc magmas (Urann et al., 2022). Such estimations attempt to support the production of crustal magmas through water-fluxed melting, effectively reducing the solidus temperatures of the lower crust (e.g. Collins et al., 2020, 2016; Weinberg and Hasalová, 2015). However, these water contents are notably high when compared with the low water contents stored in natural rocks, rarely exceeding 1 wt. % H_2O (measured as LOI – loss on ignition) stored in primary minerals. Although the water

distribution in numerical experiments results from preset parameters in the subducting oceanic crust, limited amounts of water resulted in the production of large volumes of magmatism from the mantle lithosphere. Such reduced water budget eliminates the problem of the high-water requirement for fluid-fluxed melting of the lower crust, a vastly discussed topic in literature (see references above).

The entrainment of water and foreign silicic material into the mantle lithosphere brings the spotlight into another significant transversal topic, namely the mantle metasomatism. A metasomatized mantle has been invoked for the generation of the mafic-intermediate suite of post-collisional magmas (see references above). More specifically, to account for the enriched nature of orogenic magmatism a mantle source enriched in LILE, LREE and water is required. Nevertheless, water transport in the mantle is believed to occur mainly through crack propagation (O'Reilly and Griffin, 2013, and references therein), limiting the transportation of the required trace element budget to the mantle lithosphere. Moreover, mantle xenoliths dragged in basaltic lavas rarely display hydrous metasomatic features, and when present these are limited to accessory proportions of amphibole and phlogopite (e.g. Ionov et al., 2002; Kopylova et al., 2019). Not only do these considerations support lower water contents in the mantle lithosphere than the available estimations, but also highlight the need for an additional mechanism to account for large-scale mantle modification and subsequent magma production.

In this regard, crustal relamination serves as an alternative to the exposed problematic. According to the numerical results, the introduction of silicic crustal material in the mantle is a likely phenomenon in the evolution of an orogen, triggered after the upper continental crust becoming positively buoyant in the asthenosphere. The combination of an average silicic crustal material (c.a. 63 wt. % SiO_2 as described in Rudnick and Gao, 2003) from the relaminated crust and a peridotite from the mantle lithosphere results in a silicic hybrid mantle reservoir similar to those described for arc magmatism (Castro et al., 2013b). By the time the relaminated crust interacts with the mantle lithosphere, the thermal anomaly in the mantle wedge is sufficient to allow for magma production, likely of intermediate composition. Consequently, according to the presented contrasted numerical and petrological evidence a low-water hybrid peridotite-crustal silicic

contaminant is the most plausible source for the voluminous post-collisional magmatism.

6.2 Re-evaluation of crustal evolution throughout the geological record

The evolution of the continental crust and the lithosphere over the geological record is the result of multiple simultaneously occurring competing processes. Numerical models offer evidence of large-scale destruction of lithosphere, with common processes like erosion and weathering, slab detachment or gravitational instabilities driving the destruction of significant volumes of lithosphere. On the other hand, petrological studies provide sound evidence for the main driver behind continental growth, namely I-type magmatism. Coupled numerical and petrological work allows for a yet more complex view on the problematic, pointing to potential sources for Andean-type and Caledonian-type magmas.

Throughout the past decades, classic interpretations offered a relatively simple scenario; the continental crust is mainly created in active margins since the onset of plate tectonics (Dhuime et al., 2012, 2011; Thorpe et al., 1981; Voice et al., 2011), dismissing post-collisional magmatism as a minor contribution to crustal budget. Contrary to this, the provided new evidence depicts a yet more complex problem: both arc and post-collisional magmas result from mantle magmatism triggered by crustal destruction, either by erosion and subduction in the oceanic lithosphere or by crustal subduction and relamination. Balancing crustal growth and destruction in each process remain a critical issue to address crustal evolution. While these matters have proved to be deserving of an entire doctoral dissertation on their own merits, a preliminary re-evaluation can be made in this regard.

Andean-type magmas have been referred to as the main drivers behind crustal growth (see references above). Extensive discussion on the origin of this magmatism have reached a relative consensus on their mantle origin, resulting from melting of a silicic diapir from the subduction melange (Castro et al., 2013b; Marschall and Schumacher, 2012). Nevertheless, this crustal growth mechanism is compensated by erosion during subduction, both from the structural collapse of the forearc wedge into the trench and from the abrasion and hydrofracturing above the subduction channel.

In this regard, erosion rates along different convergent plate boundaries showcase a significant variability. For instance, 90 km^3/km/My are considered average values for the Andean subduction in central Chile (Scholl and Von Huene, 2009; Scholl and von Huene, 2007), while the estimated erosion within this same plate boundary lowers to 15 km^3/km/My in Peru (Clift et al., 2009b, 2009a). While such heterogeneity created controversy over the actual net growth in active margins (Thorpe et al., 1981), the recent development of numerical models and more accurate erosion estimations suggest that erosion far exceeds the growth rates (Stern, 2011). Such conclusions are in agreement with natural inference, since continental arcs are exposed to erosion and are prone to mass loss into sediments towards the oceanic basins. The implication is that the oceanic subduction stage in active continental margins favours crustal destruction due to the more effective erosion rates compared to new magmatic input.

The effect of post-collisional magmas in crustal evolution is the result of the competing destruction from continent subduction and growth driven by the magmatic input. Post-collisional magmatism has already been discussed to be optimal for its long-term preservation in the continental crust (Gómez-Frutos et al., 2023). Nevertheless, the new insights from numerical models point to the involvement of recycled continental crust in the source of post-collisional magmas. The implication is that the new magmatic input, although shielded in the core of newly formed supercontinents, is not translated directly into continental growth. Similar to cordilleran magmas, crustal destruction through continental subduction and crustal growth through magmatism must be balanced.

Nevertheless, addressing this issue in post-collisional magmas proves to be a more difficult task, since plenty of its mechanisms have been discussed throughout this dissertation. Erosion is not the main driver behind crustal destruction in collisional settings. Instead, continental subduction and recycling serves as a significant crustal destruction mechanism, but the ratios in terms of volume of relaminated crust and peridotite needed to produce post-collisional magmatism are unknown, and so is the volumetric production of post-collisional magmatism during collision. This issue is further complicated by the progressive lithospheric thickening during collision, since thinner overriding plate favours magmatism (Hertgen et al., 2020). For these reasons, unveiling the ratio of relaminated crust needed to produce post-collisional magmas and

estimating their subsequent volume must be the subject of future petrological and numerical studies.

These considerations suggest that the evolution of the continental crust is tightly linked to the supercontinent cycle. Mass loss characterises the breakup and early assembly stages within each cycle, where magmatism is scarce and erosion is responsible for the extensive destruction of the continental crust. During the late stages of assembly, cordilleran magmatism is triggered through oceanic subduction, and the magmatic production progressively balances the erosion rates. In the latest assembly stage and early supercontinent stage, the relaminated crust triggers the production of post-collisional magmas, marking a shift towards net crustal growth during continental collision. Preservation rates reach a maximum during this stage of the supercontinent cycle, with the new magmatic input being shielded in the suture of two continents, usually distant from oceanic influence.

The former considerations offer a qualitative description of the evolution of the continental crust. Using a magmatic perspective on the problem the existing estimations on crustal growth are challenged. The previously discussed inferences suggest that crustal growth from Andean-type magmatism is limited if any, while Caledonian-type magmas are effective in growing the continents. This evidences a progressive shift from crustal destruction towards crustal growth with the course of each supercontinent cycle, potentially implying an episodic continental growth since continent were originally created. A quantitative balance between growth and destruction within each of these stages is still lacking. Hence, determining the balance between crustal growth and destruction can be considered the next milestone in understanding the evolution of the lithosphere.

In the light of the results of this PhD thesis, it is safe to surmise that the evolution of the lithosphere results from the complex multi-component interaction between mantle and crust, mostly driven by subduction in active plate boundaries. The two magmatic suites responsible for crustal growth, namely Andean-type and Caledonian-type, occur when a critical volume of crustal material is recycled back into the mantle, triggering lithospheric mantle magmatism. In such a system the continental crust is limited to a passive role and is not the source for new I-type magmas. Instead, the spotlight is brought into the mantle

lithosphere, undergoing periodic metasomatism through the input of crustal material and giving birth to new continental crust.

7. Concluding remarks

The evolution of the lithosphere and origin of continents represent one of the most important issues in Earth Sciences, responding to the long-term balance of competing crustal growth and destruction processes. Crustal growth can be described as the incorporation and preservation of igneous material generated in the mantle into the crust. Consequently, the scrutiny of the most voluminous type of magmatism driving continental growth, namely I-type, was used as a mean to re-evaluate crustal evolution throughout the geological record. Among I-type magmas, the two constituent suites, namely Andean-type and Caledonian-type, are sourced in different stages of the subduction process, the main driver behind crustal destruction.

The examination of the petrogenesis and geodynamic mechanisms involving I-type magmatism was performed through a variety of methods, including petrological experiments, numerical models and field work. The available conclusions shall be classified according to their corresponding objectives as follows:

1) Determination of the origin of Caledonian-type/post-collisional magmatism. Caledonian-type magmas are sourced in the mantle lithosphere after metasomatism with an external material.

a) Determination of the origin of the mafic-intermediate suite (i.e. sanukitoid series) and evaluating its role in post-collisional magmatism. The sanukitoid suite is sourced in a metasomatized mantle and is parental to the voluminous silicic post-collisional magmas. The common high-Mg signature results from self-contamination with the liquidus phase of the system, namely orthopyroxene.

b) Determination of the origin of the silicic suite. The silicic suite from post-collisional magmas results from the differentiation of sanukitoid magmatism. The observed geochemical signature is configured after a liquid line of descent. Post-collisional magmas represent a significant addition of mass to the continental crust, optimal for long-term preservation as they are commonly shielded in the core of newly assembled supercontinents.

c) Determination of the origin of the mafic microgranular enclaves and evaluating their relationship with the host silicic magmas. Mafic microgranular enclaves represent fragments of the parental magma to post-collisional batholiths, preserved as quenched magmas in the ascent conduits that are torn apart and dragged by subsequent pulses.

d) Determination of the thermal and water budget of the lower crust during collision. Moho temperatures are generally not affected by the collision process, limiting the viability of the lower crust as a magmatic source. Comparatively, a large thermal anomaly can be reached in the lithospheric mantle, with temperatures up to 1300 ^{o}C. Water contents are supplied via subduction and rarely exceed 4 wt. %.

2) Determination of the parental magmas to cordilleran magmatism. The parental magmas to cordilleran magmatism are intermediate in composition, and are best preserved in magma mingling zones, where quenching is a widespread phenomenon precluding fractionation.

3) Evaluation of the role of I-type magmatism on crustal evolution. The voluminous I-type magmatism represents a consistent crustal recycling mechanism, in which the addition of new mass into the continental crust is triggered by the subduction of crustal materials into the mantle. Long-term crustal evolution is ultimately determined by the balance between growth and destruction during the subduction processes, intimately linked to the periodic occurrence of the supercontinent cycle.

The ultimate implication of such conclusions is that I-type magmatism occurs as a consequence of the subduction process, inserting crustal material into the lithosphere and causing metasomatism. These conclusions offer new ways to tackle the lithosphere evolution problem. Although such new insights into the mechanisms involving orogenic magma generation have been provided, a more detailed study on the differential mantle sources of Andean-type and Caledonian-type magmas must be the focus of further petrological experiments. Likewise, the revealed mechanisms responsible for I-type magmas require recycling continental crust into the mantle lithosphere, either by oceanic or continental subduction. The quantitative balance between crustal growth and destruction in orogenic magmatism remains unknown.

8. References

Aghazadeh, M., Castro, A., Badrzadeh, Z., Vogt, K., 2011. Post-collisional polycyclic plutonism from the Zagros hinterland: the Shaivar Dagh plutonic complex, Alborz belt, Iran. Geol. Mag. 148, 980–1008.

Allègre, C., Hart, S., Minster, J.-F., 1983. Chemical structure and evolution of the mantle and continents determined by inversion of Nd and Sr isotopic data, I. Theoretical methods. Earth Planet. Sci. Lett. 66, 177–190.

Allen, J., Boettcher, A., 1978. Amphiboles in andesite and basalt: II. Stability as a function of P–T–f H2O–f O2. Am. Mineral. 63, 1074–1087.

Alonso-Perez, R., Müntener, O., Ulmer, P., 2009. Igneous garnet and amphibole fractionation in the roots of island arcs: experimental constraints on andesitic liquids. Contrib. Mineral. Petrol. 157, 541–558.

Andersson, U.B., Eklund, O., Fröjdö, S., Konopelko, D., 2006. 1.8 Ga magmatism in the Fennoscandian Shield; lateral variations in subcontinental mantle enrichment. Lithos 86, 110–136.

Andrić, N., Vogt, K., Matenco, L., Cvetković, V., Cloetingh, S., Gerya, T., 2018. Variability of orogenic magmatism during Mediterranean-style continental collisions: A numerical modelling approach. Gondwana Res. 56, 119–134.

Andronicos, C.L., Chardon, D.H., Hollister, L.S., Gehrels, G.E., Woodsworth, G.J., 2003. Strain partitioning in an obliquely convergent orogen, plutonism, and synorogenic collapse: Coast Mountains Batholith, British Columbia, Canada. Tectonics 22.

Annen, C., Blundy, J., Sparks, R., 2006. The genesis of intermediate and silicic magmas in deep crustal hot zones. J. Petrol. 47, 505–539.

Annen, C., Blundy, J.D., Sparks, R.S.J., 2008. The sources of granitic melt in Deep Hot Zones. Earth Environ. Sci. Trans. R. Soc. Edinb. 97, 297–309.

Aranovich, L.Y., Makhluf, A.R., Manning, C.E., Newton, R.C., 2014. Dehydration melting and the relationship between granites and granulites. Precambrian Res. 253, 26–37.

Armstrong, R.L., 1981. Radiogenic isotopes: the case for crustal recycling on a near-steady-state no-continental-growth Earth. Philos. Trans. R. Soc. Lond. Ser. Math. Phys. Sci. 301, 443–472.

Arndt, N.T., 2013. The formation and evolution of the continental crust. Geochem. Perspect. 2, 405–405.

Arndt, N.T., Goldstein, S.L., 1987. Use and abuse of crust-formation ages. Geology 15, 893–895.

Artemieva, I.M., Mooney, W.D., 2001. Thermal thickness and evolution of Precambrian lithosphere: A global study (Paper 2000JB900439). J. Geophys. Res.- Ser.- 106, 16–387.

Atherton, M.P., 1990. The Coastal Batholith of Peru: the product of rapid recycling of 'new'crust formed within rifted continental margin. Geol. J. 25, 337–349.

Bacon, C.R., 1986. Magmatic inclusions in silicic and intermediate volcanic rocks. J. Geophys. Res. Solid Earth 91, 6091–6112.

Bailey, D., 1982. Mantle metasomatism—continuing chemical change within the Earth. Nature 296, 525–530.

Ballmer, M.D., Lourenço, D.L., Hirose, K., Caracas, R., Nomura, R., 2017. Reconciling magma-ocean crystallization models with the present-day structure of the Earth's mantle. Geochem. Geophys. Geosystems 18, 2785–2806.

Barbarin, B., 2005. Mafic magmatic enclaves and mafic rocks associated with some granitoids of the central Sierra Nevada batholith, California: nature, origin, and relations with the hosts. Lithos 80, 155–177.

Barbarin, B., 1991. Enclaves of the Mesozoic calc-alkaline granitoids of the Sierra Nevada Batholith, California. Enclaves Granite Petrol. 135–153.

Barbarin, B., Didier, J., 1992. Genesis and evolution of mafic microgranular enclaves through various types of interaction between coexisting felsic and mafic magmas. Earth Environ. Sci. Trans. R. Soc. Edinb. 83, 145–153.

Barker, F., Arth, J.G., Stern, T.W., 1986. Evolution of the Coast batholith along the Skagway traverse, Alaska and British Columbia. Am. Mineral. 71, 632–643.

Bateman, P.C., 1992. Plutonism in the central part of the Sierra Nevada batholith, California. US Government Printing Office.

Bea, F., Gallastegui, G., Montero, P., Molina, J., Scarrow, J., Cuesta, A., González-Menéndez, L., 2021. Contrasting high-Mg, high-K rocks in Central Iberia: the appinite—vaugnerite conundrum and their (non-existent) relation with arc magmatism. J. Iber. Geol. 47, 235–261.

Belousova, E., Kostitsyn, Y., Griffin, W., Begg, G., O'reilly, S., Pearson, N., 2010. The growth of the continental crust: constraints from zircon Hf-isotope data. Lithos 119, 457–466.

Best, M., 1963. Petrology of the Guadalupe Igneous Complex South-western Sierra Nevada Foothills California. J. Petrol. 4, 223–259.

Bird, P., 1979. Continental delamination and the Colorado Plateau. J. Geophys. Res. Solid Earth 84, 7561–7571.

Bird, P., 1978. Finite element modeling of lithosphere deformation: the Zagros collision orogeny. Tectonophysics 50, 307–336.

Blanco-Quintero, I.F., Gerya, T.V., García-Casco, A., Castro, A., 2011. Subduction of young oceanic plates: A numerical study with application to aborted thermal-chemical plumes. Geochem. Geophys. Geosystems 12.

Bonin, B., 2004. Do coeval mafic and felsic magmas in post-collisional to within-plate regimes necessarily imply two contrasting, mantle and crustal, sources? A review. Lithos 78, 1–24.

Bowes, D., Košler, J., 1993. Geochemical comparison of the subvolcanic appinite suite of the British Caledonides and the durbachite suite of the Central European Hercynides: evidence for associated shoshonitic and granitic magmatism. Mineral. Petrol. 48, 47–63.

Boyd, F., England, J., 1960. Apparatus for phase-equilibrium measurements at pressures up to 50 kilobars and temperatures up to 1750° C. J. Geophys. Res. 65, 741–748.

Brophy, J.G., 1991. Composition gaps, critical crystallinity, and fractional crystallization in orogenic (calc-alkaline) magmatic systems. Contrib. Mineral. Petrol. 109, 173–182.

Brugier, Y.-A., Alletti, M., Pichavant, M., 2015. Fe pre-enrichment: A new method to counteract iron loss in experiments on basaltic melts. Am. Mineral. 100, 2106–2111.

Bunsen, R., 1851. Ueber die Processe der vulkanischen Gesteinsbildungen Islands. Ann. Phys. 159, 197–272.

Burg, J., Gerya, T., 2005. The role of viscous heating in Barrovian metamorphism of collisional orogens: thermomechanical models and application to the Lepontine Dome in the Central Alps. J. Metamorph. Geol. 23, 75–95.

Cantagrel, J.-M., Didier, J., Gourgaud, A., 1984. Magma mixing: origin of intermediate rocks and “enclaves” from volcanism to plutonism. Phys. Earth Planet. Inter. 35, 63–76.

Carracedo, M., Paquette, J.-L., Alonso Olazabal, A., Santos Zalduegui, J., García de Madinabeitia, S., Tiepolo, M., Gil Ibarguchi, J., 2009. U–Pb dating of granodiorite and granite units of the Los Pedroches batholith. Implications for geodynamic models of the southern Central Iberian Zone (Iberian Massif). Int. J. Earth Sci. 98, 1609–1624.

Carroll, M.R., Wyllie, P.J., 1990. The system tonalite-H2O at 15 kbar and the genesis of calc-alkaline magmas. Am. Mineral. 75, 345–357.

Castro, A., 2021. A non-basaltic experimental cotectic array for calc-alkaline batholiths. Lithos 382, 105929.

Castro, A., 2020. The dual origin of I-type granites: the contribution from experiments. Geol. Soc. Lond. Spec. Publ. 491, 101–145.

Castro, A., Aghazadeh, M., Badrzadeh, Z., Chichorro, M., 2013a. Late Eocene–Oligocene post-collisional monzonitic intrusions from the Alborz magmatic belt, NW Iran. An example of monzonite magma generation from a metasomatized mantle source. Lithos 180, 109–127.

Castro, A., Corretgé, L.G., De la Rosa, J., Fernández, C., López, S., García-Moreno, O., Chacón, H., 2003. The appinite–migmatite complex of Sanabria, NW Iberian massif, Spain. J. Petrol. 44, 1309–1344.

Castro, A., Gerya, T., 2008. Magmatic implications of mantle wedge plumes: Experimental study. Lithos 103, 138–148.

Castro, A., Gerya, T., García-Casco, A., Fernández, C., Díaz-Alvarado, J., Moreno-Ventas, I., Löw, I., 2010. Melting relations of MORB–sediment mélanges in underplated mantle wedge plumes; implications for the origin of Cordilleran-type batholiths. J. Petrol. 51, 1267–1295.

Castro, A., Stephens, W.E., 1992. Amphibole-rich polycrystalline clots in calc-alkaline granitic rocks and their enclaves. Can. Mineral. 30, 1093–1112.

Castro, A., Vogt, K., Gerya, T., 2013b. Generation of new continental crust by sublithospheric silicic-magma relamination in arcs: a test of Taylor's andesite model. Gondwana Res. 23, 1554–1566.

Cawthorn, R.G., O'Hara, M.J., 1976. Amphibole fractionation in calc-alkaline magma genesis. Am. J. Sci. 276, 309–329.

Chapman, D., 1986. Thermal gradients in the continental crust. Geol. Soc. Lond. Spec. Publ. 24, 63–70.

Chappell, B., 1996. Magma mixing and the production of compositional variation within granite suites: evidence from the granites of southeastern Australia. J. Petrol. 37, 449–470.

Chappell, B.W., Wyborn, D., 2012. Origin of enclaves in S-type granites of the Lachlan Fold Belt. Lithos 154, 235–247.

Chen, Y., Price, R., White, A., 1989. Inclusions in three S-type granites from southeastern Australia. J. Petrol. 30, 1181–1218.

Chung, S.-L., Chu, M.-F., Zhang, Y., Xie, Y., Lo, C.-H., Lee, T.-Y., Lan, C.-Y., Li, X., Zhang, Q., Wang, Y., 2005. Tibetan tectonic evolution inferred from spatial and temporal variations in post-collisional magmatism. Earth-Sci. Rev. 68, 173–196.

Clark, C., Fitzsimons, I.C., Healy, D., Harley, S.L., 2011. How does the continental crust get really hot? Elements 7, 235–240.

Clauser, C., Huenges, E., 1995. Thermal conductivity of rocks and minerals. Rock Phys. Phase Relat. Handb. Phys. Constants 3, 105–126.

Clemens, J., Elburg, M., Harris, C., 2017. Origins of igneous microgranular enclaves in granites: the example of Central Victoria, Australia. Contrib. Mineral. Petrol. 172, 1–27.

Clift, P., Vannucchi, P., 2004. Controls on tectonic accretion versus erosion in subduction zones: Implications for the origin and recycling of the continental crust. Rev. Geophys. 42.

Clift, P.D., Schouten, H., Vannucchi, P., 2009a. Arc-continent collisions, sediment recycling and the maintenance of the continental crust. Geol. Soc. Lond. Spec. Publ. 318, 75–103.

Clift, P.D., Vannucchi, P., Morgan, J.P., 2009b. Crustal redistribution, crust–mantle recycling and Phanerozoic evolution of the continental crust. Earth-Sci. Rev. 97, 80–104.

Cobbing, E.J., Pitcher, W.S., 1972. The coastal batholith of central Peru. J. Geol. Soc. 128, 421–454.

Codillo, E., Le Roux, V., Marschall, H., 2018. Arc-like magmas generated by mélange-peridotite interaction in the mantle wedge. Nat. Commun. 9, 2864.

Collins, W.J., Huang, H.-Q., Jiang, X., 2016. Water-fluxed crustal melting produces Cordilleran batholiths. Geology 44, 143–146.

Collins, W.J., Murphy, J., Blereau, E., Huang, H.-Q., 2021. Water availability controls crustal melting temperatures. Lithos 402, 106351.

Collins, W.J., Murphy, J.B., Johnson, T.E., Huang, H.-Q., 2020. Critical role of water in the formation of continental crust. Nat. Geosci. 13, 331–338.

Conceição, R., Green, D., 2004. Derivation of potassic (shoshonitic) magmas by decompression melting of phlogopite+ pargasite lherzolite. Lithos 72, 209–229.

Condie, K., 2014. Growth of continental crust: a balance between preservation and recycling. Mineral. Mag. 78, 623–637.

Condie, K.C., 2013a. Plate tectonics & crustal evolution. Elsevier.

Condie, K.C., 2013b. Preservation and recycling of crust during accretionary and collisional phases of Proterozoic orogens: a bumpy road from Nuna to Rodinia. Geosciences 3, 240–261.

Condie, K.C., 1998. Episodic continental growth and supercontinents: a mantle avalanche connection? Earth Planet. Sci. Lett. 163, 97–108.

Condie, K.C., Aster, R.C., 2010. Episodic zircon age spectra of orogenic granitoids: the supercontinent connection and continental growth. Precambrian Res. 180, 227–236.

Condie, K.C., Bickford, M.E., Aster, R.C., Belousova, E., Scholl, D.W., 2011. Episodic zircon ages, Hf isotopic composition, and the preservation rate of continental crust. GSA Bull. 123, 951–957.

Coombs, M.L., Eichelberger, J.C., Rutherford, M.J., 2003. Experimental and textural constraints on mafic enclave formation in volcanic rocks. J. Volcanol. Geotherm. Res. 119, 125–144.

Corradino, M., Balázs, A., Faccenna, C., Pepe, F., 2022. Arc and forearc rifting in the Tyrrhenian subduction system. Sci. Rep. 12, 4728.

Couzinié, S., Laurent, O., Moyen, J.-F., Zeh, A., Bouilhol, P., Villaros, A., 2016. Post-collisional magmatism: Crustal growth not identified by zircon Hf–O isotopes. Earth Planet. Sci. Lett. 456, 182–195.

Daignieres, M., Fremond, M., FRIAA, A., 1978. Modèle du type Norton-Hoff généralisé pour l'étude des déformations lithosphériques (exemple: la collision himalayenne).

Daly, R.A., 1925. The geology of Ascension island. Presented at the Proceedings of the American Academy of Arts and Sciences, JSTOR, pp. 3–80.

de Lima, J.V., de Pinho Guimarães, I., Neves, S.P., Basei, M.A.S., da Silva Filho, A.F., Brainer, C.C.G., 2021. Post-collisional, high-Ba-Sr Teixeira Batholith granites: evidence for recycling of Paleoproterozoic crust in the Alto Pajeú domain, Borborema Province–NE-Brazil. Lithos 404, 106469.

de Oliveira, M.A., Dall'Agnol, R., Althoff, F.J., da Silva Leite, A.A., 2009. Mesoarchean sanukitoid rocks of the Rio Maria granite-greenstone terrane, Amazonian craton, Brazil. J. South Am. Earth Sci. 27, 146–160.

de Oliveira, M.A., Dall'Agnol, R., Scaillet, B., 2010. Petrological constraints on crystallization conditions of Mesoarchean sanukitoid rocks, Southeastern Amazonian Craton, Brazil. J. Petrol. 51, 2121–2148.

Dhuime, B., Hawkesworth, C., Cawood, P., 2011. When continents formed. Science 331, 154–155.

Dhuime, B., Hawkesworth, C.J., Cawood, P.A., Storey, C.D., 2012. A change in the geodynamics of continental growth 3 billion years ago. Science 335, 1334–1336.

Didier, J., 1991. Enclaves and granite petrology. Dev. Petrol. 13 625.

Didier, J., 1973. Developments in Petrology: The Bearing of Enclaves on the Origin of Granites. Granites and Their Enclaves. Elsevier Scientific Publishing Company.

Didier, J., 1964. Etude pétrographique des enclaves de quelques granites du Massif Central français. J. de Bussac.

Didier, J., Lameyre, J., 1969. Les granites du Massif central français: étude comparée des leucogranites et granodiorites. Contrib. Mineral. Petrol. 24, 219–238.

Dodge, F., Kistler, R., 1990. Some additional observations on inclusions in the granitic rocks of the Sierra Nevada. J. Geophys. Res. Solid Earth 95, 17841–17848.

Donaire, T., Pascual, E., Pin, C., Duthou, J.-L., 2005. Microgranular enclaves as evidence of rapid cooling in granitoid rocks: the case of the Los Pedroches granodiorite, Iberian Massif, Spain. Contrib. Mineral. Petrol. 149, 247–265.

dos Santos, M.N.S., Oliveira, D.C., 2016. Rio Maria granodiorite and associated rocks of Ourilândia do Norte–Carajás province: Petrography, geochemistry and implications for sanukitoid petrogenesis. J. South Am. Earth Sci. 72, 279–301.

Duan, F., Li, Y., Zhi, Q., Yang, G., Gao, J., 2019. Petrogenesis and geodynamic implications of Late Carboniferous sanukitic dikes from the Bieluagaxi area of West Junggar, NW China. J. Asian Earth Sci. 175, 158–177.

Duque-Trujillo, J., Bustamante, C., Solari, L., Gómez-Mafla, Á., Toro-Villegas, G., Hoyos, S., 2019. Reviewing the Antioquia batholith and satellite bodies: a record of Late

Cretaceous to Eocene syn-to post-collisional arc magmatism in the Central Cordillera of Colombia. Andean Geol. 46, 82–101.

Duretz, T., Gerya, T.V., May, D.A., 2011. Numerical modelling of spontaneous slab breakoff and subsequent topographic response. Tectonophysics 502, 244–256.

Dymkova, D., Gerya, T., Burg, J.-P., 2016. 2D thermomechanical modelling of continent–arc–continent collision. Gondwana Res. 32, 138–150.

Eichelberger, J.C., 1975. Origin of andesite and dacite: evidence of mixing at Glass Mountain in California and at other circum-Pacific volcanoes. Geol. Soc. Am. Bull. 86, 1381–1391.

Eklund, O., Konopelko, D., Rutanen, H., Fröjdö, S., Shebanov, A., 1998. 1.8 Ga Svecofennian post-collisional shoshonitic magmatism in the Fennoscandian shield. Lithos 45, 87–108.

Eugster, H.P., 1971. The Beginnings of Experimental Petrology: Van't Hoff's study of marine evaporites was the first systematic effort in this field. Science 173, 481–489.

Faccenda, M., Gerya, T.V., Chakraborty, S., 2008. Styles of post-subduction collisional orogeny: Influence of convergence velocity, crustal rheology and radiogenic heat production. Lithos 103, 257–287.

Faccenda, M., Minelli, G., Gerya, T., 2009. Coupled and decoupled regimes of continental collision: Numerical modeling. Earth Planet. Sci. Lett. 278, 337–349.

Fernández-Suárez, J., Dunning, G., Jenner, G., GUTIÉRREZ-ALONSO, G., 2000. Variscan collisional magmatism and deformation in NW Iberia: constraints from U–Pb geochronology of granitoids. J. Geol. Soc. 157, 565–576.

Ferré, E., Caby, R., Peucat, J., Capdevila, R., Monié, P., 1998. Pan-African, post-collisional, ferro-potassic granite and quartz–monzonite plutons of Eastern Nigeria. Lithos 45, 255–279.

Fershtater, G., Borodina, N., 1977. Petrology of autoliths in granitic rocks. Int. Geol. Rev. 19, 458–468.

Fowler, M., 1992. Elemental and O-Sr-Nd isotope geochemistry of the Glen Dessarry syenite, NW Scotland. J. Geol. Soc. 149, 209–220.

Fowler, M., 1988. Ach'uaine hybrid appinite pipes: evidence for mantle-derived shoshonitic parent magmas in Caledonian granite genesis. Geology 16, 1026–1030.

Fowler, M., Henney, P., 1996. Mixed Caledonian appinite magmas: implications for lamprophyre fractionation and high Ba-Sr granite genesis. Contrib. Mineral. Petrol. 126, 199–215.

Fowler, M., Kocks, H., Darbyshire, D., Greenwood, P., 2008. Petrogenesis of high Ba–Sr plutons from the northern highlands Terrane of the British Caledonian Province. Lithos 105, 129–148.

Fowler, M., Rollinson, H., 2012. Phanerozoic sanukitoids from Caledonian Scotland: implications for Archean subduction. Geology 40, 1079–1082.

Frisch, W., Dunkl, I., Kuhlemann, J., 2000. Post-collisional orogen-parallel large-scale extension in the Eastern Alps. Tectonophysics 327, 239–265.

Fyfe, W., 1978. The evolution of the Earth's crust: modern plate tectonics to ancient hot spot tectonics? Chem. Geol. 23, 89–114.

Galán, G., Corretgé, L., Laurent, O., 1997. Low-potassium vaugnerites from Guéret (Massif Central, France). Mafic magma evolution influenced by contemporaneous granitoids. Mineral. Petrol. 59, 165.

Garrido, C.J., Bodinier, J.-L., Burg, J.-P., Zeilinger, G., Hussain, S.S., Dawood, H., Chaudhry, M.N., Gervilla, F., 2006. Petrogenesis of mafic garnet granulite in the lower crust of the Kohistan paleo-arc complex (Northern Pakistan): implications for intra-crustal differentiation of island arcs and generation of continental crust. J. Petrol. 47, 1873–1914.

Gaschnig, R.M., Vervoort, J.D., Lewis, R.S., Tikoff, B., 2011. Isotopic evolution of the Idaho batholith and Challis intrusive province, northern US Cordillera. J. Petrol. 52, 2397–2429.

Gaudemer, Y., Jaupart, C., Tapponnier, P., 1988. Thermal control on post-orogenic extension in collision belts. Earth Planet. Sci. Lett. 89, 48–62.

Gencalioglu Kuscu, G., Geneli, F., 2010. Review of post-collisional volcanism in the Central Anatolian Volcanic Province (Turkey), with special reference to the Tepekoy Volcanic Complex. Int. J. Earth Sci. 99, 593–621.

Gerya, T., 2022. Numerical modeling of subduction: State of the art and future directions. Geosphere 18, 503–561.

Gerya, T., 2019. Introduction to numerical geodynamic modelling. Cambridge University Press.

Gerya, T., 2014. Precambrian geodynamics: concepts and models. Gondwana Res. 25, 442–463.

Gerya, T.V., Yuen, D.A., 2007. Robust characteristics method for modelling multiphase visco-elasto-plastic thermo-mechanical problems. Phys. Earth Planet. Inter. 163, 83–105.

Gerya, T.V., Yuen, D.A., 2003. Characteristics-based marker-in-cell method with conservative finite-differences schemes for modeling geological flows with strongly variable transport properties. Phys. Earth Planet. Inter. 140, 293–318.

Ghazian, R.K., Buiter, S.J., 2013. A numerical investigation of continental collision styles. Geophys. J. Int. 193, 1133–1152.

Giuliani, A., Phillips, D., Kamenetsky, V.S., Goemann, K., 2016. Constraints on kimberlite ascent mechanisms revealed by phlogopite compositions in kimberlites and mantle xenoliths. Lithos 240, 189–201.

Goes, S., Hasterok, D., Schutt, D.L., Klöcking, M., 2020. Continental lithospheric temperatures: A review. Phys. Earth Planet. Inter. 306, 106509.

Goes, S., van der Lee, S., 2002. Thermal structure of the North American uppermost mantle inferred from seismic tomography. J. Geophys. Res. Solid Earth 107, ETG-2.

Göğüş, O.H., Pysklywec, R.N., 2008. Mantle lithosphere delamination driving plateau uplift and synconvergent extension in eastern Anatolia. Geology 36, 723–726.

Gómez-Frutos, D., Castro, A., 2023. Mafic microgranular enclaves (MMEs) trace the origin of post-collisional magmas. Geology 51, 743–747.

Gómez-Frutos, D., Castro, A., 2022. Sanukitoid crystallization relations at 1.0 and 0.3 GPa. Lithos 414, 106632.

Gómez-Frutos, D., Castro, A., Gutiérrez-Alonso, G., 2023. Post-collisional batholiths do contribute to continental growth. Earth Planet. Sci. Lett. 603, 117978.

Gorczyk, W., Hobbs, B., Gerya, T., 2012. Initiation of Rayleigh–Taylor instabilities in intra-cratonic settings. Tectonophysics 514, 146–155.

Goswami, B., Bhattacharyya, C., 2014. Petrogenesis of shoshonitic granitoids, eastern India: implications for the late Grenvillian post-collisional magmatism. Geosci. Front. 5, 821–843.

Griffin, W.L., Pearson, N.J., Belousova, E., Jackson, S. v, Van Achterbergh, E., O'Reilly, S.Y., Shee, S., 2000. The Hf isotope composition of cratonic mantle: LAM-MC-ICPMS analysis of zircon megacrysts in kimberlites. Geochim. Cosmochim. Acta 64, 133–147.

Grove, T.L., Donnelly-Nolan, J.M., Housh, T., 1997. Magmatic processes that generated the rhyolite of Glass Mountain, Medicine Lake volcano, N. California. Contrib. Mineral. Petrol. 127, 205–223.

Guo, Z., Wilson, M., Liu, J., Mao, Q., 2006. Post-collisional, potassic and ultrapotassic magmatism of the northern Tibetan Plateau: Constraints on characteristics of the mantle source, geodynamic setting and uplift mechanisms. J. Petrol. 47, 1177–1220.

Guo, Z., Wilson, M., Zhang, M., Cheng, Z., Zhang, L., 2013. Post-collisional, K-rich mafic magmatism in south Tibet: constraints on Indian slab-to-wedge transport processes and plateau uplift. Contrib. Mineral. Petrol. 165, 1311–1340.

Hacker, B.R., Kelemen, P.B., Behn, M.D., 2011. Differentiation of the continental crust by relamination. Earth Planet. Sci. Lett. 307, 501–516.

Halla, J., 2005. Late Archean high-Mg granitoids (sanukitoids) in the southern Karelian domain, eastern Finland: Pb and Nd isotopic constraints on crust− mantle interactions. Lithos 79, 161–178.

Hamilton, P.J., O'nions, R.K., Pankhurst, R.J., 1980. Isotopic evidence for the provenance of some Caledonian granites. Nature 287, 279–284.

Harmon, R.S., Halliday, A.N., Clayburn, J.A.P., Stephens, W.E., 1984. Chemical and isotopic systematics of the Caledonian intrusions of Scotland and Northern England: a guide to magma source region and magma-crust interaction. Philos. Trans. R. Soc. Lond. Ser. Math. Phys. Sci. 310, 709–742.

Hasterok, D., Chapman, D., 2011. Heat production and geotherms for the continental lithosphere. Earth Planet. Sci. Lett. 307, 59–70.

Hawkesworth, C., Cawood, P., Kemp, T., Storey, C., Dhuime, B., 2009. A matter of preservation. Science 323, 49–50.

Hawkesworth, C., Cawood, P.A., Dhuime, B., 2019. Rates of generation and growth of the continental crust. Geosci. Front. 10, 165–173.

Hawkesworth, C.J., Kemp, A., 2006. Evolution of the continental crust. Nature 443, 811–817.

Heier, K.S., 1973. A Discussion on the evolution of the Precambrian crust-Geochemistry of granulite facies rocks and problems of their origin. Philos. Trans. R. Soc. Lond. Ser. Math. Phys. Sci. 273, 429–442.

Heilimo, E., Halla, J., Andersen, T., Huhma, H., 2013. Neoarchean crustal recycling and mantle metasomatism: Hf–Nd–Pb–O isotope evidence from sanukitoids of the Fennoscandian shield. Precambrian Res. 228, 250–266.

Heilimo, E., Halla, J., Hölttä, P., 2010. Discrimination and origin of the sanukitoid series: geochemical constraints from the Neoarchean western Karelian Province (Finland). Lithos 115, 27–39.

Hertgen, S., Yamato, P., Guillaume, B., Magni, V., Schliffke, N., van Hunen, J., 2020. Influence of the thickness of the overriding plate on convergence zone dynamics. Geochem. Geophys. Geosystems 21, e2019GC008678.

Hervé, F., Munizaga, F., Parada, M., Brook, M., Pankhurst, R., Snelling, N., Drake, R., 1988. Granitoids of the Coast Range of central Chile: geochronology and geologic setting. J. South Am. Earth Sci. 1, 185–194.

Herve, F., Pankhurst, R.J., Fanning, C., Calderón, M., Yaxley, G., 2007. The South Patagonian batholith: 150 my of granite magmatism on a plate margin. Lithos 97, 373–394.

Hildebrand, R., Bowring, S., 1999. Crustal recycling by slab failure. Geology 27, 11–14.

Hildreth, W., 1981. Gradients in silicic magma chambers: implications for lithospheric magmatism. J. Geophys. Res. Solid Earth 86, 10153–10192.

Holland, J.G., Lambert, R.S.J., 1972. Major element chemical composition of shields and the continental crust. Geochim. Cosmochim. Acta 36, 673–683.

Holub, F.V., 1997. Ultrapotassic plutonic rocks of the durbachite series in the Bohemian Massif: petrology, geochemistry and petrogenetic interpretation. J Geol Sci Econ Geol Miner. 31, 5–26.

Huang, F., Chen, J.-L., Xu, J.-F., Wang, B.-D., Li, J., 2015. Os–Nd–Sr isotopes in Miocene ultrapotassic rocks of southern Tibet: Partial melting of a pyroxenite-bearing lithospheric mantle? Geochim. Cosmochim. Acta 163, 279–298.

Huet, B., Le Pourhiet, L., Labrousse, L., Burov, E., Jolivet, L., 2011. Post-orogenic extension and metamorphic core complexes in a heterogeneous crust: the role of crustal layering inherited from collision. Application to the Cyclades (Aegean domain). Geophys. J. Int. 184, 611–625.

Huppert, H., Sparks, R., 1988. The generation of granitic magmas by intrusion of basalt into continental crust. J. Petrol. 29, 599–624.

Hurley, P.M., Rand, J.R., 1969. Pre-drift continental nuclei. Science 164, 1229–1242.

Hyndman, D.W., 1983. The Idaho batholith and associated plutons, Idaho and western Montana.

Ionov, D.A., Bodinier, J.-L., Mukasa, S.B., Zanetti, A., 2002. Mechanisms and sources of mantle metasomatism: major and trace element compositions of peridotite xenoliths from Spitsbergen in the context of numerical modelling. J. Petrol. 43, 2219–2259.

Janoušek, V., Bowes, D., Rogers, G., Farrow, C.M., Jelínek, E., 2000. Modelling diverse processes in the petrogenesis of a composite batholith: the Central Bohemian Pluton, Central European Hercynides. J. Petrol. 41, 511–543.

Jayananda, M., Santosh, M., Aadhiseshan, K., 2018. Formation of Archean (3600–2500 Ma) continental crust in the Dharwar Craton, southern India. Earth-Sci. Rev. 181, 12–42.

Jiang, N., Guo, J., Fan, W., Hu, J., Zong, K., Zhang, S., 2016. Archean TTGs and sanukitoids from the Jiaobei terrain, North China craton: Insights into crustal growth and mantle metasomatism. Precambrian Res. 281, 656–672.

Kägi, R., Müntener, O., Ulmer, P., Ottolini, L., 2005. Piston-cylinder experiments on H2O undersaturated Fe-bearing systems: An experimental setup approaching f O2 conditions of natural calc-alkaline magmas. Am. Mineral. 90, 708–717.

Kampunzu, A., Tombale, A., Zhai, M., Bagai, Z., Majaule, T., Modisi, M., 2003. Major and trace element geochemistry of plutonic rocks from Francistown, NE Botswana: evidence for a Neoarchaean continental active margin in the Zimbabwe craton. Lithos 71, 431–460.

Käpyaho, A., Mänttäri, I., Huhma, H., 2006. Growth of Archaean crust in the Kuhmo district, eastern Finland: U–Pb and Sm–Nd isotope constraints on plutonic rocks. Precambrian Res. 146, 95–119.

Kargin, A., Sazonova, L., Nosova, A., Lebedeva, N., Kostitsyn, Y.A., Kovalchuk, E., Tretyachenko, V., Tikhomirova, Y.S., 2019. Phlogopite in mantle xenoliths and kimberlite from the Grib pipe, Arkhangelsk province, Russia: evidence for multi-stage mantle metasomatism and origin of phlogopite in kimberlite. Geosci. Front. 10, 1941–1959.

Kawabata, H., Shuto, K., 2005. Magma mixing recorded in intermediate rocks associated with high-Mg andesites from the Setouchi volcanic belt, Japan: implications for Archean TTG formation. J. Volcanol. Geotherm. Res. 140, 241–271.

Kawamoto, T., Hirose, K., 1994. Au-Pd sample containers for melting experiments on iron and water bearing systems. Eur. J. Mineral.-Ohne Beih. 6, 381–386.

Kay, R.W., Kay, S.M., 1993. Delamination and delamination magmatism. Tectonophysics 219, 177–189.

Kelemen, P.B., 1995. Genesis of high Mg# andesites and the continental crust. Contrib. Mineral. Petrol. 120, 1–19.

Kemp, A., Hawkesworth, C., Paterson, B., Kinny, P., 2006. Episodic growth of the Gondwana supercontinent from hafnium and oxygen isotopes in zircon. Nature 439, 580–583.

Kirscher, U., Mitchell, R.N., Liu, Y., Nordsvan, A.R., Cox, G.M., Pisarevsky, S.A., Wang, C., Wu, L., Murphy, J.B., Li, Z.-X., 2021. Paleomagnetic constraints on the duration of the Australia-Laurentia connection in the core of the Nuna supercontinent. Geology 49, 174–179.

Kopylova, M., Tso, E., Ma, F., Liu, J., Pearson, D., 2019. The metasomatized mantle beneath the North Atlantic Craton: insights from peridotite xenoliths of the Chidliak kimberlite province (NE Canada). J. Petrol. 60, 1991–2024.

Kudryashov, N., Petrovsky, M., Mokrushin, A., Elizarov, D., 2013. Neoarchean sanukitoid magmatism in the Kola region: Geological, petrochemical, geochronological, and isotopic-geochemical data. Petrology 21, 351–374.

Kushiro, I., 1972. Origin of some abyssal tholeiites from the Mid-Atlantic Ridge. Carnegie Inst Wash. Yearb. 71, 403–406.

Kusky, T.M., Polat, A., 1999. Growth of granite–greenstone terranes at convergent margins, and stabilization of Archean cratons. Tectonophysics 305, 43–73.

Lackey, J.S., Valley, J.W., Chen, J.H., Stockli, D.F., 2008. Dynamic magma systems, crustal recycling, and alteration in the central Sierra Nevada batholith: the oxygen isotope record. J. Petrol. 49, 1397–1426.

Lacroix, A., 1898. Le granite des Pyrénées et ses phénomènes de contact... Librairie polytechnique.

Lacroix, A., 1893. Les enclaves des roches volcaniques. Protat Freres.

Laurent, A., Janousek, V., Magna, T., Schulmann, K., Mikova, J., 2014. Petrogenesis and geochronology of a post-orogenic calc-alkaline magmatic association: the Zulova Pluton, Bohemian Massif. J. Geosci. 59, 415–440.

Laurent, O., Couzinié, S., Doucet, L.S., 2023. Timescales of ultra-high temperature metamorphism and crustal differentiation: Zircon petrochronology from granulite xenoliths of the Variscan French Massif Central. Earth Planet. Sci. Lett. 611, 118133.

Lee, C.-T.A., Bachmann, O., 2014. How important is the role of crystal fractionation in making intermediate magmas? Insights from Zr and P systematics. Earth Planet. Sci. Lett. 393, 266–274.

Lee, C.-T.A., Cheng, X., Horodyskyj, U., 2006. The development and refinement of continental arcs by primary basaltic magmatism, garnet pyroxenite accumulation, basaltic recharge and delamination: insights from the Sierra Nevada, California. Contrib. Mineral. Petrol. 151, 222–242.

Lee, C.-T.A., Morton, D.M., Kistler, R.W., Baird, A.K., 2007. Petrology and tectonics of Phanerozoic continent formation: From island arcs to accretion and continental arc magmatism. Earth Planet. Sci. Lett. 263, 370–387.

Li, L., Lin, S., Xing, G., Jiang, Y., He, J., 2017. First direct evidence of Pan-African orogeny associated with Gondwana assembly in the Cathaysia Block of Southern China. Sci. Rep. 7, 794.

Li, Z.-H., Liu, M., Gerya, T., 2016. Lithosphere delamination in continental collisional orogens: A systematic numerical study. J. Geophys. Res. Solid Earth 121, 5186–5211.

Liégeois, J.-P., Berza, T., Tatu, M., Duchesne, J.-C., 1996. The Neoproterozoic Pan-African basement from the Alpine Lower Danubian nappe system (South Carpathians, Romania). Precambrian Res. 80, 281–301.

Liégeois, J.-P., Navez, J., Hertogen, J., Black, R., 1998. Contrasting origin of post-collisional high-K calc-alkaline and shoshonitic versus alkaline and peralkaline granitoids. The use of sliding normalization. Lithos 45, 1–28.

Liu, D., Zhao, Z., Zhu, D.-C., Niu, Y., Widom, E., Teng, F.-Z., DePaolo, D.J., Ke, S., Xu, J.-F., Wang, Q., 2015. Identifying mantle carbonatite metasomatism through Os–Sr–Mg isotopes in Tibetan ultrapotassic rocks. Earth Planet. Sci. Lett. 430, 458–469.

Lobach-Zhuchenko, S., Rollinson, H., Chekulaev, V., Arestova, N., Kovalenko, A., Ivanikov, V., Guseva, N., Sergeev, S., Matukov, D., Jarvis, K., 2005. The Archaean sanukitoid series of the Baltic Shield: geological setting, geochemical characteristics and implications for their origin. Lithos 79, 107–128.

Lobach-Zhuchenko, S., Rollinson, H., Chekulaev, V., Savatenkov, V., Kovalenko, A., Martin, H., Guseva, N., Arestova, N., 2008. Petrology of a Late Archaean, highly potassic, sanukitoid pluton from the Baltic Shield: insights into Late Archaean mantle metasomatism. J. Petrol. 49, 393–420.

López-Moro, F.-J., López-Plaza, M., 2004. Monzonitic series from the Variscan Tormes Dome (Central Iberian Zone): petrogenetic evolution from monzogabbro to granite magmas. Lithos 72, 19–44.

Ma, C., Li, Z., Ehlers, C., Yang, K., Wang, R., 1998. A post-collisional magmatic plumbing system: Mesozoic granitoid plutons from the Dabieshan high-pressure and ultrahigh-pressure metamorphic zone, east-central China. Lithos 45, 431–456.

Maierová, P., Schulmann, K., Gerya, T., 2018. Relamination styles in collisional orogens. Tectonics 37, 224–250.

Marschall, H.R., Schumacher, J.C., 2012. Arc magmas sourced from mélange diapirs in subduction zones. Nat. Geosci. 5, 862–867.

Martin, H., Moyen, J.-F., Rapp, R., 2009. The sanukitoid series: magmatism at the Archaean–Proterozoic transition. Earth Environ. Sci. Trans. R. Soc. Edinb. 100, 15–33.

Martin, H., Smithies, R., Rapp, R., Moyen, J.-F., Champion, D., 2005. An overview of adakite, tonalite–trondhjemite–granodiorite (TTG), and sanukitoid: relationships and some implications for crustal evolution. Lithos 79, 1–24.

Matsumoto, T., Tomoda, Y., 1983. Numerical simulation of the initiation of subduction at the fracture zone. J. Phys. Earth 31, 183–194.

Meier, U., Curtis, A., Trampert, J., 2007. Global crustal thickness from neural network inversion of surface wave data. Geophys. J. Int. 169, 706–722.

Melekhova, E., Annen, C., Blundy, J., 2013. Compositional gaps in igneous rock suites controlled by magma system heat and water content. Nat. Geosci. 6, 385–390.

Minear, J.W., Toksöz, M.N., 1970. Thermal regime of a downgoing slab and new global tectonics. J. Geophys. Res. 75, 1397–1419.

Miyashiro, A., 1974. Volcanic rock series in island arcs and active continental margins. Am. J. Sci. 274, 321–355.

Moghadam, H.S., Hoernle, K.A., Hauff, F., Chiaradia, M., Garbe-Schönberg, D., Orozco-Esquivel, T., Bindeman, I.N., Karsli, O., Ghorbani, G., Mousavi, N., 2023. Middle-Late Miocene to Pleistocene post-collisional magmatism in the Arabia-Eurasia collision zone, an example from northwest Iran. J. Petrol. egad081.

Molina, J., Montero, P., Bea, F., Scarrow, J., 2012. Anomalous xenocryst dispersion during tonalite–granodiorite crystal mush hybridization in the mid crust: mineralogical and geochemical evidence from Variscan appinites (Avila Batholith, Central Iberia). Lithos 153, 224–242.

Moyen, J.-F., Laurent, O., Chelle-Michou, C., Couzinié, S., Vanderhaeghe, O., Zeh, A., Villaros, A., Gardien, V., 2017. Collision vs. subduction-related magmatism: two contrasting ways of granite formation and implications for crustal growth. Lithos 277, 154–177.

Mullen, E., Weis, D., Marsh, N., Martindale, M., 2017. Primitive arc magma diversity: New geochemical insights in the Cascade Arc. Chem. Geol. 448, 43–70.

Murphy, J.B., 2020. Appinite suites and their genetic relationship with coeval voluminous granitoid batholiths. Int. Geol. Rev. 62, 683–713.

Murphy, J.B., 2013. Appinite suites: A record of the role of water in the genesis, transport, emplacement and crystallization of magma. Earth-Sci. Rev. 119, 35–59.

Nabatian, G., Jiang, S.-Y., Honarmand, M., Neubauer, F., 2016. Zircon U–Pb ages, geochemical and Sr–Nd–Pb–Hf isotopic constraints on petrogenesis of the Tarom-Olya pluton, Alborz magmatic belt, NW Iran. Lithos 244, 43–58.

Nakajima, M., Stevenson, D.J., 2015. Melting and mixing states of the Earth's mantle after the Moon-forming impact. Earth Planet. Sci. Lett. 427, 286–295.

O'Reilly, S., Griffin, W., 2006. Imaging global chemical and thermal heterogeneity in the subcontinental lithospheric mantle with garnets and xenoliths: Geophysical implications. Tectonophysics 416, 289–309.

O'Reilly, S.Y., Griffin, W., 2013. Mantle metasomatism. Metasomatism Chem. Transform. Rock 471–533.

Orejana, D., Villaseca, C., Pérez-Soba, C., López-García, J.A., Billström, K., 2009. The Variscan gabbros from the Spanish Central System: A case for crustal recycling in the sub-continental lithospheric mantle? Lithos 110, 262–276.

Otamendi, J.E., Vujovich, G.I., de la Rosa, J.D., Tibaldi, A.M., Castro, A., Martino, R.D., Pinotti, L.P., 2009. Geology and petrology of a deep crustal zone from the Famatinian paleo-arc, Sierras de Valle Fértil and La Huerta, San Juan, Argentina. J. South Am. Earth Sci. 27, 258–279.

Pabst, A., 1928. Observations on inclusions in the granitic rocks of the Sierra Nevada. University of California Press.

Pang, K.-N., Chung, S.-L., Zarrinkoub, M.H., Khatib, M.M., Mohammadi, S.S., Chiu, H.-Y., Chu, C.-H., Lee, H.-Y., Lo, C.-H., 2013. Eocene–Oligocene post-collisional magmatism in the Lut–Sistan region, eastern Iran: Magma genesis and tectonic implications. Lithos 180, 234–251.

Pankhurst, R., Hole, M., Brook, M., 1988. Isotope evidence for the origin of Andean granites. Earth Environ. Sci. Trans. R. Soc. Edinb. 79, 123–133.

Pankhurst, R., Weaver, S., Hervé, F., Larrondo, P., 1999. Mesozoic-Cenozoic evolution of the North Patagonian batholith in Aysen, southern Chile. J. Geol. Soc. 156, 673–694.

Parada, M.A., Nyström, J., Levi, B., 1999. Multiple sources for the Coastal Batholith of central Chile (31–34 S): geochemical and Sr–Nd isotopic evidence and tectonic implications. Lithos 46, 505–521.

Parat, F., Holtz, F., René, M., Almeev, R., 2010. Experimental constraints on ultrapotassic magmatism from the Bohemian Massif (durbachite series, Czech Republic). Contrib. Mineral. Petrol. 159, 331–347.

Paterson, S., Memeti, V., Mundil, R., Žák, J., 2016. Repeated, multiscale, magmatic erosion and recycling in an upper-crustal pluton: Implications for magma chamber dynamics and magma volume estimates. Am. Mineral. 101, 2176–2198.

Paterson, S.R., Pignotta, G.S., Vernon, R.H., 2004. The significance of microgranitoid enclave shapes and orientations. J. Struct. Geol. 26, 1465–1481.

Patiño Douce, A.E., 2005. Vapor-absent melting of tonalite at 15–32 kbar. J. Petrol. 46, 275–290.

Patiño Douce, A.E., 1999. What do experiments tell us about the relative contributions of crust and mantle to the origin of granitic magmas? Geol. Soc. Lond. Spec. Publ. 168, 55–75.

Patiño Douce, A.E., 1995. Experimental generation of hybrid silicic melts by reaction of high-Al basalt with metamorphic rocks. J. Geophys. Res. Solid Earth 100, 15623–15639.

Payne, J.L., McInerney, D.J., Barovich, K.M., Kirkland, C.L., Pearson, N.J., Hand, M., 2016. Strengths and limitations of zircon Lu-Hf and O isotopes in modelling crustal growth. Lithos 248, 175–192.

Pearce, J.A., Cann, J.R., 1973. Tectonic setting of basic volcanic rocks determined using trace element analyses. Earth Planet. Sci. Lett. 19, 290–300.

Pearce, J.A., Harris, N.B., Tindle, A.G., 1984. Trace element discrimination diagrams for the tectonic interpretation of granitic rocks. J. Petrol. 25, 956–983.

Peccerillo, A., Taylor, S., 1976. Geochemistry of Eocene calc-alkaline volcanic rocks from the Kastamonu area, northern Turkey. Contrib. Mineral. Petrol. 58, 63–81.

Pfiffner, O.-A., Ellis, S., Beaumont, C., 2000. Collision tectonics in the Swiss Alps: Insight from geodynamic modeling. Tectonics 19, 1065–1094.

Philpotts, A.R., Ague, J.J., 2009. Principles of igneous and metamorphic petrology. Cambridge University Press.

Pickering, J.M., Schwab, B.E., Johnston, A.D., 1998. Off-center hot spots: double thermocouple determination of the thermal gradient in a 1.27 cm (1/2 in.) CaF2 piston-cylinder furnace assembly. Am. Mineral. 83, 228–235.

Pitcher, W.S., 1997. The nature and origin of granite. Springer Science & Business Media.

Pitcher, W.S., 1987. Granites and yet more granites forty years on. Geol. Rundsch. 76, 51–79.

Plag, H.-P., Jüttner, H.-U., 1995. Rayleigh-Taylor instabilities of a self-gravitating Earth. J. Geodyn. 20, 267–288.

Plank, T., Kelley, K.A., Zimmer, M.M., Hauri, E.H., Wallace, P.J., 2013. Why do mafic arc magmas contain~ 4 wt% water on average? Earth Planet. Sci. Lett. 364, 168–179.

Plant, J., 1983. Metalliferous and mineralized Caledonian granites in relation to regional metamorphism and fracture systems in northern Scotland. Inst. Min. Metall. Trans. 92.

Priestley, K., McKenzie, D., 2006. The thermal structure of the lithosphere from shear wave velocities. Earth Planet. Sci. Lett. 244, 285–301.

Putirka, K.D., Canchola, J., Rash, J., Smith, O., Torrez, G., Paterson, S.R., Ducea, M.N., 2014. Pluton assembly and the genesis of granitic magmas: Insights from the GIC pluton in cross section, Sierra Nevada Batholith, California. Am. Mineral. 99, 1284–1303.

Pysklywec, R.N., 2001. Evolution of subducting mantle lithosphere at a continental plate boundary. Geophys. Res. Lett. 28, 4399–4402.

Qian, Q., Hermann, J., 2013. Partial melting of lower crust at 10–15 kbar: constraints on adakite and TTG formation. Contrib. Mineral. Petrol. 165, 1195–1224.

Ranalli, G., 1995. Rheology of the Earth. Springer Science & Business Media.

Rao, K.M., Kumar, M.R., Rastogi, B.K., 2015. Crust beneath the northwestern Deccan Volcanic Province, India: Evidence for uplift and magmatic underplating. J. Geophys. Res. Solid Earth 120, 3385–3405.

Rapela, C., Pankhurst, R., 1996. Monzonite suites: the innermost Cordilleran plutonism of Patagonia. Earth Environ. Sci. Trans. R. Soc. Edinb. 87, 193–203.

Rapp, R.P., Watson, E.B., 1995. Dehydration melting of metabasalt at 8–32 kbar: implications for continental growth and crust-mantle recycling. J. Petrol. 36, 891–931.

Read, H.H., 1961. Aspects of Caledonian magmatism in Britain. Geol. J. 2, 653–683.

Reubi, O., Blundy, J., 2009. A dearth of intermediate melts at subduction zone volcanoes and the petrogenesis of arc andesites. Nature 461, 1269–1273.

Reymer, A., Schubert, G., 1984. Phanerozoic addition rates to the continental crust and crustal growth. Tectonics 3, 63–77.

Roberts, N.M., Spencer, C.J., 2015. The zircon archive of continent formation through time. The Geological Society of London London.

Rodríguez, C., Castro, A., 2019. Origins of mafic microgranular enclaves and enclave swarms in granites: Field and geochemical relations. GSA Bull. 131, 635–660.

Röhm, A.H., Snieder, R., Goes, S., Trampert, J., 2000. Thermal structure of continental upper mantle inferred from S-wave velocity and surface heat flow. Earth Planet. Sci. Lett. 181, 395–407.

Rudnick, R.L., 1995. Making continental crust. Nature 378, 571–578.

Rudnick, R.L., Fountain, D.M., 1995. Nature and composition of the continental crust: a lower crustal perspective. Rev. Geophys. 33, 267–309.

Rudnick, R.L., Gao, S., 2003. Composition of the continental crust. Treatise on Geochemistry, vol. 3. Elsevier New York.

Rudnick, R.L., McDonough, W.F., O'Connell, R.J., 1998. Thermal structure, thickness and composition of continental lithosphere. Chem. Geol. 145, 395–411.

Schilling, F., Wunder, B., 2004. Temperature distribution in piston-cylinder assemblies: Numerical simulations and laboratory experiments. Eur. J. Mineral. 16, 7–14.

Schmidt, M.W., Ulmer, P., 2004. A rocking multianvil: elimination of chemical segregation in fluid-saturated high-pressure experiments. Geochim. Cosmochim. Acta 68, 1889–1899.

Scholl, D.W., Von Huene, R., 2009. Implications of estimated magmatic additions and recycling losses at the subduction zones of accretionary (non-collisional) and collisional (suturing) orogens. Geol. Soc. Lond. Spec. Publ. 318, 105–125.

Scholl, D.W., von Huene, R., 2007. Crustal recycling at modern subduction zones applied to the past—Issues of growth and preservation of continental basement crust, mantle geochemistry, and supercontinent reconstruction.

Schutt, D.L., Lowry, A.R., Buehler, J.S., 2018. Moho temperature and mobility of lower crust in the western United States. Geology 46, 219–222.

Shapiro, N., Ritzwoller, M., 2004. Thermodynamic constraints on seismic inversions. Geophys. J. Int. 157, 1175–1188.

Shirey, S.B., Hanson, G.N., 1984. Mantle-derived Archaean monozodiorites and trachyandesites. Nature 310, 222–224.

Silver, L., Chappell, B., 1988. The Peninsular Ranges Batholith: an insight into the evolution of the Cordilleran batholiths of southwestern North America. Earth Environ. Sci. Trans. R. Soc. Edinb. 79, 105–121.

Singh, P.K., Verma, S.K., Singh, V.K., Moreno, J.A., Oliveira, E.P., Mehta, P., 2019. Geochemistry and petrogenesis of sanukitoids and high-K anatectic granites from the Bundelkhand Craton, India: Implications for late-Archean crustal evolution. J. Asian Earth Sci. 174, 263–282.

Sisson, T., Grove, T., 1993. Temperatures and H 2 O contents of low-MgO high-alumina basalts. Contrib. Mineral. Petrol. 113, 167–184.

Sisson, T., Ratajeski, K., Hankins, W., Glazner, A.F., 2005. Voluminous granitic magmas from common basaltic sources. Contrib. Mineral. Petrol. 148, 635–661.

Słaby, E., Martin, H., 2008. Mafic and felsic magma interaction in granites: the Hercynian Karkonosze Pluton (Sudetes, Bohemian Massif). J. Petrol. 49, 353–391.

Smithies, R., Champion, D., 2000. The Archaean high-Mg diorite suite: links to tonalite–trondhjemite–granodiorite magmatism and implications for early Archaean crustal growth. J. Petrol. 41, 1653–1671.

Smithies, R.H., Lu, Y., Kirkland, C.L., Johnson, T.E., Mole, D.R., Champion, D.C., Martin, L., Jeon, H., Wingate, M.T., Johnson, S.P., 2021. Oxygen isotopes trace the origins of Earth's earliest continental crust. Nature 592, 70–75.

Smithson, S.B., 1978. Modeling continental crust: structural and chemical constraints. Geophys. Res. Lett. 5, 749–752.

Solano, J., Jackson, M., Sparks, R., Blundy, J.D., Annen, C., 2012. Melt segregation in deep crustal hot zones: a mechanism for chemical differentiation, crustal assimilation and the formation of evolved magmas. J. Petrol. 53, 1999–2026.

Soller, D.R., Ray, R.D., Brown, R.D., 1982. A new global crustal thickness map. Tectonics 1, 125–149.

Spencer, C.J., Cawood, P.A., Hawkesworth, C.J., Prave, A.R., Roberts, N.M., Horstwood, M.S., Whitehouse, M.J., 2015. Generation and preservation of continental crust in the Grenville Orogeny. Geosci. Front. 6, 357–372.

Stampfli, G., Hochard, C., Vérard, C., Wilhem, C., 2013. The formation of Pangea. Tectonophysics 593, 1–19.

Stephens, W.E., Halliday, A.N., 1984. Geochemical contrasts between late Caledonian granitoid plutons of northern, central and southern Scotland. Earth Environ. Sci. Trans. R. Soc. Edinb. 75, 259–273.

Stern, C.R., 2011. Subduction erosion: rates, mechanisms, and its role in arc magmatism and the evolution of the continental crust and mantle. Gondwana Res. 20, 284–308.

Stern, R., Hanson, G.N., 1991. Archean high-Mg granodiorite: a derivative of light rare earth element-enriched monzodiorite of mantle origin. J. Petrol. 32, 201–238.

Stern, R.A., Hanson, G.N., Shirey, S.B., 1989. Petrogenesis of mantle-derived, LILE-enriched Archean monzodiorites and trachyandesites (sanukitoids) in southwestern Superior Province. Can. J. Earth Sci. 26, 1688–1712.

Stevenson, R., Henry, P., Gariépy, C., 1999. Assimilation–fractional crystallization origin of Archean sanukitoid suites: Western Superior Province, Canada. Precambrian Res. 96, 83–99.

Streck, M.J., Leeman, W.P., Chesley, J., 2007. High-magnesian andesite from Mount Shasta: a product of magma mixing and contamination, not a primitive mantle melt. Geology 35, 351–354.

Sutcliffe, R.H., Smith, A.R., Doherty, W., Barnett, R.L., 1990. Mantle derivation of Archean amphibole-bearing granitoid and associated mafic rocks: evidence from the southern Superior Province, Canada. Contrib. Mineral. Petrol. 105, 255–274.

Takahashi, E., Kushiro, I., 1983. Melting of a dry peridotite at high pressures and basalt magma genesis. Am. Mineral. 68, 859–879.

Tang, H.-Y., Zheng, J.-P., Yu, C.-M., 2009. Age and composition of the Rushan intrusive complex in the northern Sulu orogen, eastern China: petrogenesis and lithospheric mantle evolution. Geol. Mag. 146, 199–215.

Tarney, J., Jones, C.E., 1994. Trace element geochemistry of orogenic igneous rocks and crustal growth models. J. Geol. Soc. 151, 855–868.

Tatsumi, Y., Ishizaka, K., 1982. Origin of high-magnesian andesites in the Setouchi volcanic belt, southwest Japan, I. Petrographical and chemical characteristics. Earth Planet. Sci. Lett. 60, 293–304.

Tatsumi, Y., Ishizaka, K., 1981. Existence of andesitic primary magma: an example from southwest Japan. Earth Planet. Sci. Lett. 53, 124–130.

Taylor, S.R., 1967. The origin and growth of continents. Tectonophysics 4, 17–34.

Taylor, S.R., McLennan, S.M., 1995. The geochemical evolution of the continental crust. Rev. Geophys. 33, 241–265.

Taylor, S.R., McLennan, S.M., 1985. The continental crust: its composition and evolution.

Terentiev, R., Santosh, M., 2018. High magnesian granitoids in the Precambrian continental crust: Implication for the continuum between ferro–potassic and magnesio–potassic rock suites. Lithos 314, 669–682.

Tewari, H.C., Dixit, M.M., Rao, N.M., Venkateswaralu, N., Rao, V.V., 1997. Crustal thickening under the palaeo-meso-Proterozoic Delhi Fold Belt in northwestern India: evidence from deep reflection profiling. Geophys. J. Int. 129, 657–668.

Thorpe, R., Francis, P., Harmon, R., 1981. Andean andesites and crustal growth. Philos. Trans. R. Soc. Lond. Ser. Math. Phys. Sci. 301, 305–320.

Tobisch, O., McNulty, B., Vernon, R., 1997. Microgranitoid enclave swarms in granitic plutons, central Sierra Nevada, California. Lithos 40, 321–339.

Tonks, W.B., Melosh, H.J., 1993. Magma ocean formation due to giant impacts. J. Geophys. Res. Planets 98, 5319–5333.

Torrance, K.E., Turcotte, D.L., 1971. Thermal convection with large viscosity variations. J. Fluid Mech. 47, 113–125.

Turcotte, D.L., Schubert, G., 2002. Geodynamics. Cambridge university press.

Ueda, K., Gerya, T.V., Burg, J.-P., 2012. Delamination in collisional orogens: Thermomechanical modeling. J. Geophys. Res. Solid Earth 117.

Ulmer, P., Kaegi, R., Müntener, O., 2018. Experimentally derived intermediate to silica-rich arc magmas by fractional and equilibrium crystallization at 1· 0 GPa: an evaluation of phase relationships, compositions, liquid lines of descent and oxygen fugacity. J. Petrol. 59, 11–58.

Urann, B., Le Roux, V., Jagoutz, O., Müntener, O., Behn, M., Chin, E., 2022. High water content of arc magmas recorded in cumulates from subduction zone lower crust. Nat. Geosci. 15, 501–508.

van Hunen, J., Allen, M.B., 2011. Continental collision and slab break-off: A comparison of 3-D numerical models with observations. Earth Planet. Sci. Lett. 302, 27–37.

Vernon, R., 1984. Microgranitoid enclaves in granites—globules of hybrid magma quenched in a plutonic environment. Nature 309, 438–439.

Villagómez, D., Spikings, R., Magna, T., Kammer, A., Winkler, W., Beltrán, A., 2011. Geochronology, geochemistry and tectonic evolution of the Western and Central cordilleras of Colombia. Lithos 125, 875–896.

Vogt, K., Gerya, T.V., Castro, A., 2012. Crustal growth at active continental margins: Numerical modeling. Phys. Earth Planet. Inter. 192, 1–20.

Vogt, K., Matenco, L., Cloetingh, S., 2017. Crustal mechanics control the geometry of mountain belts. Insights from numerical modelling. Earth Planet. Sci. Lett. 460, 12–21.

Voice, P.J., Kowalewski, M., Eriksson, K.A., 2011. Quantifying the timing and rate of crustal evolution: global compilation of radiometrically dated detrital zircon grains. J. Geol. 119, 109–126.

von Raumer, J.F., Finger, F., Veselá, P., Stampfli, G.M., 2014. Durbachites–Vaugnerites–a geodynamic marker in the central E uropean Variscan orogen. Terra Nova 26, 85–95.

Walowski, K.J., Wallace, P.J., Clynne, M.A., Rasmussen, D., Weis, D., 2016. Slab melting and magma formation beneath the southern Cascade arc. Earth Planet. Sci. Lett. 446, 100–112.

Wang, C.Y., Campbell, I.H., Allen, C.M., Williams, I.S., Eggins, S.M., 2009. Rate of growth of the preserved North American continental crust: evidence from Hf and O isotopes in Mississippi detrital zircons. Geochim. Cosmochim. Acta 73, 712–728.

Wang, Y., Fan, W., Peng, T., Zhang, H., Guo, F., 2005. Nature of the Mesozoic lithospheric mantle and tectonic decoupling beneath the Dabie Orogen, Central China: evidence from 40Ar/39Ar geochronology, elemental and Sr–Nd–Pb isotopic compositions of early Cretaceous mafic igneous rocks. Chem. Geol. 220, 165–189.

Wang, Y., Luo, Z., Santosh, M., Wang, S., Wang, N., 2017. The Liuyuan Volcanic Belt in NW China revisited: evidence for Permian rifting associated with the assembly of continental blocks in the Central Asian Orogenic Belt. Geol. Mag. 154, 265–285.

Wareham, C., Pankhurst, R., Thomas, R., Storey, B., Grantham, G., Jacobs, J., Eglington, B., 1998. Pb, Nd, and Sr isotope mapping of Grenville-age crustal provinces in Rodinia. J. Geol. 106, 647–660.

Watson, E., Wark, D., Price, J., Van Orman, J., 2002. Mapping the thermal structure of solid-media pressure assemblies. Contrib. Mineral. Petrol. 142, 640–652.

Weinberg, R.F., Hasalová, P., 2015. Water-fluxed melting of the continental crust: A review. Lithos 212, 158–188.

Whalen, J.B., Hildebrand, R.S., 2019. Trace element discrimination of arc, slab failure, and A-type granitic rocks. Lithos 348, 105179.

White, A.J., Chappell, B.W., 1977. Ultrametamorphism and granitoid genesis. Tectonophysics 43, 7–22.

White, A.J., Chappell, B.W., Wyborn, D., 1999. Application of the Restite Model to the Deddick Granodiorite and its Enclaves—a Reinterpretation of the Observations and Data of. J. Petrol. 40, 413–421.

Whittington, A.G., Hofmeister, A.M., Nabelek, P.I., 2009. Temperature-dependent thermal diffusivity of the Earth's crust and implications for magmatism. Nature 458, 319–321.

Wiebe, R.A., 2016. Mafic replenishments into floored silicic magma chambers. Am. Mineral. 101, 297–310.

Wiebe, R.A., 1991. Commingling of contrasted magmas and generation of mafic enclaves in granitic rocks. Presented at the Enclaves and granite petrology, pp. 393–402.

Wiebe, R.A., Adams, S.D., 1997. Felsic enclave swarms in the Gouldsboro granite, coastal Maine: a record of eruption through the roof of a silicic magma chamber. J. Geol. 105, 617–628.

Williamson, B., Downes, H., Thirlwall, M., 1992. The relationship between crustal magmatic underplating and granite genesis: an example from the Velay granite complex, Massif Central, France. Earth Environ. Sci. Trans. R. Soc. Edinb. 83, 235–245.

Windley, B.F., 2010. The evolving continents: understanding processes of continental growth. Geological Society of London.

Wood, B.J., Turner, S.P., 2009. Origin of primitive high-Mg andesite: Constraints from natural examples and experiments. Earth Planet. Sci. Lett. 283, 59–66.

Xu, H., Ma, C., Song, Y., Zhang, J., Ye, K., 2012. Early Cretaceous intermediate-mafic dykes in the Dabie orogen, eastern China: Petrogenesis and implications for crust–mantle interaction. Lithos 154, 83–99.

Xu, W., Zhu, D.-C., Wang, Q., Weinberg, R.F., Wang, R., Li, S.-M., Zhang, L.-L., Zhao, Z.-D., 2020. Mafic microgranular enclaves formed by gas-driven filter pressing during rapid cooling: An example from the Gangdese batholith in southern Tibet. J. Petrol. 61, egab003.

Yin, J., Chen, W., Xiao, W., Yuan, C., Sun, M., Tang, G., Yu, S., Long, X., Cai, K., Geng, H., 2015. Petrogenesis of early-Permian sanukitoids from west Junggar, Northwest China: implications for late Paleozoic crustal growth in Central Asia. Tectonophysics 662, 385–397.

Yongfeng, Z., 1994. Petrological significance of zoned plagioclase in Eldjurti granite and mafic microgranular enclaves, North Caucasus, Russia. Chin. J. Geochem. 13, 142–155.

Yu, Y., Li, D., Chen, Y., Kang, H., Geng, J., Xu, S., Wang, Y., Sun, M., 2021. Mantle cooling and cratonization of Archean lithosphere by continuous plate subduction: Constraints from TTGs, sanukitoids, and high-K granites, eastern North China Craton. Precambrian Res. 353, 106042.

Zhang, J., Davidson, J., Humphreys, M., Macpherson, C., Neill, I., 2015. Magmatic enclaves and andesitic lavas from Mt. Lamington, Papua New Guinea: implications for recycling of earlier-fractionated minerals through magma recharge. J. Petrol. 56, 2223–2256.

Zhang, J., Zhao, Z.-F., Zheng, Y.-F., Liu, X., Xie, L., 2012. Zircon Hf–O isotope and whole-rock geochemical constraints on origin of postcollisional mafic to felsic dykes in the Sulu orogen. Lithos 136, 225–245.

Zhao, G., Li, S., Sun, M., Wilde, S.A., 2011. Assembly, accretion, and break-up of the Palaeo-Mesoproterozoic Columbia supercontinent: record in the North China Craton revisited. Int. Geol. Rev. 53, 1331–1356.